EWI Report J6098-24-92

AN INTERNATIONAL RESEARCH PROJECT TO DEVELOP SHALLOW CRACK FRACTURE MECHANICS TESTS

#124

FINAL REPORT ON NORTH AMERICAN EXPERIMENTAL PROGRAM

to

A GROUP OF SPONSORS

May 1992

J. R. Gordon and T. H M°Gaughy
EDISON WELDING INSTITUTE
1100 Kinnear Road
Columbus, Ohio 43212

and

TWI
Abington Hall
Abington, Cambridge CB1 6AL
United Kingdom

TABLE OF CONTENTS
(Continued)

TABLE OF CONTENTS
(Continued)

EXECUTIVE SUMMARY

Background

Within the last decade there has been an increasing awareness that, depending on the heterogeneity of the materials concerned, standard deep notch (a/W >0.45) fracture mechanics test specimens can result in gross over or underestimates of the true fracture toughness associated with shallow cracks (generally <5 mm deep) in structures. This knowledge, and its serious implications for structural integrity and safety assessments, especially for steel structures, led to a joint TWI/EWI project to develop more appropriate shallow crack fracture mechanics tests. The project started in October 1987, and involved a total of 34 sponsors and in-kind contributors from Europe and North America. TWI and EWI carried out experimental work, and also assessments of the in-kind contributions of numerical and analytical studies.

This report covers the experimental work performed at EWI. A complementary report of the European contribution has been prepared by TWI.

Objective

The objective of this project was to develop shallow-crack fracture-mechanics toughness test methods that would be complementary to the existing BSI and ASTM standard deep-notch test methods.

Main Conclusions

This report presents details of the fatigue precracking, instrumentation and testing procedures which were developed for SENB, SENAB and SENT specimens with a/W ratios down to 0.05 and absolute crack depths down to 1.25 mm. Details of the numerical analyses performed during the project are presented in EWI Report J6098-23-92.

The main conclusions of the North American experimental test program can be summarized as follows:

SENB Test Program (Material M3: A36 Steel)

1. Although the J and CTOD transition data obtained from testing shallow and deeply cracked SENB specimens exhibited considerable scatter there was no pronounced effect of a/W ratio, i.e., the transition temperature did not shift significantly.

2. Replicate tests performed in the ductile to brittle transition regime indicated an elevation in toughness as the a/W ratio decreased. At an a/W ratio of 0.1 the mean CTOD toughness was approximately 1.4 times greater than the toughness measured at an a/W ratio of 0.5. The corresponding toughness elevation in J was only 1.08.

3. Increasing the width (W) of the SENB specimens from B to 2B appeared to shift the J and CTOD transition curves to a slightly higher temperature and reduce the level of scatter.

4. Increasing the specimen thickness (from B to 3B) produced a reduction in toughness of more than 100% for specimens tested in the upper transition regime. This surprising trend may be due to anti-clastic curvature effects.

SENAB Test Program (Material M4: API 5CT L80 Tube)

1. The shallow cracked SENAB specimens produced higher transition temperatures than the deeply cracked samples.

2. Metallurgical examination of the pipe material revealed a microstructural gradient through the wall thickness, with significant carbide banding in the inner third of the pipe wall.

SENT Test Program (Material M3: A36 Steel)

1. Decreasing the a/W ratio in the SENT specimens resulted in a general increase in toughness, although at small a/W ratios (less than 0.2) the scatter increased significantly. Surprisingly, the lowest toughness values were obtained with the shallowest cracked specimens.

2. Unlike the SENB specimens the SENT specimens did not exhibit a thickness dependency over the width range B to 3B. However, since the replicate SENT specimens were tested at a much lower temperature than the SENB specimens, the measured toughness values were considerably lower than those obtained from the replicate SENB tests.

Future Considerations

While sponsors will clearly be able to make use of the techniques developed in this project directly, these techniques will only achieve their full potential when they have been adopted into the appropriate national and international standards. To this end, it is recommended that EWI and TWI should put forward proposals to BSI and ASTM for amendments to the deep-notch fracture mechanics test methods.

The development of fracture toughness analysis procedures performed in this project are only relevant to homogeneous materials. It is recommended that further work should be undertaken to extend these procedures to welded joints and in particular address the issue of weld metal mismatch. (EWI Proposal A6154: "The Effect of Weld Metal Mismatch on Structural Integrity Assessments".)

Commercial Aspects

It may be noted that this joint TWI/EWI project was a major international effort involving extensive experimental work and in-kind numerical and analytical studies. At current rates, the total work in this project is estimated to have cost considerably in excess of $2 M. Individual sponsors have received the full results of the program at a cost to them of $24 K.

AN INTERNATIONAL RESEARCH PROJECT TO DEVELOP SHALLOW CRACK FRACTURE MECHANICS TESTS

FINAL REPORT ON NORTH AMERICAN EXPERIMENTAL PROGRAM

1.0 INTRODUCTION

Over the last ten years a number of fracture mechanics-based assessment procedures have been developed which enable engineering structures to be assessed on a fitness-for-service basis. In performing an assessment the predicted crack driving force in the structure is compared with the material's resistance to crack extension or fracture toughness. Standard fracture toughness test procedures exist which cover the measurement of toughness in terms of K, J and CTOD.[1-6] These test procedures include minimum specimen size requirements to ensure that, wherever possible, the recorded toughness is independent of specimen size. The test standards also impose limits on the crack size and the crack depth to specimen width ratio (a/W) to ensure that the specimens provide high levels of constraint. Moreover, since the level of constraint is influenced by the mode of loading, the majority of testing procedures specify specimen geometries where the mode of loading is predominantly bending. Although the minimum specimen size requirements and the limitations on crack size and a/W ratio ensure lower-bound toughness estimates for homogeneous materials, these requirements can lead to excessively conservative assessments for structures which contain shallow cracks and/or are loaded in tension. In such cases there is an incentive to obtain toughness estimates which are more representative of the constraint associated with shallow cracks and the loading mode the structure experiences in service.

Problems can also arise in situations where the structure under consideration contains cracks which are located in regions where there is gradient in mechanical properties. In such cases the standard test procedures which only cover the testing and analysis of deeply-notched specimens (e.g., a/W = 0.45 - 0.6), can result in toughness estimates which are not representative of the microstructure in which the crack is located. Although rapidly varying

microstructures are commonly associated with welded joints they can also occur in flame cut edges, clad material, locally heat treated or corroded materials and sometimes even cast, forged and wrought materials.

Ideally, when assessing the integrity of engineering structures containing shallow cracks, the toughness used in the assessment should be obtained by testing shallow cracked samples in which the loading mode and constraint is representative of the structure. Furthermore, in situations where there is a gradient of material properties the testing of shallow cracked specimens will ensure that the toughness is representative of the microstructure sampled by the cracks in the structure.

In 1987, TWI and EWI initiated a major International Research Project to develop "Shallow Crack Fracture Mechanics Testing Procedures".[7] The major objective of the project was to develop shallow-crack fracture toughness testing and analysis procedures to cover:

- Bending and tension loading
- Testing of both flat and curved (e.g., pipe) material
- Characterization of fracture toughness in terms of K, J and CTOD.

The project, which started on October 1, 1987, attracted 34 sponsors from 7 different countries. The project contained both experimental and numerical phases. The primary objective of the experimental phase was to develop suitable fracture-toughness testing procedures including the development of appropriate fatigue precracking guidelines. In comparison, the objective of the numerical phase was to develop appropriate analysis procedures for shallow cracked specimens including J and CTOD estimation schemes.

The project was conducted jointly by EWI and TWI. EWI coordinated the experimental testing and numerical analyses conducted in North America while TWI coordinated the corresponding European work. The majority of the numerical analyses were performed by in-kind contributors in both North America and Europe. A complete list of sponsors and in-kind contributors is presented in Table 1.

This report summarizes the results from the North American experimental program. A complete list of the reports issued during the course of the project is presented in Appendix A.

2.0 SCOPE OF EXPERIMENTAL PROGRAM

The overall experimental program was broken down into the following tasks:

Task 1. Material Characterization
Task 2. Development of Fracture Toughness Specimen Geometries
Task 3. Development of Fatigue Precracking Procedures
Task 4. Development of Measurement Techniques
Task 5. Fracture Toughness Test Program.

The above tasks are described in the following sections.

3.0 MATERIALS

3.1 General

The materials chosen for the North American experimental program were a 25 mm (1 in.) thick plate to ASTM A36-84a, designated M3, and a 244 mm (9-5/8 in.) diameter, 19 mm (3/4 in.) wall thickness pipe to API 5AC L80 pipe, designated M4.

3.2 Plate Material M3

3.2.1 Plate Identification

Two consecutively produced plates, each 25.4 mm (1 in.) thick, 1930.4 mm (76 in.) wide and 6096.0 mm (240 in.) long were supplied by the Gary Works of U.S. Steel Corporation. The steel was supplied as meeting the requirements of ASTM A36 and ASSHTO M-183-84I. The steel works identification for the plates was as follows:

Heat No.:	W-63409
Slab No.:	2-3
Plate Serial:	38287 A&B.

On receipt at EWI, the plates were cut into 1524 mm (60 in.) lengths to facilitate handling. Each piece was labeled so that its position with respect to the original plate could be identified.

3.2.2 Plate Uniformity Check

3.2.2.1 General. The uniformity in plate properties was examined by taking a series of plaques from the beginning, middle and end locations along the length of the plate. At each location, three plaques were flame-cut from positions across the width of the plate, as shown in Figure 1. Coupons were machined from each of the nine plaques. The following specimens were machined from the coupons; their disposition is illustrated in Figure 2.

(1) Sample for chemical analysis
(2) Sample for metallographic examination
(3) Tensile test piece
(4) Three Charpy V-specimens.

At some locations, additional Charpy V-specimens were prepared. These were used to establish an absorbed energy versus temperature transition curve to enable an appropriate test temperature to be established for the uniformity check Charpy tests.

3.2.2.2 Chemical Analysis. Chemical analysis of the plate was carried out using a direct-spark spectrographic technique onto the central region of the plate thickness. These results are presented in Table 2 where they are compared with the requirements of ASTM 36-84a. The results of the chemical analysis confirm that the plate conformed with the requirements of the standard and the composition was uniform across both the width and along the length of the plate.

3.2.2.3 Tensile Tests. Subsize tensile test specimens to ASTM E8 were machined from the center of the plate thickness with their longitudinal axes parallel to the rolling direction. The specimens had a gauge length of 25.4 mm (1 in.) with a square cross section, 6.35 x 6.35 mm (0.25 x 0.25 in.). The tests were carried out at room temperature 21°C (70°F) at a cross head speed of 2.54 mm/min (0.1 in./min). The results are given in Table 3 and show that the plate conforms with the tensile requirements of A36-84a [cf. yield strength: 250 N/mm^2 (minimum) and tensile strength: 400-550 N/mm^2]. However, the average yield stress is about 8% lower than the figure given on the test certificate. The measured properties are relatively uniform both across the plate width and along the plate length. Most specimens exhibited Luders extension from initial yield up to approximately 0.4 to 0.5% strain. At higher strains, work hardening occurred until the tensile strength was reached.

3.2.2.4 Charpy Tests. Standard (Type A) Charpy-V notch specimens to ASTM E23 were machined from the center of the plate thickness with their longitudinal axes parallel to the rolling direction. The notch direction was transverse to the rolling direction as shown Figure 2 (this is the L-T orientation according to the nomenclature of ASTM E616).

To examine variations in Charpy-V notch toughness within the plate, a single test temperature was selected which was just above the toe regime of the absorbed energy versus temperature transition curve. The curve was obtained by testing specimens taken from various locations in the plate. The results of these tests are summarized in Table 4 and plotted as a function of temperature in Figure 3. From this, a temperature of -30°C was chosen for testing the specimens from the nine plate locations. The results of these tests are presented in Table 5. These show fairly consistent results for most of the locations. For all locations accept DE-5 and DE-6, the average notch toughness (per set of three specimens) was between 51 and 67 J at -30°C. The variation in toughness for each location was consistent with the scatter expected in the transition regime, as can be seen from inspection of the transition curve in Figure 3. At locations DE-5 and DE-6 lower notch toughness was measured.

3.2.2.5 Hardness Tests. The variations in hardness through the thickness of the plate were measured at 2 mm intervals with a Vickers microhardness indentor using a 1 kg load. The

reference surface, from which the measurements were made, was defined as the top surface of the as-received plate. This is the same as the top surface of the plate when it was rolled in the steel mill. The results of the survey are presented in Table 6 and Figures 4, 5 and 6. The average hardness was 145 HV with a standard deviation of 3.5. These values are the same irrespective of whether the calculations are based on the average through-thickness values or the average for the nine sample locations. The results show that the plate has a consistent hardness both across its thickness as well as its width and length.

3.2.2.6 Microstructure. Metallurgical samples from the nine plate locations were examined in the optical microscope. Photographs were taken of microstructures near the original top plate surface, at mid-plate thickness and near to the original bottom plate surface, at magnifications of 100 and 400×.

The microstructures through the thickness of plate and at the nine different locations were consistent. Figure 7 shows the typical microstructures observed in the plate at the top, mid-thickness and bottom plate positions. The microstructure consisted almost entirely of equiaxed ferrite and pearlite, with an ASTM grain size of about 7.

3.2.3 Stress-Strain Behavior

3.2.3.1 General. Tensile and compressive stress-strain curves were obtained for plate Material M3.

Tensile Stress-Strain Curves. The room temperature stress-strain curve for Material M3 was obtained by testing a rectangular section tensile specimen to ASTM E8. The specimen was taken from Plate M3 with the longitudinal axis parallel to the plate rolling direction. It was removed from Panel A-B close to Location 3, as defined in Figure 1. The specimen had a nominal cross section of 25.4 mm (the plate thickness) by 31.8 mm (1.25 in.). Although it had an overall gauge length of 200 mm, strain was measured over a 50 mm gauge length located midway along the length of the specimen. The specimen was loaded at a crosshead speed of 1.25 mm/min at ambient temperature (24°C).

In addition to measuring strain over the gauge length, electrical uniaxial strain gauges were attached to the specimen. These were used to obtain a direct measure of Young's modulus.

A summary of the tensile results of Material M3 is given in Table 7. This table includes the average value of Young's modulus obtained from four loadings up to 60% of the lower yield strength.

The engineering stress versus engineering strain and true stress versus natural log strain curves are presented in Figures 8 and 9. The tabulated tensile stress-strain results for Material M3 are presented in Table 8.

Compressive Stress-Strain Curves. The compressive stress-strain curves were generated from a cylindrical specimen 60.5 mm long and 20.3 mm diameter which was tested at room temperature. The longitudinal axis of the specimen was parallel to the primary plate rolling direction. During the test the applied strain was measured over a gauge length of 25.7 mm. Loading was carried out between two ground, hardened steel platens. The crosshead displacement rate was 3.1 mm/min.

The results of the compression test are summarized in Table 9 and presented as engineering stress-strain and true stress versus natural log strain curves in Figures 10 and 11, respectively. The tabulated compressive stress-strain results for Material M3 are presented in Table 10.

3.3 Pipe Material M4

3.3.1 Pipe Identification

The pipe Material M4 was obtained from the U.S. Steel Corporation, Lorain Works in three 9 m lengths. The steel was supplied to API 5CT (formerly 5AC) L80 specification. The seamless pipe had an outside diameter of 273 mm and a nominal wall thickness of 19 mm.

3.3.2 Pipe Uniformity

3.3.2.1 General. To provide information on the variability of the mechanical properties of Pipe Material M4, a set of Charpy-V notch specimens were extracted from each end of a 9 m length of pipe. These specimens were tested over a wide range of temperatures to enable Charpy impact energy transition curves to be generated. The transition curves obtained from the two ends (denoted End A and End B) are presented in Figure 12. It is evident that End A has a slightly higher transition temperature than End B. Although the difference in transition temperatures is not considered significant, it was decided to machine the SENAB specimens from End A as the slightly higher transition temperature would facilitate the fracture toughness testing.

3.3.2.2 Microstructure. Metallurgical samples were taken from both End A and End B and examined in the optical microscope. Photographs were taken of microstructures near the outer wall surface, at mid-wall thickness and near to the inside surface, at magnifications of 100 and 400×.

Although the microstructures at End A and End B were nominally identical there was a significant variation in microstructure through the pipe wall thickness. This is illustrated in Figure 13 which shows the microstructure at the three through thickness positions.

Hardness measurements performed on the macro sample indicated that the hardness was uniform across the pipe wall. Examination of the macro sample confirmed that the microstructure of the pipe material is predominantly quenched and tempered martensite with interspersed carbides. The macro sample did, however, indicate significant carbide banding in the inner third of the pipe wall. In comparison, the microstructure in the outer two thirds of the pipe wall was very uniform with evenly distributed carbides.

3.3.3 Stress-Strain Behavior

3.3.3.1 General. Tensile and compressive stress-strain curves were generated for Tube Material M4 (API 5CT L80 tubing).

3.3.3.2 Tensile Stress-Strain Curves. The room temperature stress-strain curves were obtained by testing a 6.4 mm diameter tensile specimen to ASTM E8. The axis of the specimen was tangential to the circumference of the tube. During the test the applied strain was measured over a gauge length of 25.4 mm. The specimen was loaded at a crosshead speed of 1.6 mm/min at ambient temperature (24°C).

A summary of the tensile results of Material M4 is given in Table 11. This table includes the average value of Young's modulus obtained from four loadings up to 60% of the lower yield strength.

The engineering stress versus engineering strain and true stress versus natural log strain curves are presented in Figures 14 and 15. The tabulated tensile stress-strain results for Material M4 are presented in Table 12.

3.3.3.3 Compressive Stress-Strain Curves. The compressive stress-strain curves were generated from a cylindrical specimen 38.7 mm long and 12.8 mm diameter which was tested at room temperature. The specimen was extracted from the end of the tube marked "A." The longitudinal axis of the specimen was tangential to the circumference of the tube. Loading was carried out between two ground, hardened steel platens. The crosshead displacement rate was 3.1 mm/min.

The results of the compression test are summarized in Table 13 and presented as engineering stress versus engineering strain and true stress versus natural log strain curves in Figures 16 and 17, respectively. The tabulated compressive stress-strain results for Material M4 are presented in Table 14.

4.0 DEVELOPMENT OF FRACTURE-TOUGHNESS SPECIMEN GEOMETRIES

4.1 General

The following fracture toughness specimen geometries were included in the experimental test program:

(1) Single-Edge Notch Bend (SENB)
(2) Single-Edge Notch Arc Bend (SENAB)
(3) Single-Edge Notch Tension (SENT).

A sketch illustrating the three specimen geometries is included in Figure 18.

Throughout this report the fracture toughness specimens are described as either being through thickness- or surface-notched. The surface-notched specimens correspond to the L-S orientation, i.e., the specimen axis coincides with the longitudinal (L) or rolling direction of the plate and the notch is machined from the plate surface (S). In comparison, the through thickness-notched specimens correspond to the L-T orientation, i.e., the specimen axis coincides with the longitudinal (L) plate or pipe axis and the notch is machined through the thickness (T) of the plate or pipe.

4.2 SENB Specimens

The SENB specimens were machined from Plate Material M3. Both through thickness-notched and surface-notched specimens were tested. All the through thickness-notched specimens had a nominal thickness (B) of 25 mm. Both square section (B × B) and rectangular section (B × 2B) through thickness-notched specimens were tested. In the case of the surface-notched specimens the specimen width (W) was nominally 25 mm. The specimen thicknesses, however, were varied to provide B × B, 2B × B, and 3B × B specimen geometries.

The following SENB specimen geometries were tested in the experimental program:

Notch Orientation	B × W	a/W
Through Thickness	B × B	0.05, 0.1, 0.2, 0.3 and 0.5
Through Thickness	B × 2B	0.5
Surface	B × B	0.1 and 0.5
Surface	2B × B	0.1 and 0.5
Surface	3B × B	0.1 and 0.5

Note: B = 25 mm.

4.3 SENAB Specimens

The SENAB specimen geometry provides a simple method of determining the toughness of pipe material. Nevertheless, one of the limitations of this specimen geometry is that it becomes increasingly difficult to attach clip gauges and other associated instrumentation to the specimens taken from small diameter pipes. This problem can be alleviated to some extent by machining flats on the side of the SENAB specimens as shown in Figure 19. The major advantage of machining a flat on the inside surface of the SENAB specimen geometry is that it simplifies the attachment of shim plates and subsequent knife edge fixtures and clip gauges.

Following discussions between TWI, EWI, John Underwood of the U.S. Army and Professor Bob Dodds of the University of Illinois, the following SENAB specimen geometry was selected for the North American pipe material:

Pipe Material M4 (r_1/r_2 = 0.92) (r_1 = 114.0 mm) (r_2 = 135.0 mm)

(a) S/W = 4.0
(b) z/W = 0.1
(c) F/S = 0.5

where S = loading span
W = specimen width
z = height from specimen surface to loading surface
F = total width of machined flats
r_1 = inner radius
r_2 = outer radius.

Professor Dodds and his co-workers conducted finite element analyses of the proposed SENAB specimen geometries to determine the influence of the machined flat on the stress intensity function. The results of this study indicated that the machined flats have a negligible effect on the stress intensity functions of the SENAB specimens. Details of this study are presented in Appendix B.

The final North American SENAB specimen geometry is illustrated in Figure 20. Tests were performed for a/W ratios of 0.1, 0.15 and 0.5.

4.4 SENT Specimens

Both through thickness-notched and surface-notched SENT specimens were tested in the experimental program. All the through thickness specimens had a nominal thickness of 25 mm and were square in section, i.e., (B × B). Details of the through thickness-notched SENT specimen geometry are presented in Figure 21.

Two different surface-notched SENT specimen geometries were studied in the current program. Initially, the through thickness-notched specimen geometry was adopted for the surface-notched tests but with the notch machined from the surface rather than through the thickness. However, later in the program it became apparent that the loads required to test the replicate surface-notched SENT specimens to assess thickness effects exceeded the load capacity of the testing machines at EWI (500 kN). As a result, it was decided to reduce the thickness (B) of the replicate surface-notched SENT specimens to 18 mm. Furthermore, since the loading pin arrangement only provides rotation for through thickness-notched specimens it was decided to further simplify the surface-notched SENT specimen geometry

to a fixed grip arrangement. This necessitated increasing the length of the specimens to approximately 1000 mm. Details of both surface-notched SENT specimen geometries are presented in Figure 22.

The following SENT specimen geometries were tested in the experimental program:

(1) Initial SENT Specimens

Notch Orientation	B × W	a/W
Through Thickness	B × B	0.05, 0.1, 0.2, 0.3 and 0.5
Surface	B × B	0.1 and 0.5

Note: B = 25 mm.

(2) Replicate Surface-Notched SENT Specimens

Notch Orientation	B × W	a/W
Surface	B × B	0.1 and 0.5
Surface	2B × B	0.1 and 0.5
Surface	3B × B	0.1 and 0.5

Note: B = 18 mm.

5.0 DEVELOPMENT OF FATIGUE PRECRACKING PROCEDURES

5.1 General

Fatigue precracking procedures for "deep notch" fracture toughness specimens with a/W ratios around 0.5 are well established and documented in relevant national standards.[1-6] However, procedures for shallow notches with a/W ratios as low as 0.05 are not, and it was

therefore necessary to develop these for particular application to the specimen geometries and a/W ratios covered in this project.

5.2 Notching Methods for SEN Specimens (SENB, SENT and SENAB)

For the deep notch tests (a/W = 0.50), the notches were machined using a standard 3.2 mm wide milling cutter with a 60 degree included angle V nose. For specimens with smaller a/W ratios the notches were machined using a 0.15-mm wide slitting disc. TWI also investigated the possibility of using a hardened tool steel knife edge having a 60 degree included angle to plastically form a notch in a manner similar to a hardness indenter. Although the slitting disc produced a squarish notch tip with corner radii approximately equal to 0.04 mm compared to the pressed-notch tip radius of approximately 0.02 mm, it was concluded that the slitting disc was much more versatile particularly for notch depths grater than 1.0 mm.

In view of this, it was concluded that the pressed notch offered no advantage over the slit notch, and was not as versatile in terms of notch depth produced. It was also established that there was no evidence of multiplanar crack initiation from the slit notch. Therefore, the slit notch method was adopted for all subsequent starter notches for shallow cracks.

5.3 Fatigue Precracking Procedures for SEN Specimens (SENB, SENAB and SENT)

5.3.1 SENB Specimens

Most fracture toughness testing procedures include requirements on fatigue precracking. These requirements either limit the load or the stress intensity factor which can be applied during the fatigue precracking operation. The objective of these requirements is to limit the size of the plastic zone at the crack tip. The most common restriction is to limit the maximum permissible load to a certain fraction of the limit load or general yield load of the specimen.

Since there was no clear justification for using any one of the various fatigue precracking procedures included in test procedures for deeply-cracked specimens, a purely experimental

approach was adopted. The approach attempted to define the lowest value of stress intensity factor for fatigue precracking (K_f) that would give uniform fatigue crack growth across the full specimen thickness of shallow-notched specimens (a/W = 0.05). At the same time, it was required to produce an acceptable crack growth rate for crack length monitoring and control at a cyclic rate up to approximately 150 Hertz (Hz).

Using approximately 0.15 mm wide by 0.5 mm deep starter notches, TWI obtained acceptable shallow crack (a/W = 0.05) shapes in SENB specimens manufactured from Plate Material M1 (BS4360 Grade 50D: σ_{YS} = 388 N/mm^2) with final K_f values of approximately 1200 Nmm$^{-3/2}$. Subsequently, this nominal value of K_f was used to prepare a set of a/W = 0.05 SENB specimens from Plate Material M1 that were tested over a wide range of temperatures to produce a ductile/brittle transition curve. On completion of the tests, the final fatigue stress intensity factors were compared with the maximum stress intensity factors (K_{max}) encountered in each test. It was found that the ratio K_f/K_{max} was in all cases less than 0.57. Since this satisfies the K_{IC} test requirements,[1,3] the fatigue precracking procedure was considered acceptable.

In the case of Plate Material M3, it was not possible to apply the fatigue precracking procedure developed by TWI for shallow-cracked specimens, as the loads required to produce a K_f value of 1200 Nmm$^{-3/2}$ would have resulted in gross plastic deformation of the specimens. An estimate of the general yield load (P_{YS}) of an SENB specimen can be obtained from the following expression:

$$P_{YS} = \frac{4WB\,(W-a)^2\,\sigma_{ys}}{3WS} \qquad (1)$$

where
- B = specimen thickness
- W = specimen width
- a = crack depth
- S = loading span
- σ_{YS} = yield strength.

Based on a yield strength of 282 N/mm^2, the above equation predicts a general yield load of 53.2 kN for a 25 × 25 mm (B × B) SENB specimen with an a/W ratio of 0.05. In comparison, the applied load required to produce a stress intensity factor of 1200 $Nmm^{-3/2}$ is approximately 60 kN.

To study this effect further, a study was undertaken to compare the ratio of fatigue load (P_F) to general yield load (P_{YS}) for various levels of fatigue stress intensity factor and specimen a/W ratio. This study was performed for both the European and North American plate materials (i.e., Materials M1 and M3) assuming a square section 25 × 25 mm (B × B) SENB specimen geometry. The results of this study are presented in Figures 23 and 24.

It is evident from Figure 23 that in the case of the European Plate Material M1, an applied stress intensity factor of 1200 $Nmm^{-3/2}$ results in a P_F/P_{YS} ratio of less than 1.0 over the entire a/W ratio studied, i.e., $0.05 \leq a/W \leq 0.6$. In particular, for an a/W ratio of 0.05, the P_F/P_{YS} ratio is approximately 0.8, i.e., under these conditions the maximum fatigue load is 80 percent of the specimen's general yield load.

In the case of Plate Material M3, it is clear from Figure 24 that an applied stress intensity factor of 1200 $Nmm^{-3/2}$ results in a P_F/P_{YS} ratio larger than 1.0 for a/W ratios less than approximately 0.1. As a result, if a stress intensity factor of 1200 $Nmm^{-3/2}$ was employed to fatigue precrack a 25 mm thick (B × B) SENB specimen with an a/W ratio of 0.05 made from Material M3, gross plastic deformation of the specimen would occur. To prevent gross plastic deformation, the applied stress intensity factor would need to be reduced to approximately 1000 $Nmm^{-3/2}$.

Based on the results displayed in Figures 23 and 24, the following fatigue precracking procedures were employed for the SENB specimens from Plate Material M3:

Specimen Size (B × W) (mm)	a/W	Max K ($Nmm^{-3/2}$)	P_F/P_{YS}
25 × 25	0.05	700	0.65
25 × 25	0.1	800	0.62
25 × 25	0.5	800	0.64
25 × 50	0.5	800	0.45

The maximum fatigue stress intensity factors employed to fatigue precrack the SENB specimens are compared with the maximum values of K_f permitted by the ASTM CTOD[6] and J_{IC}[4] standards in Table 15. It is evident from Table 15 that the fatigue precracking stress intensity factors employed to precrack the B × B, a/W = 0.1 and B × B, a/W = 0.5 SENB specimens are slightly in excess of the maximum permitted by the testing standards. Nevertheless, since the results of the tests on the different specimen geometries are to be compared, it was considered important to employ nominally similar fatigue stress intensity factors. Furthermore, the results presented in Table 16 demonstrate that the maximum stress intensity factors produced in the subsequent fracture tests (which were performed over a wide range of temperature to provide failures ranging from lower shelf to upper shelf) were in all cases significantly larger than the K_f values employed to fatigue precrack the specimens. Indeed, the ratios K_f/K_{max} were in all cases less than 0.5 which is consistent with the ASTM and BSI K_{IC} test requirements.[1,3]

The fatigue precracking procedures employed for the shallow-crack SENB specimens produced acceptable fatigue cracks in terms of uniform crack shape. Photographs of two fracture faces of shallow-crack SENB specimens are presented in Figure 25.

5.3.1.1 SENT Specimens. To simplify the fatigue precracking operation all the SENT specimens were fatigue precracked in three point bending using the procedures previously developed for the SENB specimens.

5.3.1.2 **SENAB Specimens.** Since the yield strength of the North American pipe material (M4) was significantly higher than Plate Material M3 (yield strength of Pipe Material M4 = 590 N/mm^2: yield strength of Plate Material M3 = 282 N/mm^2), larger fatigue stress intensity factors could have been employed for the SENAB specimens without the risk of gross plastic deformation. Nevertheless, to maintain consistency with the fatigue precracking procedures employed for the SENB and SENT specimens, it was decided to fatigue all the SENAB specimens using a maximum fatigue stress intensity factor of 800 $Nmm^{-3/2}$. The fatigue stress intensity factors were estimated using the standard K solution for the SENB specimen geometry.

The fatigue precracking procedures employed for the shallow-notched SENAB specimens produced acceptable fatigue cracks in terms of uniform crack shape.

The fatigue stress intensity factors were compared with the maximum stress intensity factors (K_{max}) encountered in the subsequent fracture tests. It was found that in all cases the K_f/K_{max} ratios were significantly less than 0.5 which is consistent with the ASTM and BSI K_{IC} test requirements.[1,3]

6.0 DEVELOPMENT OF MEASUREMENT TECHNIQUES

6.1 General

This aspect of the project concentrated on methods of attaching clip gauges to measure mouth opening displacement and the measurement of load point displacement. These topics are discussed below.

6.2 Attachment of Clip Gauges

6.2.1 SENB Specimens

It was proposed that double-clip gauge monitoring would be used for all tests. Initial development work was carried out with SENB specimens. The standard knife edge arrangement could be used, but special attention was required regarding the attachment of knife edges to the specimens. EWI's standard procedure for attachment, which involves the use of threaded studs resistance welded to the specimen some distance from the notch mouth, is not suitable for shallow crack specimens because the attachment points would fall outside the "dead zone" (the region bounded by a 30 degree included angle radiating from the crack tip away from the loaded surface). For a/W ratios as low as 0.05, it was clearly necessary to mount the knife edges as close to the mouth of the notch as possible.

To satisfy the "dead zone" requirement, a procedure was developed, involving the use of steel shims. These shims, of dimensions 25 × 25 × 1.25 mm, were TIG welded to the notch mouth along a length of approximately 5 mm over the specimen centerline. A threaded stud, previously resistance welded to the center of the shim, could then be used for attachment of the knife edges. This arrangement is shown in Figures 26 and 27. A macro-photograph of a section through one of the welds is shown in Figure 28. It is evident from Figure 28 that the HAZ associated with the TIG weld extends into the SENB specimen to approximately 0.5 mm. As a result the TIG welding operation will not influence the microstructure sampled by fatigue cracks which are deeper than approximately 1.0 mm. To assess if residual stresses introduced by the TIG welding operation could influence toughness measurements a simple test was devised by TWI to determine the influence of TIG welding on fatigue precracking. A 25 × 25 mm SENB specimen (Material M1: BS4360 Grade 50D) was prepared by slitting to a depth of 0.47 mm. Shim plates were then micro-TIG welded to the specimen using the standard procedure. The specimen was then fatigue precracked. After fatigue precracking the specimen was cooled in liquid nitrogen and broken open. Examination of the fracture face revealed no apparent change in fatigue crack length and surface appearance in the region near the micro-TIG weld. Based on this observation it was concluded that the fatigue

crack had grown beyond the zone of influence of the residual stress from the TIG weld and, hence, the residual stresses should not influence the fracture behavior.

A photograph of an SENB specimen with the shim plate knife edge assembly and clip gauges is presented in Figure 29.

6.2.2 SENAB Specimens

The modified-SENAB specimen design (Figure 20) allowed the use of the shim and knife edge arrangement developed previously for the SENB specimen geometry. A photograph of this arrangement is presented in Figure 30.

6.2.3 SENT Specimens

The shim plate and knife edge arrangement developed for the SENB specimen geometry was also adopted for the SENT specimens.

6.3 Measurement of Load Point Displacement

6.3.1 SENB Specimens

Measurement of load point displacement was satisfactorily accomplished using a standard comparator bar technique,[1] illustrated in Figure 31.

6.3.2 SENAB Specimens

The standard comparator bar arrangement used for SENB specimens was found to be equally suitable for the SENAB specimen geometry as shown in Figure 32.

6.3.3 SENT Specimens

For the SENT specimens, a telescopic device was used in conjunction with a standard clip gauge. This enabled the linear displacement between the two reference points (100 mm apart) on the specimen sides to be measured regardless of specimen bending during a test. The instrumentation arrangement for the SENT specimens is shown in Figure 33.

6.4 Measurements at Low Temperatures

Testing SENB and SENAB specimens at low temperatures is relatively straightforward, since the specimen can be orientated so that all the instrumentation is above the cooling medium. SENT specimens, however, are normally tested vertically. This can lead to problems when performing low temperature tests, as it is difficult to cool the specimen without exposing the instrumentation to the cooling medium.

As a result of the problems associated with performing low temperature SENT tests in the vertical axis it was decided to test the specimens horizontally. This was achieved by dropping a 500 kN servohydraulic test machine on its side. The major advantage with a horizontal loading arrangement is that the whole specimen can be immersed in liquid coolant during testing, as is normal practice for bend test specimens. The testing arrangement adopted for the pin loaded through thickness-notched SENT specimens is shown in Figure 34. U-shaped links were designed to fit over the cooling bath so that the whole of the central portion of the specimen could be immersed in the coolant. Close-up photographs of the test rig are shown in Figure 35. This testing arrangement was used successfully to test the pin-loaded SENT specimens over a wide temperature range.

The fixed-grip loaded surface-notched SENT specimens were also tested horizontally. In this case, the specimens passed through a sealed opening in the cooling bath.

6.5 Measurement Errors Associated with Clip Gauge Arrangement

6.5.1 General

The main measurement error in the clip gauge arrangement is associated with rotation of the knife edge block. Three distinct sources of error were identified, associated with:

- Elastic behavior of the shim
- Elastic plastic behavior of the micro-TIG weld
- Contact with the specimen.

Analytical studies were performed by TWI to determine the errors associated with each of the above sources. Details of the study are reproduced in the following sections.

6.5.2 Elastic Behavior of the Shim

The shim is loaded by the clip gauges and the elastic response is calculable. Treating the shim as a simple cantilever and assuming the knife edge block to be rigid, the loading system created by the clip gauges becomes that shown in Figure 36a. Cantilever AB sees a rotation θ at A where:

$$\theta = \frac{ML}{EI} \qquad (2)$$

and

$M = (2.75 + 12.75)F$ (Nmm)

$L = 8.0$ mm

$E = 207000$ N/mm^2

$I = (25 \times 1.25^3)/12$ mm^4.

If AC is rigid, the deflection Δ at C is given by:

$$\Delta = 12.75 \sin\theta \ (mm) \qquad (3)$$

Simple experiments performed at TWI using a standard clip gauge, with an unloaded span of 17 mm, have shown that Force F of 22 N on the tips of the legs is required to compress the legs to fit the initial 6 mm gap between the knife edges. Therefore, assuming as a worst case that F decreases from 22 N to zero in the course of a test, then the error (Δ) in the upper clip gauge measurement is obtained from Eqs. (2) and (3) and is Δ = 0.038 mm.

6.5.3 Elastic-Plastic Behavior of the Micro-TIG Weld

Taking the typical dimensions of the weld to be throat t = 0.7 mm and effective length l = 4 mm, the maximum elastic bending stress σ in the weld due to the clip gauge load is:

$$\sigma = \frac{6M}{lt^2} = 1044 \ N/mm^2 \qquad (4)$$

Since this is likely to be well in excess of the yield strength of the weld, the weld will act as a plastic hinge.

In practice, however, the shim is initially supported by the surface of the specimen so the clip gauge force merely ensures that the shim remains bedded down to the specimen surface.

6.5.4 Contact with the Specimen

This has been observed experimentally and is best explained graphically. The specimen shapes under load as observed in tests on ductile specimens are shown exaggerated in Figures 36c and d. In deep notch specimens the shim tends to remain in full contact during the test. However, for the shallow-notched specimens, the exaggerated shapes shown in the figure illustrate the "lipping" behavior which occurred at the crack mouth. Here, the shim is

restrained by the upper surface of the specimen and is unable to follow the rotation of the material near the crack mouth.

The above cases demonstrate the error in measurement of crack flank rotation during testing, but measurement of crack mouth opening displacement (CMOD) can still be calculated with good accuracy from the double-clip gauge data. Referring to Figure 37 and regardless of the sources of knife edge rotation θr:

$$CMOD = V_1 - 2z_1\left(\frac{x_2-x_1}{z_2-z_1}\right) - 2x\cos\left[\sin^{-1}\left(\frac{x_2-x_1}{z_2-z_1}\right)\right] + 2x \qquad (5)$$

where x, z_1 and z_2 are known dimensions, $(x_2 - x_1) = (V_2 - V_1)/2$ and V_1 and V_2 are the lower- and upper-clip gauge displacements, respectively. For small displacements, the last two terms cancel out and Eq. (5) is reduced to the familiar form based on similar triangles.

In order to illustrate the difference between V_1 and CMOD in real terms, a selection of test data were analyzed using Eq. (5) above and the results are presented in Table 17. For the shallow notch bend specimens the ratio of CMOD to V_1 was in the range 76 to 83%. For the deep-notch bend specimens the ratio was a little nearer unity, in the range 85 to 87%. For the shallow-notch tensile specimens in which there is very little local bending the ratio increased further, in the range 93 to 98%. For the deep-notch tensile specimens the ratio fell to the range 80 to 82%. Hence, it can be seen that significant errors would arise if the CMOD was assumed to be equal to the displacement measured by Clip Gauge 1 above the specimen surface.

The factors that influence $CMOD/V_1$ are the degree of rotation of the knife edges with respect to each other, the distance of the knife edges above the specimen and the value of CMOD itself. The rotation is influenced by the deformation of the specimen surface during the test and the associated behavior of the micro-TIG welded shims. However, it seems that for any combination of geometry and loading, the knife edge rotation is linearly proportional to CMOD so that the value of $CMOD/V_1$ remains constant over a large range of CMOD. For the shallow-notched tension specimens which exhibit very little local bending the knife edge

rotation is relatively small and the value of CMOD/V_1 is close to unity. In comparison, the shallow-notch bend tests produced the greatest relative knife-edge rotation, giving the lowest values of CMOD/V_1 of the four cases considered in Table 17.

If CMOD is used to determine a value of fracture toughness it is clearly important to make a correction for the difference between CMOD and the measured value of V_1. This is recognized in the standard CTOD bend test methods,[1,2,6] in which the plastic component of CTOD is determined from the plastic component of CMOD, i.e., $CMOD_p$. In these tests,[1,2,6] the approximate correction for $CMOD_p$ is given by

$$\frac{CMOD_p}{V_{pl}} = \frac{a+r_p(W-a)}{a+r_p(W-a)+z_1} \qquad (6)$$

where V_{pl} is the plastic component of V_1, and r_p is an assumed plastic rotational factor. For comparison with Eq. (6), Eq. (5) may be rewritten as:

$$\frac{CMOD_p}{V_{pl}} = 1 - \frac{1}{V_{pl}}\left\{2z_1\left(\frac{x_2-x_1}{z_2-z_1}\right) - 2x\cos\left[\sin^{-1}\left(\frac{x_2-x_1}{z_2-z_1}\right)\right] + 2x\right\} \qquad (7)$$

where $x_2 - x_1 = (V_{p2} - V_{pl})/2$ and V_{p2} is the plastic component of V_2.

The bend test data from Table 17 have been recalculated according to Eqs. (6) and (7) to give the values shown in Table 18. These data indicate that the CTOD standards[1,2,6] provide reasonably accurate predictions of CMOD for bend specimens, with BS5762 providing the more conservative result for the shallow notch, i.e., a/W = 0.095. For application to tensile specimens, especially for the more deeply notched ones (e.g., a/W = 0.5), there presently appear to be no alternatives to using Eqs. (5) and (7) for accurate measurements of CMOD and $CMOD_p$, respectively. However, there will be situations when the last two terms of Eq. (6) cancel out, leaving a relatively simple equation based on similar triangles.

6.6 Alternative Methods of Measuring CMOD

Although the double-clip gauge method (described in this report) can provide reasonably accurate estimates of crack mouth opening displacement (CMOD), there are other alternative measurement techniques which are capable of measuring CMOD directly. One of the most attractive measurement techniques is non-contact laser extensometry. The advantages of adopting laser extensometers are:

(1) Laser extensometers can measure CMOD directly whereas the double-clip gauge method estimates CMOD by extrapolation.

(2) Since laser extensometers are non-contact, this measurement technique is better suited for tests at both low and high temperature than techniques which use clip gauges.

(3) The use of non-contact laser extensometers avoids the need for attaching shim plates to the specimens.

Although the use of laser extensometers was not studied in this project, in the opinion of the authors, non-contact laser extensometers probably provides a more accurate and reliable method of measuring CMOD than the double-clip gauge technique.

7.0 TEST PROGRAM

7.1 General

The overall test matrix is summarized in Tables 19 and 20. The following fracture toughness specimen geometries were tested in the experimental program:

(1) SENB
(2) SENAB
(3) SENT.

To provide an indication of the effect of a/W ratio on the overall fracture behavior of the various specimen geometries transition curves were obtained for each specimen geometry by testing both shallow- and deeply-cracked specimens over a wide temperature range. In the case of the SENB and SENT specimen geometries, transition curves were obtained for both through thickness-notched and surface-notched orientations.

Replicate tests were then performed for each specimen geometry to establish the effect of a/W ratio and specimen thickness. The replicate tests to determine the effect of a/W ratio were performed at a temperature which corresponded to mid-transition. The replicate tests to assess specimen thickness effects were performed at a temperature corresponding to upper transition/upper shelf fracture behavior.

Since the J and CTOD estimation schemes included in the current fracture toughness testing standards are not appropriate for shallow cracked specimens, the following J and CTOD expressions were used to analyze the specimens tested in this project:

$$\delta = \frac{K^2(1-\nu^2)}{2E\sigma_{YS}} + \eta_\delta \, CMOD_{pl} \tag{8}$$

$$J = \frac{K^2(1-\upsilon^2)}{E} + \frac{\eta_c A_{pl}}{B(W-a)} \tag{9}$$

where

	K	=	stress intensity factor
	E	=	Young's modulus
	σ_{YS}	=	yield strength
	ν	=	Poisson's ratio
	W	=	specimen width
	B	=	specimen thickness
	a	=	crack length
	$CMOD_{pl}$	=	plastic component of CMOD calculated using double clip gauge arrangement
	η_δ	=	CTOD calculation parameter to determine $CTOD_{pl}$
	η_c	=	J calculation parameter to determine J_{pl}

A_{pl} = plastic component of area under the load versus CMOD record.

Values of η_δ and η_c were determined for each specimen at the failure condition (either the onset of unstable fracture, maximum load conditions or test stopped conditions) from the results of the finite element analyses performed in the numerical phase of this project.[8] Note η_δ and η_c are functions of the specimen a/W ratio, $CMOD_{pl}$ and A_{pl}. The η_δ and η_c finite element results for the SENB, SENAB and SENT specimen geometries are summarized in Figures 38-43. Since the finite element analyses modeled the specimen geometries and materials tested in the experimental program, the J and CTOD estimation procedures should provide accurate predictions of the applied crack driving force in the test specimens.

It is worth noting that the conventional J and CTOD estimation schemes for deeply-cracked specimens can result in significant overestimates of the applied J or CTOD in shallow cracked samples, particularly for high work hardening materials (e.g., Material M3). As a result the use of the conventional J and CTOD estimation procedures to compare and contrast the behavior of shallow and deeply-cracked fracture toughness specimens can introduce trends which may be a direct consequence of the estimation schemes.

Throughout the test program the following notation has been used to describe the fracture behavior of the specimens:

Type of Result	Description
c	Unstable fracture with no preceding slow stable crack growth.
u	Unstable fracture preceded by slow stable crack growth.
m	Toughness corresponding to the conditions at the first attainment of maximum load.
ts	Toughness corresponding to the conditions at which the test was stopped. (This type of result is obtained when the specimen exhibits fully ductile behavior, the test being terminated when the range of the clip gauge is exceeded.)

7.2 SENB Test Program: Material M3

7.2.1 Transition Curve Tests on Through Thickness-Notched Specimens

Tests on through thickness-notched and fatigue precracked SENB specimens were carried out over a wide range of temperature to obtain fractures ranging from completely ductile to brittle. The following specimen geometries were tested:

- 25 x 25 mm (B × W) SENB a/W = 0.05
- 25 x 25 mm (B × W) SENB a/W = 0.5
- 25 x 50 mm (B × W) SENB a/W = 0.5.

The results of the fracture toughness tests are summarized in Tables 21-23 and presented as CTOD and J transition curves in Figures 44-49.

To enable the temperature for the replicate tests to be determined, the J and CTOD transition curves obtained from the (B × B) a/W = 0.05 and (B × B) a/W = 0.5 specimens were plotted together. The resulting plots are presented in Figures 50 and 51. It is apparent from Figures 50 and 51 that the transition curves for the two a/W ratios are very similar. This is rather surprising as it is generally accepted that increasing the a/W ratio produces higher levels of constraint which, in turn, causes the transition curve to shift to a higher temperature. Indeed, preliminary analyses of the through thickness-notched SENB transition curve tests (using the standard CTOD estimation approach) had indicated that the CTOD transition curve for the B × B, a/W = 0.5 specimens exhibited a slightly higher transition temperature than the corresponding a/W = 0.05 curve. This effect was, no doubt, exaggerated by the standard CTOD estimation procedure which can significantly overestimate CTOD for shallow cracked specimens particularly for high work hardening materials such as Material M3. The comparison of the transition curves for the two a/W ratios was also complicated by scatter. Based on the results presented in Figures 50 and 51, it was decided to perform the replicate tests on the through thickness-notched SENB specimens at a temperature T_{m1} of -40°C.

The J and CTOD transition curves obtained from the square and rectangular section deeply-notched (a/W = 0.5) specimens are compared in Figures 52 and 53. It would appear that the rectangular section (B × 2B) deeply-notched SENB specimens exhibit a slightly higher transition temperature than the corresponding square section (B × B) specimens. It should be stressed, however, that the square section specimens produced considerably more scatter in the transition region than the rectangular SENB specimens, thus making it difficult to estimate a representative transition curve.

The J and CTOD results obtained from the (B × B) a/W = 0.05 and (B ×2B) a/W = 0.5 SENB specimens are compared in Figures 54 and 55. It is interesting to note that although these specimen geometries have similar initial uncracked ligaments, the maximum load toughness results (which are generally assumed to scale with initial ligament size) are significantly different. Indeed, closer examination of Figures 50 and 51 indicates that the (B × B) a/W = 0.05 and (B × B) a/W = 0.5 through thickness-notched SENB specimens produced similar maximum load toughness values despite the fact that the initial uncracked ligaments in the shallow cracked specimens were approximately twice as large as the initial ligaments in the a/W = 0.5 specimens. It is interesting to note that preliminary analyses of the through thickness-notched SENB transition curve tests (using the standard CTOD estimation procedure) had indicated similar maximum load CTOD values for the B × B, a/W = 0.05 and B × 2B, a/W = 0.5 specimens suggesting that maximum load toughness did scale with ligament size, even for shallow cracked specimens.

7.2.2 Transition Curve Tests on Surface-Notched Specimens

Tests on surface-notched and fatigue precracked SENB specimens were carried out over a wide range of temperatures to obtain fractures ranging from completely ductile to brittle. The following specimen geometries were tested:

- 25 x 25 mm (B × B) SENB a/W = 0.1
- 25 x 25 mm (B × B) SENB a/W = 0.5.

The results of the fracture toughness tests are summarized in Tables 24 and 25 and presented as J and CTOD transition curves in Figures 56-59. To enable the two surface-notched specimen geometries to be compared, the J and CTOD transition curves obtained from the two specimen geometries are compared in Figures 60 and 61. Based on these results it was decided to perform the replicate rests on the a/W = 0.1 and a/W = 0.5 SENB specimens at -25°C (i.e., T_1 and T_2 are both equal to -25°C).

7.2.3 Replicate Tests on Through Thickness-Notched Specimens

Through thickness-notched SENB replicate tests were performed to determine the influence of crack size (or a/W ratio) on the measured toughness in the ductile-to-brittle transition regime. All the tests in this phase were performed at -40°C with specimens of the following geometries:

- 25 x 25 mm (B × W) SENB a/W = 0.05
- 25 x 25 mm (B × W) SENB a/W = 0.10
- 25 x 25 mm (B × W) SENB a/W = 0.15
- 25 x 25 mm (B × W) SENB a/W = 0.20
- 25 x 25 mm (B × W) SENB a/W = 0.30
- 25 X 25 mm (B × W) SENB a/W = 0.50.

For each specimen geometry five specimens were tested, i.e., a total of 30 specimens. The test temperature of -40°C was selected as J and CTOD transition curves for the through thickness-notched SENB specimens with a/W ratios of 0.05 and 0.5 (Figures 50 and 51) had indicated that this temperature coincided with the ductile-to-brittle transition regime for both specimen geometries.

The results of the replicate fracture toughness tests are summarized in Table 26 and presented as plots of J and CTOD versus a/W ratio in Figures 62 and 63.

It is clear from Figures 62 and 63 that there is considerable scatter in the J and CTOD results. It should be stressed, however, that the load displacement traces obtained from the

specimens exhibited widely different behavior and as a result, regardless of the method of analyzing the data, the subsequent fracture toughness results will exhibit a large degree of scatter. Nevertheless, even with the scatter it is evident that, as a general trend, the measured toughness decreases with a/W ratio. Moreover, the results suggest that the amount of scatter reduces as the a/W ratio is increased.

Linear regression analyses performed on the data presented in Figures 62 and 63 yielded the following equations:

$$CTOD = -0.259(a/W) + 0.516 \quad (10)$$

$$J = -82.66(a/W) + 470 \quad (11)$$

The above equations predict the following elevation in toughness for a/W = 0.1 specimens compared to a/W = 0.5 specimens:

$$\frac{CTOD_{(a/W-0.1)}}{CTOD_{(a/W-0.5)}} = 1.4 \quad (12)$$

$$\frac{J_{(a/W-0.1)}}{J_{(a/W-0.5)}} = 1.08 \quad (13)$$

It is evident that the CTOD toughness elevation is considerably larger than the J toughness elevation. Indeed, the J results show little elevation in toughness as the a/W ratio decreases.

It is interesting to note that the preliminary analysis of the through thickness-notched SENB replicate tests (using the standard CTOD estimation procedure) predicted a CTOD toughness elevation (a/W = 0.1 to a/W = 0.5) of 1.9.

Although the toughness elevations exhibited by the SENB replicate tests is much smaller than that predicted using the Dodds-Anderson constraint model (see Appendix C) it should be

noted that the measured toughness levels were high, e.g., at a/W = 0.1 the measured CTODs were approximately 20% of the crack size.

Dodds and Anderson have recently proposed the following minimum specimen size requirements for deeply-cracked SENB specimens to guarantee size independent results:

$$a_1 B_1 (W-a) \geq 400 \frac{J}{\sigma_{flow}} \qquad (14)$$

and

$$a_1 B_1 (W-a) \geq 300\ \delta \qquad (15)$$

For the B x B (B = 25 mm), a/W = 0.5 SENB specimens (Material M3) tested in this project the above requirements predict geometry independent results for J and CTOD values less than 25 kJ/m^2 and 0.05 mm, respectively. It is clear that in the case of Material M3 these toughness levels correspond to lower shelf behavior.

7.2.4 Replicate Tests on Surface-Notched Specimens

The replicate tests on the surface-notched SENB specimens were performed to determine the effect of specimen thickness on the measured toughness in the upper transition regime, i.e., brittle fracture preceded by slow stable crack growth. All the tests in this study were performed at -25°C with specimens of the following geometries:

- 25 x 25 mm (B x W) SENB a/W = 0.1
- 50 x 25 mm (B x W) SENB a/W = 0.1
- 75 x 25 mm (B x W) SENB a/W = 0.1
- 25 x 25 mm (B x W) SENB a/W = 0.5
- 50 x 25 mm (B x W) SENB a/W = 0.5
- 75 x 25 mm (B x W) SENB a/W = 0.5.

For each specimen geometry, five specimens were tested, i.e., a total of 30 specimens. The test temperature of -25°C was selected as the J and CTOD transition curves presented in Figures 60 and 61 indicated that this temperature coincided with upper transitional fracture behavior for both a/W ratios.

The results of the fracture toughness tests are summarized in Table 27 and 28 and presented as plots of J and CTOD versus B/W ratio in Figs 64-67 for the shallow- and deeply-notched specimen geometries.

It is evident from Figures 64-67 that, in general, as the specimen thickness is increased the measured toughness decreases. In the case of the shallow-notched specimens the fracture behavior of the specimens ranged from fully ductile (i.e., test stopped because clip gauge range was exceeded) to unstable fracture before maximum load. Two of the square section shallow-notched SENB specimens exhibited fully ductile behavior, the other three exhibiting unstable fracture after maximum load. In comparison four of the 2B × B and all of the 3B × B shallow-notched SENB specimens exhibited unstable fracture before maximum load. The remaining 2B × B shallow-cracked SENB specimen exhibited unstable fracture after maximum load.

In the case of the deeply-notched SENB specimens, all the specimens exhibited unstable fracture. Three of the square section (B × B) specimens exhibited unstable fracture after maximum load. The remainder of the deeply-notched specimens (i.e., two B × B and all the 2B × B and 3B × B specimens) exhibited unstable fracture before maximum load.

It is generally accepted that once the specimen thickness exceeds the remaining ligament the overall specimen constraint is controlled by the ligament and, as a result, toughness should be independent of B/W ratio (provided B is greater than W-a). Unlike the results obtained from the North American surface notched-replicate SENB tests, the results obtained from the corresponding European tests (conducted at TWI) did not exhibit a dependence on B/W ratio.

On completion of the surface-notched SENB replicate test program the fracture faces of the specimens were examined to determine the point of crack initiation. The objective of this exercise was to determine if anti-clastic curvature effects were responsible for the unusual CTOD and J results obtained from the replicate tests which indicate that the measured fracture toughness in the ductile to brittle transition regime decreases as the specimen thickness is increased from B to 3B.

The results of the sectioning study are summarized in Tables 27 and 28 and presented in Figures 68 and 69 as plots of initiation position versus B/W ratio for a/W ratios of 0.1 and 0.5, respectively. The initiation position was defined as the distance from the initiation point to the nearest side of the specimen expressed as a percentage of the specimen breadth, i.e., a value of 50% corresponds to the mid-thickness position, whereas a value of 20% corresponds to an initiation position 20% of the specimens thickness from the specimen surface. The results presented in Figures 68 and 69 have been rounded off to the nearest 5%.

It would appear from the results presented in Figure 68 that as the B/W ratio is increased for the shallow-cracked specimens, there is a tendency for the point of crack initiation to move from the specimen center out towards the specimen surface. This trend is most evident with the (3B $\times$ B) specimens where initiation generally occurred at approximately 20% of the specimen thickness from the surface of the specimen. The results presented in Figure 69 also suggest that in the case of the deeply-notched specimens the point of crack initiation moves from the specimen center out towards the specimen surface as the specimen thickness is increased, although the trend is not as pronounced as that exhibited by the shallow cracked specimens.

The results of the sectioning study indicate that anti-clastic curvature affects probably influenced the results of the surface notched-SENB replicate tests, particularly the shallow cracked tests. It is important to appreciate that anti-clastic curvature effects are more significant when the loading mode is bending rather than tension. Furthermore, anti-clastic curvature effects increase as the level of overall plasticity increases. Moreover, when the

mode of loading is bending anti-clastic curvature effects should increase as the a/W ratio decreases.

With this in mind, it is worth noting that the surface notched-SENB replicate specimens were tested in bending and the high measured toughness values indicate large levels of global plasticity. If the specimens had been tested at a lower temperature, which would have produced lower values of toughness and a decrease in the level of plasticity, it is conceivable that the results would have been independent of B/W ratio. Additional replicate tests are being performed at a lower test temperature in a follow-on project to investigate the effect of specimen thickness and anti-clastic curvature effects in more detail.

The results of the North American finite element analyses of the SENB specimens with different a/W ratio were re-analyzed to determine if they could provide evidence of anti-clastic curvature effects. The variation in applied crack driving force (CTOD and J) across the specimen thickness was studied for several a/W ratios and levels of applied crack driving force. It was found that:

(1) In the case of the deeply-cracked SENB specimens (a/W = 0.5) the applied crack driving force was uniform in the central section of the specimen. Closer to the specimen surface the applied crack driving force started to fall off due to plane stress effects. This trend was exhibited at all levels of applied crack driving force.

(2) The shallow-cracked SENB specimens (a/W = 0.1) exhibited the same trend as the deeply-cracked SENB specimens at low levels of applied crack driving force. As the applied crack driving force increased in the shallow-cracked specimens, the maximum crack driving force (J_{max}) shifted from the specimen mid-thickness to a position between the specimen mid-thickness and the specimen surface. Further increases in applied crack driving force resulted in an increase in the ratio $J_{max}/J_{mid\text{-}thickness}$. Moreover, the position corresponding to J_{max} shifted closer to the specimen surface as the applied crack driving force increased.

The trends exhibited by the shallow cracked-SENB finite element analyses support the view that anti-clastic curvature effects can become significant in shallow cracked-SENB specimens at high levels of applied crack driving force.

A more detailed study of anti-clastic curvature effects in shallow cracked-SENB and SENT specimens is currently underway at EWI as part of the Cooperative Research Program.

7.3 SENAB Test Program: Material M4

7.3.1 Transition Curve Tests on Surface-Notched SENAB Specimens

Tests on surface-notched and fatigue precracked SENAB specimens were performed over a wide range of temperature to obtain fractures ranging from completely brittle to fully ductile. The following specimen geometries were tested:

- 21 x 21 mm (B × W) SENAB a/W = 0.1
- 21 x 21 mm (B × W) SENAB a/W = 0.5.

The results of the fracture toughness tests are summarized in Tables 29 and 30 and presented as J and CTOD transition curves in Figures 70-73. The J and CTOD transition curves for the two a/W ratios are compared in Figures 74 and 75.

It is evident from Figures 74 and 75 that the J and CTOD transition curves for the shallow-notched specimens lie to the right of the curves for the deeply-notched specimens, i.e., the shallow-notched specimens exhibited brittle fracture at higher temperatures than the corresponding deeply-notched specimens. Indeed, the results presented in Tables 28 and 29 confirm that above -80°C the deeply-notched SENAB specimens exhibited fully ductile behavior. In comparison the shallow-notched SENAB specimens exhibited brittle fracture up to test temperatures of -55°C.

This behavior is rather surprising as it is generally accepted that shallow-notched specimens provide less constraint than deeply-notched specimens. As a result, shallow-notched

specimens should produce fracture toughness transition curves which lie to the left of the corresponding curves obtained from deeply-notched specimens, i.e., increasing the crack size increases the constraint thereby increasing the likelihood of brittle fracture.

It is also interesting to note the difference in maximum load toughness values produced by the shallow- and deeply-notched SENAB specimens. For a homogeneous material it is generally found that, for a given specimen thickness, the maximum load toughness is directly proportional to the size of the uncracked ligament. In the case of the SENAB specimens, the shallow-notched (a/W = 0.1) specimens produced maximum load toughness values in the range 0.66-0.81 mm. In comparison, the deeply-notched specimens produced maximum load toughness values in the range 0.21-0.28 mm. Consequently, the maximum load toughness values obtained from the shallow-notched samples were typically three times larger than those obtained from the deeply-notched specimens. In comparison, the ligaments in the shallow-notched specimens were only 1.8 times larger than the deeply-notched specimens.

The unexpected trends exhibited in Figures 74 and 75 suggest that there is a gradient in toughness through the wall of the pipe. To provide more information on the variation of properties through the wall of the pipe a full thickness macro sample was extracted from the pipe. Hardness measurements performed on the macro sample indicated that the hardness was uniform across the pipe wall. Examination of the macro sample confirmed that the microstructure of the pipe material is predominantly quenched and tempered martensite with interspersed carbides. Initially, it was assumed that the variation in toughness through the pipe wall could be due to carburization of the inner surface. Examination of the macro sample confirmed that there was no significant carburization. The macro sample did, however, indicate significant carbide banding in the inner third of the pipe wall as shown in Figure 13. In comparison, the microstructure in the outer two thirds of the pipe wall was very uniform with evenly distributed carbides. The reason the shallow-notched SENAB specimens exhibited a higher transition temperature than the deeply-notched specimens is, therefore, considered to be a result of the cracks in the shallow-notched specimens sampling the low toughness heavily carbide-banded microstructure, whereas, the cracks in the deeply-notched

SENAB specimens sampled the higher toughness microstructure found in the outer two thirds of the pipe wall.

As a result of the variation in microstructure through the pipe wall thickness, it was decided to terminate the SENAB test program since the variation in toughness through the pipe wall would complicate the interpretation of the fracture toughness results.

7.4 SENT Test Program: Material M3

7.4.1 Transition Curve Tests on Through Thickness-Notched Specimens

Through thickness-notched and fatigue-precracked SENT specimens were tested over a wide range of temperatures to enable J and CTOD transition curves to be developed. The following specimen geometries were tested:

- 25 × 25 mm (B × B) SENT a/W = 0.1
- 25 × 25 mm (B × B) SENT a/W = 0.5.

The results of the fracture toughness tests are summarized in Tables 31 and 32 and presented as J and CTOD transition curves in Figures 76 to 79.

The J and CTOD transition curves for the a/W = 0.05 and a/W = 0.5 through thickness-notched SENT specimens are compared in Figures 80 and 81. It is evident from Figures 80 and 81 that increasing the a/W ratio from 0.05 to 0.5 has not resulted in major changes to the transition curves. This behavior is consistent with the J and CTOD results obtained from the through thickness-notched SENB specimens presented in Figures 50 and 51.

Based on the results presented in Figures 80 and 81, it was decided that the replicate tests on the through thickness-notched SENT specimens with different a/W ratios would be performed at a test temperature (T_{m2}) of -90°C.

7.4.2 Transition Curve Tests on Surface-Notched Specimens

Surface-notched and fatigue-precracked SENT specimens were tested over a wide range of temperature to enable J and CTOD transition curves to be developed. The following specimen geometries were tested:

- 25 x 25 mm (B × B) SENT a/W = 0.1
- 25 x 25 mm (B × B) SENT a/W = 0.5.

The specimens were tested using the same procedures as the through thickness-notched SENT specimens except that transition attachments were used in the loading shackles to rotate the specimen axis through 90 degrees so that the double-clip gauge arrangement could be mounted on the top surface of the specimens.

The results of the fracture toughness tests are summarized in Tables 33 and 34 and presented as J and CTOD transition curves in Figures 82 to 85.

The J and CTOD transition curves for the a/W = 0.1 and a/W = 0.5 surface-notched SENT specimens are compared in Figures 86 and 87. The results presented in Figures 86 and 87 indicate that increasing the a/W ratio from 0.1 to 0.5 may have caused the J and CTOD transition curves to move to a slightly higher temperature.

Based on the results presented in Figures 86 and 87 a test temperature (T_2) of -80°C was selected for the replicate tests on the surface-notched SENT specimens of different thicknesses.

7.4.3 Replicate Tests on Through Thickness-Notched Specimens

Through thickness-notched SENT replicate tests were performed to determine the influence of crack size (or a/W ratio) on the measured toughness in the ductile-to-brittle transition regime. All the tests in this phase were performed at -90°C with specimens of the following geometries:

- 25 x 25 mm (B × B) SENT a/W = 0.10
- 25 x 25 mm (B × B) SENT a/W = 0.15
- 25 x 25 mm (B × B) SENT a/W = 0.20
- 25 x 25 mm (B × B) SENT a/W = 0.30
- 25 x 25 mm (B × B) SENT a/W = 0.50.

The results of the SENT fracture toughness tests are summarized in Table 35 and presented as plots of CTOD and J versus a/W ratio in Figures 88 and 89. All specimens produced δ_c and J_c results, i.e., unstable fracture with no preceding stable crack growth.

It is evident from Figures 88 and 89 that the J and CTOD results display significant scatter. Nevertheless, the results indicate that, in general:

(1) The average measured toughness decreases as the a/W ratio increases.
(2) The degree of scatter decreases as the a/W ratio increases.

A more surprising feature of the results presented in Figures 88 and 89 is that the lowest toughness values were obtained from the shallowest notched specimens. (Note, the lowest recorded toughness values corresponded to fracture under nominally linear elastic loading conditions.) Initially, it was thought that this unusual trend may have been produced by the HAZ of the shim plate welds extending to the tip of the crack. Sectioning the samples which produced low toughness values confirmed that this was not the case. The reason the shallow notched samples produced such low toughness values is still not clear.

7.4.4 Replicate Tests on Surface-Notched Specimens

As a result of the changes to the surface-notched SENT replicate specimen geometry it was agreed to machine and test a total of 18 surface-notched SENT specimens; 9 each of the B × B and 3B × B geometries. The test matrix was as follows (W = 18 mm in each case):

- B = 18 mm (B × B) a/W = 0.1
- B = 18 mm (B × B) a/W = 0.5

- B = 54 mm (B × 3B) a/W = 0.1
- B = 54 mm (3B × B) a/W = 0.5.

Initially, four specimens for each geometry and a/W ratio were tested, leaving two specimen blanks; one a B × B geometry and the other a 3B × B specimen. After analyzing the results of the 16 replicate tests, the most appropriate a/W ratio for the remaining two specimens was selected.

Based on the CTOD and J transition curves developed for the surface-notched SENT specimens, a test temperature of -80°C was selected for the replicate surface-notched SENT tests.

The results of the B × B and 3B × B surface-notched SENT tests are summarized in Tables 36 and 37 and plotted in Figures 90-93, respectively. It is apparent from Figures 90-93 that the degree of scatter is considerably larger for the shallow-notched specimens. This trend was also observed for the through thickness-notched SENT results.

The results also indicate that, unlike the surface notched-SENB replicate tests, increasing the specimen thickness from B to 3B has little effect on the measured toughness. It should, nevertheless, be emphasized that the toughness values obtained from the SENT specimens (which were tested at -80°C) were much lower than the corresponding results obtained from the surface notched-SENB replicate specimens (which were tested at -25°C). The CTOD toughness values obtained from the SENT replicate tests ranged from approximately 0.05 to 0.35 mm. The corresponding CTOD toughness range obtained from the SENB replicate tests was 0.1 to 1.6 mm.

7.4.5 Metallographic Assessment of SENT Specimens

Several shallow-notched SENT specimens produced very low values of CTOD and J. Nine specimens were selected for metallurgical sectioning to determine if the heat-affected zone (HAZ) associated with the shim plate weld had influenced the toughness behavior. These specimens were examined in the scanning electron microscope to identify the fracture

initiation site. If the initiation site was located near the shim plate weld, the specimen was sectioned through the initiation site to determine the presence of HAZ microstructure.

The following specimens were examined (a/W values are nominal):

- M3-108 TT-notched B × B a/W = 0.05
- M3-109 TT-notched B × B a/W = 0.05
- M3-114 TT-notched B × B a/W = 0.05
- M3-118 TT-notched B × B a/W = 0.05
- M3-150 S-notched B × B a/W = 0.10
- M3-224 S-notched B × B a/W = 0.10
- M3-247 S-notched B × B a/W = 0.10
- M3-258 S-notched B × B a/W = 0.10
- M3-265 S-notched 3B × B a/W = 0.10.

The metallurgical assessments found no indications of HAZ microstructure near the fracture initiation sites in any of these specimens. The visible HAZ boundary did not extend to the fatigue crack tip in any of the sectioned specimens. This indicates that the low CTOD and J values were not produced by the specimen preparation procedures.

7.5 Comparison of SENB and SENT Results

To provide an indication of the effect of loading mode on the fracture toughness transition behavior the J and CTOD transition curves obtained from the through thickness-notched, a/W = 0.05, SENB and SENT specimens are compared in Figures 94 and 95. The J and CTOD transition curves obtained from the through thickness-notched, a/W = 0.05, SENB and SENT specimens are compared in Figures 96 and 97.

As expected, the results presented in Figures 94-97 indicate that the SENB transition curves exhibit a higher transition temperature than the corresponding SENT transition curves. It is also interesting to note that this trend is more evident for the deeply-notched (a/W = 0.5) specimens than the shallow notched specimens (a/W = 0.05).

8.0 CONCLUSIONS

In 1987 TWI and EWI initiated a major international research project to develop "Shallow Crack Fracture Mechanics Testing Procedures". The major objective of the project was to develop shallow crack fracture toughness testing and analysis procedures to cover:

- Bending and tension loading
- Testing of both flat and curved (e.g., pipe) material
- Characterization of fracture toughness in terms of K, J and CTOD.

The project was conducted jointly by EWI and TWI. EWI coordinated the experimental and numerical analyses conducted in North America while TWI coordinated the corresponding European work. The majority of the numerical analyses were performed by in-kind contributors in both North America and Europe. The primary objective of the experimental phase was to develop suitable fracture toughness testing procedures including the development of appropriate fatigue precracking guidelines. In comparison the objective of the numerical phase was to develop appropriate analysis procedures for shallow cracked specimens including J and CTOD estimation schemes.

This report presents details of the fatigue precracking, instrumentation and testing procedures which were developed for SENB, SENAB and SENT specimens with a/W ratios down to 0.05 and absolute crack depths 1.25 mm. The main conclusions of the North American experimental test program can be summarized as follows:

SENB Test Program (Material M3: A36 Steel)

1. Although the J and CTOD transition data obtained from testing shallow and deeply cracked SENB specimens exhibited considerable scatter there was no pronounced effect of a/W ratio.

2. Replicate tests performed in the ductile to brittle transition regime indicated an elevation in toughness as the a/W ratio decreased. At an a/W ratio of 0.1 the mean CTOD

toughness was approximately 1.4 times greater than the toughness measured at an a/W ratio of 0.5. The corresponding toughness elevation in J was only 1.08.

3. Increasing the width (W) of the SENB specimens from B to 2B appeared to shift the J and CTOD transition curves to a slightly higher temperature and reduce the level of scatter.

4. Increasing the specimen thickness (from B to 3B) produced a reduction in toughness of more than 100% for specimens tested in the upper transition regime. This surprising trend may be due to anti-clastic curvature effects.

SENAB Test Program (Material M4: API 5CT L80 Tube)

1. The shallow cracked SENAB specimens produced higher transition temperatures than the deeply cracked samples.

2. Metallurgical examination of the pipe material revealed a microstructural gradient through the wall thickness, with significant carbide banding in the inner third of the pipe wall.

SENT Test Program (Material M3: A36 Steel)

1. Decreasing the a/W ratio in the SENT specimens resulted in a general increase in toughness, although at small a/W ratios (less than 0.2) the scatter increased significantly. Surprisingly the lowest toughness values were obtained with the shallowest cracked specimens.

2. Unlike the SENB specimens the SENT specimens did not exhibit a thickness dependency over the width range B to 3B. However since the replicate SENT specimens were tested at a much lower temperature than the SENB specimens the measured toughness values were considerably lower than those obtained from the replicate SENB tests.

9.0 RECOMMENDATIONS

While sponsors will clearly be able to make use of the techniques developed in this project directly, these techniques will only achieve their full potential when they have been adopted into the appropriate national and international standards. To this end, it is recommended that TWI and EWI submit proposals to BSI and ASTM for amendments to the deeply-notch fracture-mechanics test methods.

Although the current project has laid the groundwork for the development of shallow-crack fracture toughness testing and analysis procedures, there are still areas where further work is required. These include:

(1) The development of fatigue precracking procedures for low strength materials (less than 300 N/mm^2) which are suitable for K_{Ic} testing, as described in EWI Proposal A6098-1.[9]

(2) The development of shallow crack K_{Ic} and shallow crack J and CTOD R-curve test procedures as described in EWI Proposal A6098-1.[9]

(3) The development of shallow-crack fracture toughness testing and analysis procedures for welded joints as described in EWI Proposal A6154.[10]

10.0 ACKNOWLEDGEMENTS

The authors are grateful to the sponsors of this project for their financial support and technical input, particularly Dr. Walt Reuter of EG&G Idaho and Dr. Alan Glover of NOVA Corporation of Alberta who chaired the North American Sponsor Group Meetings. The authors also wish to thank their colleagues at TWI who coordinated the experimental work and numerical analyses performed in Europe.

Finally, EWI and TWI would like to extend their gratitude to the in-kind contributors not only for their generous contributions, but also for the helpful suggestions and comments.

11.0 REFERENCES

1. BS7448:Part 1:1991, "Fracture Mechanics Toughness Tests, Part 1. Method for the Determination of K_{Ic}, Critical CTOD and Critical J Values of Metallic Materials," (this standard replaced BS5447:1977:K_{Ic} tests and BS5762:1979:CTOD tests.)

2. BS6729:1987, "British Standard Method for Determination of the Dynamic Fracture Toughness of Metallic Materials."

3. ASTM E399-90, "Standard Test Method for Plane-Strain Fracture Toughness of Metallic Materials."

4. ASTM E813-89, "Standard Test for J_{Ic}, a Measure of Fracture Toughness."

5. ASTM E1152-87, "Standard Test Method for Determining J-R Curves."

6. ASTM E1290-89, "Standard Test Method for Crack-Tip Opening Displacement (CTOD) Fracture Toughness Measurement."

7. Contract Proposal TWI Ref. CP/MAN/3299-1, EWI Ref. A6098, "An International Research Project to Develop Shallow Crack Fracture Mechanics Tests," July 1987.

8. Gordon, J. R. and Wang, Y-Y., "An International Research Project to Develop Shallow Crack Fracture Mechanics Tests - North American Contribution, Final Report on North American Finite Element Analyses, EWI Report," No. J6098-23-91, May 1992.

9. EWI Proposal A6098-1, "An International Research Project to Develop Shallow Crack Fracture Mechanics Tests - Additional Testing and Analysis," January 1991.

10. EWI Proposal A6154, "The Effect of Weld Metal Mismatch on Structural Integrity Assessments," July 1991.

TABLE 1. SPONSORS AND IN-KIND CONTRIBUTORS

No.	Sponsor	Country
North American Sponsors		
1	Chevron Corporation	US
2	EG&G Idaho	US
3	Electric Power Research Institute	US
4	Exxon Production Research Company	US
5	National Aeronautics and Space Administration	US
6	National Institute of Standards and Technology	US
7	NOVA Corporation of Alberta	Canada
8	Oak Ridge National Laboratories	US
9	Ontario Hydro	Canada
10	USS Division of USX Corporation	US
European Sponsors		
11	AEA Technology	UK
12	BASF Aktiengesellschaft	Germany
13	British Steel plc	UK
14	Bureau Veritas	France
15	Conoco (UK) Ltd.	UK
16	Defence Research Agency	UK
17	Health & Safety Executive	UK
18	Imperial Chemical Industries plc	UK
19	NEI Parsons	UK
20	Nuclear Electric	UK
21	Rolls-Royce and Associates Ltd.	UK
22	Saga Petroleum AS	Norway
23	Shell Exploration & Production	UK
24	STATOIL	Norway

TABLE 1. (Continued)

No.	Sponsor	Country
	In-Kind Contributors	
25	Billiton/Shell Research BV	The Netherlands
26	ESIS TCI Subcommittee on Local Approach	Europe
27	NASA Langley Research Center	US
28	Netherlands Energy Research Centre	The Netherlands
29	Sandia National Laboratory	US
30	SINTEF	Norway
31	Texas A&M University	US
32	University of Aachen	Germany
33	University of Illinois at Urbana-Champaign	US
34	University of Kansas	US

TABLE 2. CHEMICAL ANALYSIS OF PLATE, M3

(Element, weight percent)

Sample Identification[a]	C	Mn	P	S	Si	Cu	Ni	Cr	Mo	Al	Ti
ASTM A36-84a Mill Cert.	0.25 max 0.17	0.80- 1.20 1.07	0.04 max. 0.011	0.05 max. 0.006	--	--	--	--	--	--	--
AB1 AB2 AB3	0.18 0.18 0.18	1.02 1.00 1.00	0.010 0.009 0.010	0.005 0.004 0.004	0.19 0.19 0.19	0.024 0.023 0.023	0.009 0.008 0.008	0.022 0.021 0.021	0.011 0.009 0.010	0.024 0.023 0.024	0.001 0.001 0.001
DE4 DE5 DE6	0.018 0.018 0.018	1.01 1.00 0.98	0.009 0.009 0.008	0.003 0.004 0.003	0.19 0.19 0.18	0.022 0.022 0.020	0.006 0.006 0.005	0.021 0.021 0.020	0.008 0.009 0.007	0.023 0.022 0.020	0.000 0.001 0.000
HI7 HI8 HI9	0.18 0.18 0.18	1.02 1.02 1.02	0.010 0.009 0.009	0.005 0.004 0.005	0.19 0.20 0.19	0.23 0.23 0.23	0.006 0.006 0.007	0.21 0.21 0.21	0.010 0.010 0.009	0.023 0.024 0.022	0.001 0.001 0.000

(a) See Figure 1.

Sn = 0.001
Nb, V, Zr <.001
B, Ca <0.0001
W, Pb <0.01
Co <0.003

TABLE 3. TENSILE TEST RESULTS AT ROOM TEMPERATURE

Sample Identification	0.2% Yield Strength, N/mm^2 (ksi)	Tensile Strength, N/mm^2 (ksi)	Elongation[(a)] (%)	Reduction of Area (%)
AB1	280 (40.5)	491 (71.2)	43	67
AB2	283 (41.1)	487 (70.6)	43	67
AB3	276 (40.1)	492 (71.5)	42	67
DE4	297 (43.1)	496 (71.9)	54	65
DE5	276 (40.0)	485 (70.5)	46	69
DE6	291 (42.1)	493 (71.4)	44	69
HI7	283 (41.1)	496 (71.9)	42	68
HI8	285 (41.3)	487 (70.6)	43	68
HI9	281 (40.7)	493 (71.4)	41	68
Mill Cert.	308 (44.6)	500 (72.5)	45[(b)]	--

(a) 25.4 mm (1.0 in.) gauge length.

(b) Over 50.8-mm (2-in.) gauge length (24% over 8 in.).

TABLE 4. CHARPY V-NOTCH TOUGHNESS OF PLATE M3 - TRANSITION DATA

Specimen Location	Specimen Identification M3 -	Temperature (°C)	Charpy J	Energy ft-lbs
AB1	13 14 15	20	274 288 250	202 212 184
AB2	16 17 18	0	267 270 124	197 199 91.5
AB3	19 20 21	-20	57 84 93	42.5 62 68.5
AB1	8 9 10	-30	61 62 29	45 46 21.5
DE4	22 23 24	-40	29 23 21	21 17 15
DE5	25 26 27	-60	8 4 7	6 3 5

TABLE 5. CHARPY V-NOTCH TOUGHNESS AT -30°C

Specimen Location	Identification M3-	Charpy Energy	
		J	ft-lbs
AB1	8	61	45
	10	62	46
	12	29	21.5
AB2	40	46	33.5
	41	60	44.5
	42	46	33.5
AB3	43	62	46
	44	52	38
	45	48	35
DE4	46	60	44.5
	47	55	40.5
	48	87	64
DE5	49	17	12.5
	50	6	4.5
	51	--	--
DE6	55	37	28
	56	23	17.5
	57	--	--
HI7	31	63	46.5
	32	66	48.5
	33	49	36.5
HI8	34	20	14.5
	35	86	63
	36	54	40
HI9	37	71	52
	38	53	39.1
	39	60	44.5

TABLE 6. MICROHARDNESS (HV1) RESULTS FOR PLATE M3

Distance from Top (mm)	Specimen Identification										
	AB1	AB2	AB3	DE4	DE5	DE6	HI7	HI8	HI9	Mean	Standard Deviation
1	147	148	149	147	153	145	140	144	140	146	4.7
3	145	144	143	143	148	143	147	148	154	146	3.6
5	143	144	147	145	140	143	140	143	150	144	3.2
7	142	150	147	145	143	145	144	146	142	145	2.6
9	150	143	148	145	150	152	140	149	145	147	3.9
11	147	150	152	147	140	142	138	146	145	145	4.5
13	151	142	148	149	147	142	144	143	156	147	4.7
15	147	147	144	150	142	147	148	144	145	146	2.5
17	142	142	139	149	144	148	143	144	139	143	3.2
19	148	147	147	149	145	142	145	143	149	146	2.5
21	144	144	144	144	144	144	145	139	143	143	1.7
23	143	142	145	150	142	142	147	151	142	146	3.8
25	138	138	139	150	142	139	140	145	140	141	4.0
Mean	145	145	146	147	145	144	143	145	145		
Standard Deviation	3.6	3.5	3.8	2.5	4.1	3.3	3.2	3.0	5.3		

TABLE 7. SUMMARY OF TENSILE PROPERTIES FOR PLATE MATERIAL M3

Steel specification	ASTM A36-84a (25.4 mm thick) to ASSHTO M-183-841
Test temperature	24°C
Young's modulus	207×10^3 N/mm^2
Poisson's ratio	0.3 (assumed)
Yield strength	283 N/mm^2
Tensile strength	491 N/mm^2

TABLE 8. IDEALIZED TENSILE STRESS-STRAIN CURVE FOR PLATE MATERIAL M3

Engineering Stress (N/mm^2)	Engineering Strain	True Stress (N/mm^2)	True Strain
0	0	0	0
283.4	0.00136	283.4	0.00136
283.4	0.01050	286.4	0.01044
323.8	0.01958	330.2	0.01939
354.3	0.02832	364.3	0.02792
376.8	0.03691	390.7	0.03624
395.8	0.04595	414.0	0.04492
410.2	0.05493	432.8	0.05347
423.5	0.06416	450.6	0.06218
432.7	0.07352	464.6	0.07096
440.6	0.08315	477.2	0.07988
446.8	0.09287	488.3	0.08880
450.6	0.09980	495.6	0.09513

TABLE 9. SUMMARY OF COMPRESSIVE PROPERTIES FOR PLATE MATERIAL M3

Steel specification	ASTM A36-84a (25.4 mm thick) to ASSHTO M-183-841
Test temperature	24°C
Young's modulus	203.2×10^3 N/mm^2
Poisson's ratio	0.3 (assumed)
Yield strength	276 N/mm^2

TABLE 10. IDEALIZED COMPRESSIVE STRESS-STRAIN CURVE FOR PLATE MATERIAL M3

Engineering Stress (N/mm^2)	Engineering Strain	True Stress (N/mm^2)	Log (e) Strain
0	0	0	0
276.0	0.00136	275.6	0.00136
276.0	0.00703	274.1	0.00701
299.4	0.01006	296.4	0.01001
354.3	0.02002	347.2	0.01982
401.2	0.03008	389.1	0.02963
440.1	0.04014	422.4	0.03935
473.5	0.05000	449.8	0.04879
503.0	0.06001	472.8	0.05832
528.5	0.07021	491.4	0.06786
552.6	0.08027	508.2	0.07721
574.0	0.09023	522.2	0.08639
594.1	0.10000	534.7	0.09531
614.2	0.11005	546.6	0.10441
624.9	0.11631	552.2	0.11003

TABLE 11. SUMMARY OF TENSILE PROPERTIES FOR TUBE MATERIAL M4

Steel specification	API 5CT L80 tubing (270 mm OD, 21 mm wall thickness)
Test temperature	24°C
Young's modulus	202.5×10^3 N/mm^2
Poisson's ratio	0.3 (assumed)
Yield strength	590 N/mm^2
Tensile strength	705 N/mm^2

TABLE 12. IDEALIZED TENSILE STRESS-STRAIN CURVE FOR TUBE MATERIAL M4 (END "A")

Engineering Stress (N/mm^2)	Engineering Strain	True Stress (N/mm^2)	True Strain
0	0	0	0
590.0	0.00291	591.7	0.00290
590.0	0.01318	597.8	0.01309
609.8	0.02002	622.0	0.01982
639.8	0.03017	659.1	0.02973
662.8	0.04004	689.3	0.03926
680.2	0.05039	714.5	0.04916
691.3	0.06054	733.1	0.05878
696.9	0.07061	746.1	0.06822
701.1	0.08037	757.4	0.07730
703.2	0.09013	766.6	0.08630
703.2	0.10029	773.7	0.09557
701.8	0.11005	779.0	0.10441
701.1	0.12011	785.3	0.11343
695.5	0.13193	787.3	0.12392
692.1	0.14023	789.1	0.13122
683.7	0.15000	786.3	0.13976

TABLE 13. SUMMARY OF COMPRESSIVE PROPERTIES FOR TUBE MATERIAL M4

Steel specification	API 5CT L80 tubing (270 mm OD, 21 mm wall thickness)
Test temperature	24°C
Young's modulus	239.1×10^3 N/mm^2
Poisson's ratio	0.3 (assumed)
Yield strength	634.6 N/mm^2

TABLE 14. IDEALIZED COMPRESSIVE STRESS-STRAIN CURVE FOR TUBE MATERIAL M4 (END "A")

Engineering Stress (N/mm^2)	Engineering Strain	True Stress (N/mm^2)	Log (e) Strain
0	0	0	0
634.6	0.00266	632.9	0.00268
634.6	0.00938	628.6	0.00933
653.0	0.01533	643.0	0.01521
674.8	0.02011	661.2	0.01992
718.3	0.03017	696.7	0.02973
758.5	0.04004	728.1	0.03926
792.0	0.05020	752.2	0.04900
822.2	0.06025	772.7	0.05851
847.2	0.07051	787.5	0.06813
869.0	0.08008	799.4	0.07703
890.8	0.09014	810.5	0.08630
907.5	0.10000	816.8	0.09531
926.0	0.10830	825.7	0.10282

TABLE 15. COMPARISON OF FATIGUE PRECRACKING STRESS INTENSITY FACTORS

Specimen Size, mm (B × B)	Notch[1] Orientation	a/W	Actual K_f ($N/mm^{-3/2}$)	ASTM[2] CTOD ($N/mm^{-3/2}$)	ASTM[2] J_{Ic} ($N/mm^{-3/2}$)
25 × 25	TT	0.05	700	545	581
25 × 25	TT	0.5	800	643	686
25 × 50	TT	0.5	800	910	971
25 × 25	S	0.1	800	663	707
25 × 25	S	0.5	800	643	686

Notes: (1) TT = through-thickness, S = surface
(2) Maximum fatigue stress intensity factors permitted by test procedure.

TABLE 16. COMPARISON OF FATIGUE STRESS INTENSITY FACTORS AND MAXIMUM STRESS INTENSITY FACTORS ENCOUNTERED IN FRACTURE TOUGHNESS TESTS

Specimen Geometry, mm (B × W)	Notch[1] Orientation	a/W	K_f ($N/mm^{-3/2}$)	K_{max}[2] ($N/mm^{-3/2}$)	K_f/K_{max}
25 × 25	TT	0.05	700	1455	0.48
25 × 25	TT	0.5	800	1692	0.47
25 × 50	TT	0.5	800	1711	0.47
25 × 25	S	0.1	800	1906	0.42
25 × 25	S	0.5	800	1743	0.46

Notes: (1) TT = through-thickness, S = surface
(2) Minimum value of K_{max} tests.

TABLE 17. COMPARISON OF CMOD AND V_1 FOR A SELECTION OF TEST RESULTS FROM B × B SPECIMENS

Specimen Type	Specimen No.	a/W	Upper Clip Gauge Output, V_2 (mm)	Lower Clip Gauge Output, V_1 (mm)	CMOD (mm)	CMOD/V_1
SENB/TT	5574M1/ 40	0.05	0.246	0.161	0.133	0.83
SENB/TT	5574M1/ 29	0.05	1.556	0.941	0.742	0.79
SENB/TT	5574M1/ 31	0.05	2.960	1.681	1.271	0.76
SENB/TT	5574M1/ 32	0.05	3.964	2.371	1.863	0.79
SENB/TT	5574M1/ 37	0.05	4.532	2.632	2.028	0.77
SENB/TT	5574M1/ 55	0.50	0.808	0.575	0.499	0.87
SENB/TT	5574M1/ 56	0.50	2.183	1.482	1.256	0.85
SENB/TT	5574M1/ 44	0.50	4.150	2.852	2.438	0.85
SENB/TT	5574M1/ 50	0.50	7.169	4.882	4.165	0.85
SENB/TT	5574M1/ 53	0.50	8.553	5.898	5.070	0.86
SENT/TT	5574M1/116	0.05	0.115	0.097	0.091	0.94
SENT/TT	5574M1/112	0.05	0.387	0.367	0.360	0.98
SENT/TT	5574M1/113	0.05	0.923	0.765	0.714	0.93
SENT/TT	5574M1/129	0.50	0.148	0.092	0.074	0.80
SENT/TT	5574M1/123	0.50	1.683	1.062	0.860	0.81
SENT/TT	5574M1/124	0.50	3.649	2.363	1.945	0.82

TABLE 18. COMPARISON OF $CMOD_p/v_{pl}$ CALCULATED FROM SINGLE- AND DOUBLE-CLIP GAUGE MEASUREMENTS

Specimen No.	Actual a/W	Assumed Value of r_p	$CMOD_p/V_{pl}$	
			Eq. (6)	Eq. (7)
5574M1/29	0.095	0.4[(a)]	0.80	0.79
5574M1/56	0.525	0.4[(a)]	0.85	0.85
5574M1/29	0.095	0.45[(b)]	0.78	0.79
5574M1/56	0.525	0.45[(b)]	0.85	0.85

(a) According to BS5762.
(b) According to ASTM E1290.

TABLE 19. SPECIMENS FOR PLATE MATERIAL TESTS

Specimen No. J6098	Specimen Type	Size (B × W)	a/W	Temperature
M3/28-42	SENB/TT	B × B	0.05	Tr
M3/43-57	SENB/TT	B × B	0.5	Tr
M3/58-72	SENB/TT	B × 2B	0.5	Tr
M3/73-77	SENB/TT	B × B	0.05	Tm1
M3/78-82	SENB/TT	B × B	0.10	Tm1
M3/88-92	SENB/TT	B × B	0.15	Tm1
M3/93-97	SENB/TT	B × B	0.20	Tm1
M3/98-102	SENB/TT	B × B	0.30	Tm1
M3/103-107	SENB/TT	B × B	0.50	Tm1
M3/108-122	SENT/TT	B × B	0.05	Tr
M3/123-137	SENT/TT	B × B	0.50	Tr
M3/138-142	SENT/TT	B × B	0.05	Tm2
M3/143-147	SENT/TT	B × B	0.10	Tm2
M3/153-157	SENT/TT	B × B	0.15	Tm2
M3/158-162	SENT/TT	B × B	0.20	Tm2
M3/163-167	SENT/TT	B × B	0.30	Tm2
M3/168-172	SENT/TT	B × B	0.50	Tm2
M3/173-182	SENB/S	B × B	0.10	Tr
M3/183-192	SENB/S	B × B	0.50	Tr
M3/193-197	SENB/S	B × B	0.10	T1
M3/198-202	SENB/S	3B × B	0.10	T1
M3/203-207	SENB/S	2B × B	0.10	T1
M3/208-212	SENB/S	B × B	0.50	T2
M3/213-217	SENB/S	3B × B	0.50	T2
M3/218-222	SENB/S	2B × B	0.50	T2

TABLE 19. (Continued)

Specimen No. J6098	Specimen Type	Size (B × W)	a/W	Temperature
M3/223-232	SENT/S	B × B	0.10	Tr
M3/233-242	SENT/S	B × B	0.50	Tr
M3/243-247	SENT/S	B × B	0.10	T1
M3/248-252	SENT/S	3B × B	0.10	T1
M3/253-257	SENT/S	2B × B	0.10	T1
M3/258-262	SENT/S	B × B	0.50	T2
M3/263-267	SENT/S	3B × B	0.50	T2
M3/268-272	SENT/S	2B × B	0.50	T2

Test temperature: T1, T2 - Defined in proposal
Tr - Various temperatures in transition regime
Tm1, Tm2 - Intermediate temperatures.

TABLE 20. PLAIN MATERIAL TESTS, PIPE MATERIAL M4

Specimen Type	Size (B × W)	a/W	Specimen No.	Test Temperature
SENAB/ISR	B × B	0.10	6098M4/13-22	T_v
SENAB/ISR	B × B	0.50	6098M4/23-32	T_v
SENAB/ISR	B × B	0.10	6098M4/33-37	T_m
SENAB/ISR	B × B	--	6098M4/38-42	--
SENAB/ISR	B × B	0.15	6098M4/43-47	T_m
SENAB/ISR	B × B	0.20	6098M4/48-52	T_m
SENAB/ISR	B × B	0.30	6098M4/53-57	T_m
SENAB/ISR	B × B	0.50	6098M4/58-62	T_m

Test temperature: T1, T2 - Defined in proposal
Tr - Various temperatures in transition regime
Tm1, Tm2 - Intermediate temperatures.

TABLE 21. RESULTS OF FRACTURE TOUGHNESS TESTS ON THROUGH-THICKNESS NOTCHED, a/W = 0.05, B x B, SENB SPECIMENS

Specimen No.	Test Temperature (°C)	CTOD (mm)	J (kJ/m^2)	Type of Result[(a)]
M3-29	-120	0.0027	2	c
M3-28	-100	0.121	77	c
M3-30	-80	0.105	66	c
M3-31	-70	0.043	27	c
M3-33	-60	0.26	162	u
M3-32	-50	0.29	186	u
M3-34	-40	0.51	325	u
M3-41	-40	0.65	414	u
M3-35	-30	0.66 0.73	421 463	m u
M3-36	-20	0.75 0.95	476 606	m u
M3-42	-20	0.41	260	u
M3-38	-10	0.67	424	u
M3-37	0	0.72 1.25	456 794	m u
M3-39	+5	0.60 0.86	382 545	m u
M3-40	+5	0.78 1.50	494 952	m ts

(a) c = brittle fracture with no preceding stable crack growth
u = brittle fracture preceded by stable crack growth
m = toughness evaluated at maximum load conditions
ts = test stopped because range of transducers exceeded.

TABLE 22. RESULTS OF FRACTURE TOUGHNESS TESTS ON THROUGH THICKNESS-NOTCHED, a/W = 0.5, B × B, SENB SPECIMENS

Specimen No.	Test Temperature (°C)	CTOD (mm)	J (kJ/m^2)	Type of Result[a]
M3-44	-120	0.049	36	c
M3-43	-100	0.048	35	c
M3-48	-80	0.19	137	c
M3-46	-70	0.24	175	c
M3-45	-60	0.11	83	c
M3-49	-50	0.44	326	u
M3-50	-40	0.70 0.75	516 552	m u
M3-51	-30	0.36	265	c
M3-52	-20	0.63 0.77	466 567	m u
M3-54	-20	0.68 1.23	502 909	m u
M3-55	-10	0.39	291	u
M3-47	-10	0.96 1.09	708 804	m u
M3-53	0	0.71 1.16	527 853	m u
M3-56	0	0.69 1.36	512 1004	m ts
M3-57	+10	0.60 1.19	441 879	m ts

(a) c = brittle fracture with no preceding stable crack growth
u = brittle fracture preceded by stable crack growth
m = toughness evaluated at maximum load conditions
ts = test stopped because range of transducers exceeded.

TABLE 23. RESULTS OF FRACTURE TOUGHNESS TESTS ON THROUGH THICKNESS-NOTCHED, a/W = 0.5, B × 2B, SENB SPECIMENS

Specimen No.	Test Temperatures (°C)	CTOD (mm)	J (kJ/m^2)	Type of Result[a]
M3-61	-120	0.037	27	c
M3-58	-100	0.12	90	c
M3-62	-80	0.098	72	c
M3-63	-70	0.048	35	c
M3-64	-60	0.12	90	c
M3-65	-50	0.20	151	c
M3-66	-40	0.21	155	c
M3-67	-30	0.43	316	u
M3-59	-20	0.24	175	c
M3-69	-20	0.31	225	c
M3-68	-10	0.71	527	u
M3-72	0	1.32 1.57	974 1160	m ts
M3-60	0	1.39 1.70	1024 1255	m u
M3-70	+10	1.33	979	u
M3-71	+20	1.27 1.67	939 1230	m ts

(a) c = brittle fracture with no preceding stable crack growth
u = brittle fracture preceded by stable crack growth
m = toughness evaluated at maximum load conditions
ts = test stopped because range of transducers exceeded.

TABLE 24. RESULTS OF FRACTURE TOUGHNESS TESTS ON THROUGH THICKNESS-NOTCHED, a/W = 0.1, B × B, SENB SPECIMENS

Specimen No.	Test Temperatures (°C)	CTOD (mm)	J (kJ/m^2)	Type of Result[(a)]
M3-173	-100	0.077	72	c
M3-176	-80	0.054	51	c
M3-178	-65	0.60	562	u
M3-174	-50	0.41	385	u
M3-177	-40	1.16 1.25	1094 1174	m u
M3-180	-30	0.60	562	u
M3-182	-20	0.47	438	u
M3-179	-20	0.55	518	u
M3-181	-10	1.20 1.54	1130 1453	m u
M3-175	0	1.07 1.65	1005 1550	m u

(a) c = brittle fracture with no preceding stable crack growth
u = brittle fracture preceded by stable crack growth
m = toughness evaluated at maximum load conditions
ts = test stopped because range of transducers exceeded.

TABLE 25. RESULTS OF FRACTURE TOUGHNESS TESTS ON THROUGH THICKNESS-NOTCHED, a/W = 0.5, B × B, SENB SPECIMENS

Specimen No.	Test Temperatures (°C)	CTOD (mm)	J (kJ/m^2)	Type of Result[(a)]
M3-184	-120	0.031	35	c
M3-183	-100	0.066	74	c
M3-185	-80	0.038	43	c
M3-186	-70	0.20	229	c
M3-187	-60	0.25	283	c
M3-188	-50	0.20	220	c
M3-189	-40	0.24	264	c
M3-190	-30	0.77	863	u
M3-191	-20	0.88 1.29	985 1451	m u
M3-192	0	0.67 0.88	756 985	m u

(a) c = brittle fracture with no preceding stable crack growth
u = brittle fracture preceded by stable crack growth
m = toughness evaluated at maximum load conditions
ts = test stopped because range of transducers exceeded.

TABLE 26. RESULTS OF REPLICATE FRACTURE TOUGHNESS TESTS ON THROUGH THICKNESS-NOTCHED (B × B) SENB SPECIMENS
(All specimens tested at -40°C)

Specimen No.	a_o/W	CTOD[a] (mm)	J (kJ/m^2)	Type of Result[a]
M3-73	0.065	0.38	354	u
M3-74	0.063	0.26	245	u
M3-75	0.065	0.54	509	u
M3-76	0.177	0.88	833	u
M3-77	0.076	0.29	269	u
M3-78	0.148	0.64	614	u
M3-79	0.150	0.48	461	u
M3-80	0.112	0.68	651	u
M3-81	0.108	0.40	379	u
M3-82	0.132	0.79	759	u
M3-88	0.179	0.30	291	u
M3-89	0.187	0.30	286	u
M3-90	0.213	0.48	459	u
M3-91	0.210	0.60	575	u
M3-92	0.240	0.65	619	u
M3-93	0.20	0.40	385	u
M3-94	0.25	0.38	386	u
M3-95	0.22	0.20	200	u
M3-96	0.28	0.13	135	c
M3-97	0.25	0.72	734	u
M3-98	0.35	0.35	365	u
M3-99	0.36	0.35	373	u

TABLE 26. (Continued)

Specimen No.	a_o/W	CTOD[(a)] (mm)	J (kJ/m^2)	Type of Result[(a)]
M3-100	0.37	0.45	508	u
M3-101	0.38	0.80	838	u
M3-102	0.27	0.19	200	c
M3-103	0.54	0.45	508	u
M3-104	0.54	0.23	261	u
M3-105	0.55	0.34	566	u
M3-106	0.53	0.53	600	u
M3-107	0.54	0.15	170	c

(a) c = brittle fracture with no preceding stable crack growth
u = brittle fracture preceded by stable crack growth.

TABLE 27. RESULTS OF REPLICATE FRACTURE TOUGHNESS TESTS ON SHALLOW-NOTCHED (a/W = 0.1) SURFACE-NOTCHED (B × B) SENB SPECIMENS (All tests conducted at -25°C.)

Specimen No.	B/W	CTOD (mm)	J (kJ/m^2)	Type of Result[a]	Initiation Position (%)
M3-193	1	0.96 1.60	908 1497	m ts	25
M3-194	1	0.91 1.22	859 1146	m u	40
M3-195	1	0.87 1.29	820 1213	m u	25
M3-196	1	0.92	868	u	40
M3-197	1	0.94 1.38	885 1297	m ts	40
M3-198	3	0.56	527	u	20
M3-199	3	0.28	266	u	30
M3-200	3	0.57	540	u	20
M3-201	3	0.78	735	u	15
M3-202	3	0.37	346	u	15
M3-203	2	0.67	633	u	30
M3-204	2	0.97	912	u	25
M3-205	2	0.88	828	u	25
M3-206	2	0.99 1.05	938 992	m u	25
M3-207	2	0.48	456	u	45

(a) m = toughness calculated at maximum load conditions
u = brittle fracture preceded by stable crack growth
ts = test stopped because range of transducers exceeded.

TABLE 28. RESULTS OF FRACTURE TOUGHNESS TESTS ON SHALLOW-NOTCHED (a/W = 0.5) SURFACE-NOTCHED (B × B) SENB SPECIMENS (All tests conducted at -25° C.)

Specimen No.	B/W	CTOD (mm)	J (kJ/m^2)	Type of Result[a]	Initiation Position (%)
M3-208	1	0.74 0.83	 932	m u	45
M3-209	1	0.58 0.73	 824	m u	50
M3-210	1	0.25	283	c	50
M3-211	1	0.49	550	u	45
M3-212	1	0.76 0.92	 1031	m u	45
M3-213	3	0.22	252	c	35
M3-214	3	0.088	99	c	20
M3-215	3	0.44	496	u	20
M3-216	3	0.39	442	u	40
M3-217	3	0.16	175	c	45
M3-218	2	0.64	718	u	30
M3-219	2	0.52	589	u	40
M3-220	2	0.27	305	c	25
M3-221	2	0.29	321	c	30
M3-222	2	0.73	824	u	15

(a) m = toughness calculated at maximum load conditions
u = brittle fracture preceded by stable crack growth
ts = test stopped because range of transducers exceeded.

TABLE 29. RESULTS OF FRACTURE TOUGHNESS TESTS ON SURFACE-NOTCHED SENAB SPECIMENS, a/W = 0.1

Specimen No.	Test Temperature (°C)	CTOD (mm)	J (kJ/m^2)	Type of Result[a]
M4-18	-120	0.12	102	c
M4-17	-100	0.090	76	c
M4-20	-100	0.085 0.19	70 164	p u
M4-15	-90	0.13	108	c
M4-16	-80	0.46	386	u
M4-64	-80	0.29	245	u
M4-8	-70	0.80	680	u
M4-14	-70	0.39	330	u
M4-21	-70	0.17	141	c
M4-19	-65	0.77 0.95	652 805	m u
M4-13	-55	0.63 1.16	531 982	m u
M4-22	-40	0.75 1.58	636 1336	m ts

TABLE 30. RESULTS OF FRACTURE TOUGHNESS TESTS ON SURFACE-NOTCHED SENAB SPECIMENS, a/W = 0.5

Specimen No.	Test Temperature (°C)	CTOD (mm)	J (kJ/m^2)	Type of Result[(a)]
M4-31	-130	0.032	35	c
M4-26	-120	0.083	92	c
M4-30	-110	0.10	115	c
M4-32	-105	0.27 0.37	303 409	m u
M4-23	-100	0.09 0.33 0.68	99 370 756	p m u
M4-28	-95	0.16	172	c
M4-29	-90	0.22 0.49	245 544	m u
M4-66	-90	0.30	245	u
M4-65	-85	0.28	320	u
M4-25	-80	0.26 0.99	293 1100	m ts
M4-27	-60	0.35 1.00	384 1113	m ts
M4-24	-40	0.33 1.09	368 1207	m ts

(a) c = brittle fracture with no preceding stable crack growth
u = brittle fracture preceded by stable crack growth
m = toughness calculated at maximum load conditions
ts = test stopped
p = pop-in.

TABLE 31. RESULTS OF FRACTURE TOUGHNESS TESTS ON THROUGH THICKNESS-NOTCHED SENT SPECIMENS, a/W = 0.05

Specimen No.	Test Temperature (°C)	a/W	CTOD (mm)	J (kJ/m^2)	Type of Result[a]
M3-114	-150	0.07	0.011	9	c
M3-109	-120	0.06	0.023	18	c
M3-118	-110	0.06	0.041	33	c
M3-108	-100	0.06	0.069	56	c
M3-122	-90	0.06	0.147	111	c
M3-119	-80	0.04	0.239	187	u
M3-113	-80	0.08	0.294	240	u
M3-121	-70	0.06	0.309	244	u
M3-111	-70	0.07	0.166	127	c
M3-115	-60	0.06	0.415	330	u
M3-112	-60	0.07	0.308	243	u
M3-110	-50	0.06	0.268	210	u
M3-117	-50	0.06	0.382	311	u

(a) c = unstable fracture with no preceding slow stable crack growth
u = unstable fracture preceded by slow stable crack growth
m = toughness calculated at maximum load conditions.

TABLE 32. RESULTS OF FRACTURE TOUGHNESS TESTS ON THROUGH THICKNESS-NOTCHED SENT SPECIMENS, a/W = 0.50

Specimen No.	Test Temperature (°C)	a/W	CTOD (mm)	J (kJ/m^2)	Type of Result[(a)]
M3-133	-120	0.52	0.046	44	c
M3-127	-110	0.54	0.076	74	c
M3-126	-100	0.55	0.045	44	c
M3-135	-90	0.52	0.046	44	c
M3-137	-80	0.54	0.090	88	c
M3-124	-80	0.56	0.150	146	c
M3-134	-70	0.51	0.255	248	u
M3-123	-70	0.56	0.074	72	c
M3-125	-60	0.53	0.188	183	c
M3-136	-60	0.53	0.213	207	u
M3-131	-50	0.52	0.263	256	u
M3-128	-50	0.53	0.415	404	u
M3-130	-40	0.53	0.686	667	u
M-132	-40	0.54	0.664	646	u
M-129	-40	0.53	0.875	852	u

(a) c = unstable fracture with no preceding slow stable crack growth
u = unstable fracture preceded by slow stable crack growth
m = toughness calculated at maximum load conditions.

TABLE 33. RESULTS OF FRACTURE TOUGHNESS TESTS ON SURFACE-NOTCHED SENT SPECIMENS, a/W = 0.1

Specimen No.	Test Temperature (°C)	a/W	CTOD (mm)	J (kJ/m^2)	Type of Result[(a)]
M3-150	-120	0.14	0.03	24	c
M3-224	-100	0.10	0.05	41	c
M3-232	-90	0.09	0.20	165	u
M3-226	-80	0.13	0.40	330	u
M3-230	-70	0.13	0.32	257	u
M3-225	-60	0.13	0.26	212	u
M3-228	-60	0.06	0.38	313	u
M3-229	-50	0.10	0.94	764	u
M3-151	-50	0.10	0.73	591	u
M3-227	-40	0.08	1.0	815	u

(a) c = unstable fracture with no preceding slow stable crack growth
u = unstable fracture preceded by slow stable crack growth
m = toughness calculated at maximum load conditions.

TABLE 34. RESULTS OF FRACTURE TOUGHNESS TESTS ON SURFACE-NOTCHED SENT SPECIMENS, a/W = 0.5

Specimen No.	Test Temperature (°C)	a/W	CTOD (mm)	J (kJ/m^2)	Type of Result[(a)]
M3-240	-120	0.54	0.095	92	c
M3-241	-100	0.55	0.100	97	c
M3-233	-90	0.55	0.065	63	c
M3-242	-80	0.54	0.175	170	c
M3-234	-70	0.58	0.099	96	c
M3-239	-60	0.58	0.106	103	c
M3-235	-60	0.57	0.186	181	c
M3-236	-50	0.57	0.617	600	u
M3-238	-50	0.54	0.449	457	u
M3-237	-40	0.55	0.800	778	u

(a) c = unstable fracture with no preceding slow stable crack growth
u = unstable fracture preceded by slow stable crack growth
m = toughness calculated at maximum load conditions.

TABLE 35. RESULTS OF FRACTURE TOUGHNESS TESTS ON THROUGH THICKNESS-NOTCHED SENT SPECIMENS (TEST TEMPERATURE = -90°C)

Specimen No.	a/W	CTOD (mm)	J (kJ/m^2)	Type of Result[a]
M3-138	0.03	0.17	14	c
M3-139	0.06	0.006	5	c
M3-141	0.05	0.020	17	c
M3-142	0.04	0.13	103	c
M3-143	0.12	0.092	78	c
M3-144	0.11	0.024	20	c
M3-145	0.14	0.041	35	c
M3-146	0.18	0.18	172	c
M3-147	0.16	0.041	38	c
M3-153	0.14	0.095	82	c
M3-154	0.16	0.14	124	c
M3-155	0.14	0.095	82	c
M3-156	0.16	0.14	184	c
M3-157	0.16	0.069	62	c
M3-158	0.26	0.098	93	c
M3-159	0.23	0.10	95	c
M3-160	0.23	0.10	81	c
M3-161	0.22	0.15	142	c
M3-162	0.26	0.15	142	c
M3-163	0.34	0.12	114	c
M3-164	0.35	0.13	123	c
M3-165	0.36	0.097	92	c
M3-167	0.52	0.056	56	c

TABLE 35. (Continued)

Specimen No.	a/W	CTOD (mm)	J (kJ/m^2)	Type of Result[(a)]
M3-168	0.52	0.073	72	c
M3-169	0.54	0.041	76	c
M3-170	0.51	0.073	72	c
M3-171	0.52	0.041	41	c
M3-172	0.44	0.041	39	c

(a) c = unnstable fracture with no preceding stable crack growth.

TABLE 36. RESULTS OF FRACTURE TOUGHNESS TESTS ON B × B SURFACE-NOTCHED SENT SPECIMENS (TEST TEMPERATURE = -80°C)

Specimen No.	a/W	CTOD (mm)	J (kJ/m^2)	Type of Result[a]
M3-246	0.12	0.222	181	u
M3-247	0.13	0.069	56	u
M3-258	0.13	0.112	91	u
M3-259	0.08	0.319	260	u
M3-260	0.11	0.237	193	u
M3-268	0.09	0.254	207	u
M3-243	0.57	0.111	108	u
M3-244	0.63	0.242	235	u
M3-261	0.52	0.113	110	u

(a) u = unstable fracture preceded by slow stable crack growth.

TABLE 37. RESULTS OF FRACTURE TOUGHNESS TEST ON 3B × B SURFACE-NOTCHED SENT SPECIMENS (TEST TEMPERATURE = -80°C)

Specimen No.	a/W	CTOD (mm)	J (kJ/m^2)	Type of Result[(a)]
M3-251	0.15	0.285	232	u
M3-263	0.26	0.158	129	u
M3-264	0.13	0.132	107	u
M3-265	0.10	0.034	28	u
M3-266	0.10	0.194	158	u
M3-267	0.11	0.230	187	u
M3-248	0.49	0.096	93	u
M3-249	0.46	0.123	119	u
M3-250	0.51	0.194	189	u

(a) u = unstable fracture preceded by slow stable crack growth.

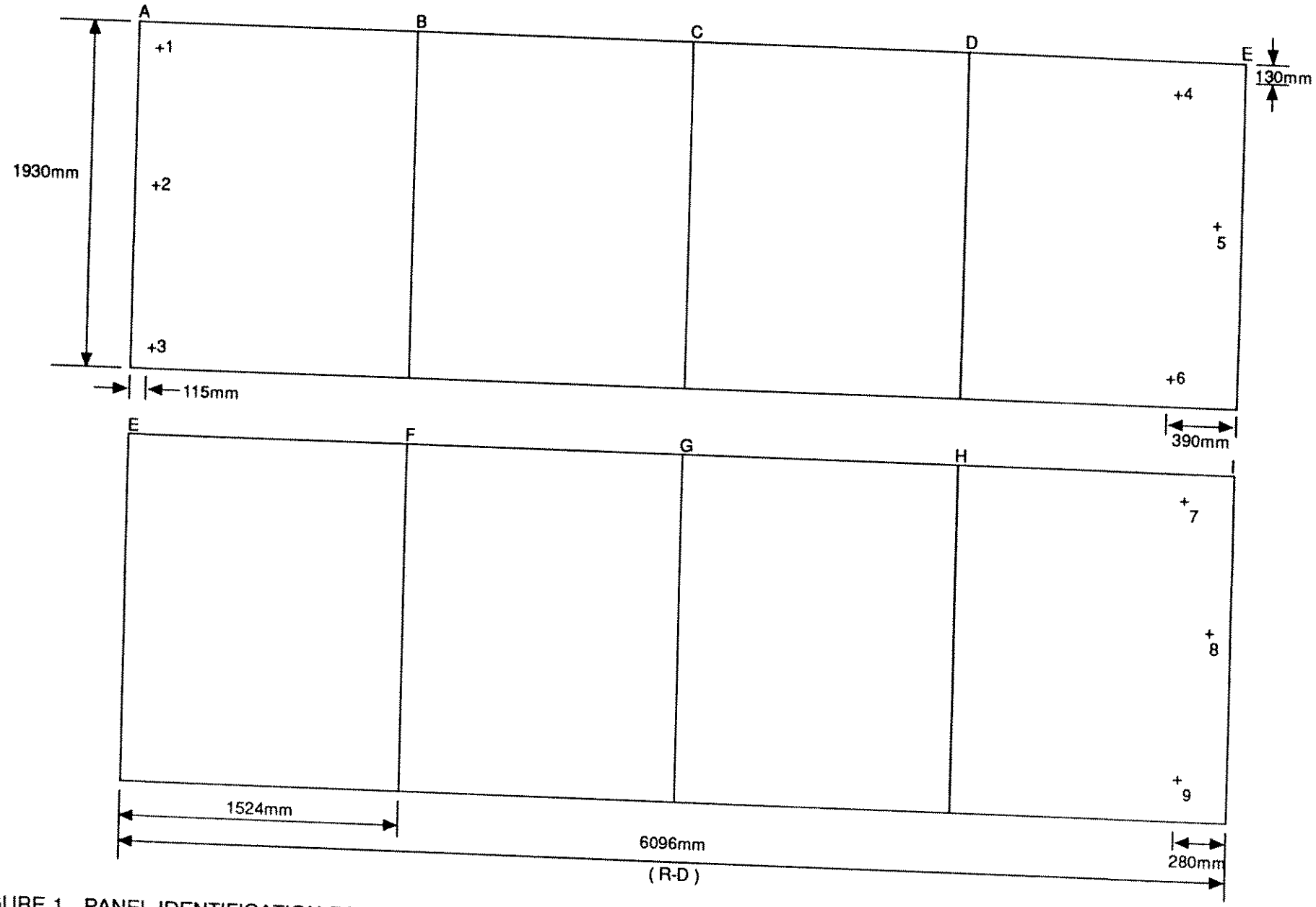

FIGURE 1. PANEL IDENTIFICATION FOR PLATE MATERIAL M3 ("+" INDICATES THE TOP FELT HAND CORNER OF TEST COUPONS)

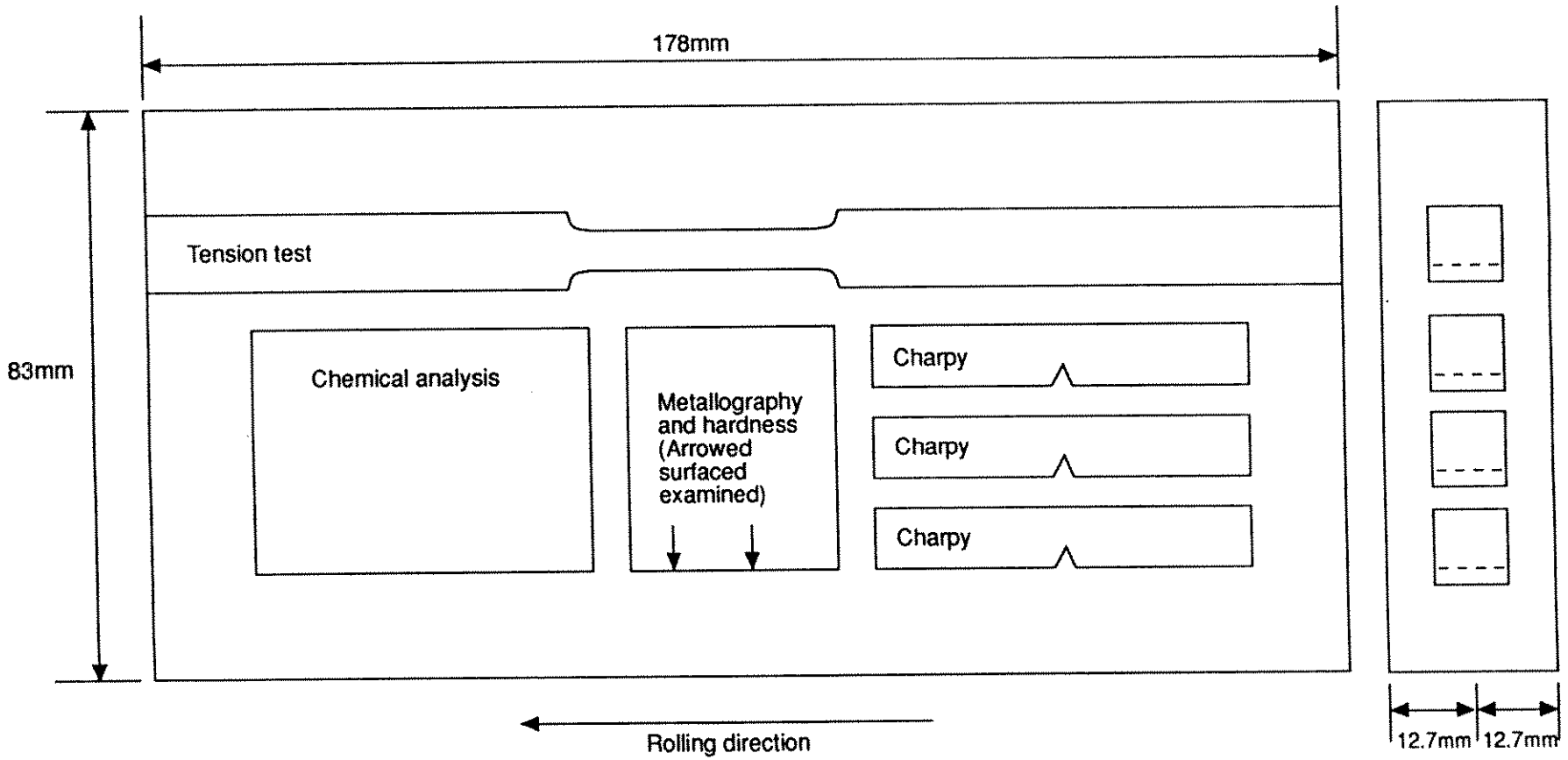

FIGURE 2. TEST COUPON SHOWING DISPOSITION OF SPECIMENS

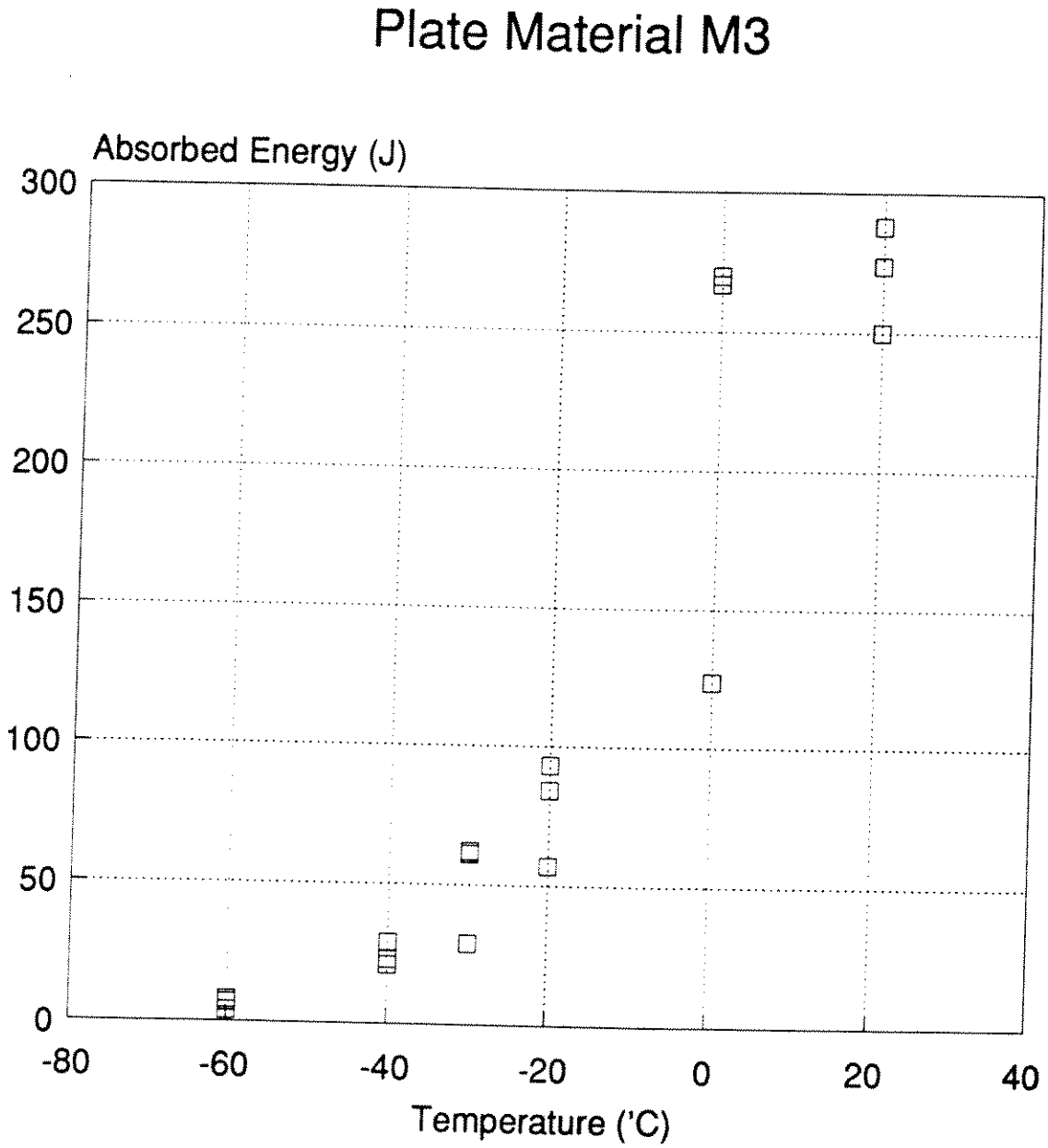

FIGURE 3. CHARPY V-NOTCH TRANSITION CURVE FOR PLATE MATERIAL M3

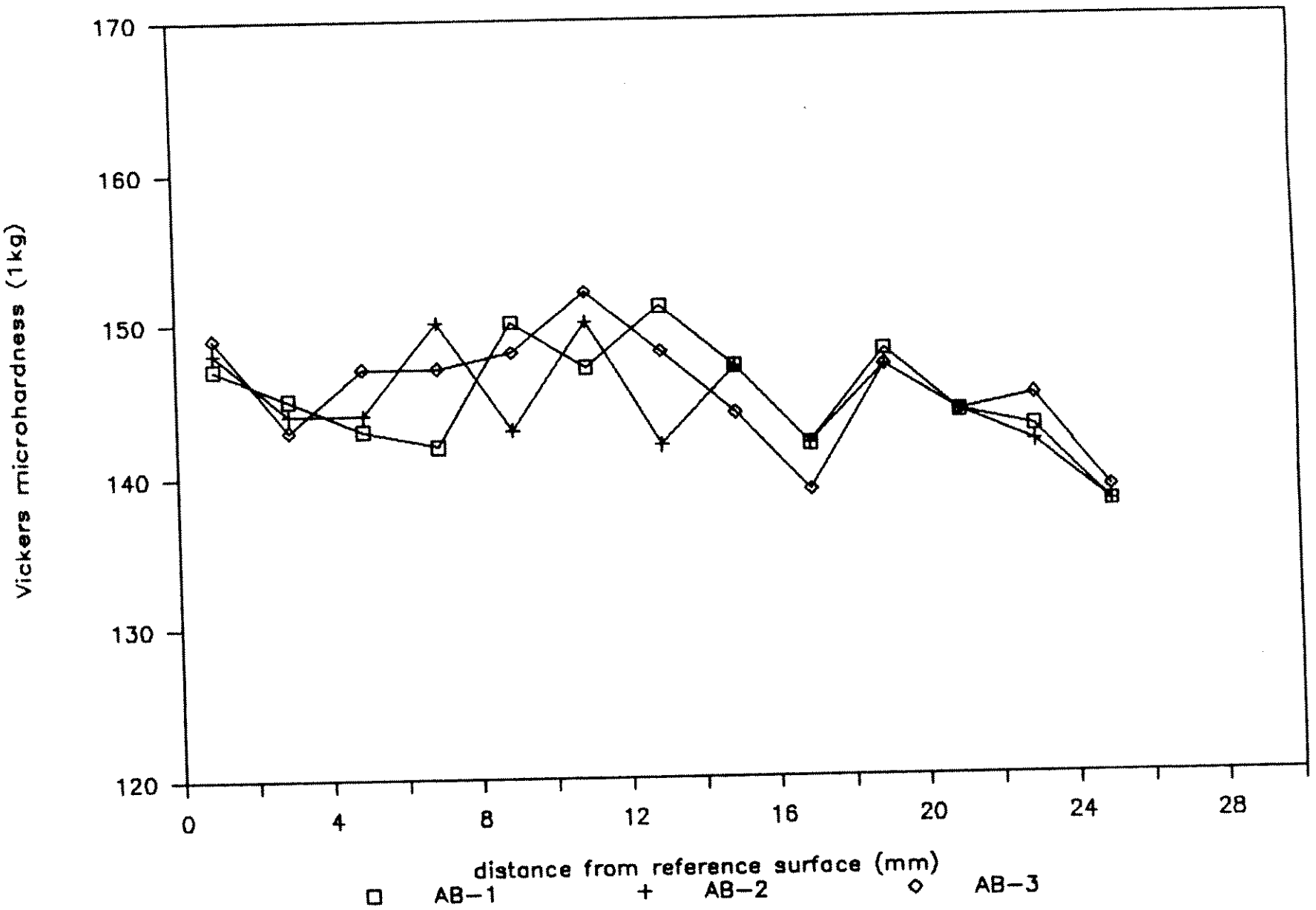

FIGURE 4. VICKERS MICROHARDNESS SURVEY THROUGH THICKNESS OF PLATE M3 (LOCATIONS AB-1, -2 AND -3)

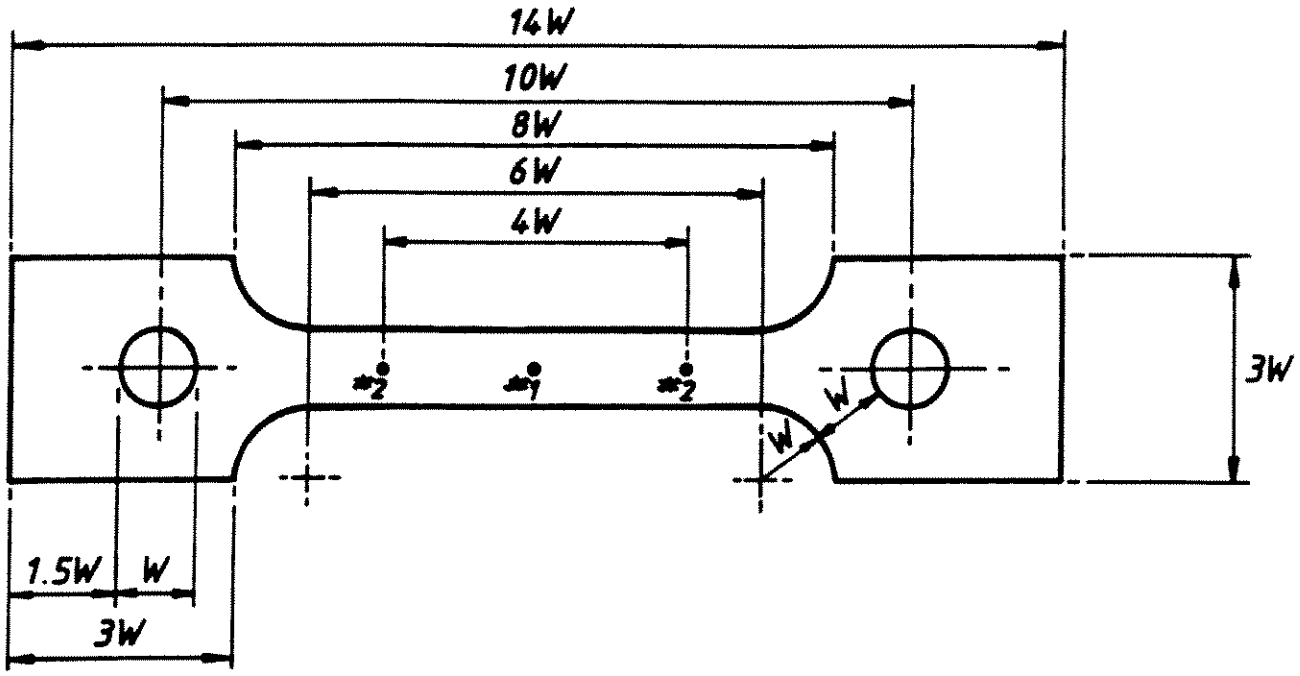

FIGURE 21. THROUGH THICKNESS NOTCHED SENT SPECIMEN GEOMETRY

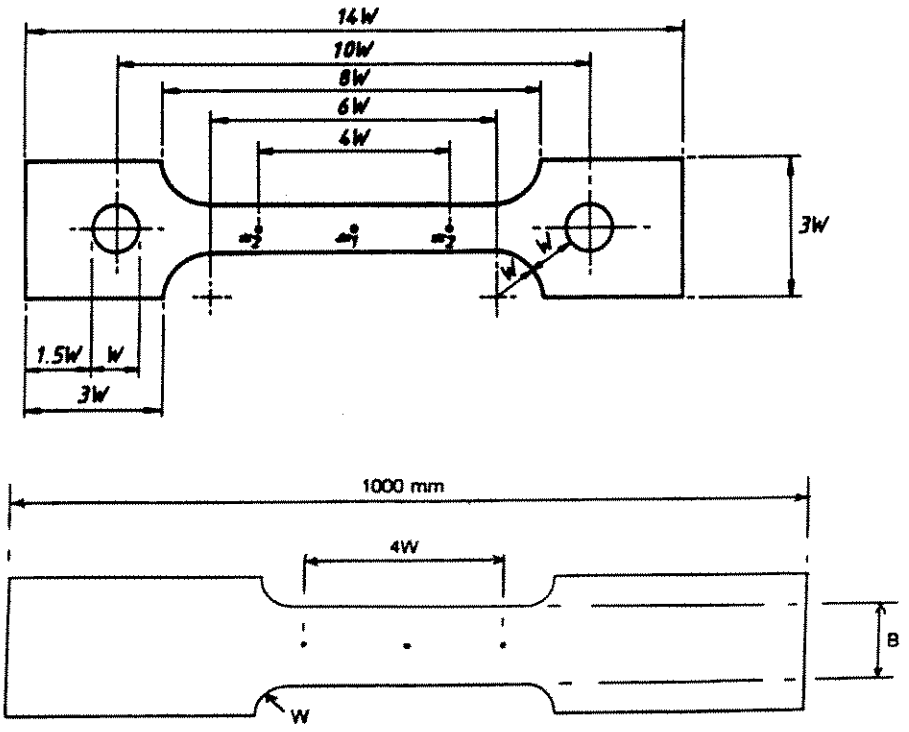

FIGURE 22. SURFACE NOTCHED SENT SPECIMEN GEOMETRIES (ORIGINAL + MODIFIED)

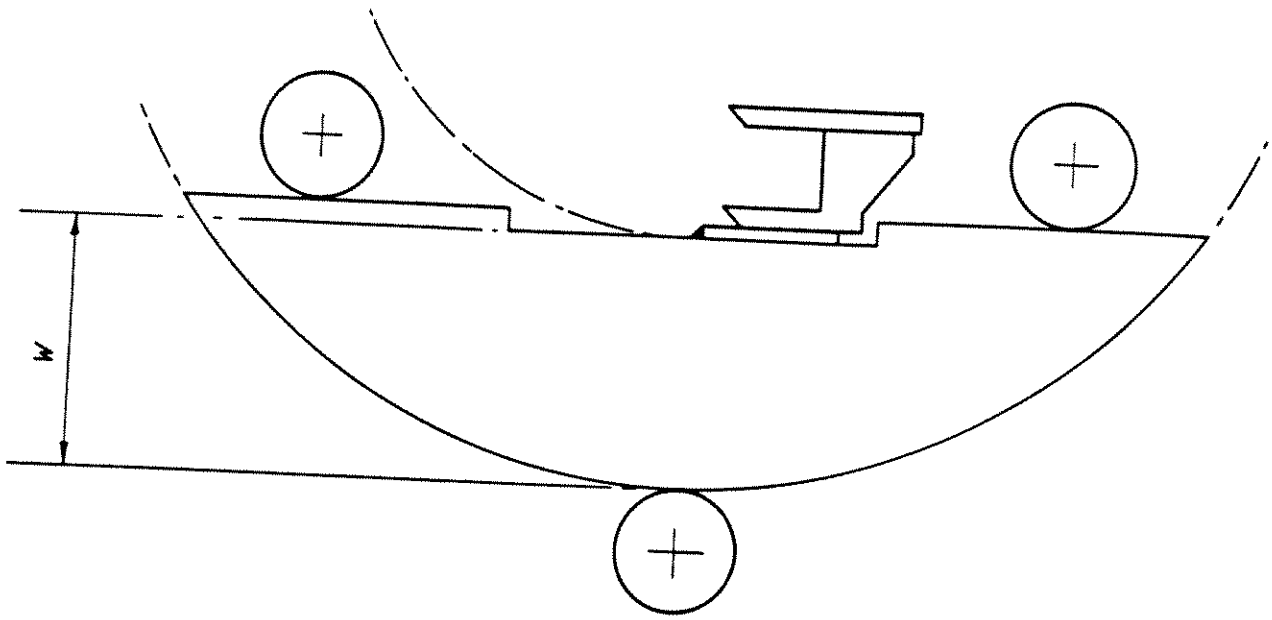

FIGURE 19. MODIFIED SENAB SPECIMEN GEOMETRY

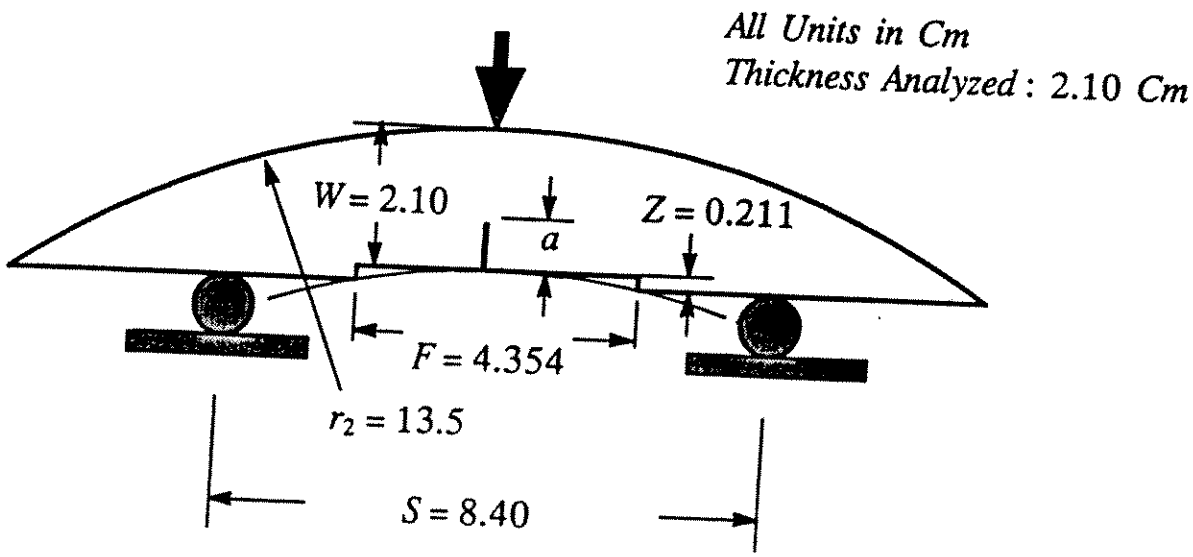

FIGURE 20. FINAL U.S. SENAB SPECIMEN GEOMETRY FOR PIPE MATERIAL M4

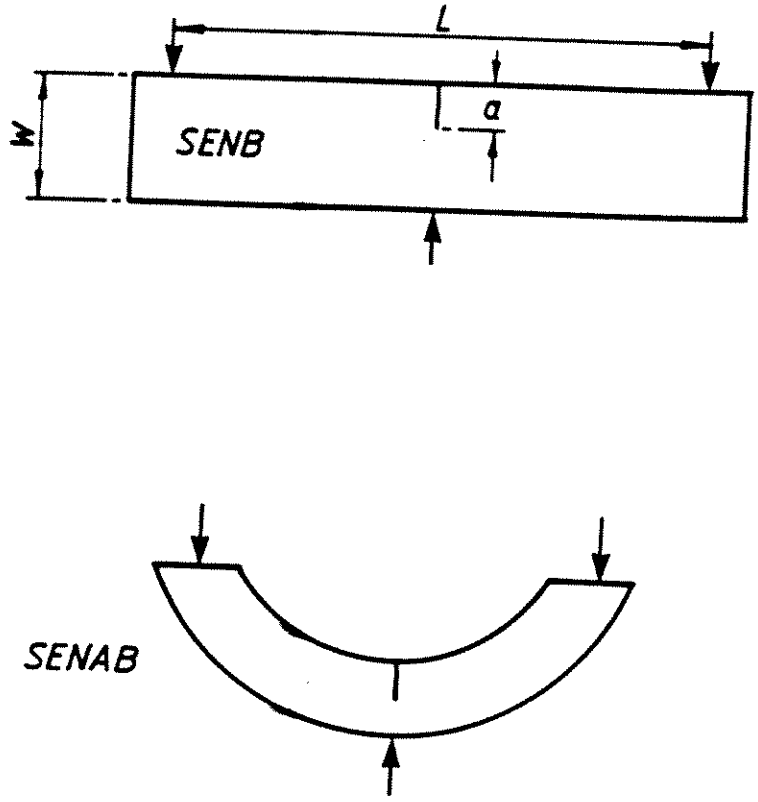

FIGURE 18. COMPARISON OF SPECIMEN GEOMETRIES

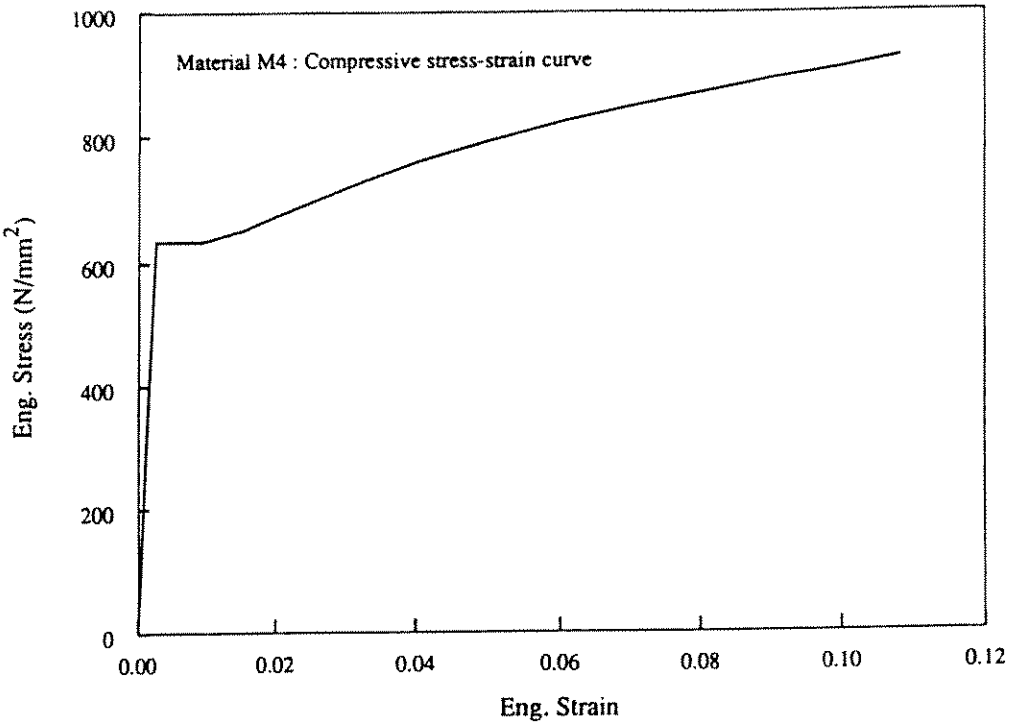

FIGURE 16. COMPRESSIVE ENGINEERING STRESS-STRAIN CURVE FOR MATERIAL M4

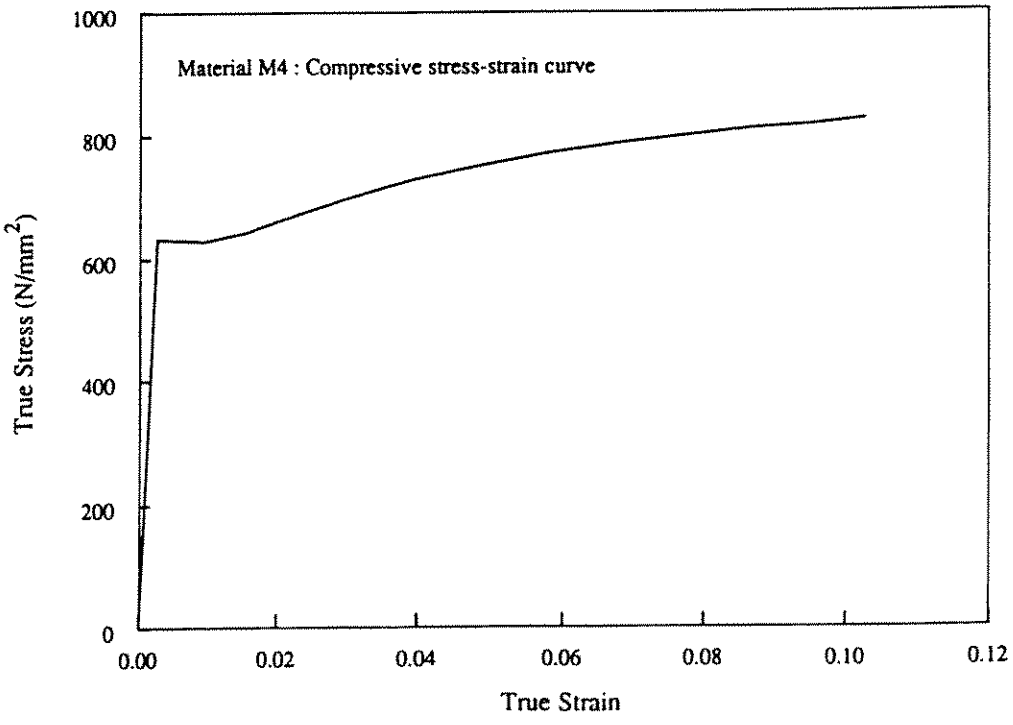

FIGURE 17. COMPRESSIVE TRUE STRESS-STRAIN CURVE FOR MATERIAL M4

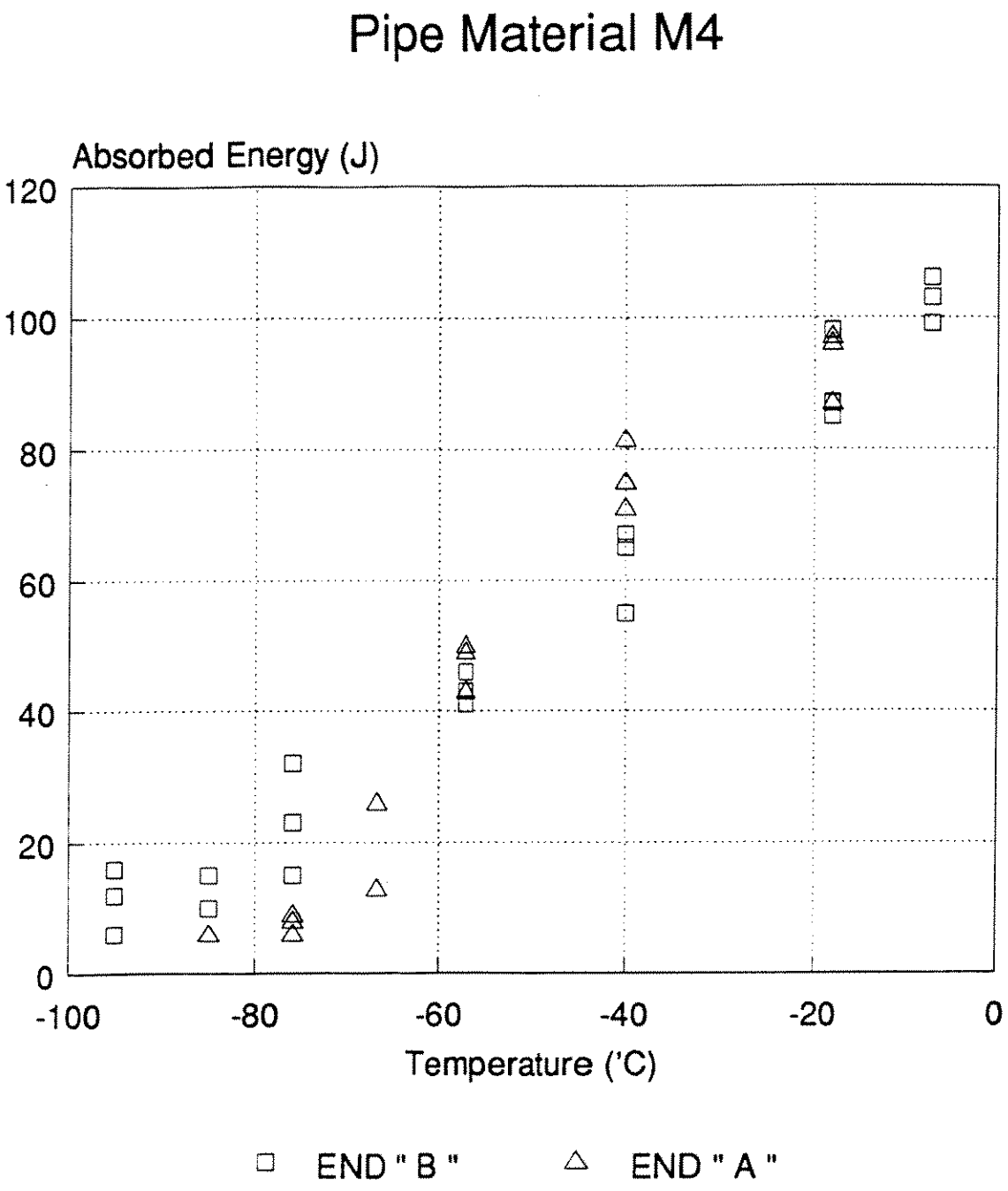

FIGURE 12. CHARPY V-NOTCH TRANSITION CURVES FROM ENDS A AND B OF PIPE MATERIAL M4

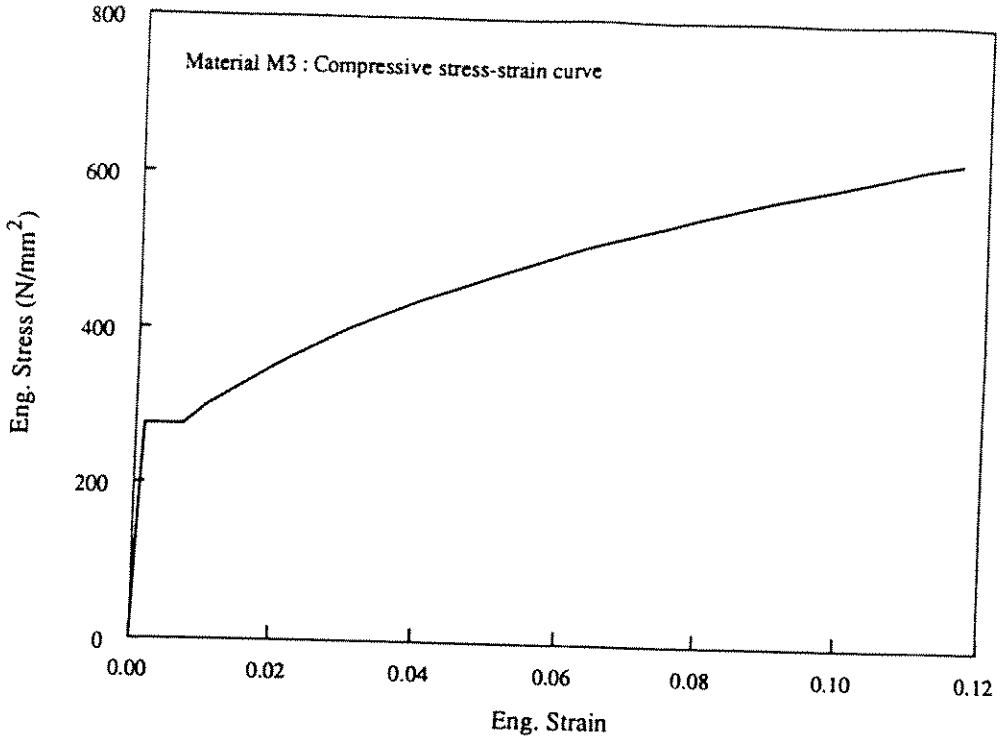

FIGURE 10. COMPRESSIVE ENGINEERING STRESS-STRAIN CURVE FOR MATERIAL M3

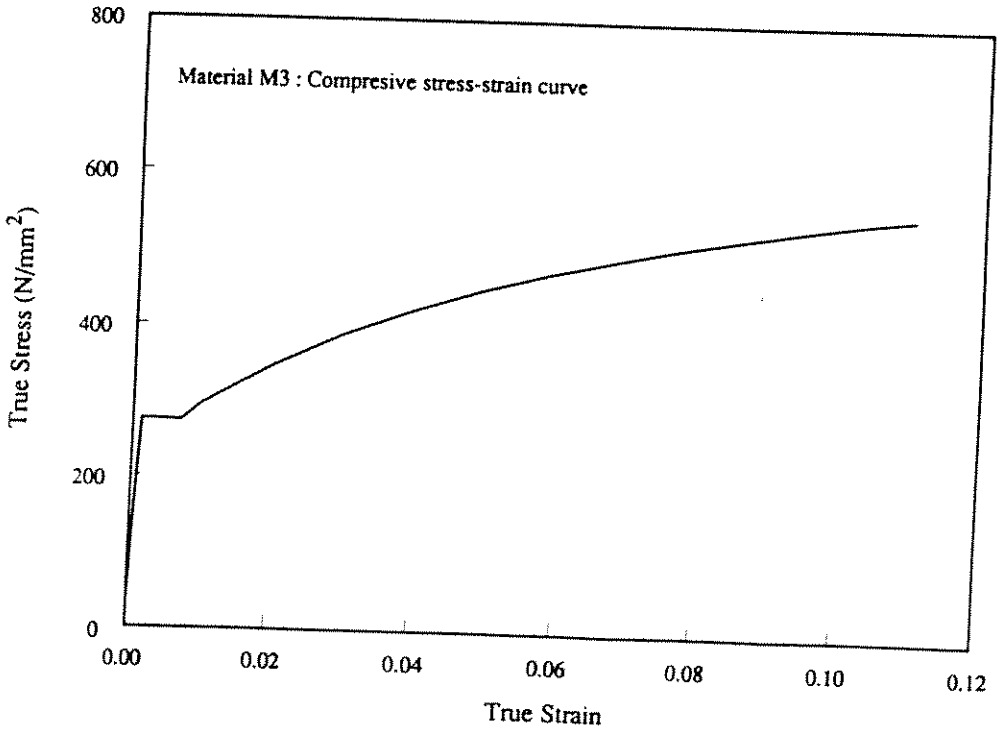

FIGURE 11. COMPRESSIVE TRUE STRESS-STRAIN CURVE FOR MATERIAL M3

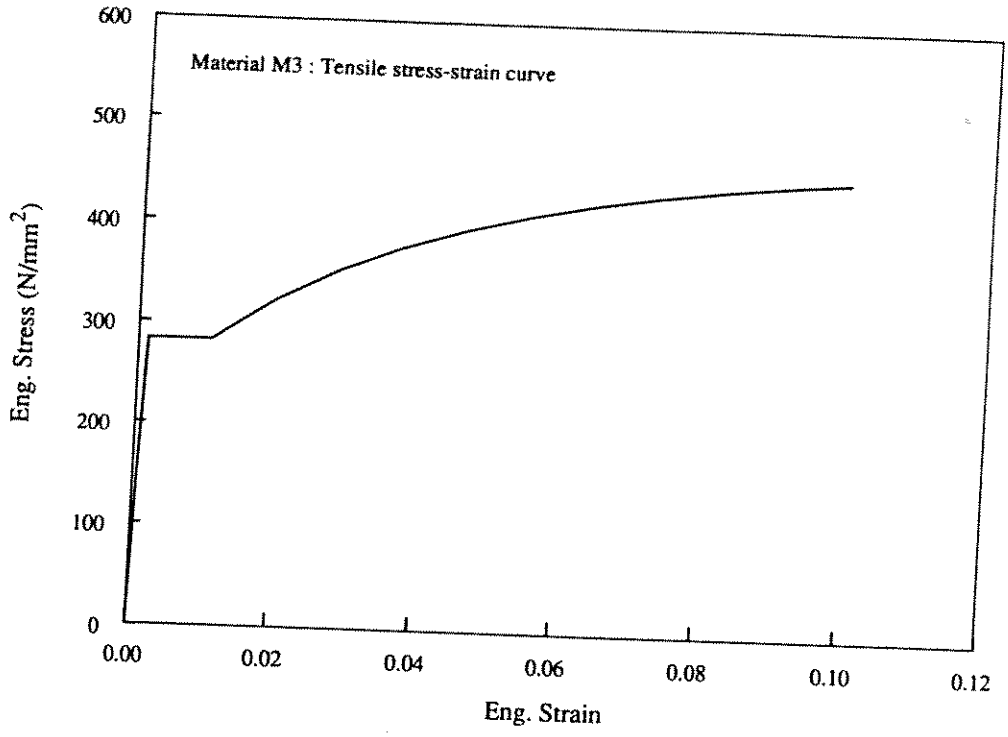

FIGURE 8. TENSILE ENGINEERING STRESS-STRAIN CURVE FOR MATERIAL M3

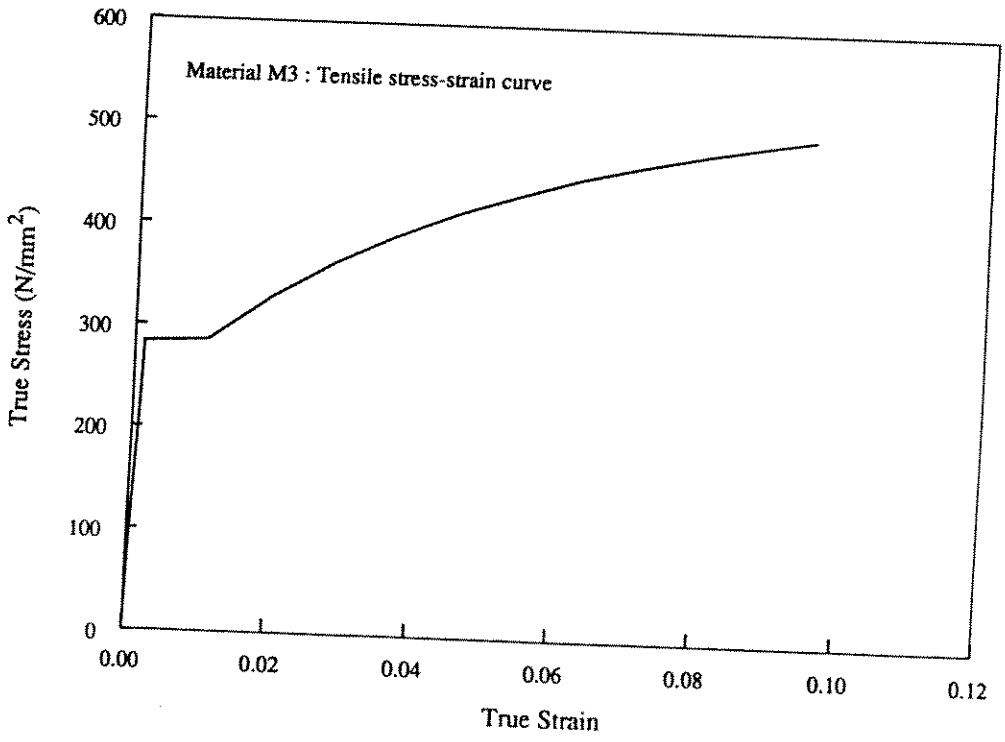

FIGURE 9. TENSILE TRUE STRESS-STRAIN CURVE FOR MATERIAL M3

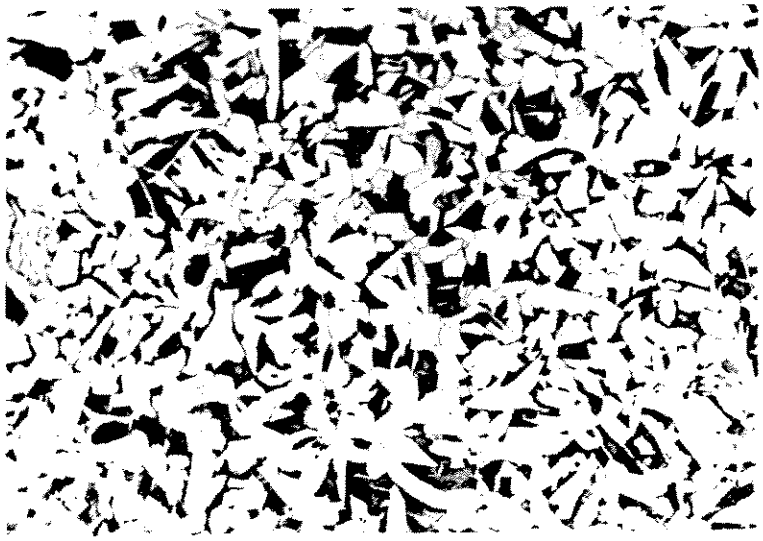

(A) ×100 Negative No. 6098-3-10

(B) ×100 Negative No. 6098-3-11

(C) ×100 Negative No. 6098-3-12

FIGURE 7. PLATE MATERIAL M3 MICROSTRUCTURE [(A) TOP SURFACE, (B) MID-THICKNESS AND (C) BOTTOM SURFACE]

(A) ·100 Negative No. 6098-6

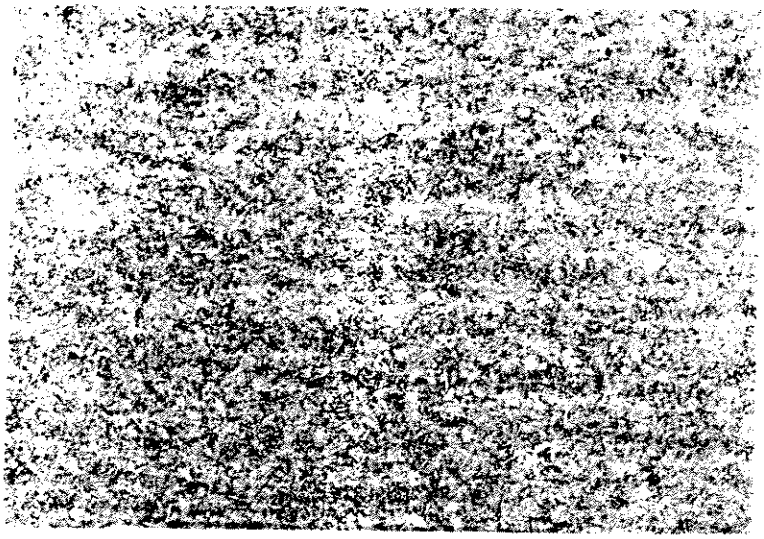

(B) ·100 Negative No. 6098-4

(C) ·100 Negative No. 6098-2

FIGURE 13. PIPE MATERIAL M4 MICROSTRUCTURE [(A) OUTSIDE SURFACE, (B) MID THICKNESS AND (C) INSIDE SURFACE]

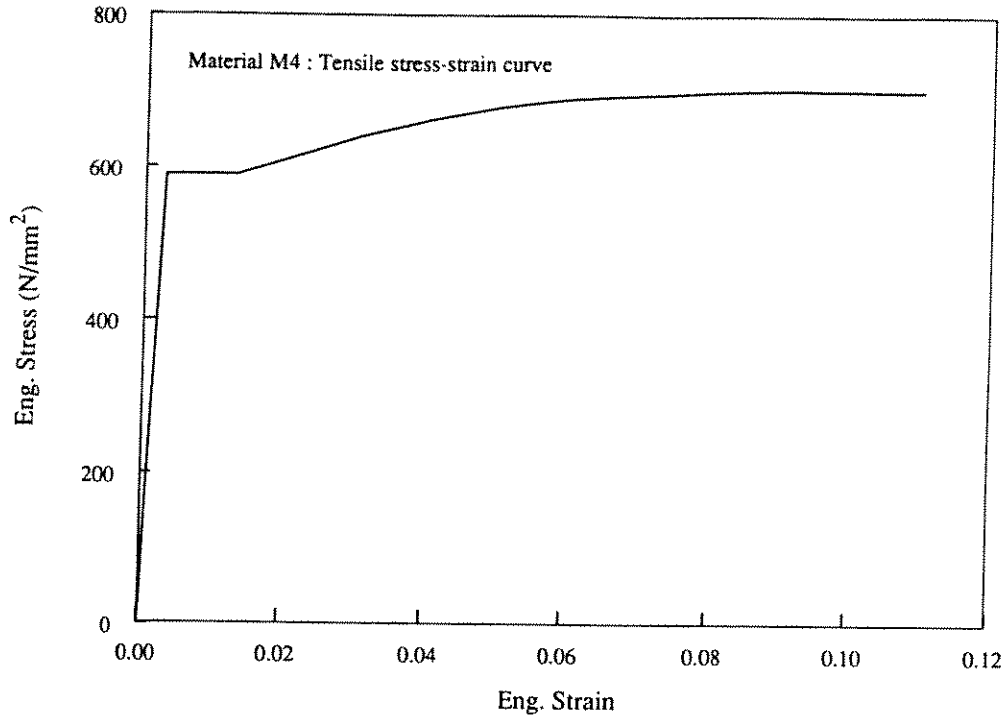

FIGURE 14. TENSILE ENGINEERING STRESS-STRAIN CURVE FOR MATERIAL M4

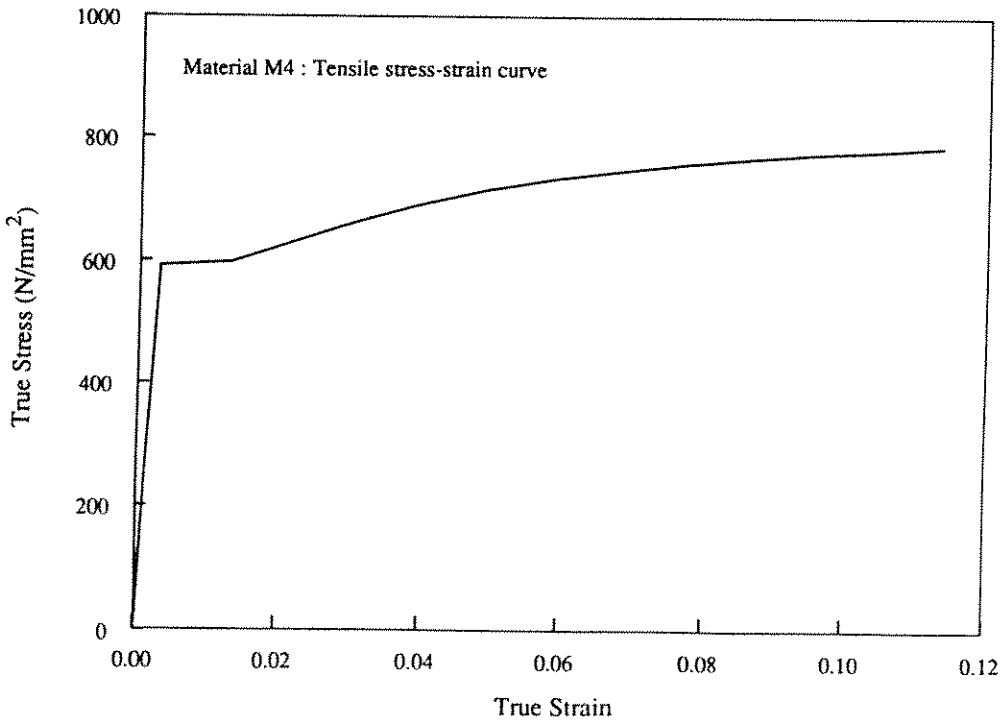

FIGURE 15. TENSILE TRUE STRESS-STRAIN CURVE FOR MATERIAL M4

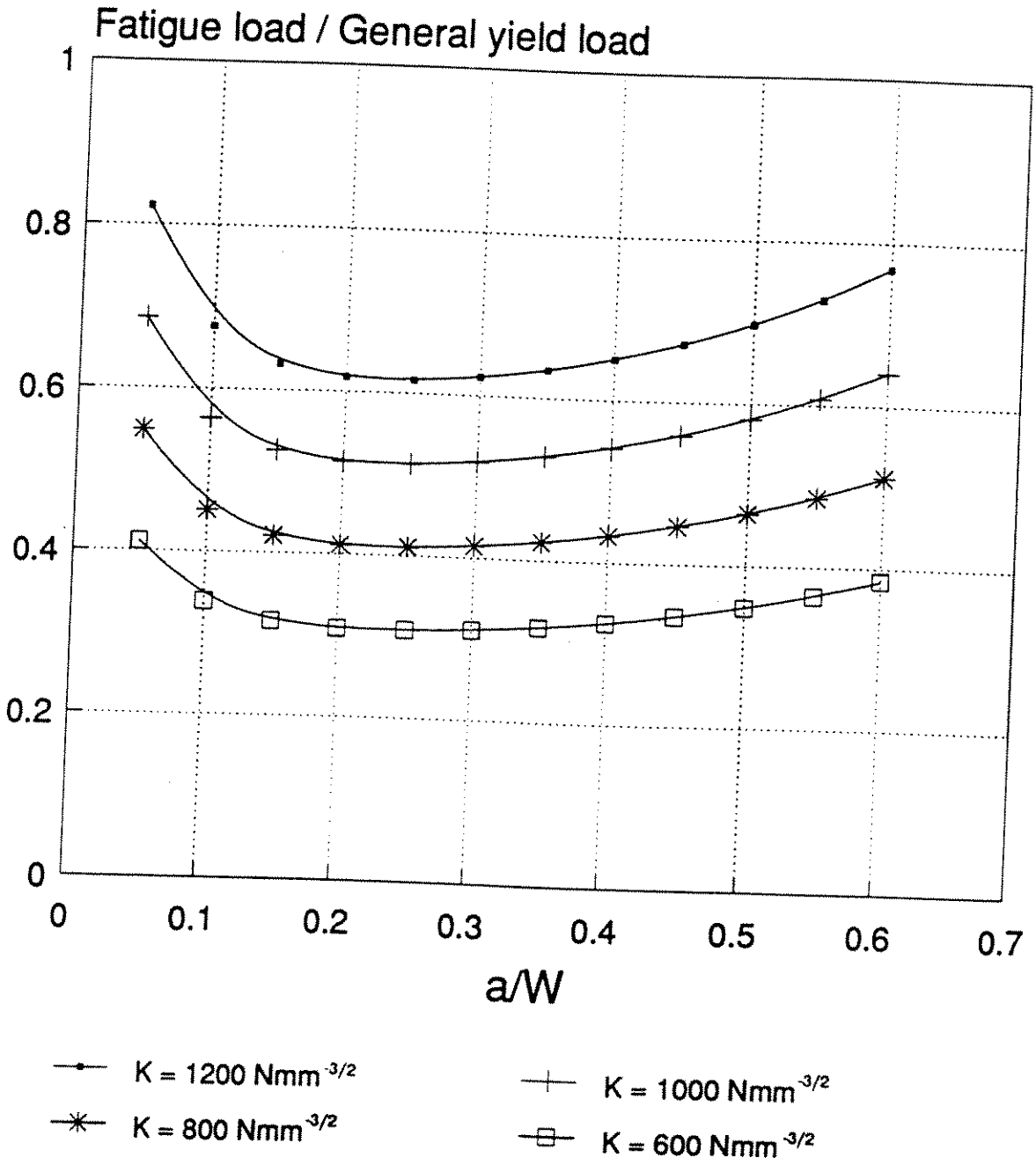

FIGURE 23. COMPARISON OF FATIGUE LOADS FOR EUROPEAN PLATE MATERIAL M1

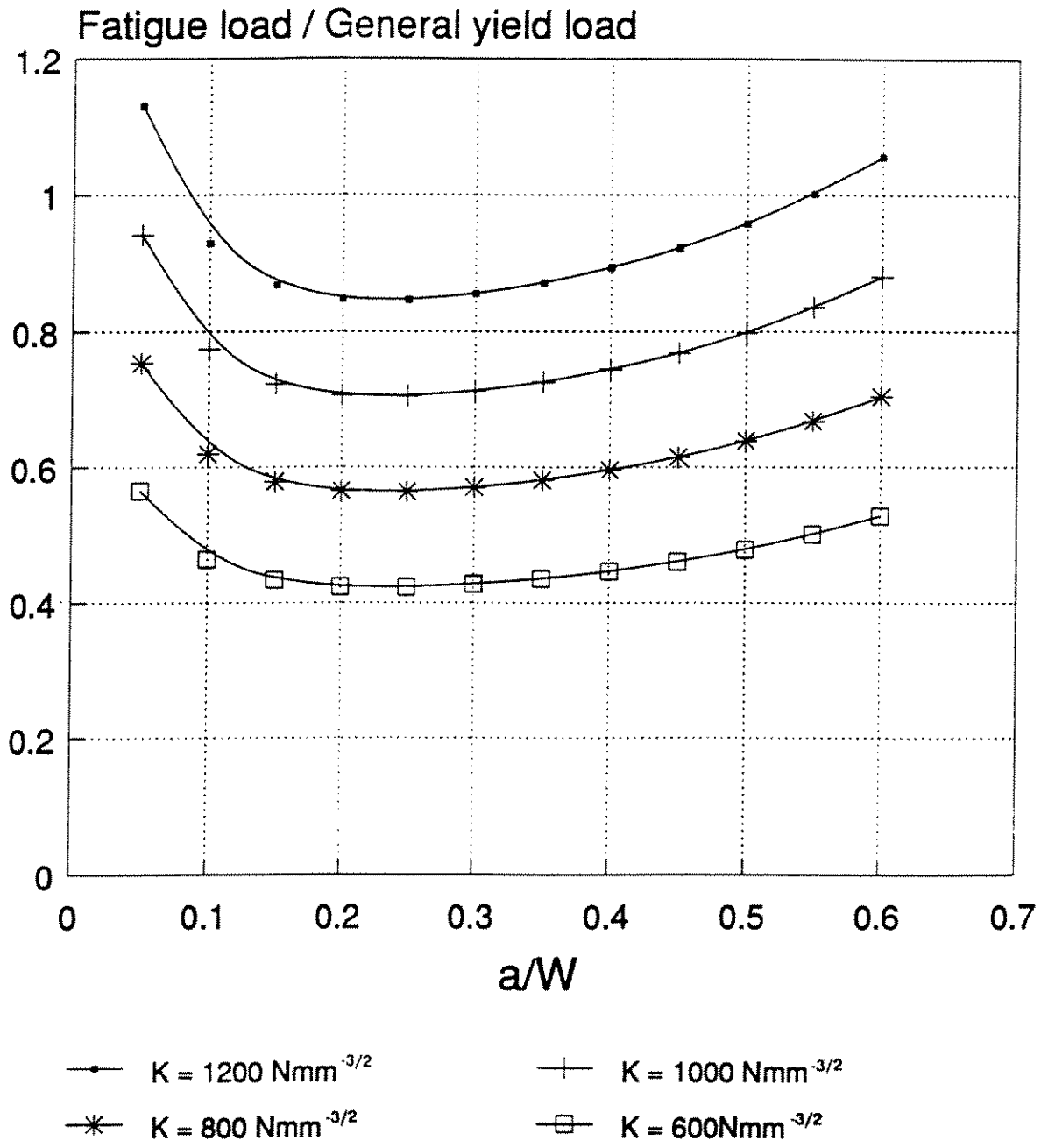

FIGURE 24. COMPARISON OF FATIGUE LOADS FOR NORTH AMERICAN PLATE MATERIAL M3

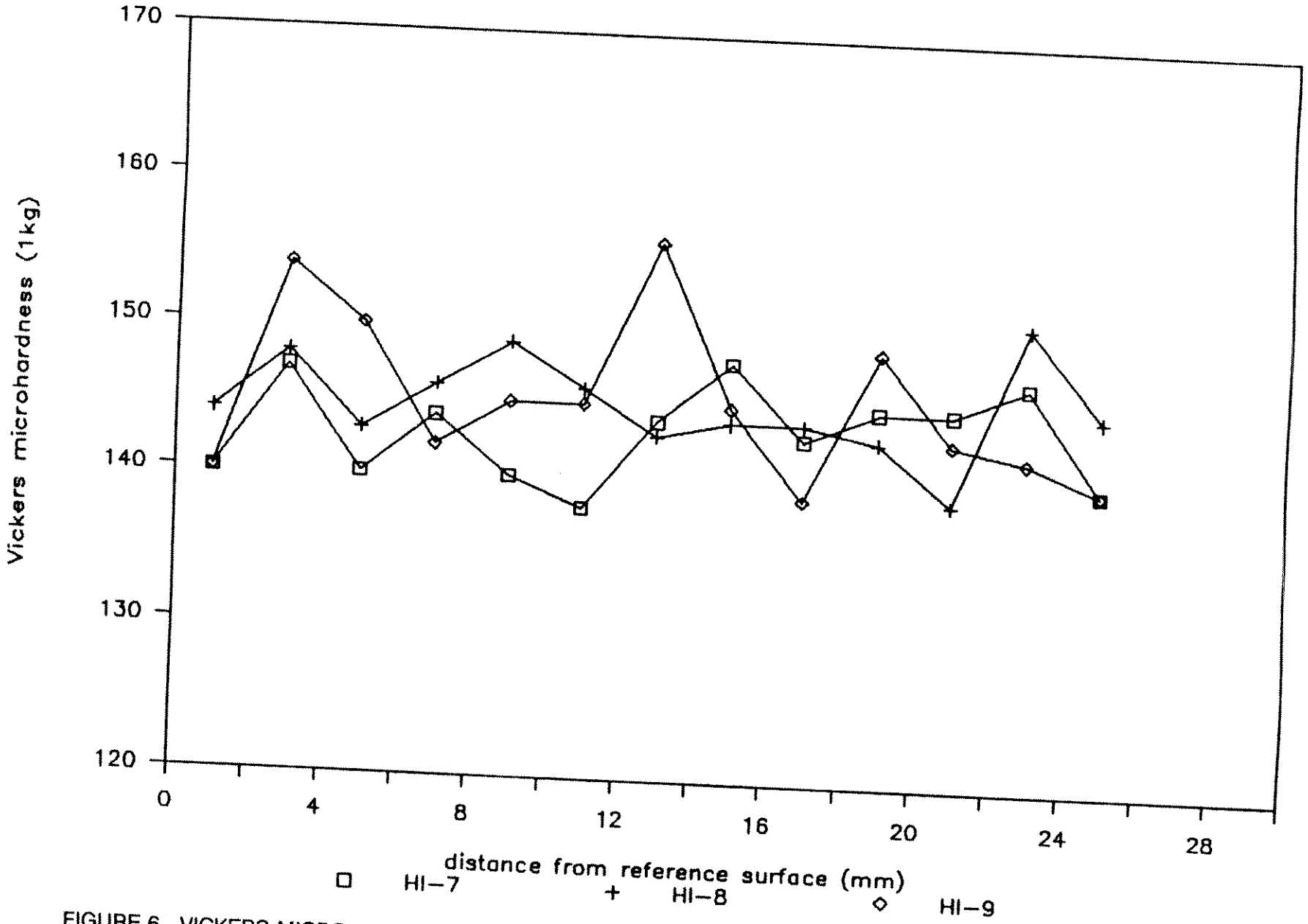

FIGURE 6. VICKERS MICROHARDNESS SURVEY THROUGH THICKNESS OF PLATE M3 (LOCATIONS HI-7, -8 AND -9)

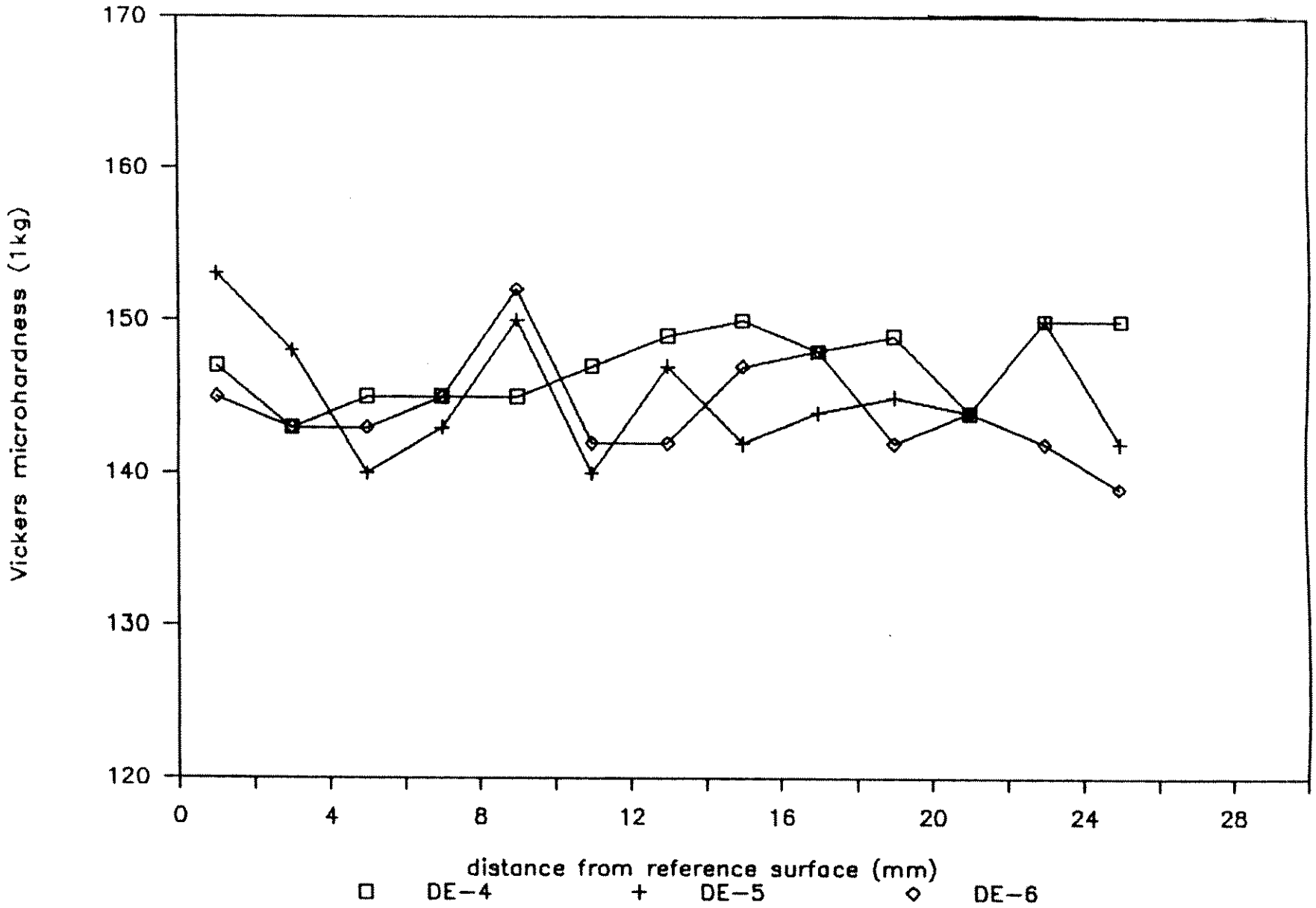

FIGURE 5. VICKERS MICROHARDNESS SURVEY THROUGH THICKNESS OF PLATE M3 (LOCATIONS DE-4, -5 AND -6)

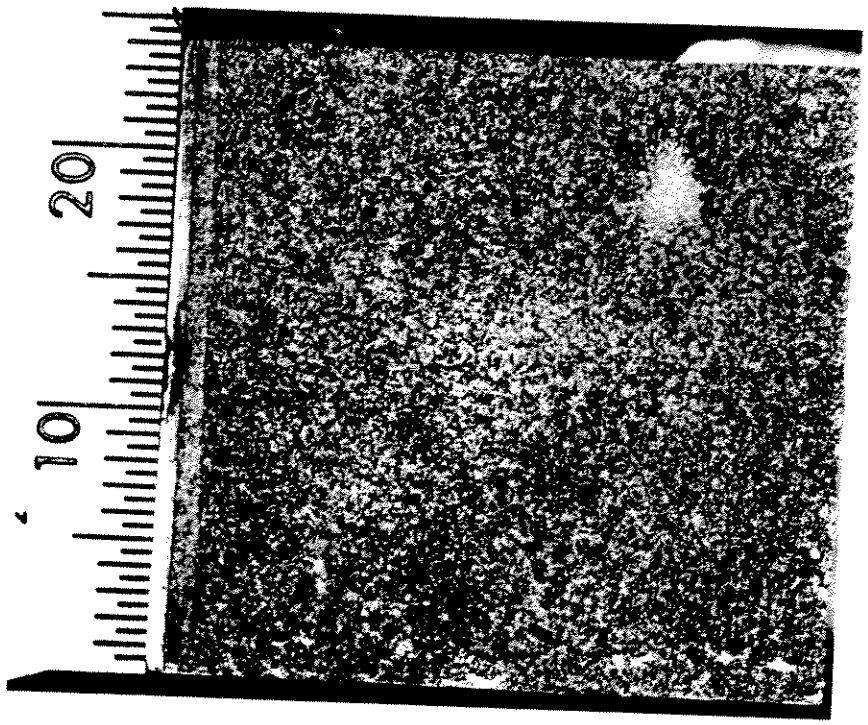

(A) Specimen M3-114, a/W = 0.05

Negative No. M92-04(

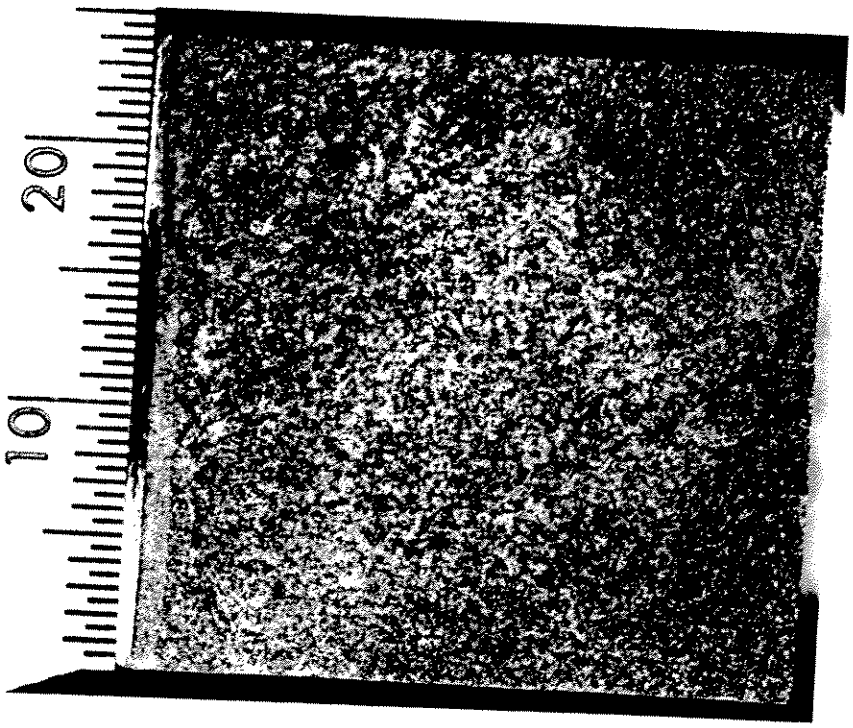

(B) Specimen M3-118, a/W = 0.05

Negative No. M92-04

FIGURE 25. FRACTURE FACES OF SHALLOW-CRACKED SENB SPECIMENS

×50

Negative No. 6098-8

FIGURE 28. SECTION THROUGH SHIM PLATE TIG WELD

Negative No. 6098-1-15

FIGURE 29. PHOTOGRAPH OF SENB WITH SHIM PLATE/KNIFE EDGE ASSEMBLY AND CLIP GAUGES

Negative No. 6098-1-14

FIGURE 30. PHOTOGRAPH OF SENAB WITH SHIM PLATE/KNIFE EDGE ASSEMBLY AND CLIP GAUGES

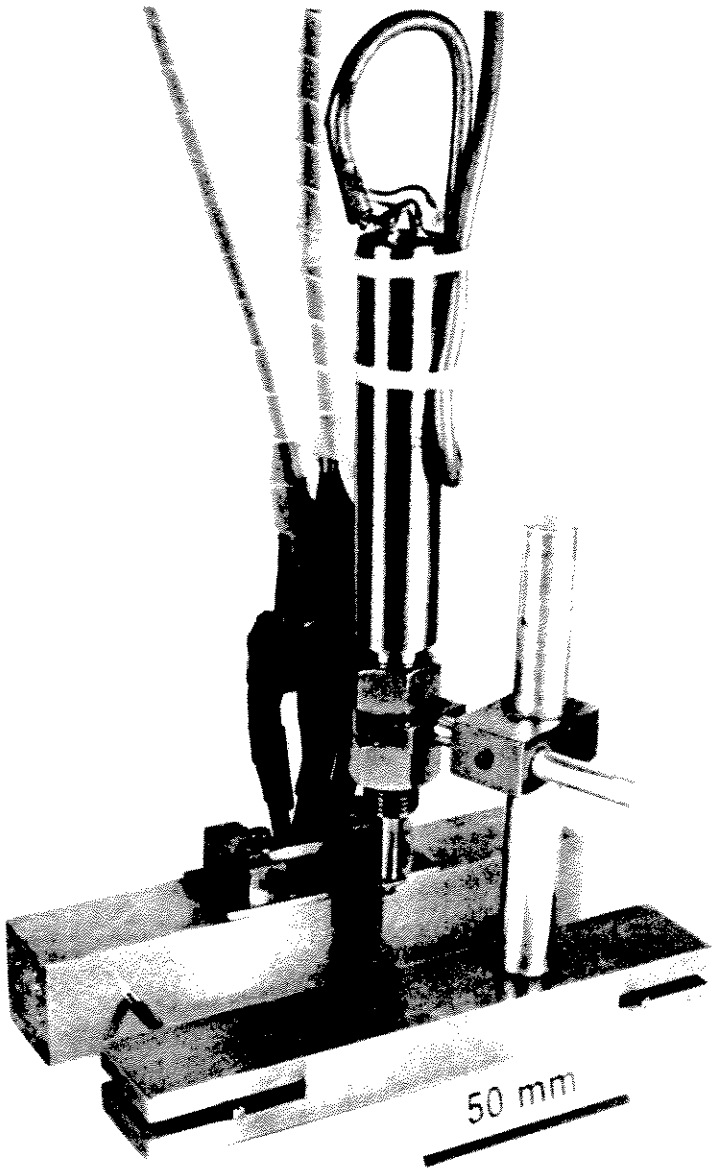

Negative No. 6098-1-15

FIGURE 31. SENB COMPARATOR BAR ARRANGEMENT

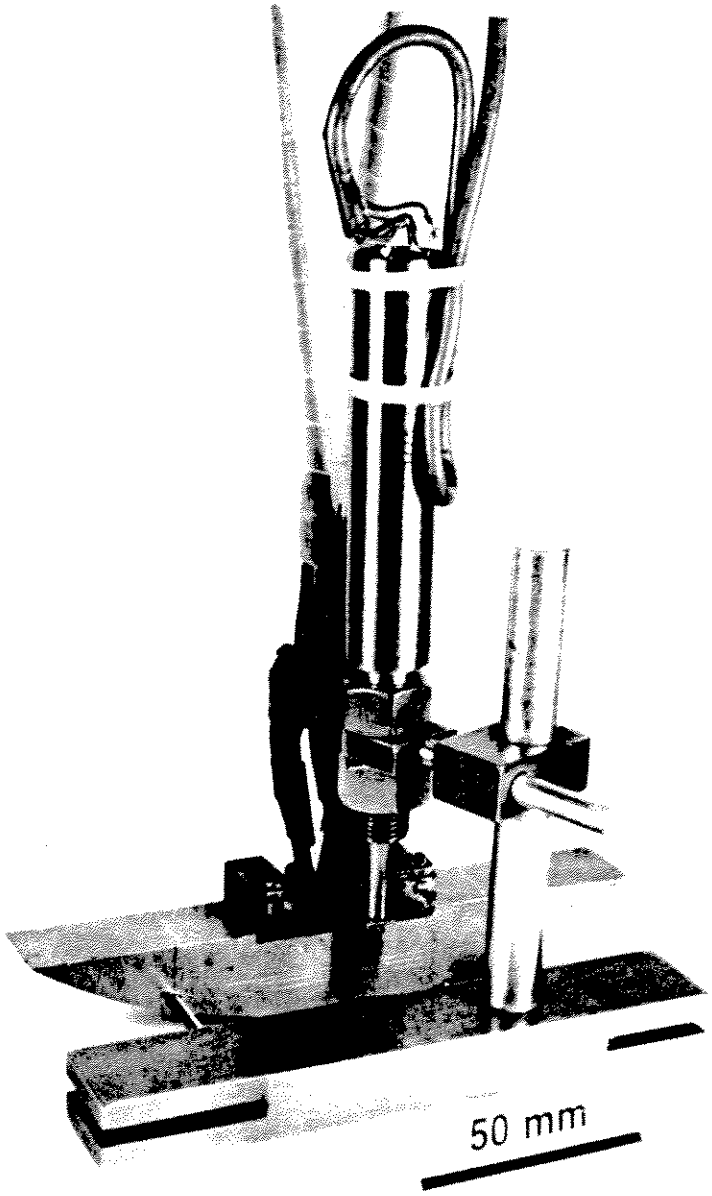

Negative No. 6098-1-17

FIGURE 32. SENAB COMPARATOR BAR ARRANGEMENT

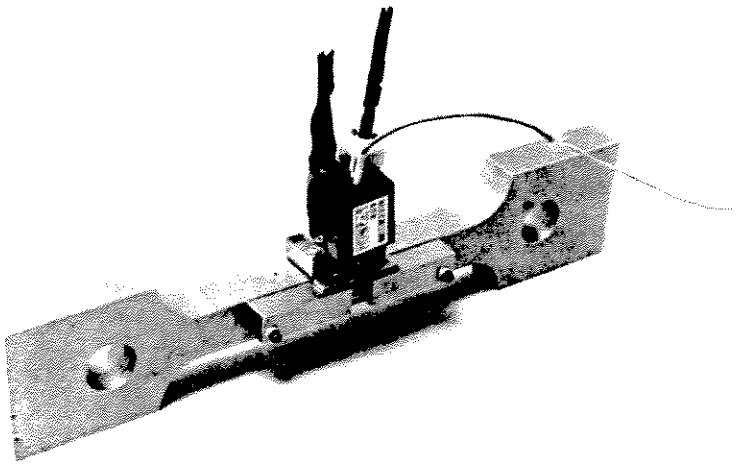

Negative No. 6098-5-6

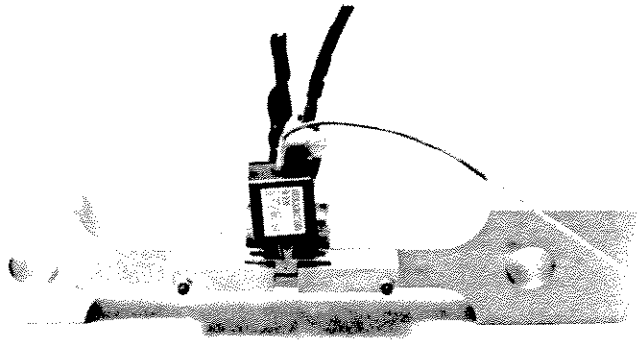

Negative No. 6096-5-4

FIGURE 33. PHOTOGRAPH OF SENT INSTRUMENTATION SET-UP

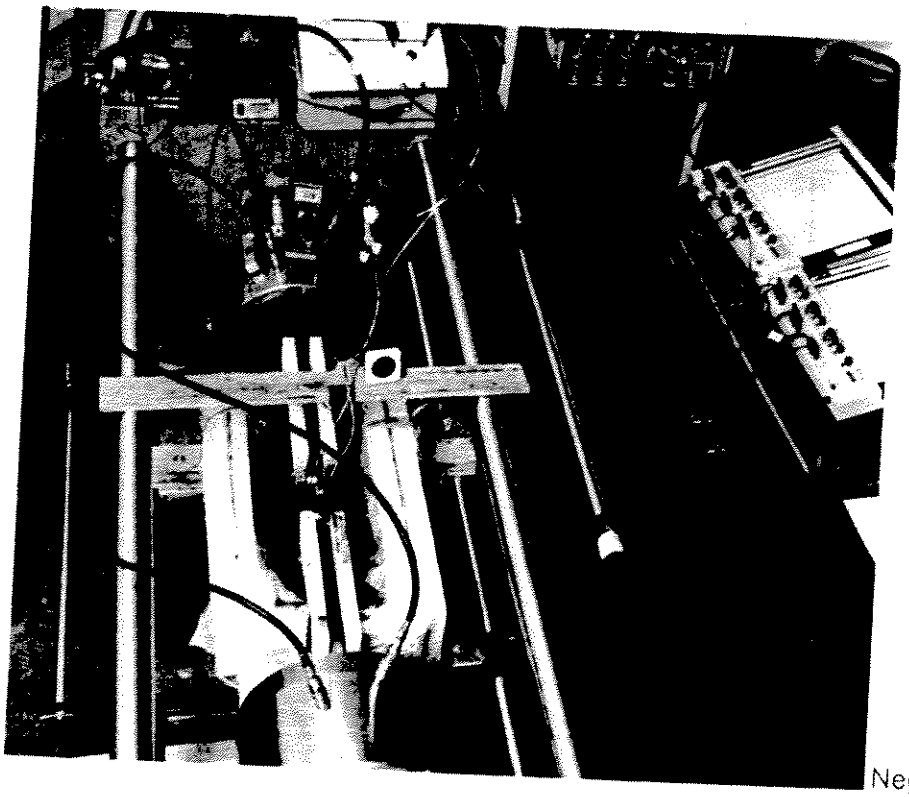

Negative No. 6098-4-9

FIGURE 34. SENT TEST ARRANGEMENT

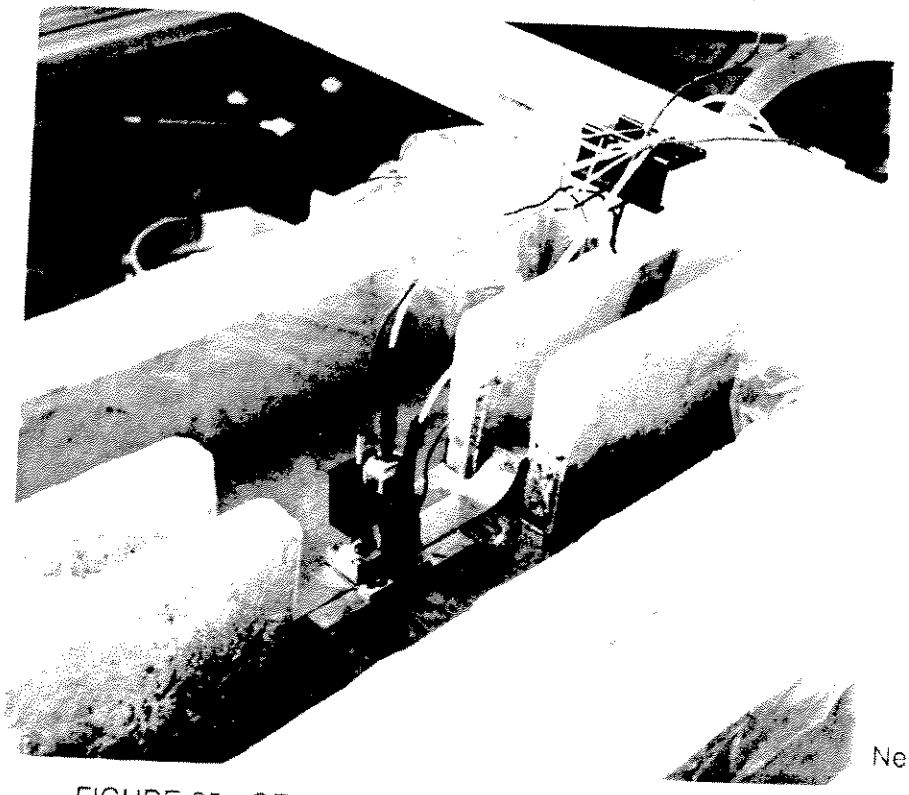

Negative No. 6098-5-1

FIGURE 35. SENT TEST ARRANGEMENT (CLOSE-UP)

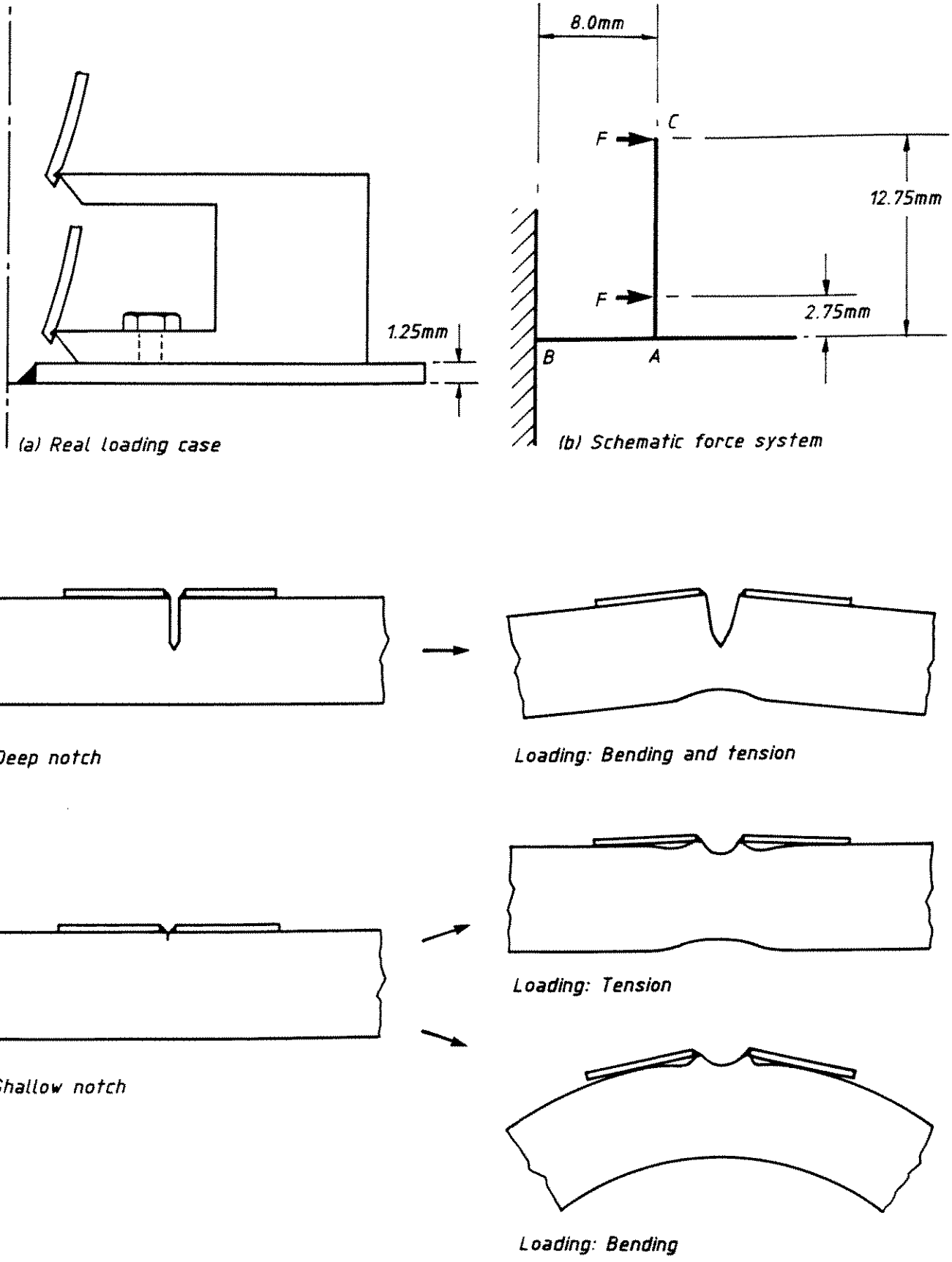

FIGURE 36. CRACK MOUTH OPENING AND SHIM BEHAVIOR

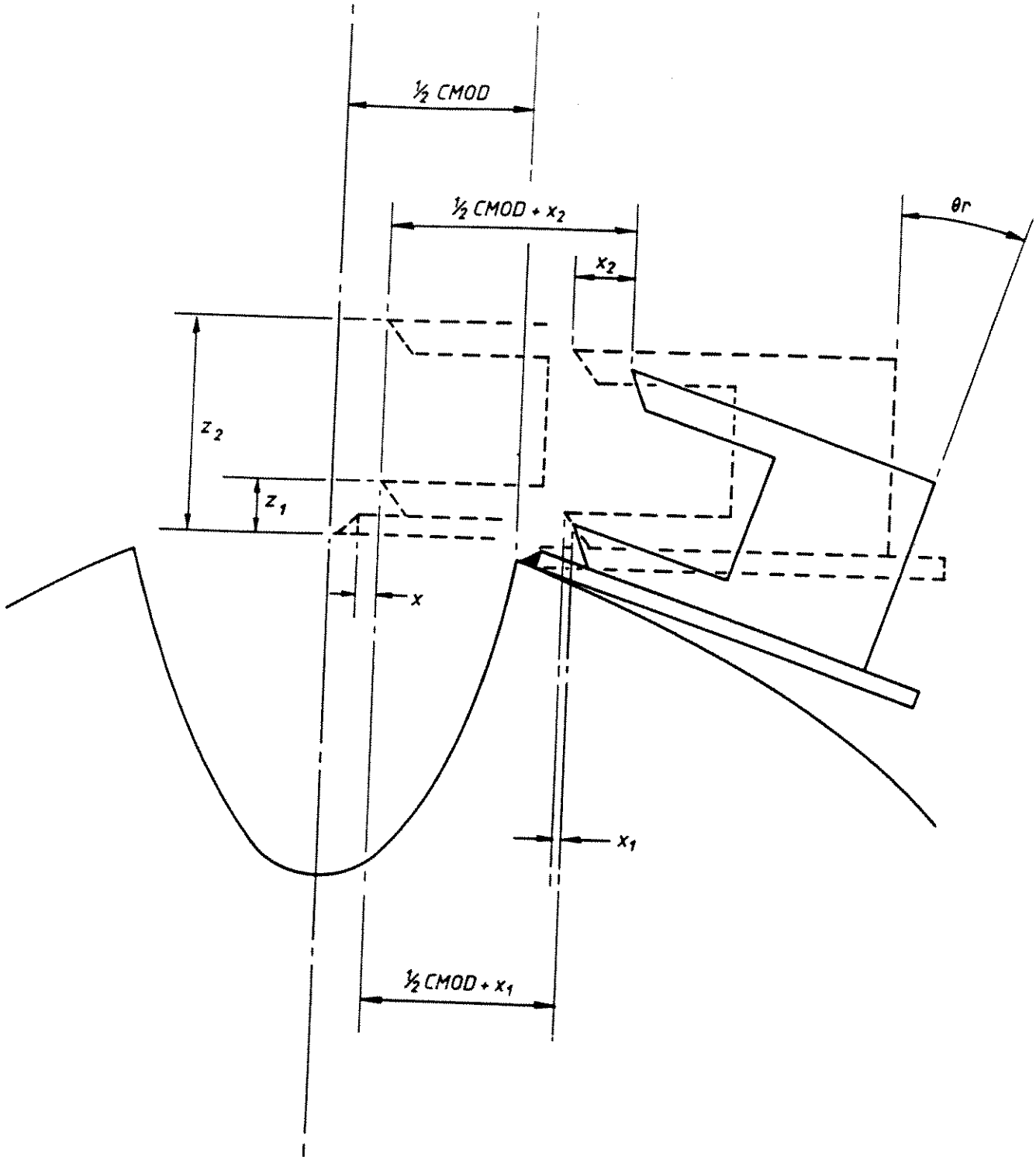

FIGURE 37. EFFECT OF KNIFE EDGE ROTATION ON MEASUREMENT OF CMOD

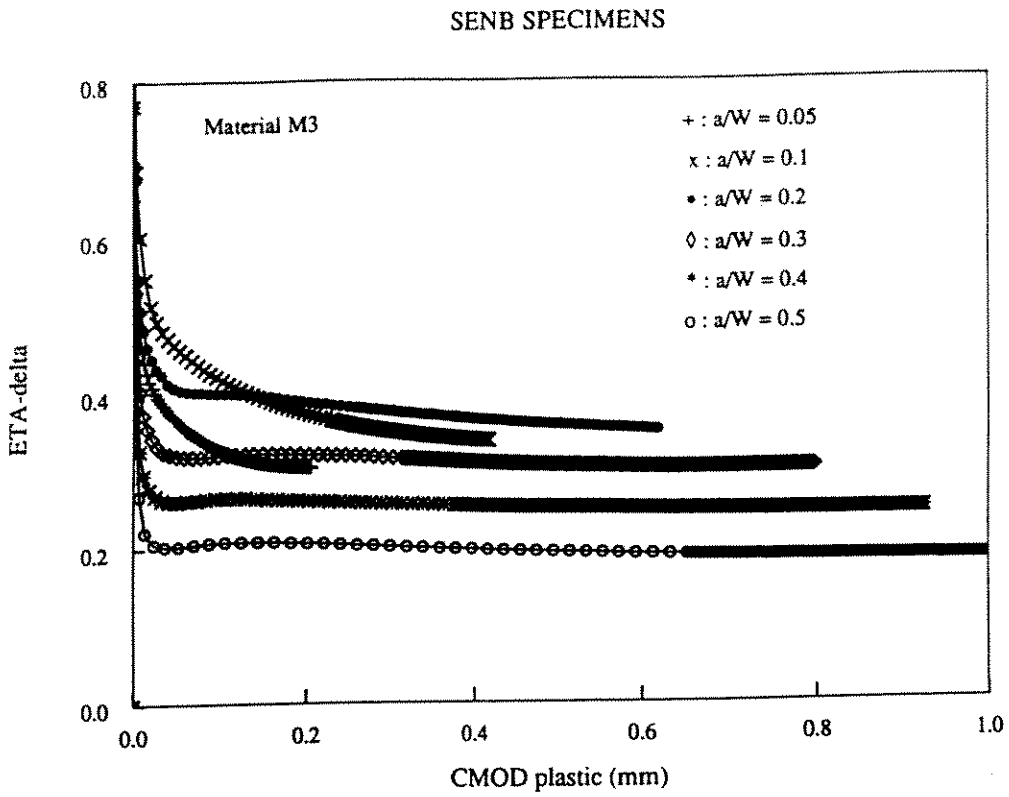

FIGURE 38. VARIATION OF η_δ WITH $CMOD_{PL}$ (SENB: MATERIAL M3)

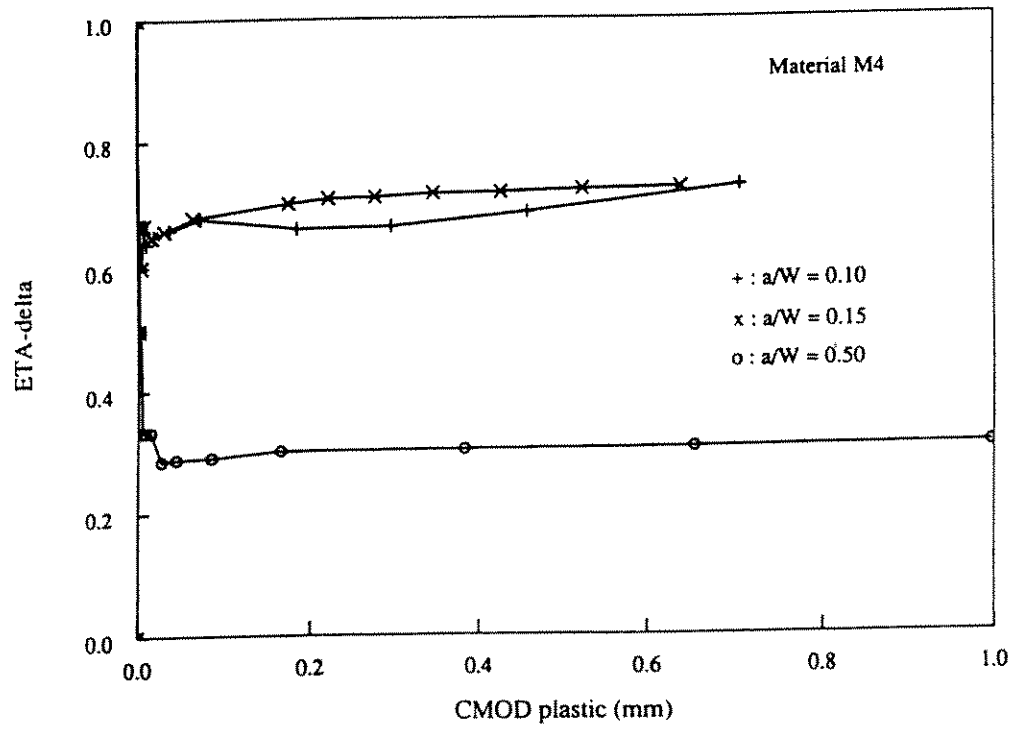

FIGURE 39. VARIATION OF η_δ WITH $CMOD_{PL}$ (SENAB: MATERIAL M4)

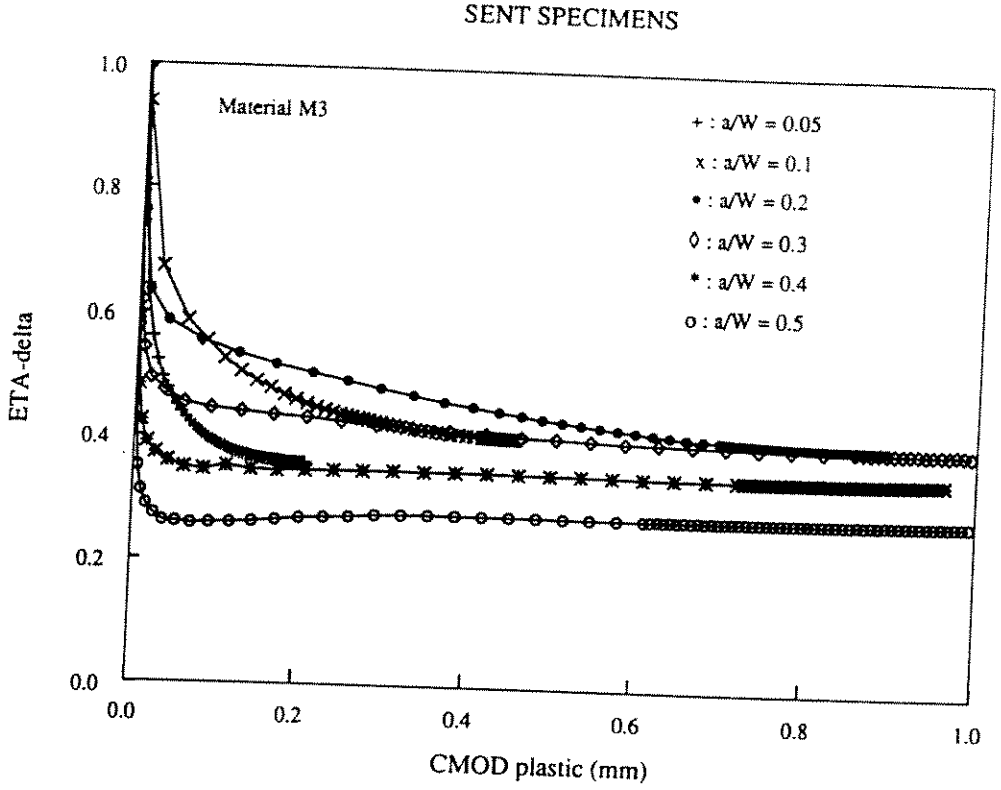

FIGURE 40. VARIATION OF η_δ WITH $CMOD_{PL}$ (SENT: MATERIAL M3)

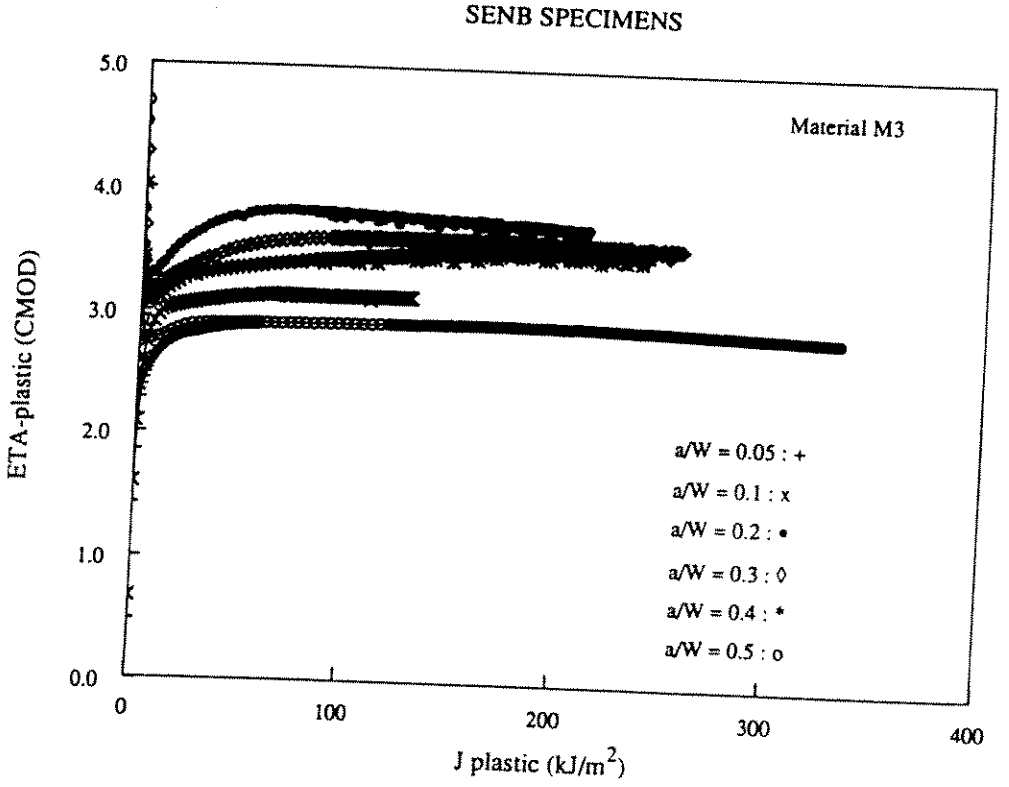

FIGURE 41. VARIATION OF η_c WITH J_{PL} (SENB: MATERIAL M3)

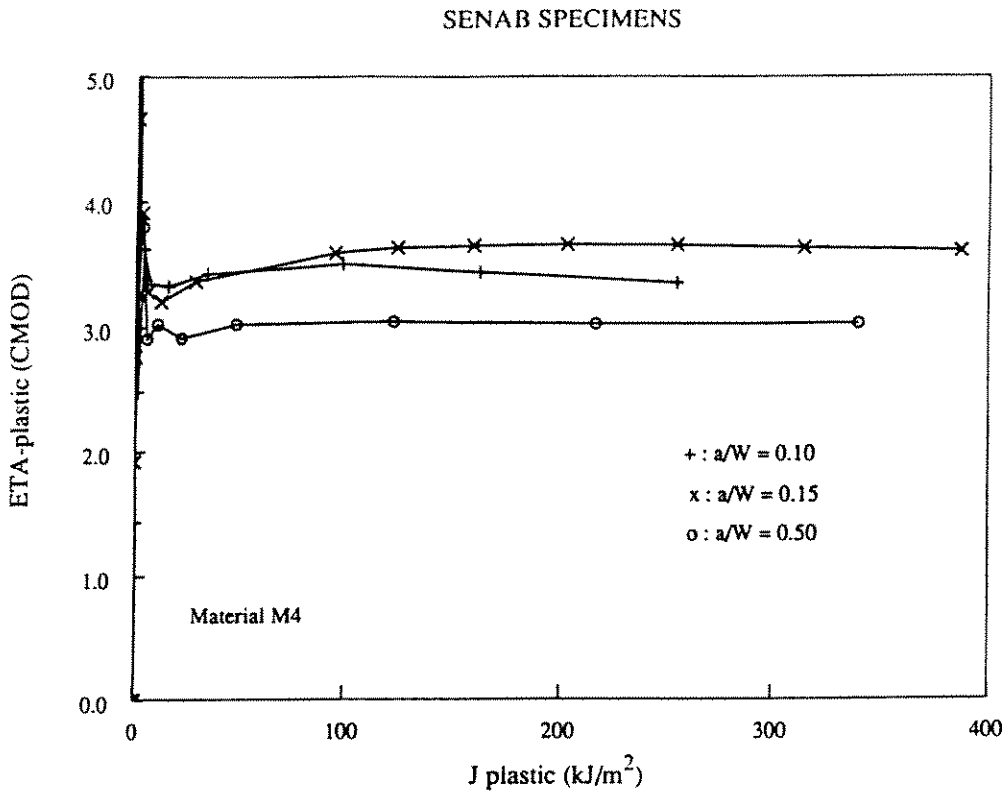

FIGURE 42. VARIATION OF η_c WITH J_{PL} (SENAB: MATERIAL M4)

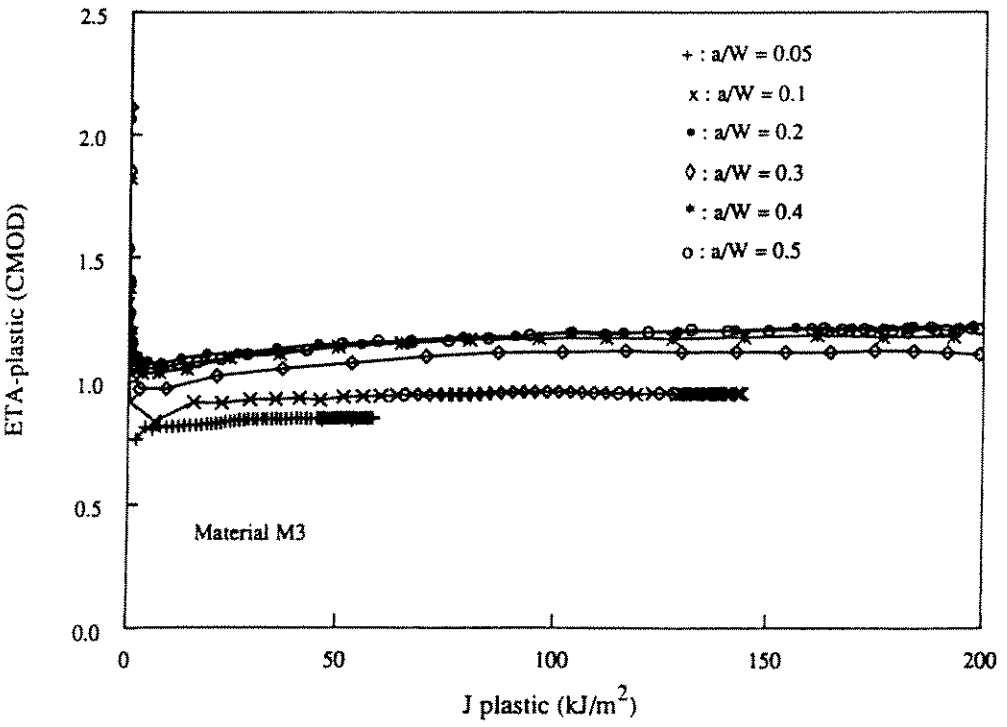

FIGURE 43.VARIATION OF η_c WITH J_{PL} (SENT: MATERIAL M3)

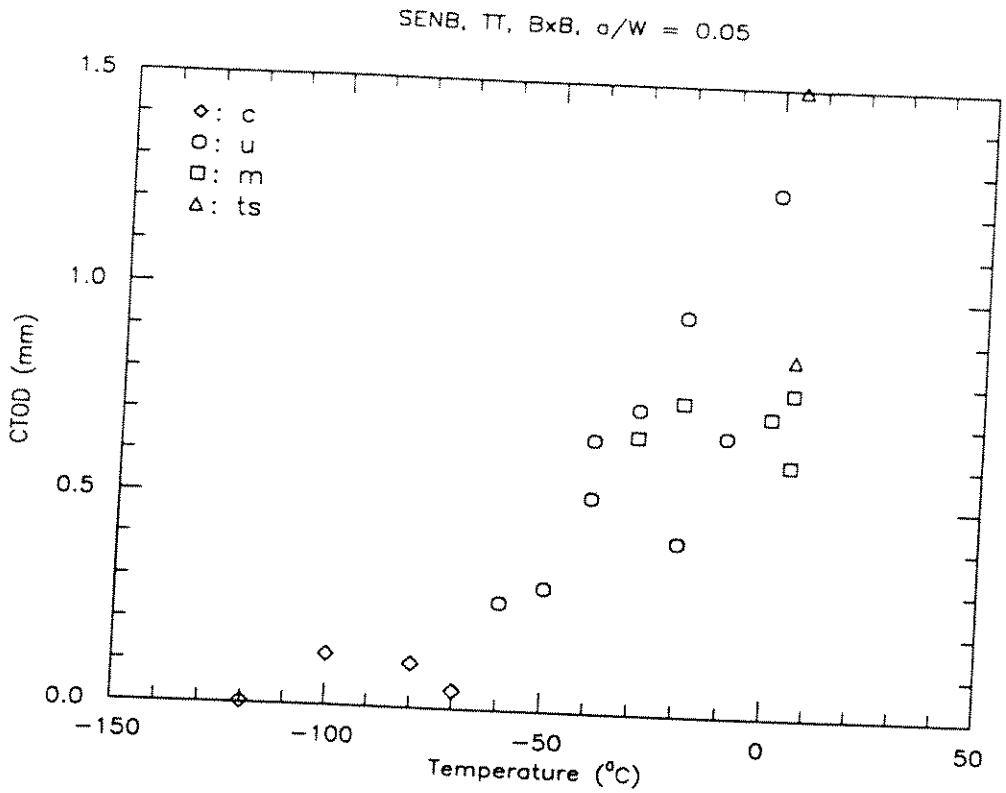

FIGURE 44. CTOD TRANSITION CURVE (SENB, B × B, a/W = 0.05, THROUGH THICKNESS NOTCHED)

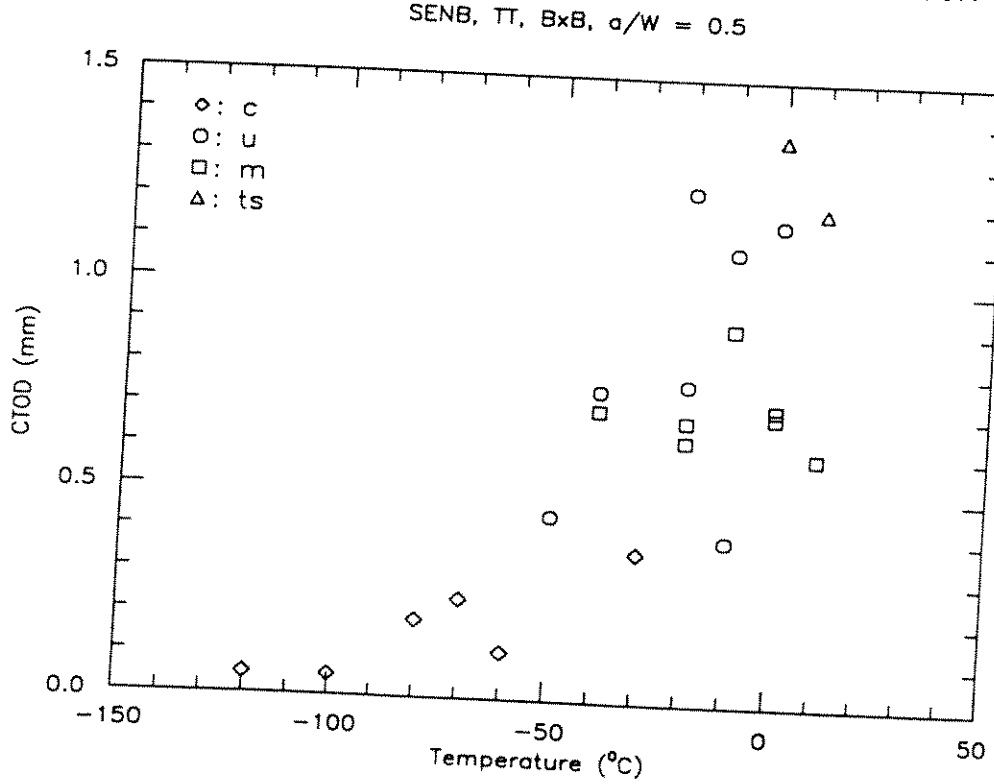

FIGURE 45. CTOD TRANSITION CURVE (SENB, B × B, a/W = 0.5, THROUGH THICKNESS NOTCHED)

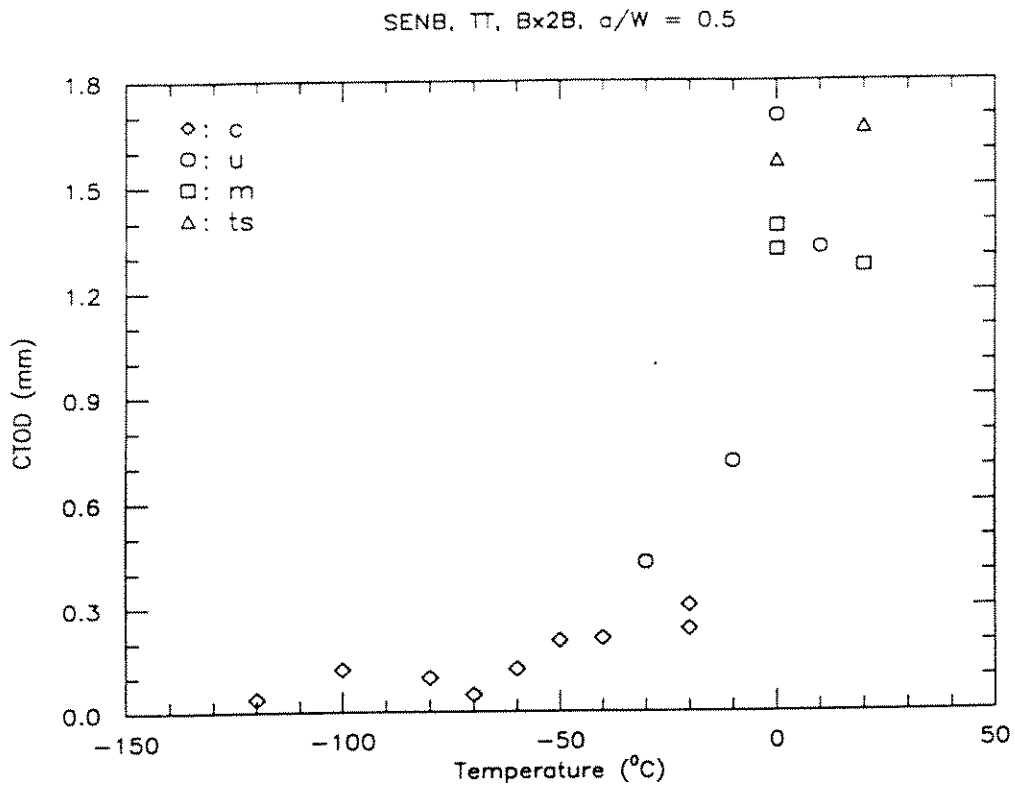

FIGURE 46. CTOD TRANSITION CURVE (SENB, B × 2B, a/W = 0.5, THROUGH THICKNESS NOTCHED)

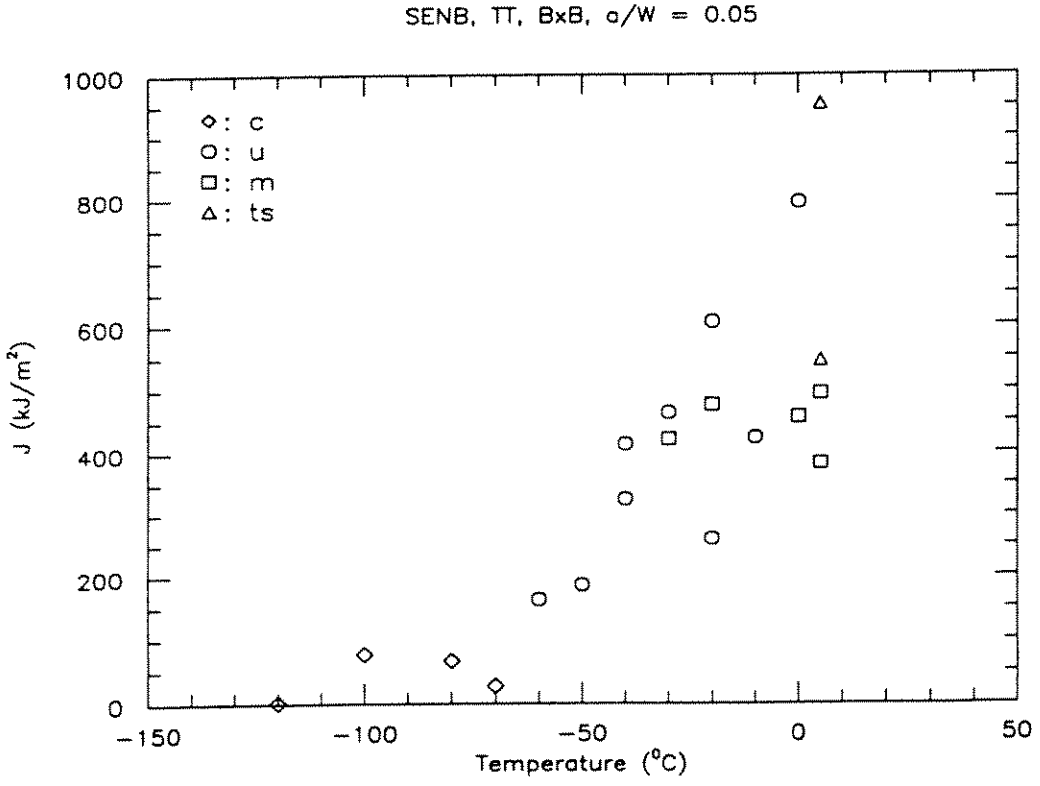

FIGURE 47. J TRANSITION CURVE (SENB, B × B, a/W = 0.05, THROUGH THICKNESS NOTCHED)

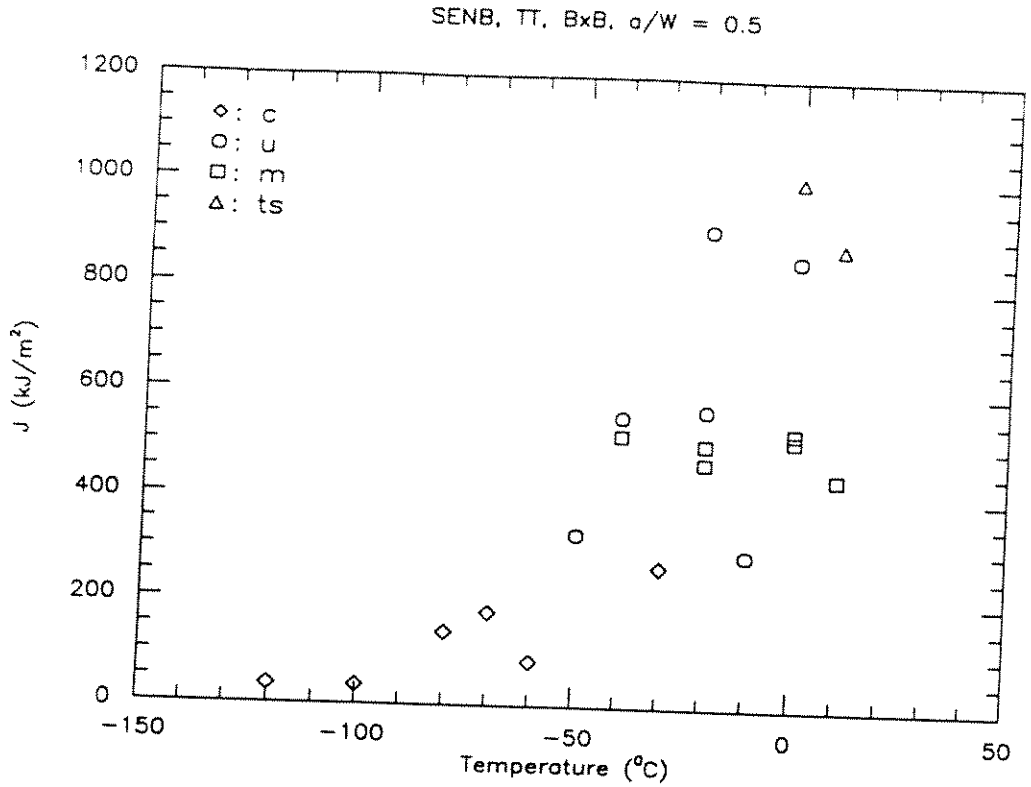

FIGURE 48. J TRANSITION CURVE (SENB, B × B, a/W = 0.5, THROUGH THICKNESS NOTCHED)

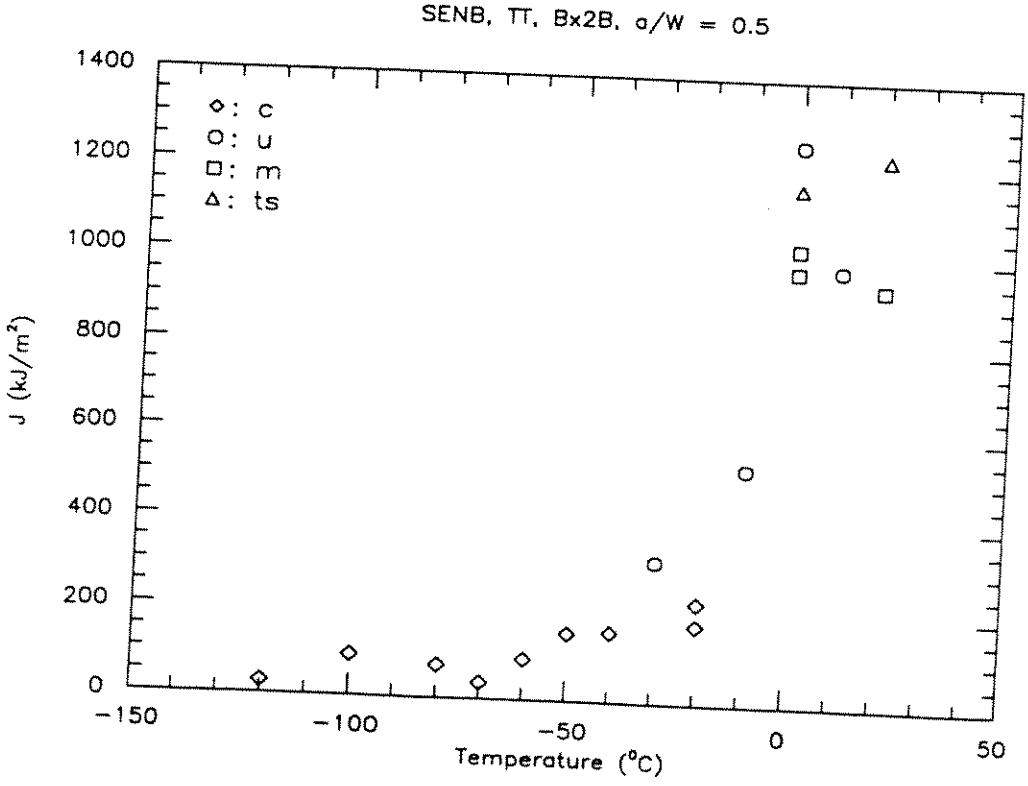

FIGURE 49. J TRANSITION CURVE (SENB, B × 2B, a/W = 0.5, THROUGH THICKNESS NOTCHED)

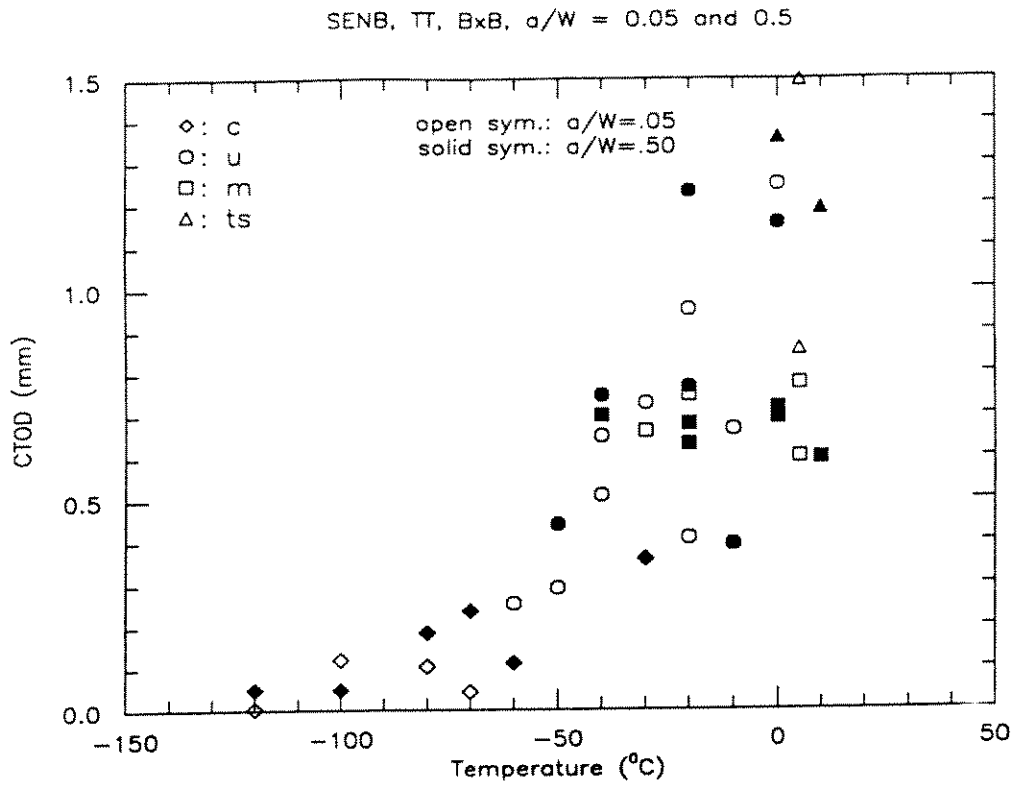

FIGURE 50. COMPARISON OF a/W = 0.05 AND a/W = 0.5 CTOD TRANSITION CURVES (SENB, B × B, THROUGH THICKNESS NOTCHED)

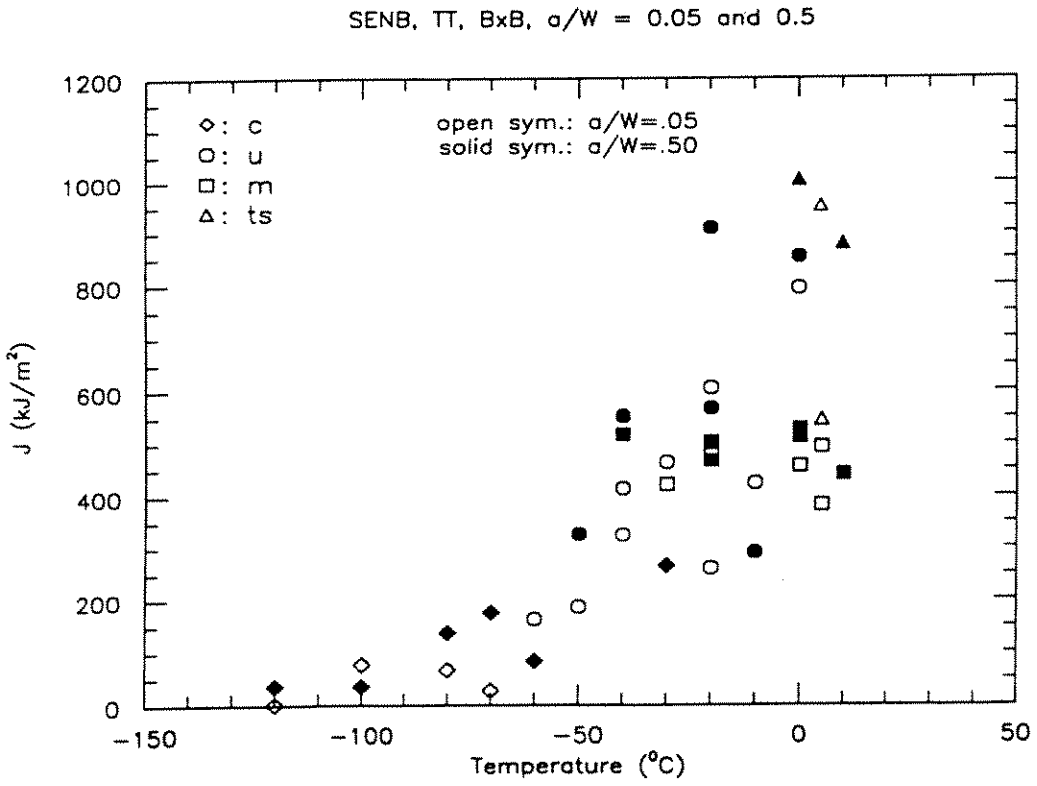

FIGURE 51. COMPARISON OF a/W = 0.05 AND a/W = 0.5 J TRANSITION CURVES (SENB, B × B, THROUGH THICKNESS NOTCHED)

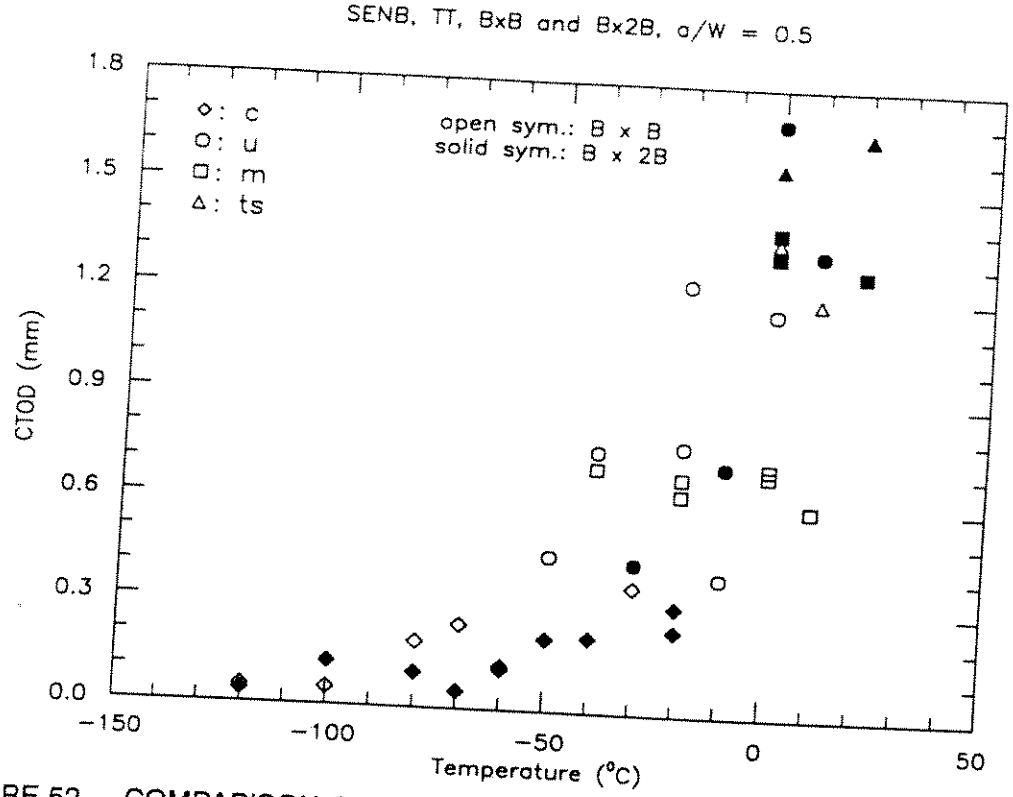

FIGURE 52. COMPARISON OF B × B AND B × 2B CTOD TRANSITION CURVES (SENB, a/W = 0.5, THROUGH THICKNESS NOTCHED)

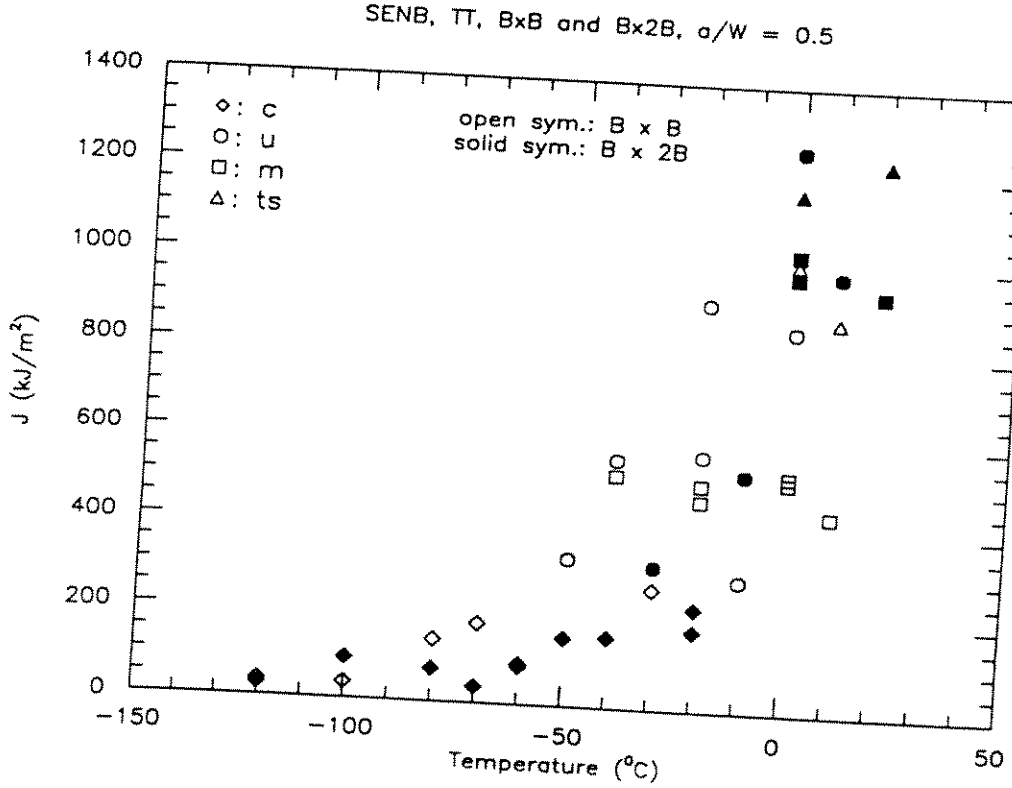

FIGURE 53. COMPARISON OF B × B AND B × 2B J TRANSITION CURVES (SENB, a/W = 0.5, THROUGH THICKNESS NOTCHED)

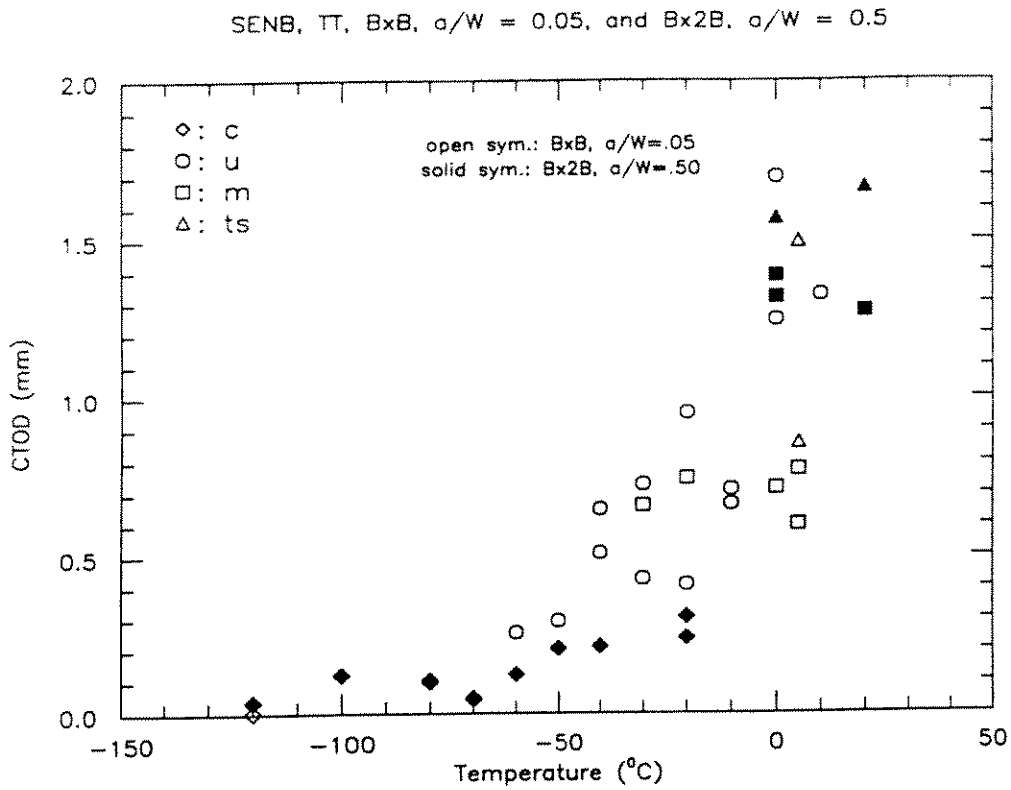

FIGURE 54. COMPARISON OF B × B, a/W = 0.05 AND B × 2B, a/W = 0.5 CTOD TRANSITION CURVES (SENB, THROUGH THICKNESS NOTCHED)

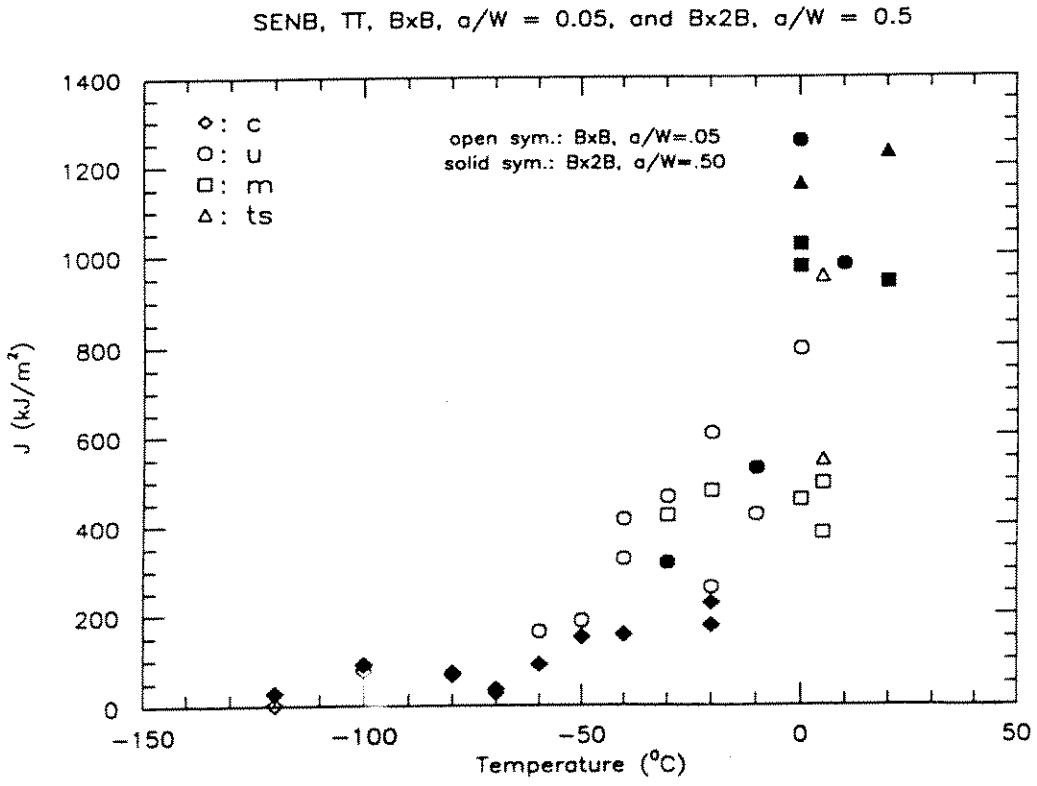

FIGURE 55. COMPARISON OF B × B, a/W = 0.05 AND B × 2B, a/W = 0.5 CTOD TRANSITION CURVES (SENB, THROUGH THICKNESS NOTCHED)

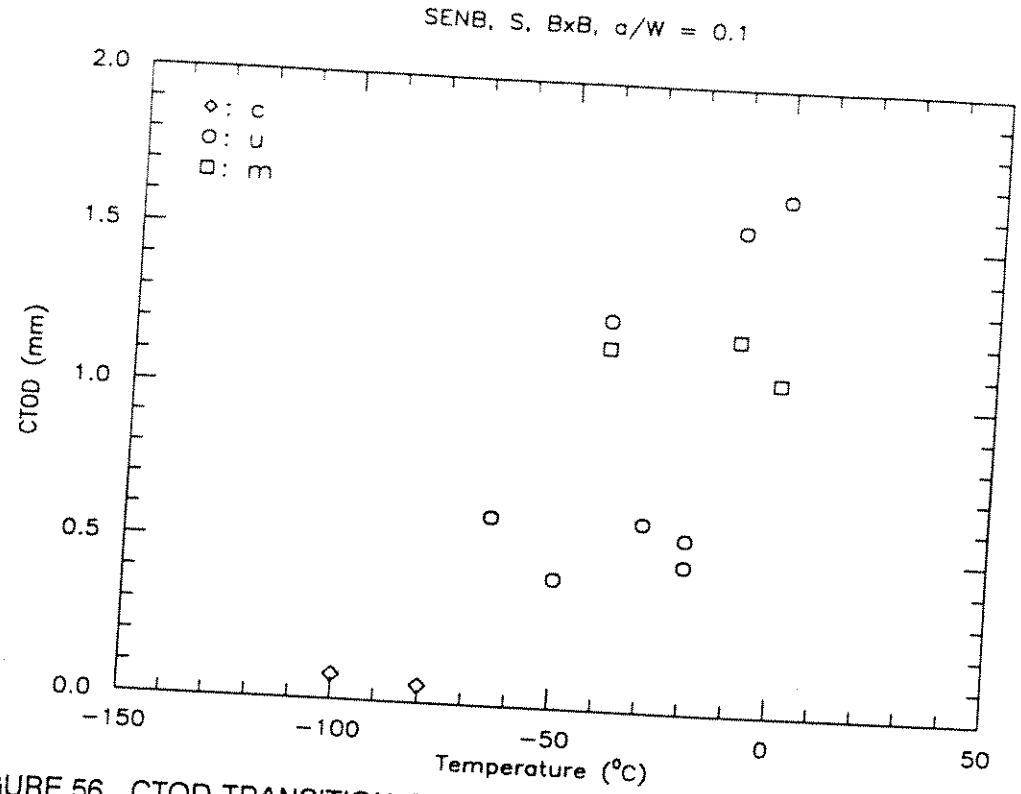

FIGURE 56. CTOD TRANSITION CURVE (SENB, B × B, a/W = 0.1, SURFACE NOTCHED)

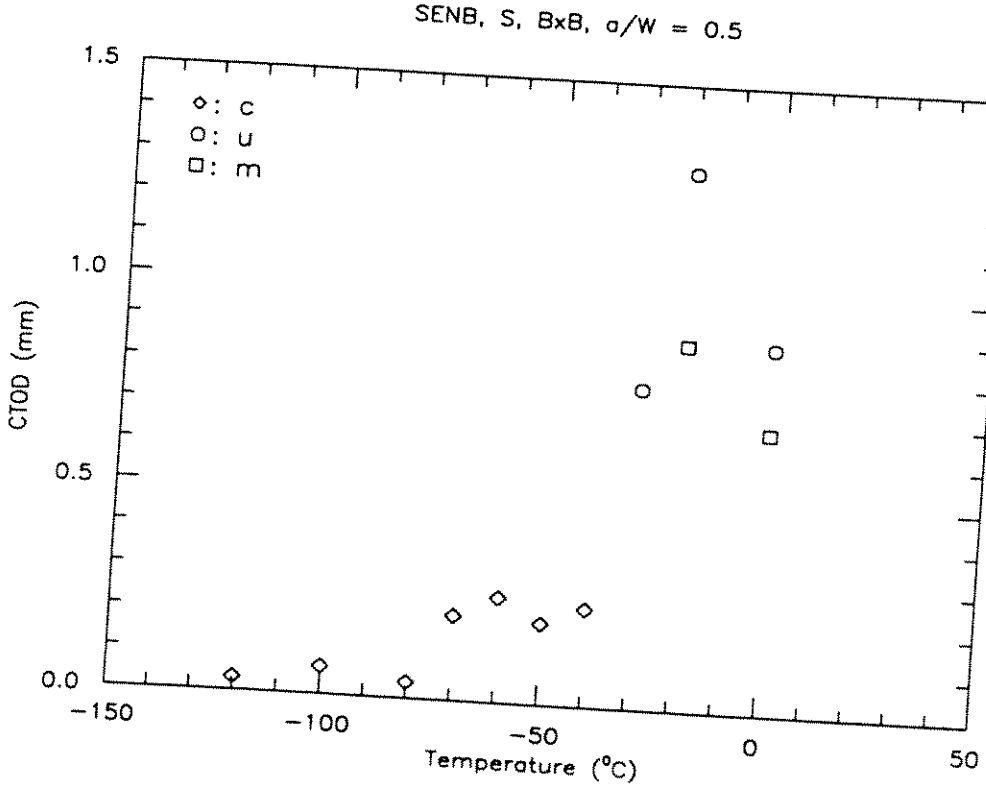

FIGURE 57. CTOD TRANSITION CURVE (SENB, B × B, a/W = 0.5, SURFACE NOTCHED)

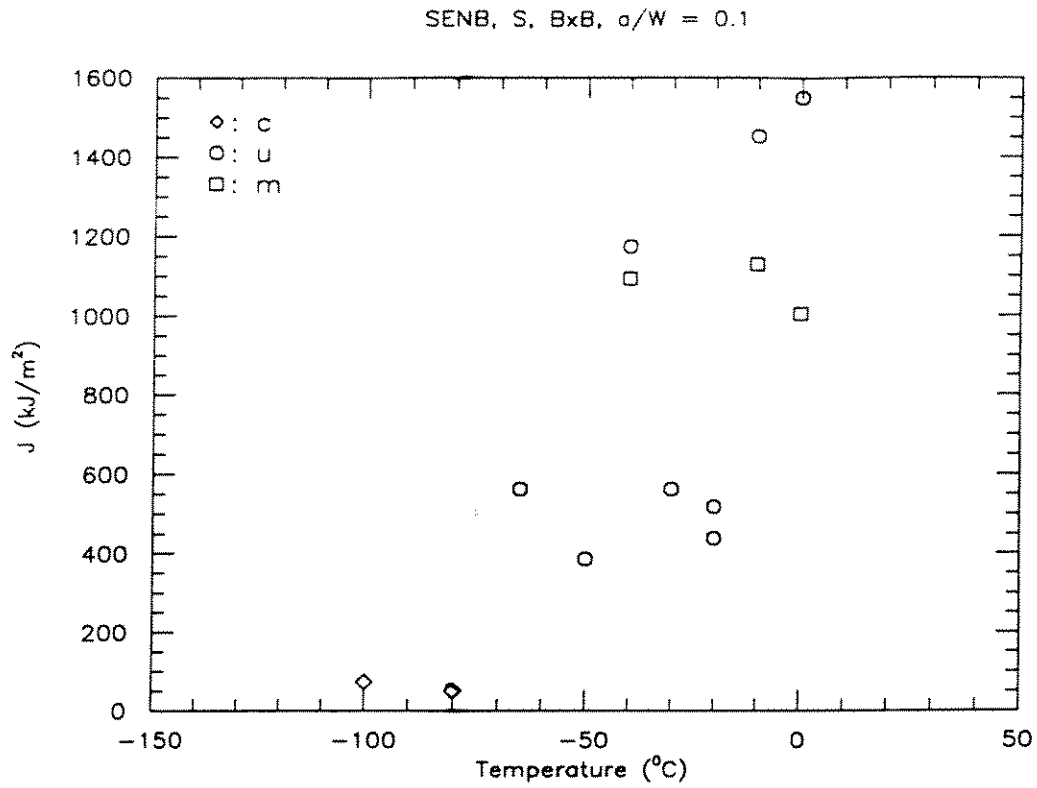

FIGURE 58. J TRANSITION CURVE (SENB, B × B, a/W = 0.1, SURFACE NOTCHED)

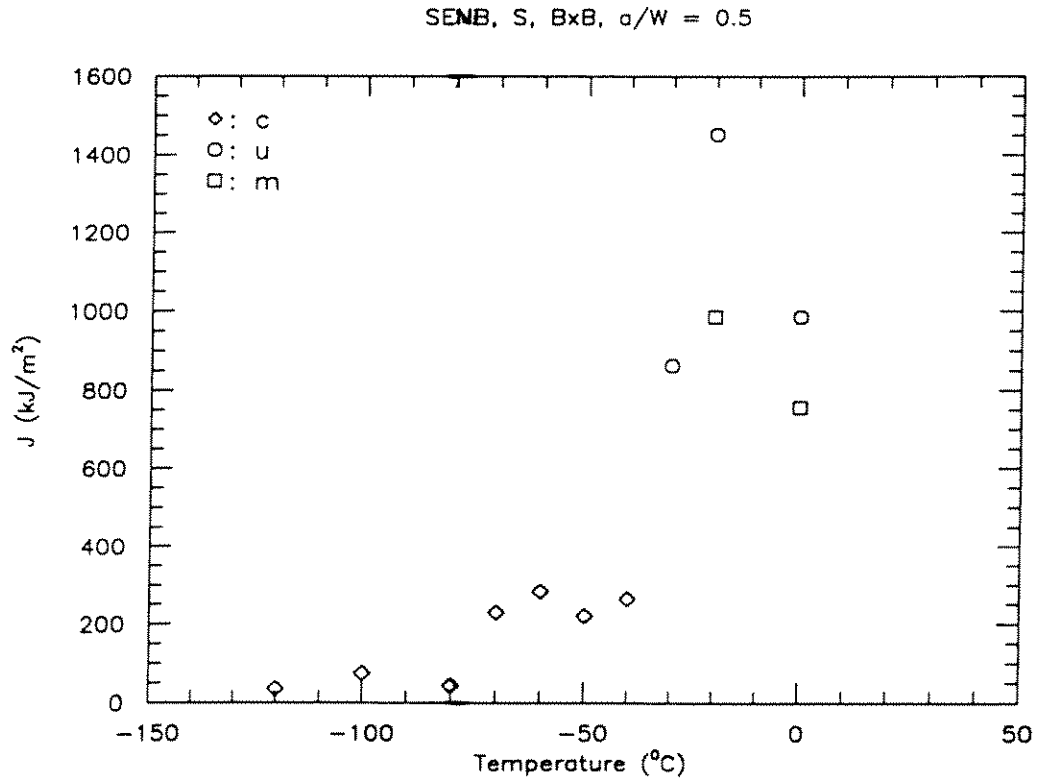

FIGURE 59. J TRANSITION CURVE (SENB, B × B, a/W = 0.5, SURFACE NOTCHED)

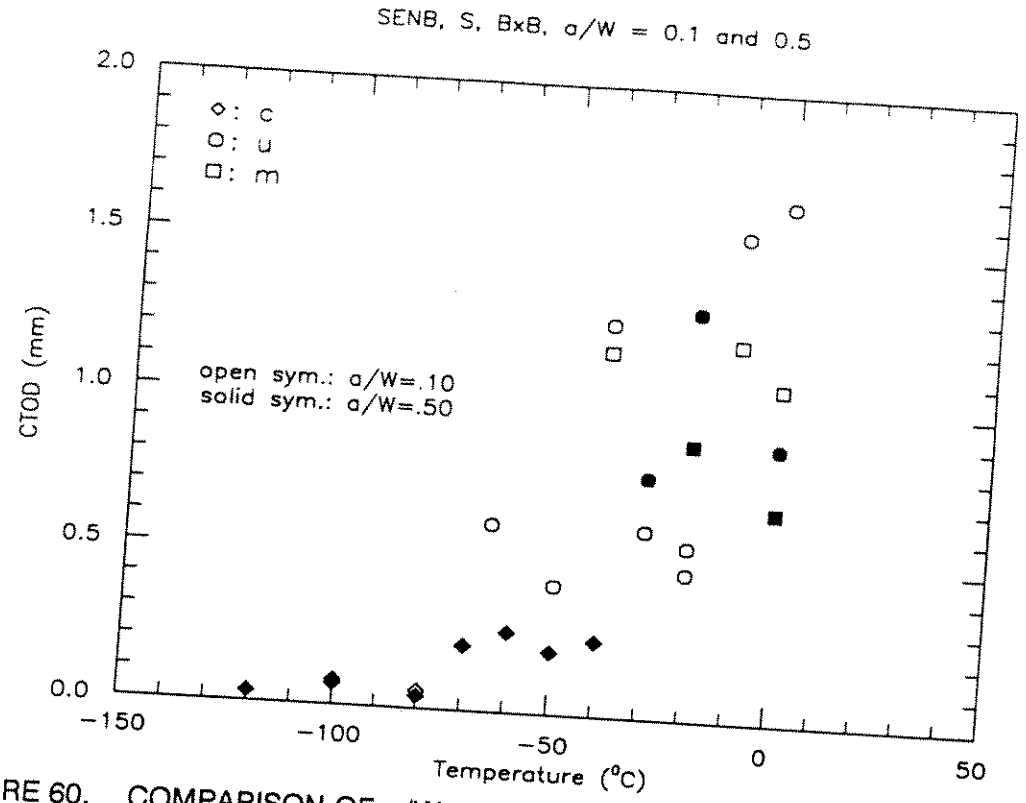

FIGURE 60. COMPARISON OF a/W = 0.1 AND a/W = 0.5 CTOD TRANSITION CURVES (SENB, B x B, SURFACE NOTCHED)

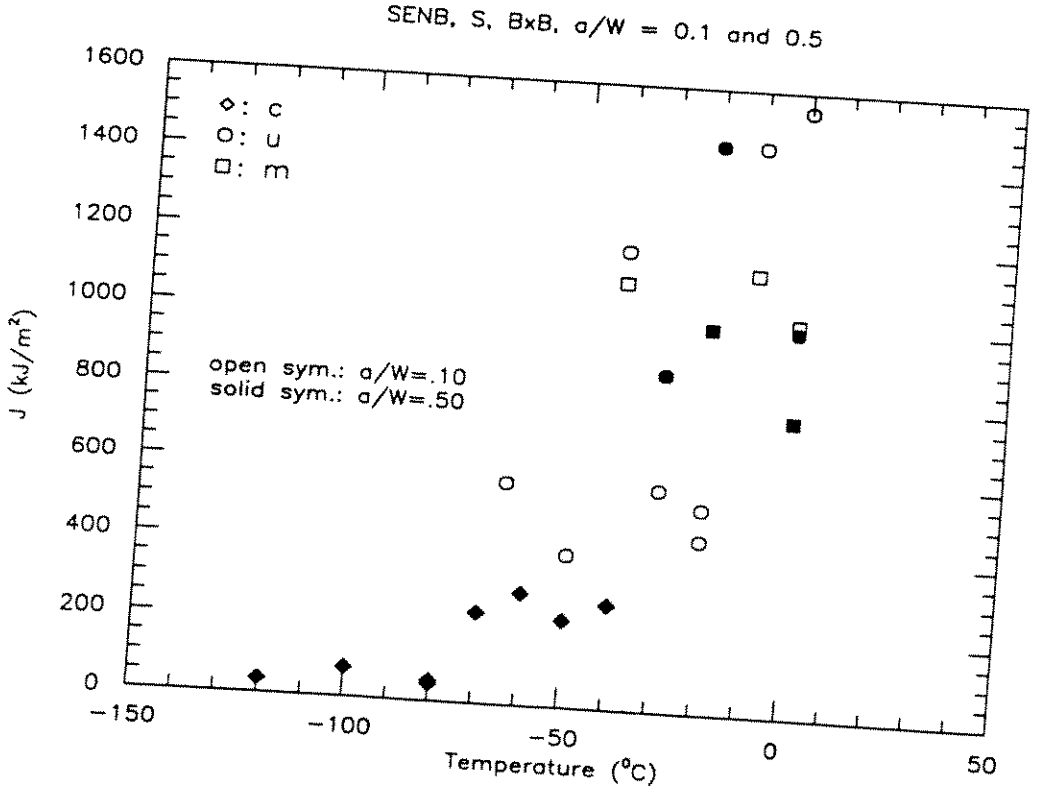

FIGURE 61. COMPARISON OF a/W = 0.1 AND a/W = 0.5 J TRANSITION CURVES (SENB, B x B, SURFACE NOTCHED)

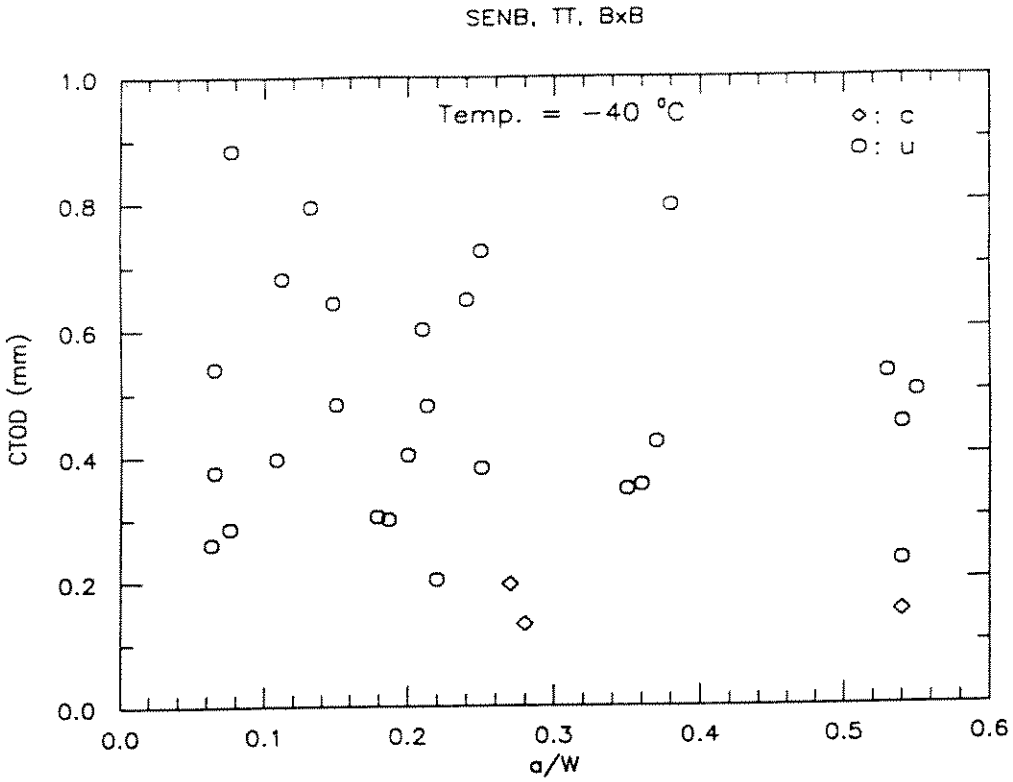

FIGURE 62. CTOD RESULTS FROM THROUGH THICKNESS NOTCHED SENB REPLICATE TESTS

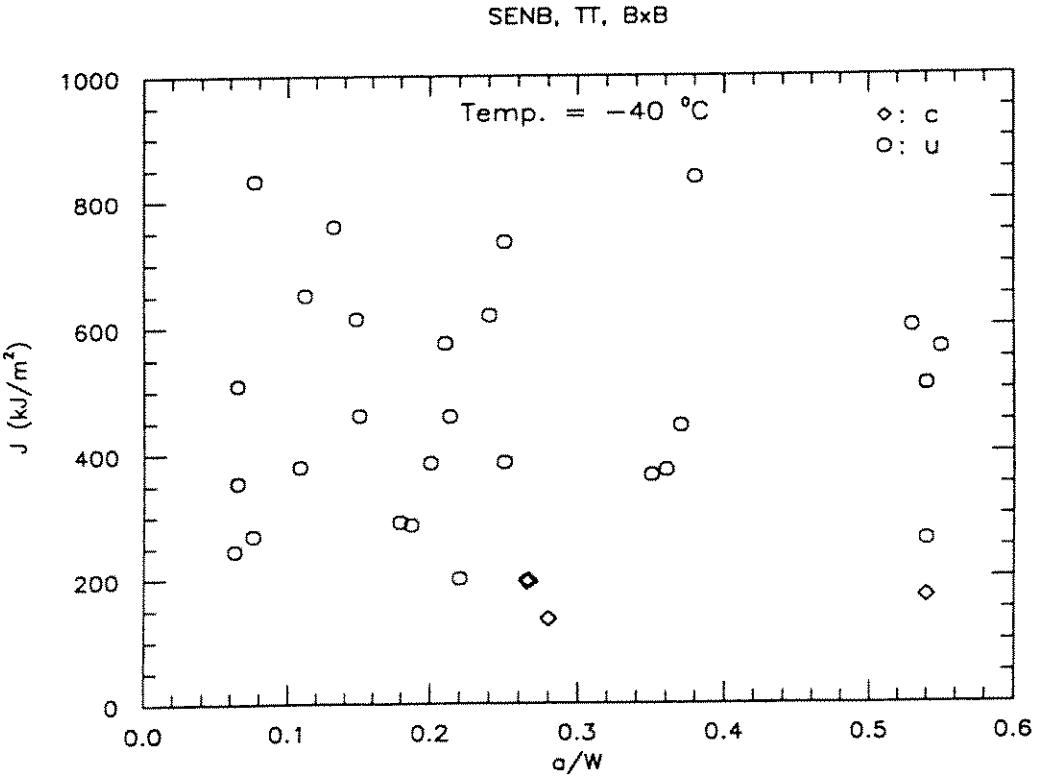

FIGURE 63. J RESULTS FROM THROUGH THICKNESS NOTCHED SENB REPLICATE TESTS

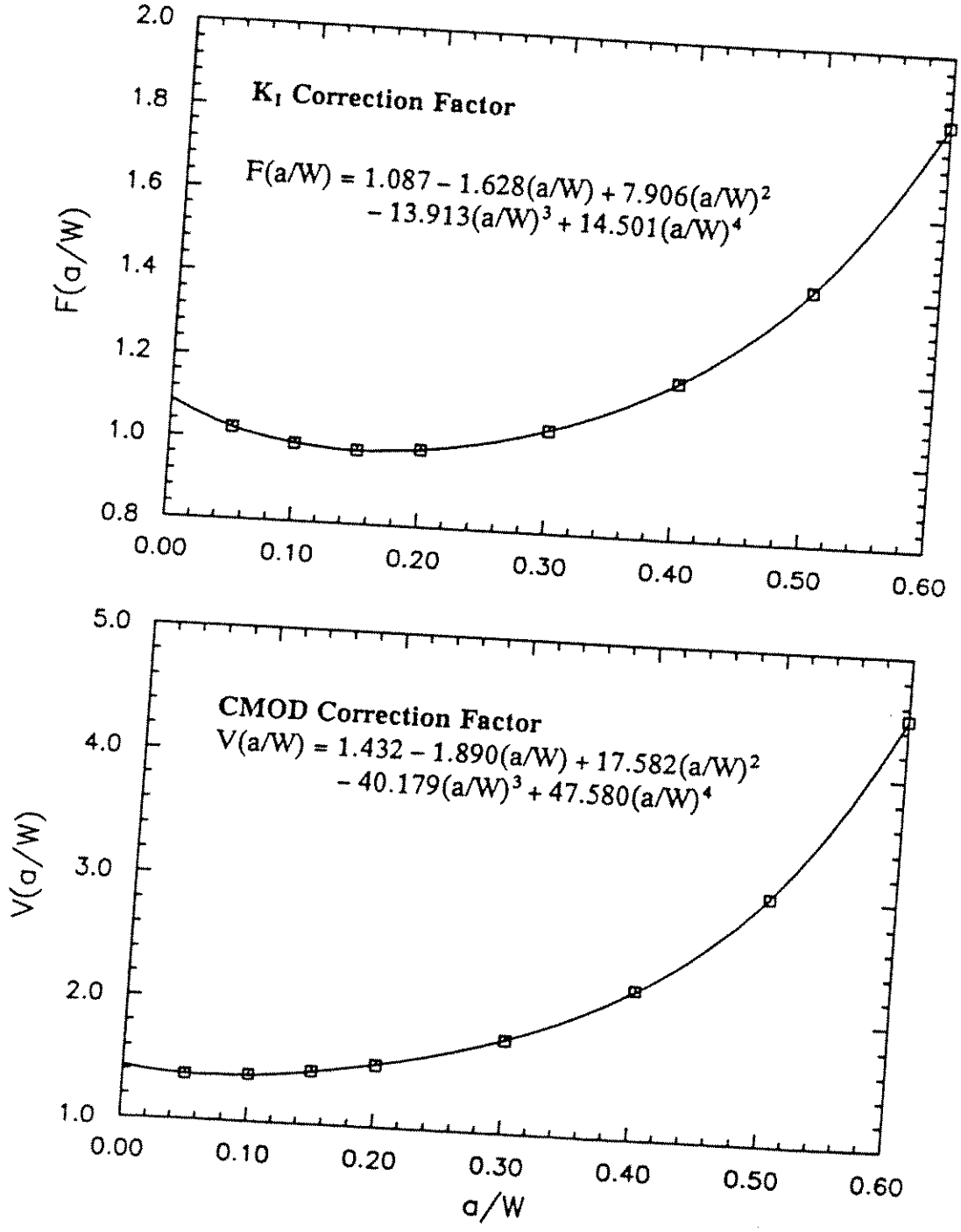

Figure 6. Correction Factors for SENAB Specimen for Pipe Material "M4" with Machined Slot

APPENDIX C

IN KIND CONTRIBUTION FROM TEXAS A&M UNIVERSITY AND THE UNIVERSITY OF ILLINOIS/URBANA-CHAMPAIGN

SPECIMEN SIZE REQUIREMENTS FOR FRACTURE TOUGHNESS TESTING IN THE TRANSITION REGION

Ted L. Anderson,
Department of Mechanical Engineering
Texas A&M University,
College Station, TX 77843

Robert H. Dodds Jr.,
Department of Civil Engineering
University of Illinois,
Champaign-Urbana, IL 61801

Submitted to

Journal of Testing and Evaluation

December 1989

ABSTRACT

This article utilizes plane strain elastic-plastic finite element analysis and a local criterion for cleavage fracture to establish specimen size requirements for the ductile-brittle transition region. Critical J and CTOD values, relative to the small scale yielding value, were predicted as a function of specimen size, strain hardening exponent, and a/W. These analyses predict an increase in the apparent toughness with decreasing specimen size due to a loss in crack tip constraint; this effect is particularly pronounced in shallow notched specimens and low hardening materials. For deeply notched bend and compact specimens, the following size requirement must be met for critical J values for cleavage to be size independent:

$$b, B, a > \frac{200\, J_c}{\sigma_Y}$$

where b is ligament length, B is thickness, and a is crack length and σ_Y is the flow stress. This criterion is eight times more severe than the size requirements in ASTM E 813-87, but is less stringent than the requirements of E 399-83. In order for a CTOD value to be nearly size independent, it must be less than 1/300 times the relevant specimen dimensions.

The constraint loss in shallow notched specimens is usually far too rapid to obtain J controlled cleavage fracture, but the analyses presented in this article provide a means for correcting fracture toughness data for constraint loss. Predictions of the effect of a/W on toughness in the transition region agree favorably with experimental data.

Future work will consider the effects of specimen thickness and ductile tearing on transition region toughness.

KEY WORDS: fracture toughness, cleavage, ductile-brittle transition, constraint, size effects, J integral, crack tip opening displacement (CTOD), finite element analysis.

Introduction

One of the fundamental assumptions of fracture mechanics is that the crack tip conditions can be uniquely characterized by a single parameter such as the stress intensity factor (K) or the J integral. When this assumption is valid, the critical value of the crack tip parameter represents a size-independent measure of fracture toughness. The ASTM Standards for K_{IC} and J_{IC} testing (E 399-83 and E 813-87, respectively) include minimum specimen size requirements which are designed to ensure a single parameter description of crack tip behavior. However, these standards are unsuitable for the transition region, as discussed below.

Existing Standards

The ASTM Standard for K_{IC} testing has very strict size requirements because the stress intensity factor is based on a linear elastic stress analysis; K is meaningless when there is significant crack tip plasticity. The size requirements in E 399-83 ensure that the crack tip plastic zone is small compared to specimen dimensions:

$$B, a \geq 2.5\left(\frac{K_{IC}}{\sigma_{YS}}\right)^2 \tag{1a}$$

$$0.45 \leq a/W \leq 0.55 \tag{1b}$$

where B is the specimen thickness, a is crack length, W is width, and σ_{YS} is the 0.2 % offset yield strength. The requirements in Eq. (1) restrict the K_{IC} test to brittle materials or very large specimens. In the case of most structural steels, valid K_{IC} tests are only possible on the lower shelf of toughness.

The size requirements in E 813 are much more lenient than E 399, primarily because the J integral is better suited to nonlinear material behavior. The minimum specimen dimensions for a valid J_{IC} result are as follows:

$$B, b \geq \frac{25\, J_{IC}}{\sigma_Y} \tag{2}$$

where b is the uncracked ligament length (W-a) and σ_Y is the flow stress, defined as the average of the yield and tensile strength. The J_{IC} test measures a critical J near

the onset of stable crack growth; E 813 is not valid when the specimen fails in an unstable manner. Thus E 813 cannot be used to quantify fracture toughness in the ductile-brittle transition region of steels, where the primary failure mechanism is cleavage. While Eq. (2) has been shown to be sufficient to guarantee nearly size-independent J_{IC} values for initiation of ductile tearing, this requirement is inappropriate for cleavage toughness, which is more sensitive to specimen size [1].

The only ASTM Standard that permits fracture toughness testing in the transition region is E 1290-89, the *Standard Test Method for Crack-Tip Opening Displacement (CTOD) Fracture Toughness Measurement*. The CTOD test applies to all micromechanisms of failure in metals, but there are no minimum specimen size requirements. The lack of size requirements in this standard is consistent with the pragmatic philosophy of the CTOD design curve approach developed in the United Kingdom [2,3]. This approach, which is usually applied to welded steel structures, concedes that critical CTOD values may vary with size and geometry, but states that CTOD data can be applied to fitness-for-purpose assessments if the test specimens possess at least as much crack tip constraint as the structure under consideration. The CTOD design approach recommends that the specimen thickness match the section thickness of the structure. The British CTOD testing standard [4] permits a/W ratios as small as 0.15, which facilitates weldment testing and allows shallow structural flaws to be simulated in the laboratory. Early drafts of the ASTM E 1290 included liberal tolerances on a/W, but these were deleted from the the final version.

Size Criteria for the Transition Region

The ductile-brittle transition region of structural steels is not adequately addressed by existing ASTM Standards. The K_{IC} test is not applicable because too much plastic deformation precedes failure in the transition region. The J_{IC} test is valid only on the upper shelf, while the CTOD standard does not guarantee a size-independent measure of fracture toughness.

There is a pressing need for rational specimen size criteria for the transition region. Such criteria are proposed in this article, where the minimum specimen size for cleavage fracture to be characterized by J or CTOD is quantified by means of finite element analysis. These analyses also make it possible to predict the size dependence of fracture toughness when the single parameter assumption is no longer valid. Both shallow and deep notched specimens are considered, as well as a wide range of strain hardening behavior.

Analysis Procedures

This investigation utilized elastic-plastic finite element analysis to quantify the size dependence of cleavage fracture toughness and to develop size criteria for single parameter characterization. Crack tip stress fields obtained from specimens of finite size were compared to the corresponding stress fields for small scale yielding.

Relationship to Previous Work

Previous investigators, such as Shih and German [5] and McMeeking and Parks [6], used finite element analysis to develop specimen size criteria for J controlled fracture. Shih and German analyzed both bending and tension, and compared the computed stress fields with the Hutchinson, Rice and Rosengren (HRR) [7,8] singularity. Shih and German arbitrarily stated that the specimen was J controlled if the computed stresses near the crack tip were within 10% of the HRR solution. Shih [9] later applied this same approach to derive size criteria for combined loading, ranging from pure tension to pure bending.

The procedure employed in the present study differs from the Shih and German approach in two major respects. First, the crack tip stresses in finite size specimens are compared to the actual small scale yielding stress fields rather than the HRR singularity, which only applies to a limited region ahead of the crack tip. The other main difference in the present approach is that the micromechanism of fracture is considered when quantifying the size dependence of fracture toughness. An arbitrary criterion based on 10% deviation in stress from small scale yielding is not appropriate for stress-controlled cleavage fracture, because even a slight deviation in stress can result in a significant elevation of the critical J value [1]. In the present study, the size dependence of cleavage toughness is computed directly; the proposed size requirements ensure that the measured fracture toughness is nearly equal to the toughness in small scale yielding.

Finite Element Analysis

Plane strain elastic-plastic finite element analysis was performed on four configurations with three strain hardening rates, resulting in a total of twelve cases (see Table 1). The crack tip stress fields for small scale yielding were evaluated, as well as single edge notched bend (SENB) specimens with a/W ratios of 0.05, 0.15, and 0.50. The material stress-strain behavior was modeled with a Ramberg-Osgood power law expression:

$$\frac{\varepsilon}{\varepsilon_o} = \frac{\sigma}{\sigma_o} + \alpha\left(\frac{\sigma}{\sigma_o}\right)^n \tag{3}$$

where ε is strain, σ is stress, σ_o is a reference stress, $\varepsilon_o = \sigma_o/E$, and α and n are dimensionless constants. For the present study, $\alpha = 1.0$, $\varepsilon_o = 0.002$, and $\sigma_o = 60$ ksi (414 MPa); in this case σ_o corresponds to the 0.2% offset yield strength, σ_{YS}. The strain hardening exponent, n, was assigned values of 5, 10 and 50, which correspond to high, medium and low work hardening, respectively.

Figure 1 shows the finite element mesh that was used for the small scale yielding analyses. The circular domain with a crack reduces to a semicircle because of symmetry. The finite element mesh contains 720 elements and 2300 nodes. The mesh was scaled geometrically in order to concentrate elements and nodes near the crack tip. Displacements of the elastic (Mode I) singular field were imposed at the boundary of the domain; in all cases K was sufficiently low to confine the plastic zone well within the domain. This model is designed to simulate a crack in an infinite body; Rice and Tracey [10] and McMeeking and Parks [6] were among the first to apply this approach to crack tip stress analysis.

Finite element meshes of SENB specimens were generated with a/W = 0.05, 0.15, 0.50. Each of these meshes contained approximately 350 elements and 1200 nodes, with most of the elements and nodes concentrated near the crack tip.

For each analysis, the J integral was evaluated by means of the energy domain integral approach [11]. The CTOD was defined as the intersection of the crack flanks with a 90° vertex emanating from the crack tip.

Additional details of the finite element analysis are given in Reference [12].

Cleavage Fracture Criterion

Under small scale yielding conditions, the crack tip stresses and strains are uniquely characterized by J, and the onset of fracture is uniquely defined by a critical value of J, irrespective of the micromechanism of failure. When J dominance is lost, the stresses and strains no longer increase in proportion to one another, and critical J values are size dependent. The magnitude of this size dependence depends on the micromechanism of failure. For example, a material that fails when a critical strain is reached locally would exhibit a different fracture toughness size dependence from a material that fails at a critical local stress.

In order to quantify size effects on fracture toughness, one must assume a local failure criterion. In the case of cleavage fracture, a number of micromechanical models have recently been proposed [13-16], most based on weakest-link statistics. The weakest-link models assume that cleavage failure is controlled by the largest or most favorably oriented fracture-triggering particle. The actual trigger event involves a local Griffith instability of a microcrack which forms from a microstructural feature such as a carbide or inclusion; the Griffith energy balance is satisfied when a critical stress is reached in the vicinity of the microcrack. The size and location of the critical microstructural feature dictate the fracture toughness; thus cleavage toughness is subject to considerable scatter [16].

The Griffith instability criterion implies fracture at a critical normal stress near the tip of the crack; the statistical sampling nature of cleavage initiation (i.e., the probability of finding a critical microstructural feature near the crack tip) suggests that the volume of the process zone is also important. Thus the probability of cleavage fracture in a cracked specimen can be expressed in the following general form:

$$F = F(\sigma_1, V(\sigma_1)) \tag{4}$$

where F is the failure probability, σ_1 is the maximum principle stress at a point, and $V(\sigma_1)$ is the cumulative volume sampled where the principal stress is $\geq \sigma_1$. Equation (4) is sufficiently general to apply to any fracture process controlled by maximum principal stress, not just weakest link failure. For a specimen subjected to plane strain conditions, V = BA, where A is cumulative area on the x-y plane. (This article uses the conventional fracture mechanics coordinate axes, where x is the direction of crack propagation, y is normal to the crack plane, and z is parallel to

the crack front.) For small scale yielding, dimensional analysis shows that the principal stress ahead of the crack tip can be written as

$$\frac{\sigma_1}{\sigma_o} = g\left(\frac{J}{\sigma_o r}, \theta\right) \tag{5a}$$

or

$$\frac{\sigma_1}{\sigma_o} = h\left(\frac{J^2}{\sigma_o^2 A}\right) \tag{5b}$$

It can be shown that the HRR singularity is a special case of Eq. (5). When J dominance is lost, there is a relaxation in triaxiality; the principal stress at a fixed r and θ is less than the small scale yielding value (Eq. (5a)). Stated another way, the cumulative area for a given σ_1 is less than implied by Eq. 5b. However, it is possible to define an *effective J* that satisfies Eq. (5b):

$$\frac{J_{ssy}^2}{A} = \frac{J^2}{A_{ssy}} \quad \text{for a fixed } \sigma_1 \tag{6}$$

where J and A are the actual applied J integral and area in the specimen and A_{ssy} is the area which corresponds to J and σ_1 under small scale yielding conditions. The small scale yielding J value (J_{ssy}) can be viewed as *the effective driving force for cleavage*.

The procedure for determining J_{ssy} is illustrated schematically in Fig. 2. When the cumulative area ahead of the crack tip is normalized by the actual applied J, the large scale yielding curve lies below the small scale yielding curve. The lower curve is collapsed onto the upper curve when A is normalized by J_{ssy}.

The ratio J/J_{ssy} at the moment of fracture is a measure of the size dependence of cleavage fracture toughness. When the specimen is sufficiently large to maintain J controlled conditions, this ratio should equal 1.0.

Results

Small Scale Yielding

Figures 3 to 5 show nondimensionalized plots of the stress normal to the crack plane for small scale yielding. The corresponding HRR solution is included on each

plot for comparison. Elastic K values of 25 and 50 ksi $\sqrt{in}$ (27.6 and 55.2 MPa $\sqrt{m}$) were imposed in each case. The corresponding J values were computed from the finite element results and converted to equivalent K values, which are slightly lower than the elastic stress intensities; this discrepancy in applied and computed K values is caused by crack tip plasticity.

Although the finite element solutions do not agree with the HRR singularity except very near the crack tip, the computed stress fields scale with J/r, as expected from dimensional analysis (Eq. (5a)). The crack tip stress fields need not agree with the HRR solution for J controlled fracture; the precise functional relationship of the crack tip fields is unimportant as long as the stresses obey Eq. (5).

The crack tip fields in small scale yielding can be modeled by infinite series, where the HRR singularity is the leading term. This term dominates as $r \rightarrow 0$, but the asymptotic HRR solution is invalid for distances less than ~ 2 times the CTOD, because the crack tip fields are influenced by blunting and large strain effects. Thus there is a very limited region where the HRR solution applies; crack tip stress fields in finite specimens should be compared to the complete small scale yielding solution rather than the HRR singularity.

Figure 6 shows principal stress contours in nondimensional coordinates for small scale yielding with n = 10. This graph demonstrates that the principal stress scales with r/J at all angles (Eq. (5a); the areas bounded by the contours also scale, as predicted by Eq. (5b). Note that the contours have a similar shape, implying that that the small scale yielding stress fields can be written as the product of separable functions of r and θ:

$$\sigma_{ij} = c_{ij}\left(\frac{J}{\sigma_o r}\right) d_{ij}(\theta) \qquad (7)$$

This relationship appears to hold for r values ranging from 2 to 20 times the CTOD.

SENB Specimens

Figure 7 compares the nondimensional principal stress contours for the small scale yielding solution with an SENB specimen with a/W = 0.5; the latter approximates small scale yielding behavior because it is loaded to a relatively low J value. Note that the contours coincide except for the sharp spike at $\theta = 45°$ in the SENB specimen. This slight difference in the shape of the contours is probably a mesh effect

rather than a real phenomena; the finite element mesh for the small scale yielding analysis was approximately twice as refined near the crack tip as the SENB mesh. The areas bounded by the contours for the two cases agree to within 3%.

Figure 8a illustrates the effect of large scale yielding on nondimensional principal stress contours for n = 10 and a/W = 0.5. Although the contours maintain a constant shape, their size (when normalized by J) decreases with plasticity. (The *absolute size* of the contour actually increases with J, but at a slower rate than predicted from Eq. (5).) The equivalent small scale yielding J values, J_{ssy}, are chosen so that the contours coincide for a constant σ_1 (Fig. 8b).

Computed J_{ssy} values are plotted as a function of J and σ_1 in Fig. 9. The ratio J/J_{ssy} increases with J due to constraint loss. This ratio is insensitive to the principal stress; the deviation at high stress levels can be discounted because this is near the large strain region, where the accuracy of the finite element solution (based on small strain theory) is suspect.

The nearly constant J/J_{ssy} ratio at a fixed J is an important result. Critical J values can be corrected for constraint loss be means of a single constant; the applied J and the J/J_{ssy} ratio completely characterize the principal stress distribution ahead of the crack tip.

Effect of Specimen Dimensions on J_c

Figures 10 to 12 illustrate the effect of crack length, a/W and hardening exponent on the J/J_{ssy} ratio. Since a critical value of J_{ssy} represents a size-independent cleavage toughness, the J/J_{ssy} ratio quantifies the geometry dependence of J_c, the measured fracture toughness. For the deeply notched specimens (a/W = 0.5), J_c approaches the small scale yielding value when the ratio $a\sigma_0/J$ is greater than ~200, but the shallow notched specimens do not produce small scale yielding behavior unless the specimen is very large relative to J/σ_0. The relative crack tip constraint increases as strain hardening rate increases, i.e., as n decreases.

The effective driving force for cleavage, J_{ssy}, is plotted against the apparent driving force, J, in Figs 13 to 15. The dashed line in each graph represents the small scale yielding limit, where $J = J_{ssy}$ by definition. Each of the curves in Figs 13 to 15 agrees with the small scale yielding limit at low J values but deviates as J increases. The deviation from small scale yielding occurs more rapidly and at lower J values in shallow notched specimens and in low hardening materials. For n = 50 (Fig. 15), the effective driving force saturates at a constant value; further increases in J do not af-

fect J_{ssy}. Once a specimen reaches the saturation value of J_{ssy}, the likelihood of cleavage fracture with further loading decreases considerably. Such a specimen could cleave only if the crack grew by ductile tearing and sampled a critical microstructural feature.

Figure 16 is a plot of J/J_{ssy} as a function of n and specimen size, which is normalized by flow stress in order to be consistent with the E 813 size criteria (Eq. (2)) and to reduce the effect of strain hardening on the size dependence. The flow stress for the Ramberg-Osgood materials was estimated from the following relationship:

$$\sigma_Y = \frac{\sigma_o}{2}\left[1 + \frac{\left(\frac{N}{0.002}\right)^N}{\exp(N)}\right] \tag{8}$$

where $N = 1/n$. Equation (8) was derived by solving for the tensile instability point in Eq. (3), converting true stress to engineering stress, and averaging σ_o and the estimated tensile strength. The J/J_{ssy} ratio becomes relatively flat and approaches 1.0 when the $a\sigma_Y/J$ ratio exceeds ~200, although the rate at which each curve approaches the small scale yielding limit depends on the hardening exponent.

The effect of specimen size on critical CTOD is shown in Fig. 17. The curves for the three hardening exponents converge and approach $\delta/\delta_{ssy} = 1.0$ when the a/δ ratio is greater than ~ 300.

Effect of Thickness

All of the results presented so far are based on plane strain finite element analysis. When the specimen thickness is finite, however, the through-thickness constraint can be considerably less than plane strain.

Three-dimensional elastic plastic finite element analyses of flawed structures and test specimens are rarely performed because of the substantial computational requirements. Even rarer are three dimensional analyses with sufficient mesh refinement to analyze crack tip stresses. One such analysis, which was recently performed by Narishimhan and Rosakis [17], provides some insight regarding the thickness required to maintain nearly plane strain conditions. They analyzed an SENB specimen where the crack length and ligament length were three and six times the thickness, respectively; thus thickness was the governing dimension. The hardening exponent, n, was 22 in their analysis.

Figure 18, which was constructed from the results of Narishimhan and Rosakis, is a plot of stress normal to the crack plane, relative to the midthickness value. Three load steps are plotted, corresponding to $B\sigma_Y/J$ ratios of 235, 103, and 26.3. The relative distance ahead of the crack tip is in the range of 2 to 4 times the CTOD in each case. For the lowest J value, the stress is nearly constant except close to the free surface. At the intermediate load step, the stress is relatively constant through the middle 40% of the thickness. The stress at the highest J value varies continuously though the thickness.

Narishimhan and Rosakis did not report strain values, so it is not possible to state with certainty that the middle of the specimen is in plane strain at low and moderate J values. However, the crack tip stress fields at midthickness agree very closely with values obtained by Narishimhan and Rosakis from a two-dimensional plane strain analysis of the SENB specimen. Thus it is reasonable to assume that the midthickness principal stress corresponds to the plane strain value, at least for the two lowest J values in Fig. 18.

According to Fig. 18, an SENB specimen maintains nearly plane strain constraint through a significant portion of the thickness for $B\sigma_Y/J$ ratios up to 100. The size of the plane strain region can be defined as the *effective thickness*, which decreases as J increases.

In the case of cleavage fracture, there is a statistical thickness effect on fracture toughness, as first reported by Landes and Schaffer [18]. Because of the weakest link nature of cleavage initiation, a population of large specimens has a lower average toughness than small specimens of the same material, because more material is sampled along the crack front in a large specimen and there is a higher probability of sampling a brittle region. Thus as constraint relaxes in a test specimen, the probability of cleavage fracture is influenced by the decrease in effective thickness.

Comparison with Experimental Data

Figures 10 to 17 provide the capability to correct cleavage fracture toughness for constraint loss. Given the measured toughness, specimen size, and material hardening characteristics it is possible to estimate the toughness of the specimen if its dimensions were infinite.

Fracture toughness data recently published by Sorem [19] were used in the present investigation to assess the ability of these analyses to characterize constraint loss. Sorem performed fracture toughness tests on SENB specimens of A 36 steel

over a range of temperatures. The specimens were square section (B x B) with the thickness equal to 31.8 mm (1.25 in). Two aspect ratios were tested: a/W = 0.50 and a/W = 0.15. Since the material is a mild steel that exhibits a yield point, the flow behavior does not match the Ramberg-Osgood expression perfectly, but a slight deviation from the Ramberg-Osgood idealization should not affect the results significantly. Based on the σ_{TS}/σ_{YS} ratio and Eq. (8), we estimated n = 6 for this material.

Figure 19 shows CTOD data for the A 36 steel at two temperatures in the transition region. The solid diamonds represent the experimental data, while the crosses indicate predicted small scale yielding values. Every specimen but one (the highest CTOD value for a/W = 0.15 at -43°C) failed by cleavage without significant prior stable crack growth. At both temperatures, the shallow notched specimens have a higher apparent toughness than the deep notched specimens but the corrected values agree reasonably well. Relatively small corrections are needed for specimens with a/W = 0.50, but the small scale yielding correction has a major effect when a/W = 0.15. The small scale yielding CTOD values appear to be less scattered than the uncorrected data.

Figures 20 and 21 are Weibull plots of the A 36 data at - 76 and - 43°C, respectively. In both cases, there is a significant difference between the experimental data for a/W = 0.15 and 0.50, but the small scale yielding values are similar for the two geometries. At the higher temperature, the a/W = 0.15 data appear to be slightly over-corrected (or the a/W = 0.50 data are under-corrected), but this difference is not statistically significant. Although Fig. 19 shows an apparently dramatic decrease in scatter when the small scale yielding correction is applied, the Weibull slopes in Figs. 20 and 21 decrease by only a modest amount for small scale yielding.

Discussion

Based on Figs. 16 to 18, we recommend the following specimen size limits for cleavage fracture in deeply notched bend specimens:

$$B, b, a \geq \frac{200\, J_c}{\sigma_Y} \qquad (9)$$

or

$$B, b, a \geq 300\, \delta_c \qquad (10)$$

These requirements, which should also apply to deeply notched compact specimens, guarantee fracture toughness results that are nearly size independent, but only when cleavage occurs without significant prior stable crack growth.

Equation (9) is eight times as severe as the size requirements in E 813-87 (Eq. (2)) but is not as severe as E 399-83 (Eq. (1)). Consider, for example, a material with J_c = 200 kPa m, σ_{YS} = 450 MPa, and σ_Y = 500 MPa. The minimum thickness required for a valid K_{IC} test is 570 mm (22.4 in), while a 10 mm (0.39 in) thick specimen would satisfy E 813-87. An 80 mm (3.15 in) thick specimen is required to satisfy Eq. (9).

Wallin [20] recently proposed that the J_c/σ_Y ratio be greater than 50 times the thickness and ligament length for J controlled cleavage. Although Wallin used a local failure criterion similar to the present study, he did not evaluate size effects in J_c directly. Also, he did not have detailed crack tip stress solutions such as those used in this investigation. According to Fig. 16, Wallin's proposed size limit is insufficient to ensure size-independent fracture toughness measurements; the more strict requirement of Eq. (9) appears to be necessary.

It is very difficult (and sometimes impossible) to achieve J controlled fracture in shallow notched specimens, but the measured toughness can be corrected for constraint loss with Figs. 10 to 12. Figures 19 to 21 show that this approach successfully removed the geometry dependence of fracture toughness in A 36 steel.

This study focused primarily on the effect of in-plane dimensions on fracture toughness; the effect of thickness requires further study. Figure 18 shows that test specimens can maintain nearly plane strain conditions at midthickness to relatively high J values, but the size of the plane strain region decreases with plasticity. It should be possible to define an effective thickness, which equals the actual thickness for small scale yielding but decreases with J. The effective thickness can then be taken into account through statistical models for cleavage fracture [13-16].

The effect of prior ductile crack growth also requires further study. The results presented in this article apply only to stationary cracks. Ductile crack growth affects the cleavage toughness in at least two ways: (1) the crack tip stress field ahead of a growing crack is undoubtedly different from that of a stationary crack; and (2) the growing crack samples more material than a stationary crack, increasing the likelihood of finding a critical cleavage trigger.

Conclusions

1. In order to obtain J controlled cleavage fracture in a deeply notched bend or compact specimen, the specimen should be at least eight times as large as required by ASTM E 813-87.

2. A critical CTOD value in a deep notched specimen should be less than 1/300 times the characteristic specimen dimensions in order to be size independent.

3. Shallow notched specimens lose constraint at very low J values, but measured fracture toughness values can be corrected for this constraint loss.

4. Further work is required to quantify the effect of specimen thickness and prior ductile crack growth on fracture toughness.

Acknowledgements

The finite element analysis was sponsored by the David Taylor Research Center, Code 2812. Mr. Nalini Mohan Rao Vanaparthy assisted with post-processing of the results.

References

1. Anderson, T.L., "Crack Tip Parameters for Large Scale Yielding and Low Constraint Configurations." Accepted for publication in *International Journal of Fracture*, to appear 1989.

2. Burdekin, F.M. and Dawes, M.G., "Practical Use of Linear Elastic and Yielding Fracture Mechanics with Particular Reference to Pressure Vessels." Proceedings of the Institute of Mechanical Engineers Conference, London, May 1971, p.28.

3. PD 6493:1980, "Guidance on Some Methods for the Derivation of Acceptance Levels for Defects in Fusion Welded Joints." British Standards Institution, March 1980.

4. BS 5762: 1979, "Methods for Crack Opening Displacement (COD) Testing." British Standards Institution, London, 1979.

5. Shih, C.F. and German, M.D., "Requirements for a One Parameter Characterization of Crack Tip Fields by the HRR Singularity." *International Journal of Fracture*, Vol. 17, 1981, pp. 27-43.

6. McMeeking, R.M. and Parks, D.M., "On Criteria for J-Dominance of Crack-Tip Fields in Large-Scale Yielding." ASTM STP 668, American Society of Testing and Materials, Philadelphia, PA, 1979, pp. 175-194.

7. Hutchinson, J.W., "Singular Behavior at the End of a Tensile Crack Tip in a Hardening Material." *Journal of the Mechanics and Physics of Solids*, Vol. 16, 1968, pp. 13-31.

8. Rice, J.R. and Rosengren, G.F., Plane Strain Deformation near a Crack Tip in a Power-Law Hardening Material." *Journal of the Mechanics and Physics of Solids*, Vol. 16, 1968, pp. 1-12.

9. Shih, C.F. "J-Dominance under Plane Strain Fully Plastic Conditions: the Edge Crack Panel Subject to Combined Tension and Bending." *International Journal of Fracture*, Vol. 29, 1985, pp. 73-84.

10. Rice, J.R. and Tracey, D.M. "Computational Fracture Mechanics." In: Numerical Computer Methods in Structural Mechanics." S.J. Fanves, et al., Eds., Academic Press, New York, 1973, pp. 585-623.

11. Shih, C.F., Moran, B., and Nakamura, T., "Energy Release Rate along a Three-Dimensional Crack Front in a Thermally Stressed Body." *International Journal of Fracture*, Vol. 30, 1986, pp. 79-102.

12. Dodds, R.H., Anderson, T.L., and Kirk, M.T., "A Framework to Assess a/W Ratio Effects on Elastic-Plastic Fracture Toughness (Jc) in SENB Specimens." to be presented at the 5th International Conference on Numerical Methods in Fracture Mechanics, Frieburg, Germany, April, 1990.

13. Lin, T., Evans, A.G. and Ritchie, R.O., "Statistical Model of Brittle Fracture by Transgranular Cleavage." *Journal of the Mechanics and Physics of Solids*, Vol 34, 1986, pp. 477-496.

14. Wallin, K., Saario, T., and Törrönen, K., "Statistical Model for Carbide Induced Brittle Fracture in Steel." *Metal Science*, Vol. 18, 1984, p. 13.

15. Beremin, F.M., "A Local Criterion for Cleavage Fracture of a Nuclear Pressure Vessel Steel." *Metallurgical Transactions*, Vol. 14A, 1983, p. 2277.

16. Anderson, T.L. and Stienstra, D., "A Model to Predict the Sources and Magnitude of Scatter in Toughness Data in the Transition Region." *Journal of Testing and Evaluation*, Vol. 17, 1989, pp. 46-53.

17. Narasimhan, R. and Rosakis A.J., "Three Dimensional Effects Near a Crack Tip in a Ductile Three Point Bend Specimen - Part I: A Numerical Investigation." California Institute of Technology, Division of Engineering and Applied Science, Report SM 88-6, Pasadena, CA, January 1988.

18. Landes J.D. and Shaffer, D.H., "Statistical Characterization of Fracture in the Transition Region." ASTM STP 700, American Society of Testing and Materials, Philadelphia, PA, 1980, p. 368.

19. Sorem, W.A., "The Effect of Specimen Size and Crack Depth on the Elastic-Plastic Fracture Toughness of a Low-Strength High-Strain Hardening Steel." Ph.D. Dissertation, University of Kansas, Lawrence, KS, May 1989.

20. Wallin, K. Fracture Toughness Testing in the Ductile-Brittle Transition Region." In: *Advances in Fracture Research, Proceedings of the Seventh International Conference on Fracture (ICF7)*, K. Salama, et. al., Eds., Pergamon Press, Oxford, UK, 1989, pp. 267-276.

Table 1. Matrix of finite element solutions.

Geometry:	Hardening Exponent:		
	n = 5	n = 10	n = 50
Small Scale Yielding	X	X	X
a/W = 0.50	X	X	X
a/W = 0.15	X	X	X
a/W = 0.05	X	X	X

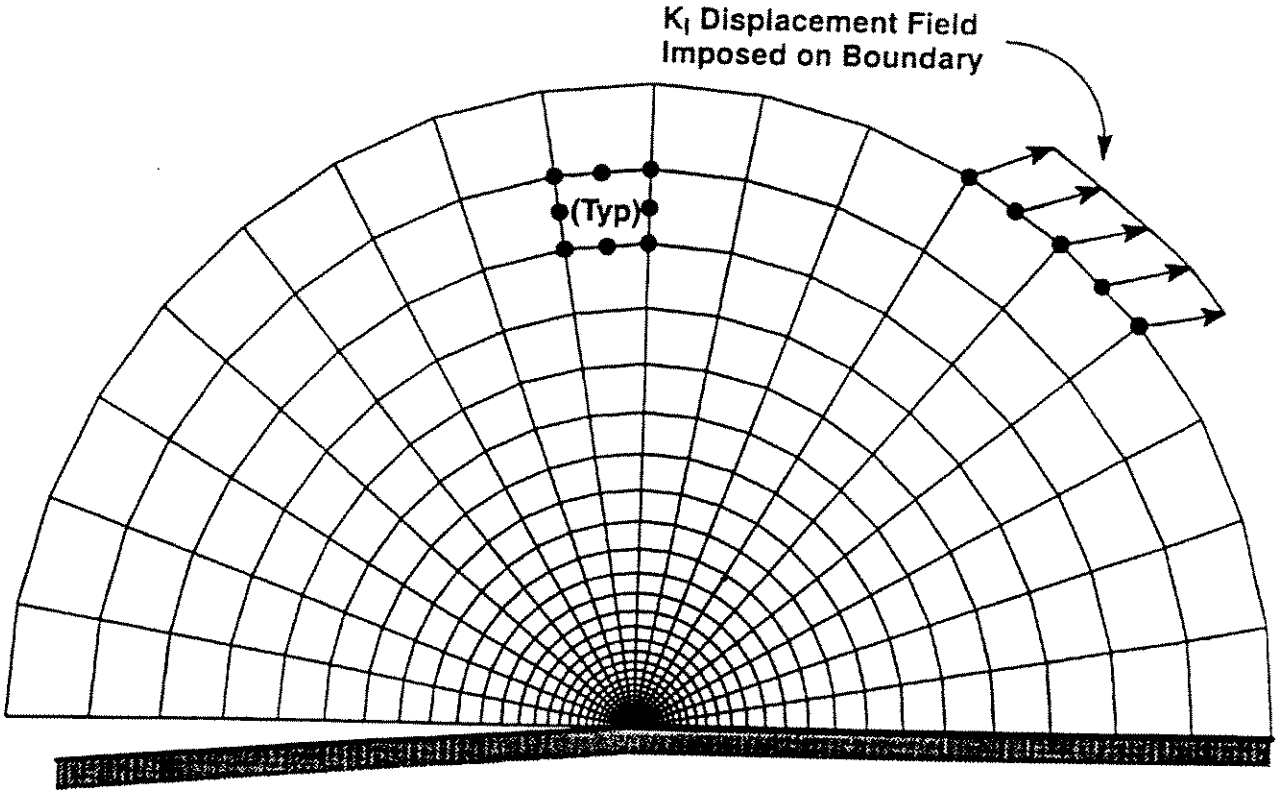

FIG. 1 Finite element mesh used for the small scale yielding analysis (720 elements, 2277 nodes).

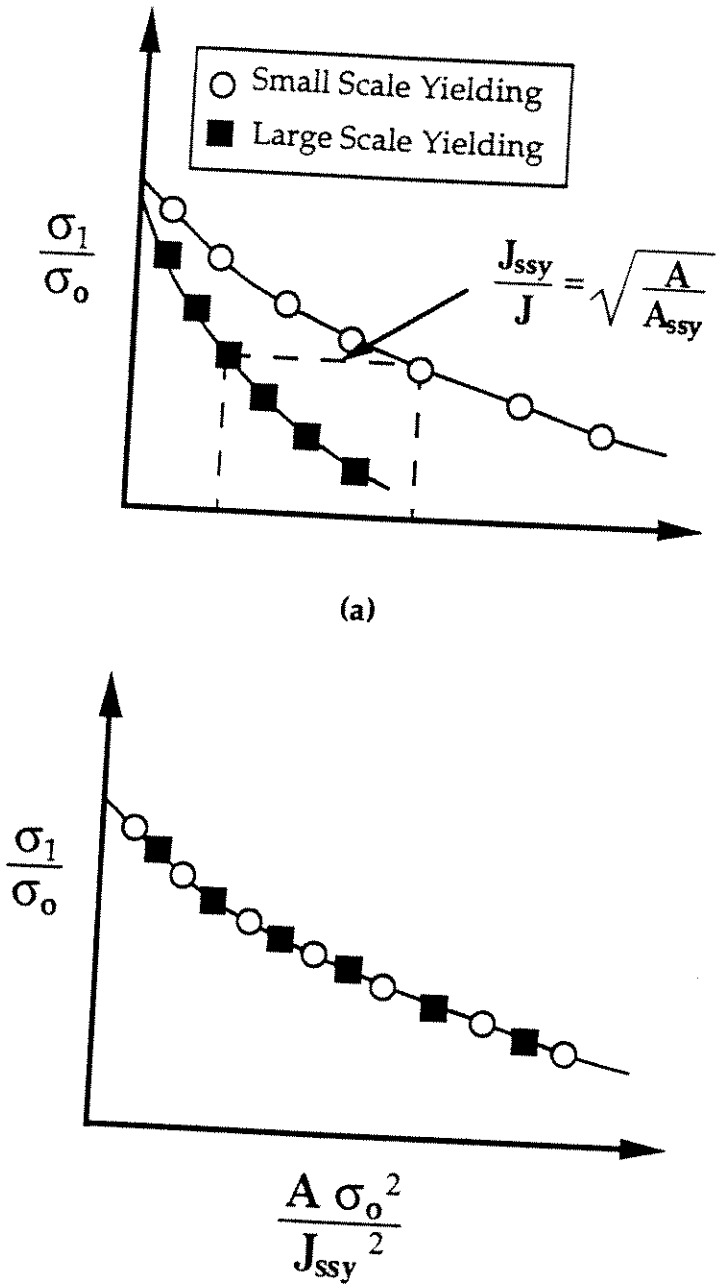

FIG 2. Definition of the effective small scale yielding J integral, J_{ssy}.

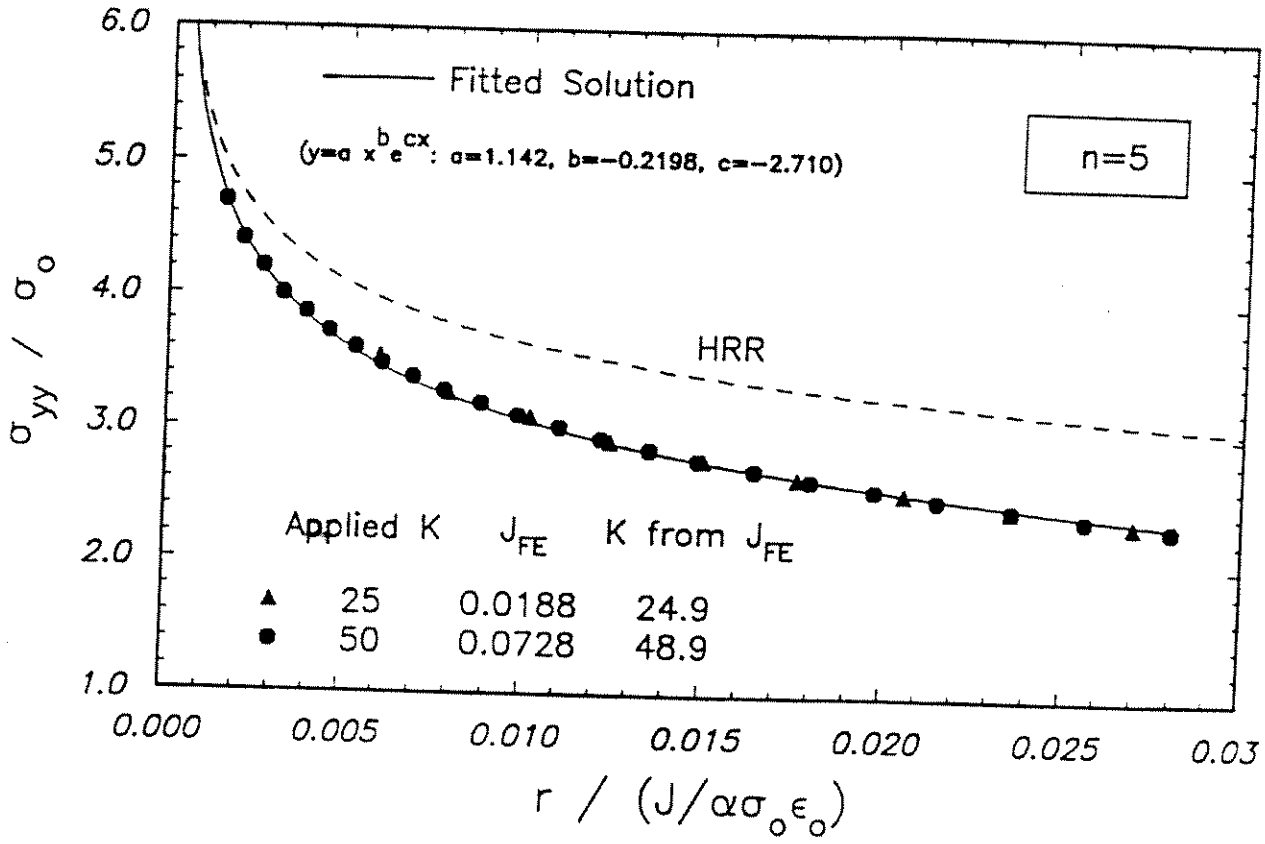

FIG. 3 Stress normal to the crack plane in small scale yielding for n = 5.

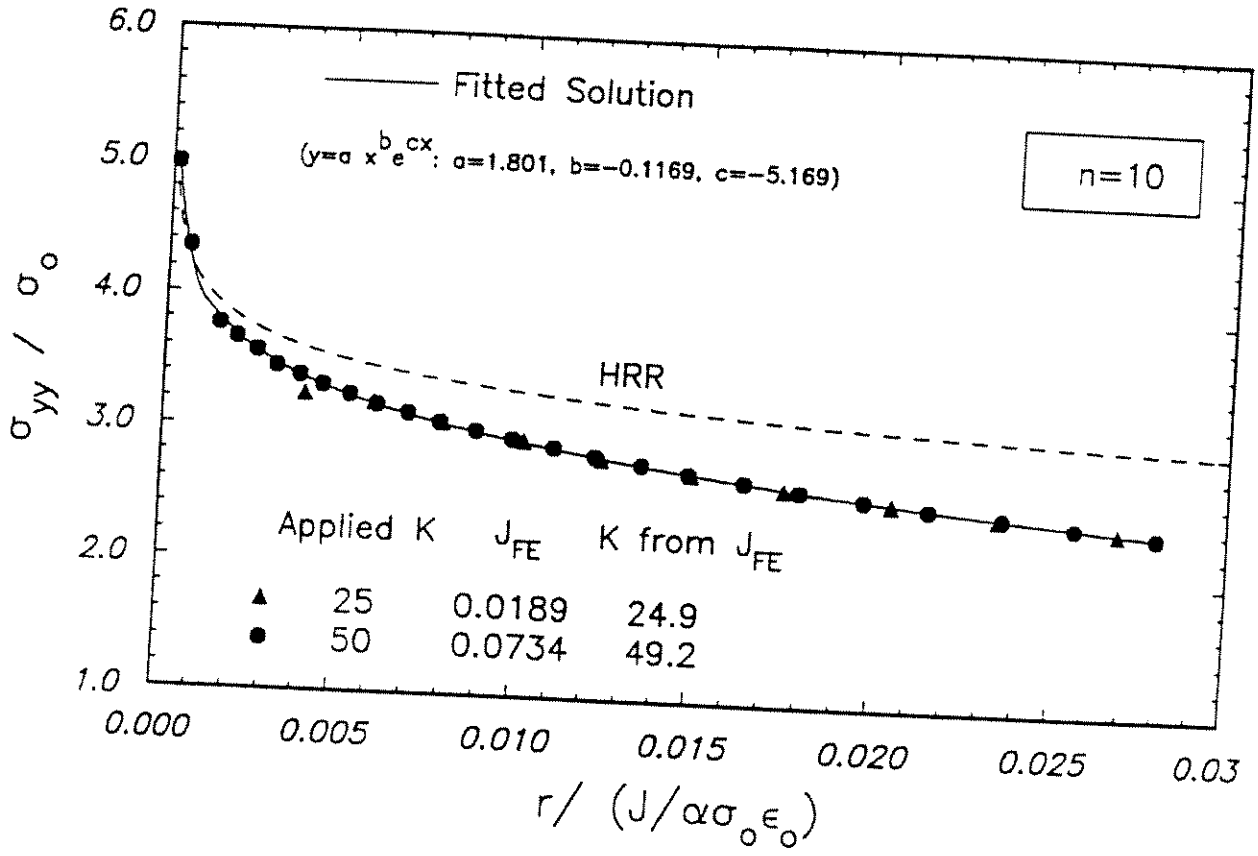

FIG. 4 Stress normal to the crack plane in small scale yielding for n = 10.

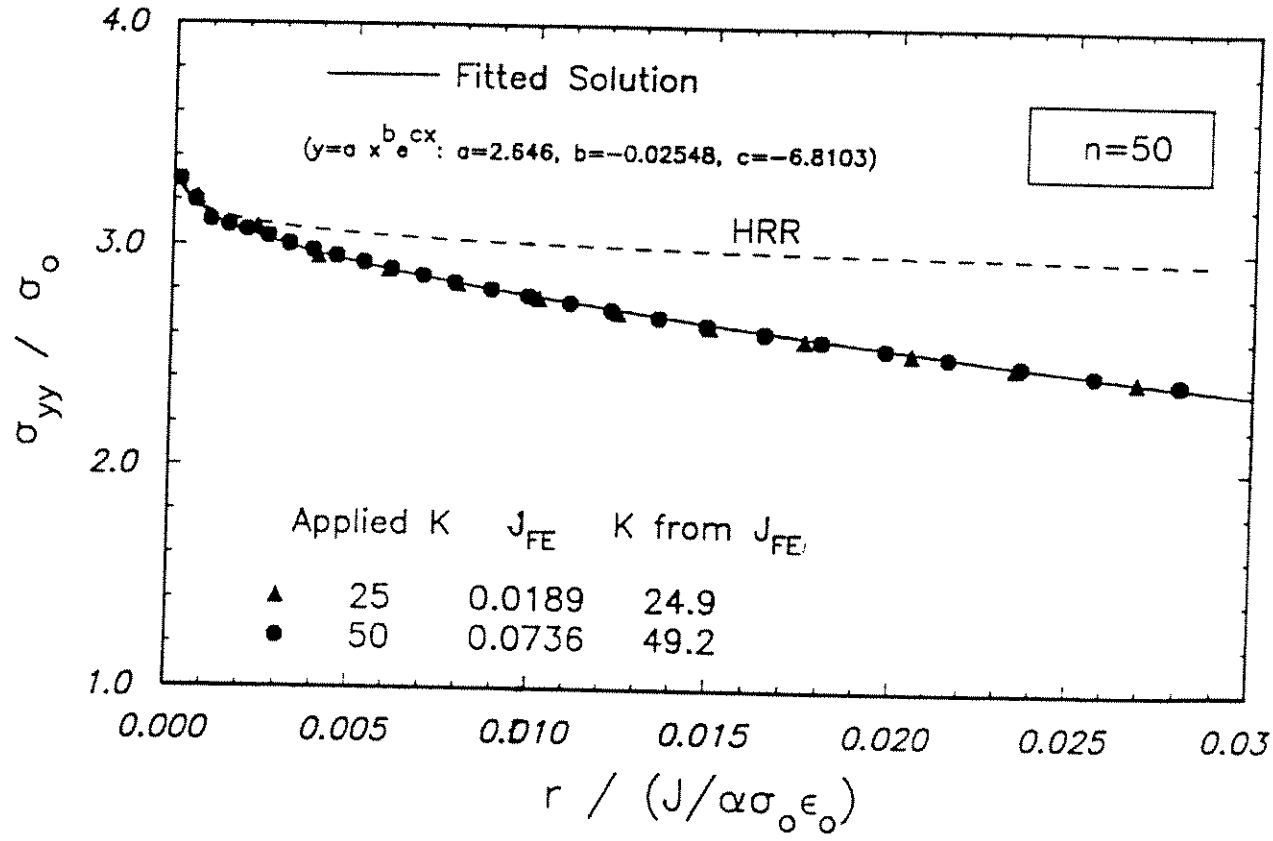

FIG. 5 Stress normal to the crack plane in small scale yielding for n = 50.

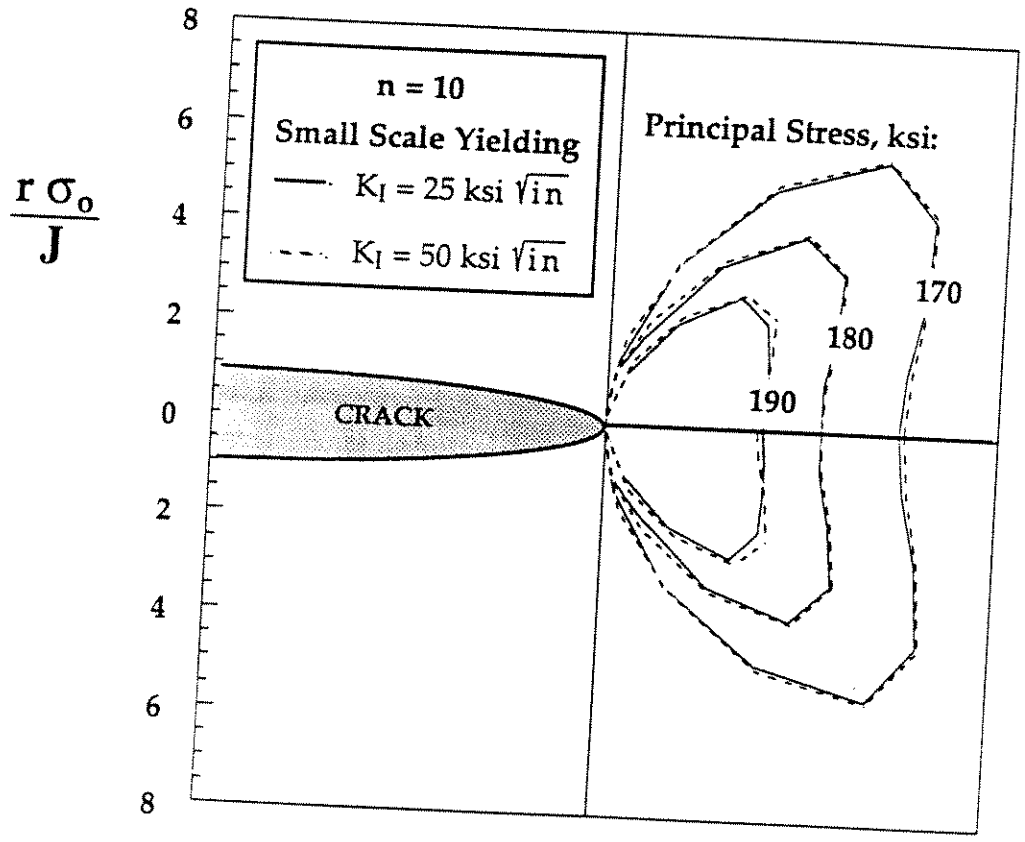

FIG 6. Maximum principal stress contours ahead of a crack in small scale yielding for n = 10.

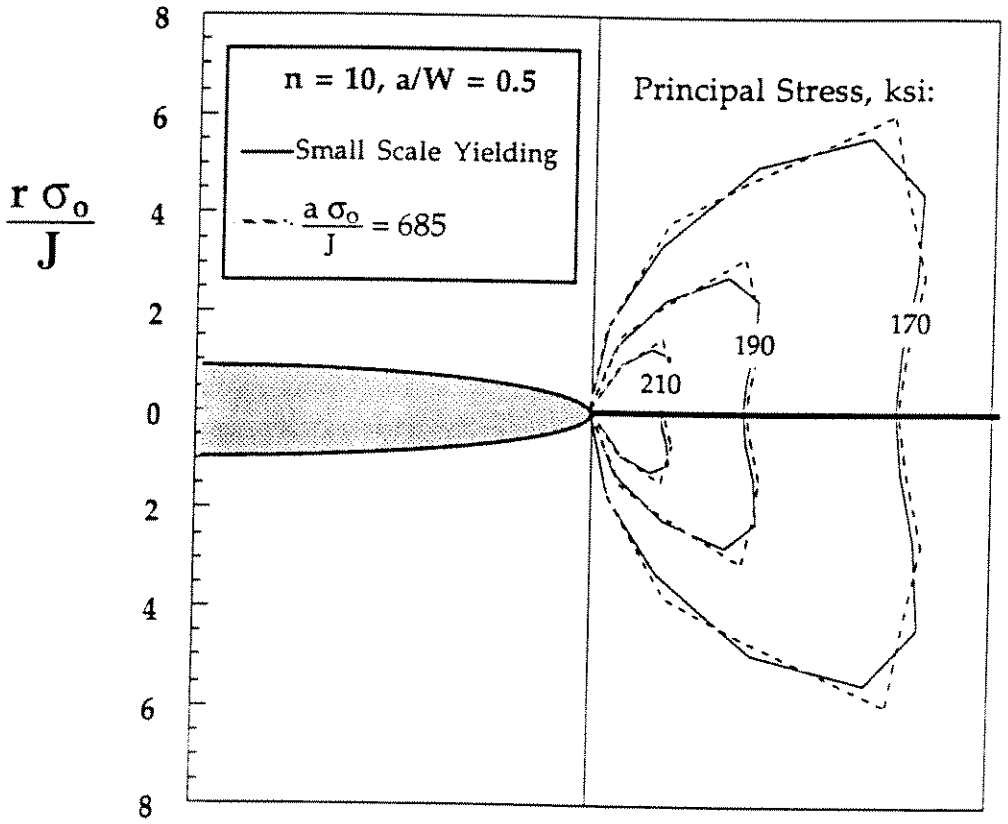

FIG. 7 **Comparison of principal stress contours in small scale yielding and in an SENB specimen with a/W = 0.5 and $a\sigma_o/J = 665$.**

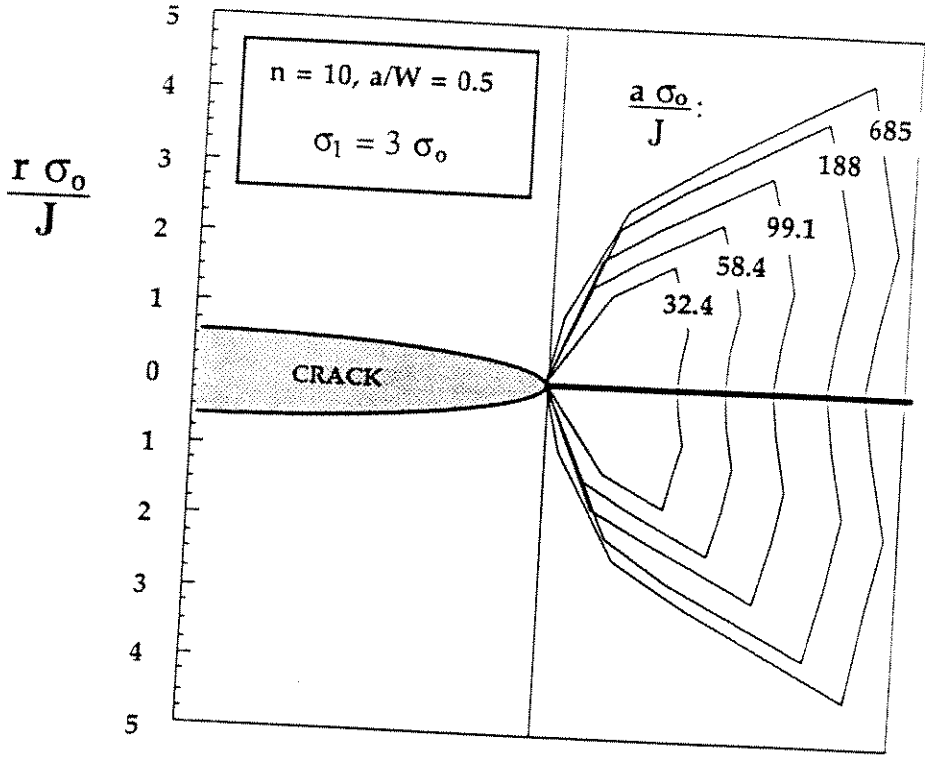

(a) Normalized by J

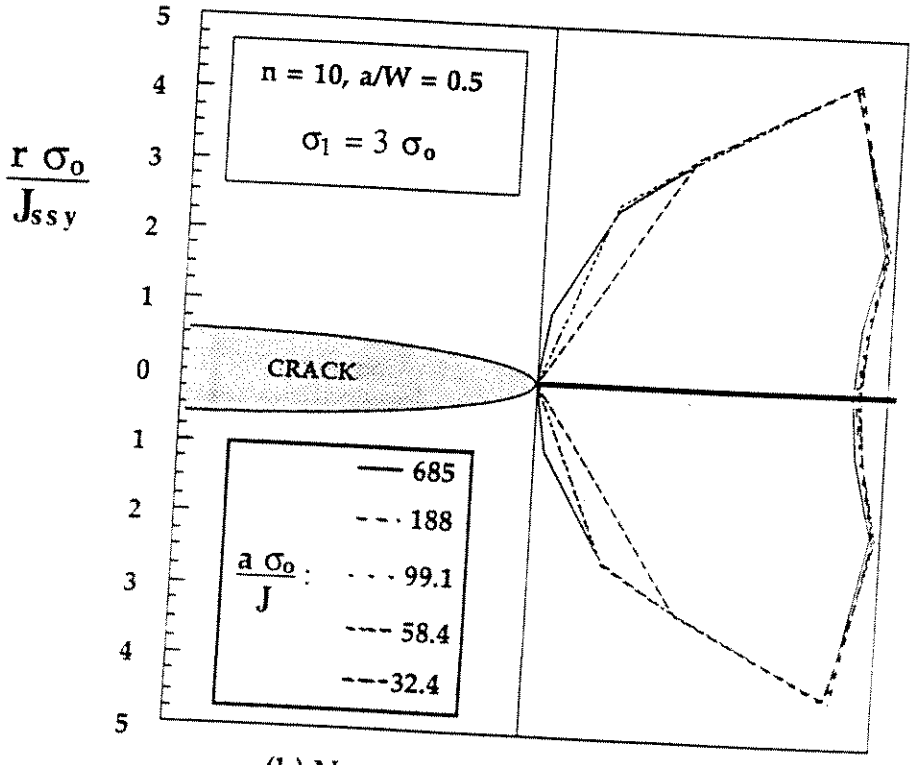

(b) Normalized by Jssy.

FIG 8. Principal stress contours for n = 10 and a/W = 0.5.

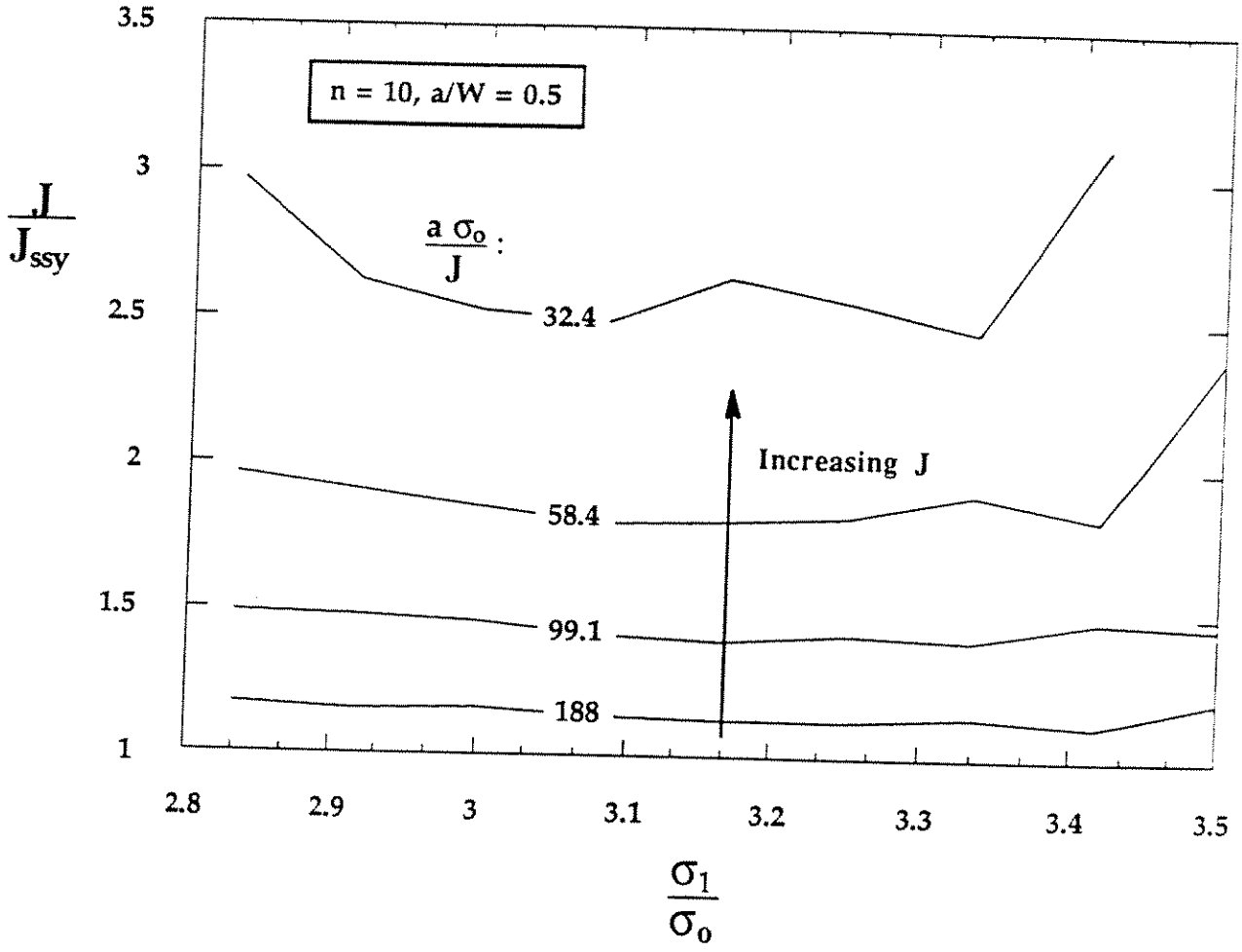

FIG 9. Effect of principal stress on the computed J/J_{ssy} ratio.

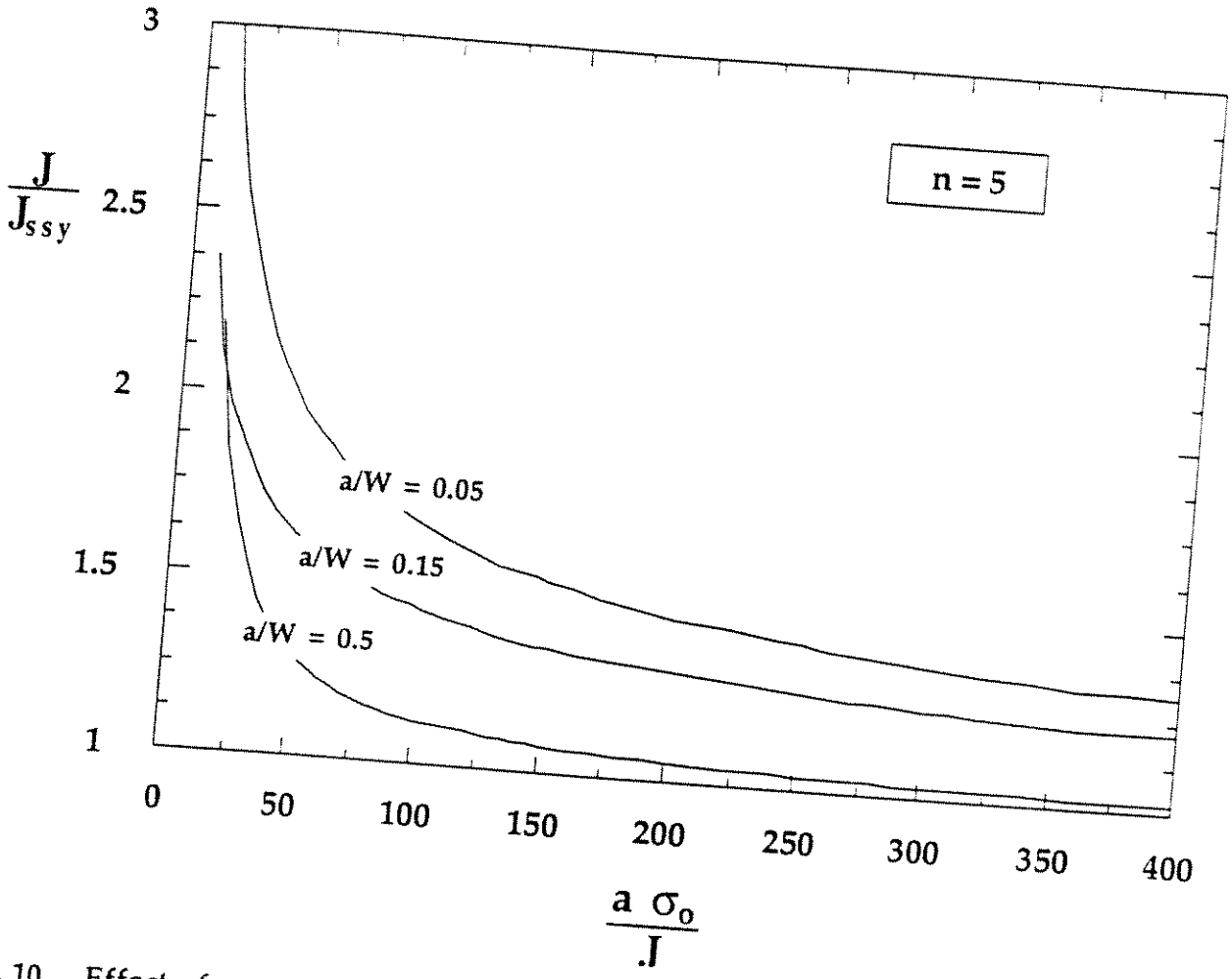

FIG. 10 Effect of crack length and a/W on the J/J_{ssy} ratio for n = 5.

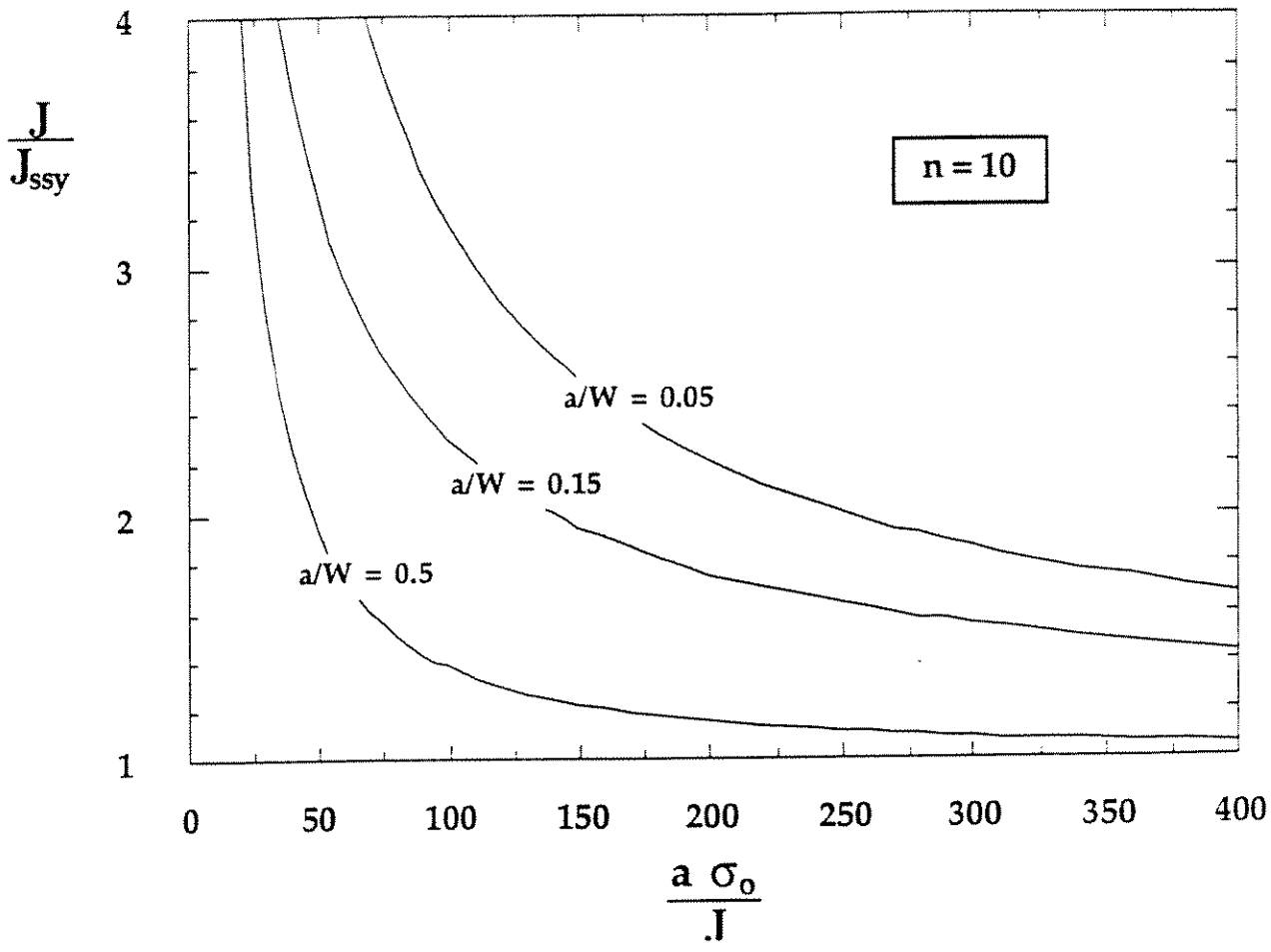

FIG. 11 Effect of crack length and a/W on the J/Jssy ratio for n = 10.

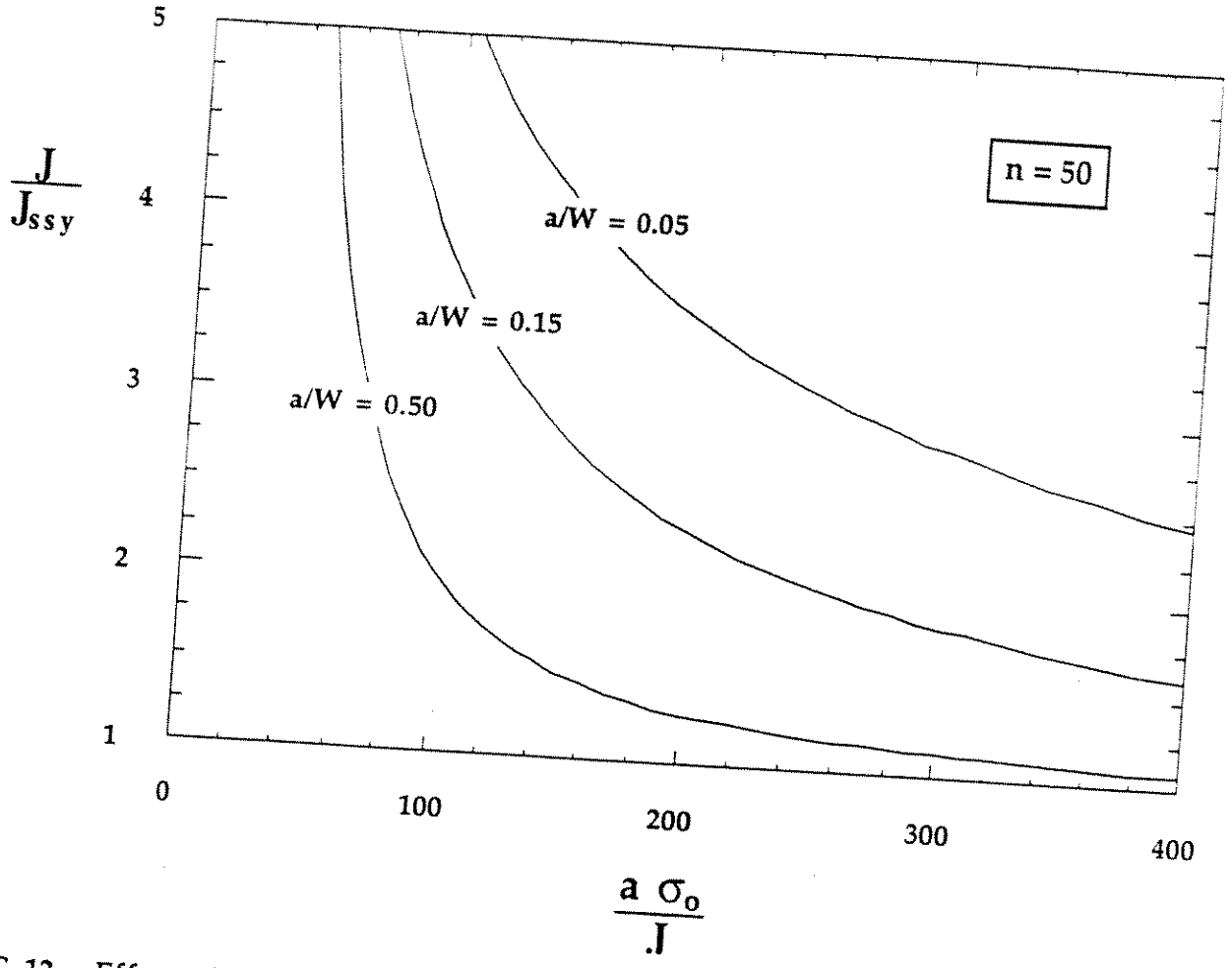

FIG. 12 Effect of crack length and a/W on the J/J_{ssy} ratio for n = 50.

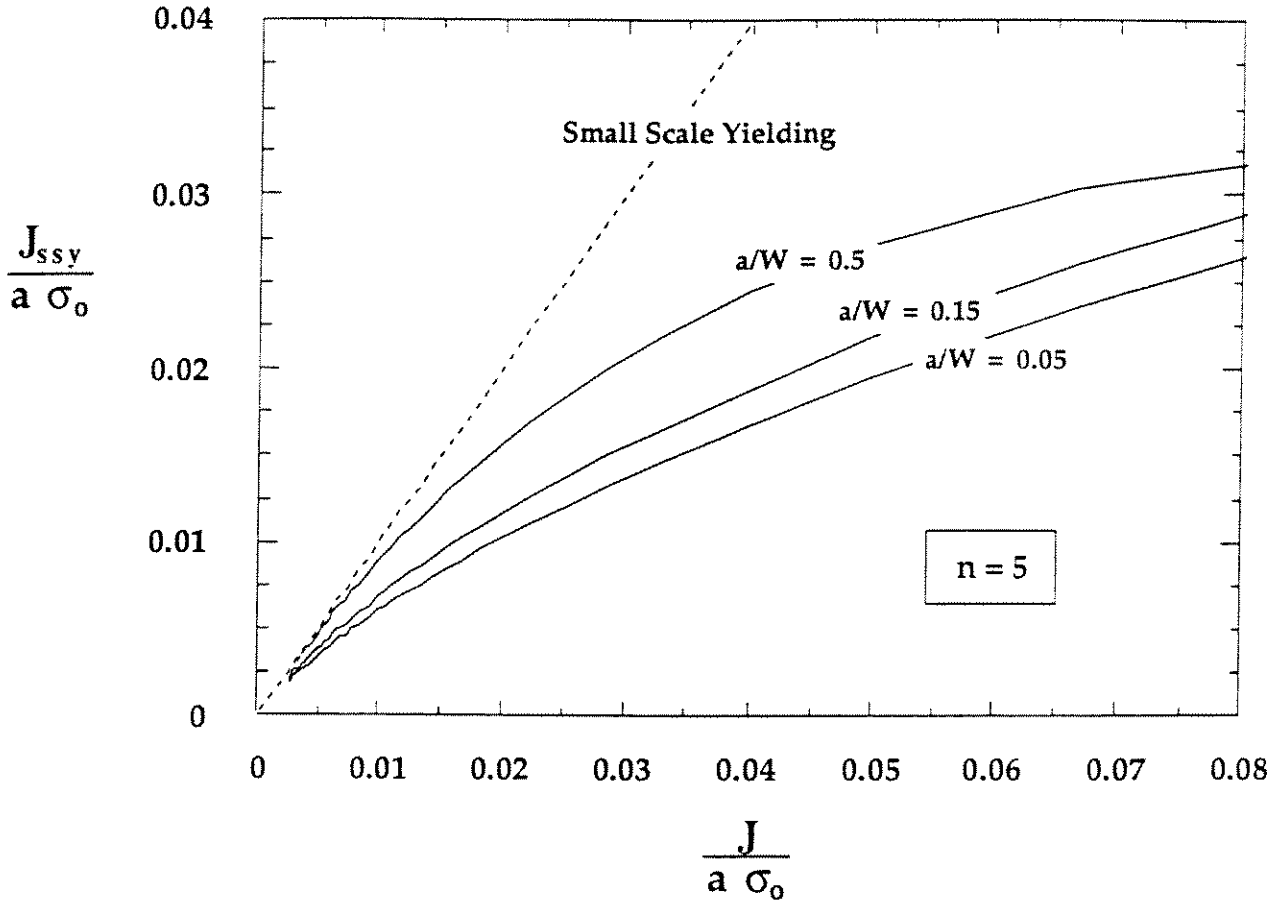

FIG. 13 Comparison of effective and apparent driving force for n = 5

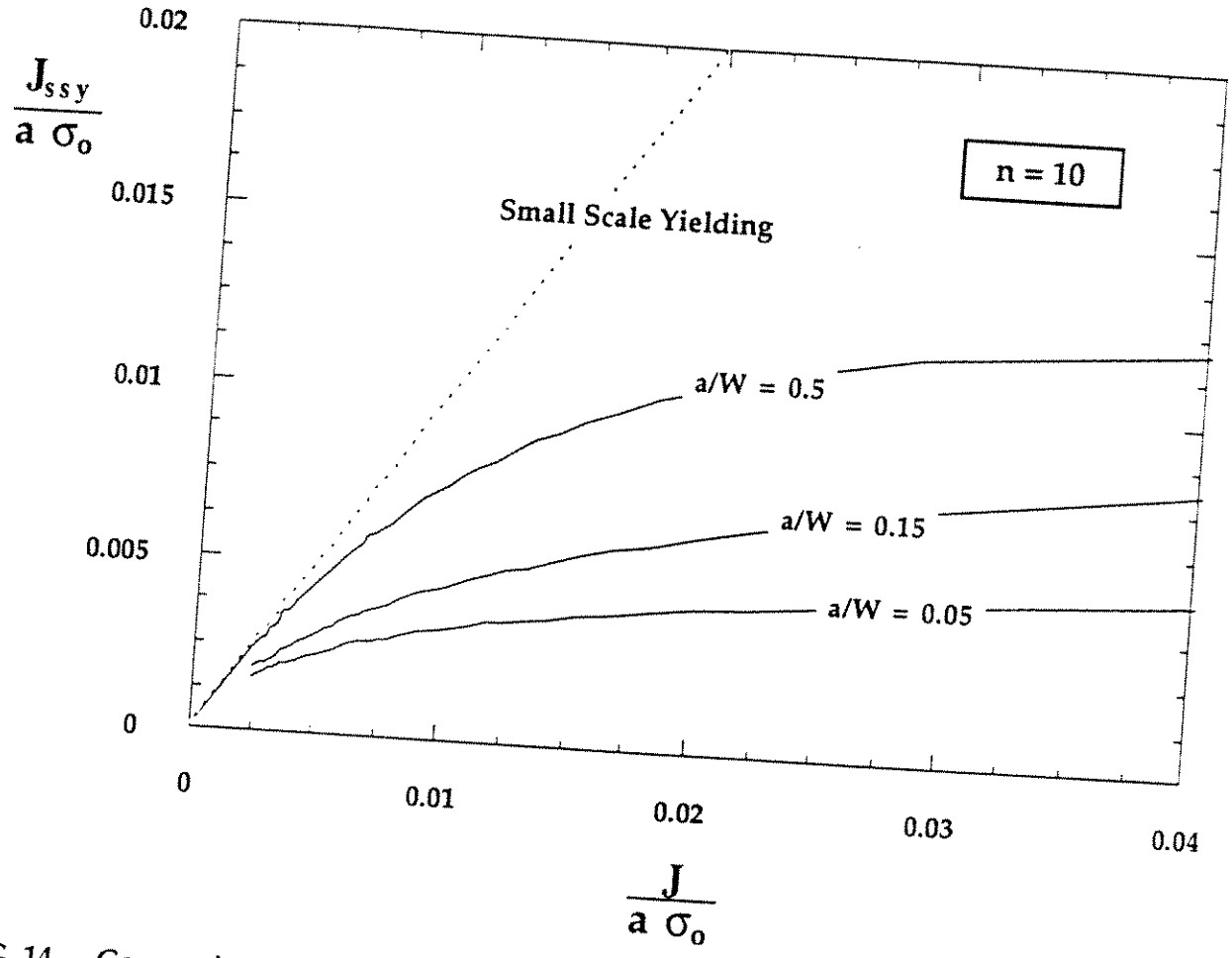

FIG. 14 Comparison of effective and apparent driving force for n = 10

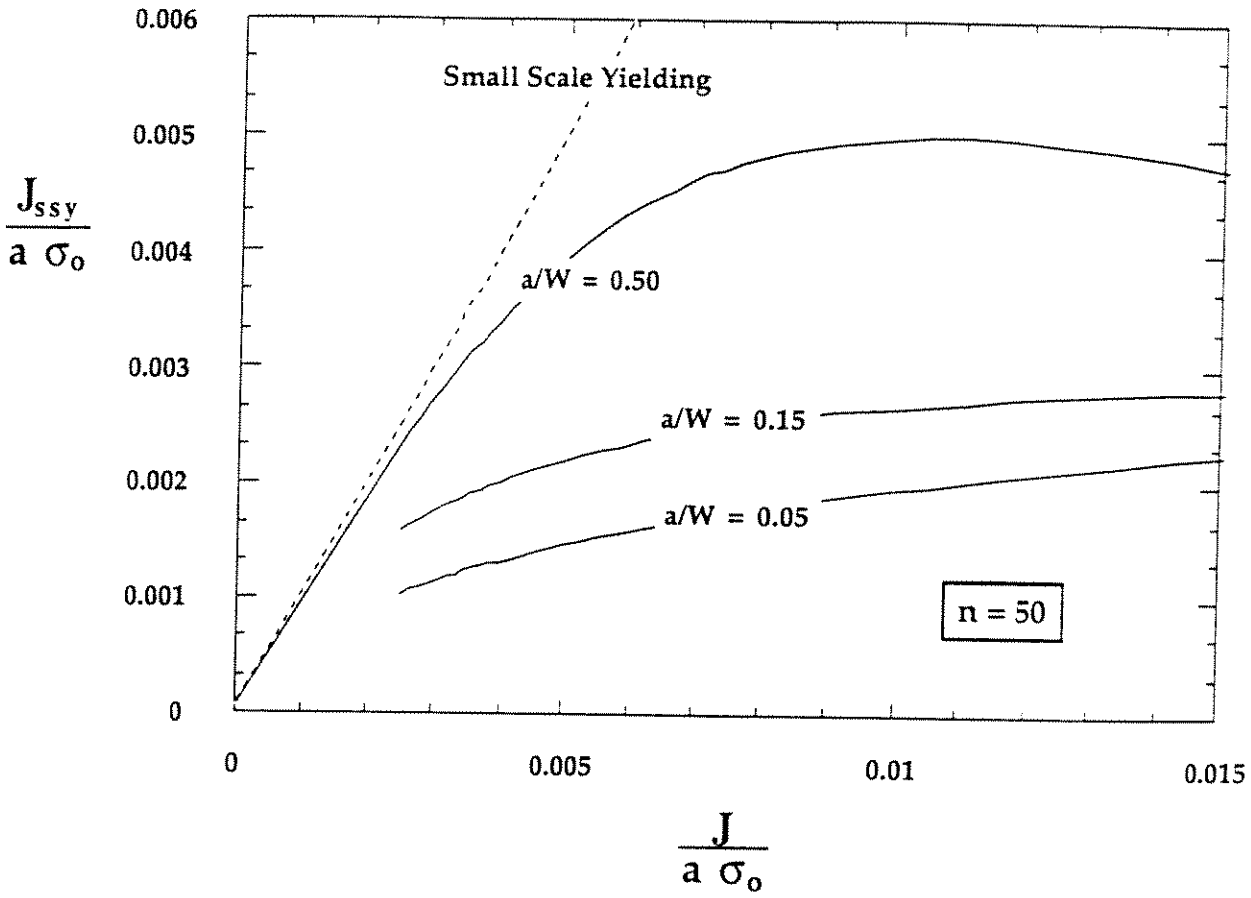

FIG. 15 Comparison of effective and apparent driving force for n = 50

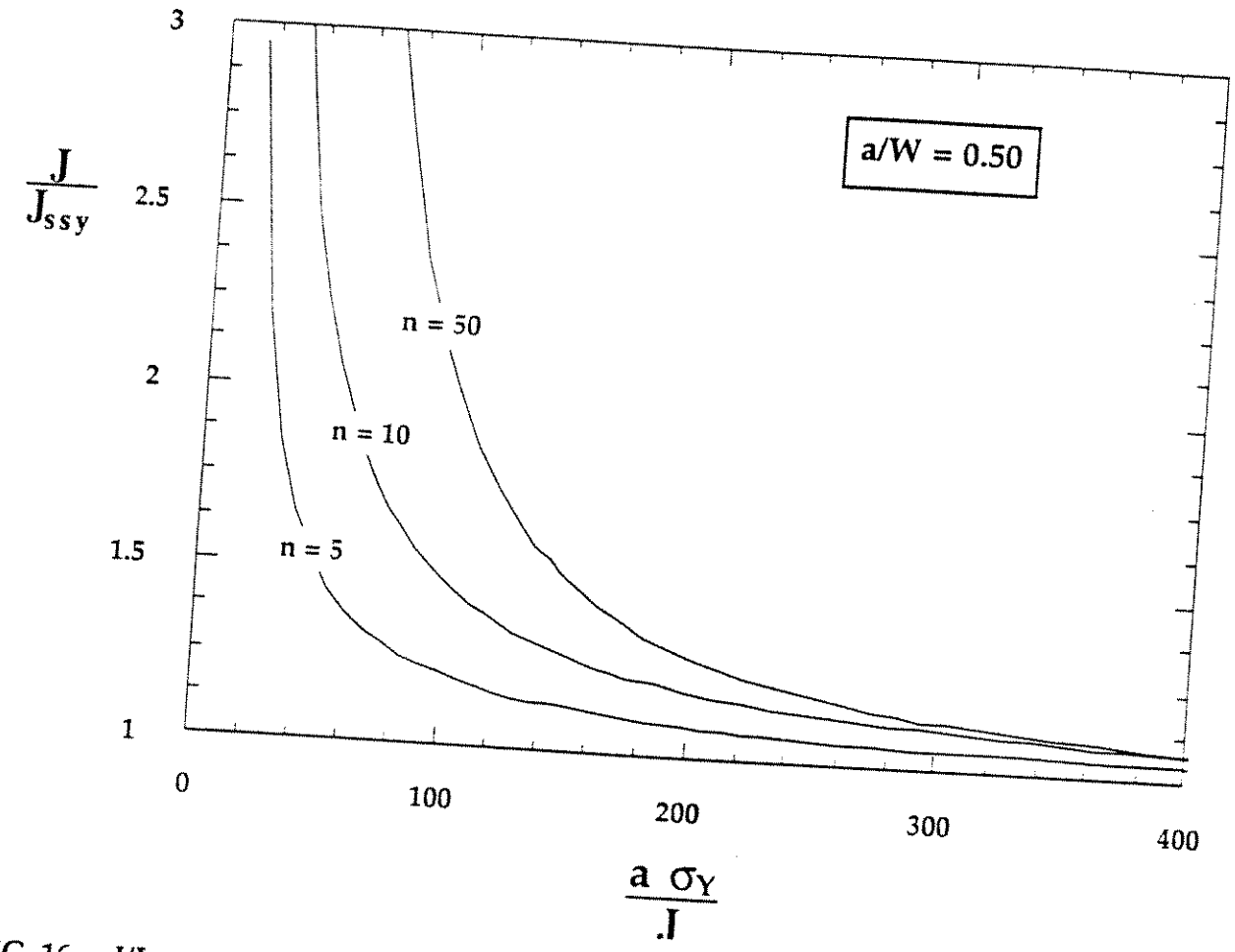

FIG. 16 J/J_{ssy} as a function of strain hardening, J and flow stress.

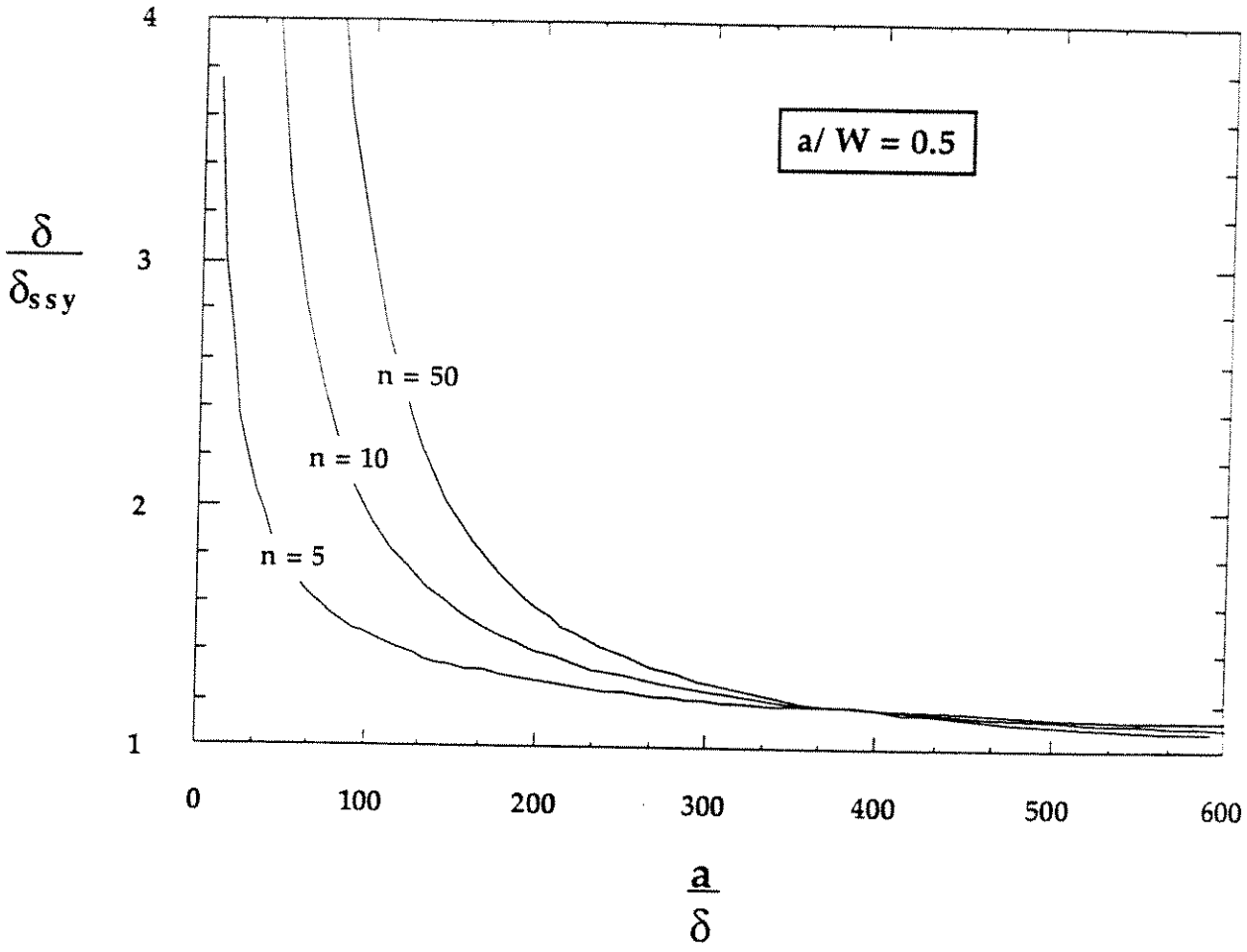

FIG. 17 Effect of specimen size on critical CTOD values for a/W = 0.5

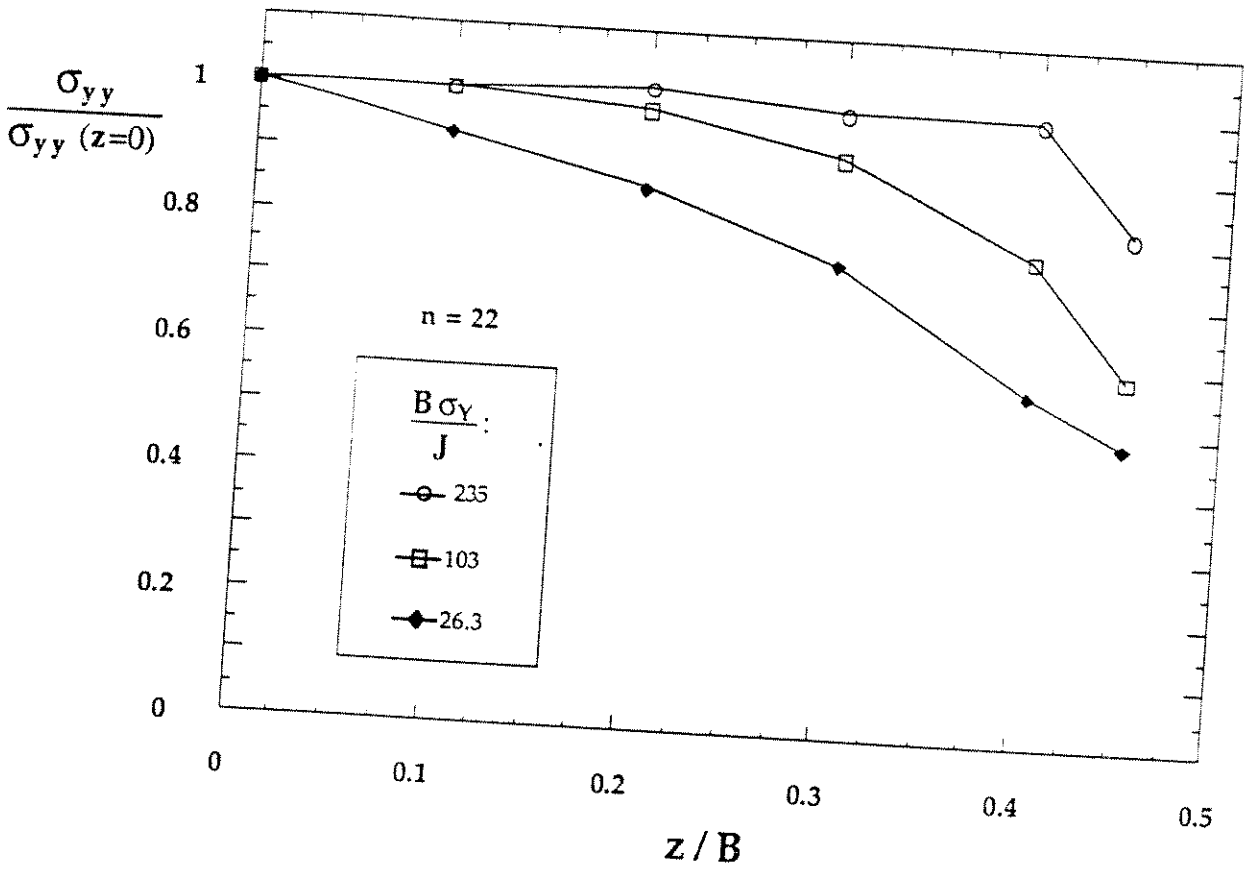

FIG. 18 Variation of normal stress through the thickness of an SENB specimen [17].

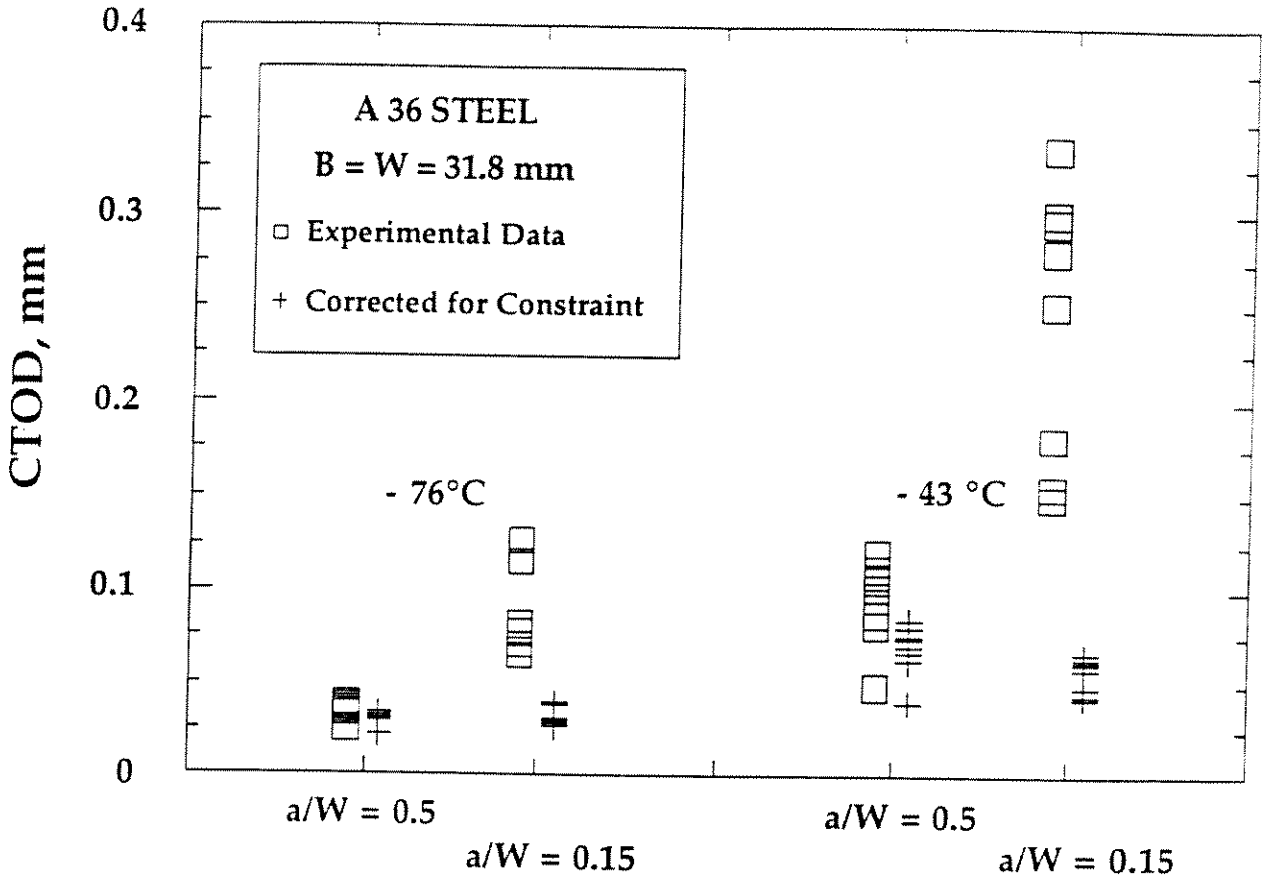

FIG. 19 Comparison of experimental CTOD values for A 36 steel with CTOD corrected for constraint loss. Data were obtained from Sorem [19].

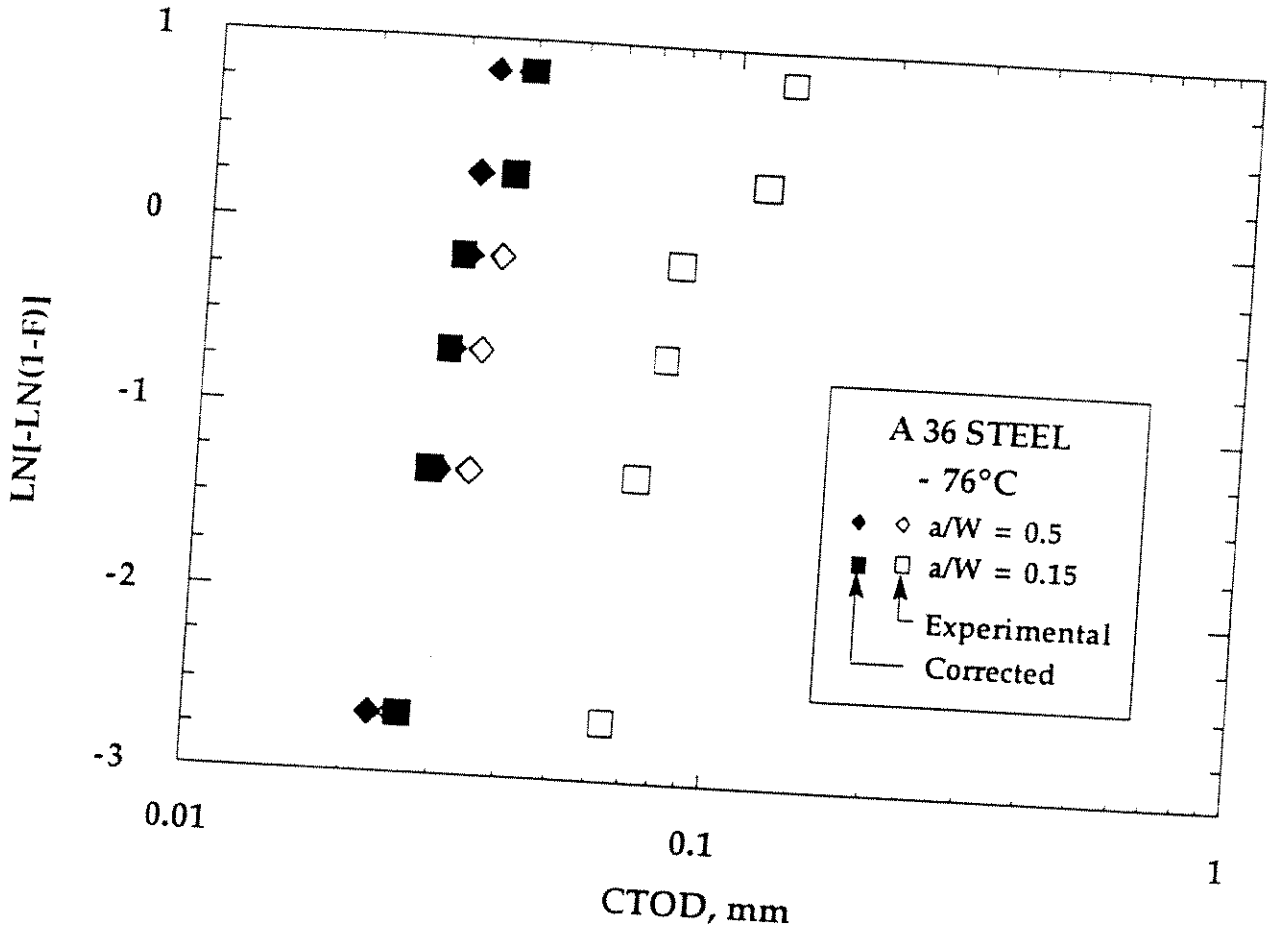

FIG. 20. Weibull plot of A 36 steel CTOD data at - 76°C.

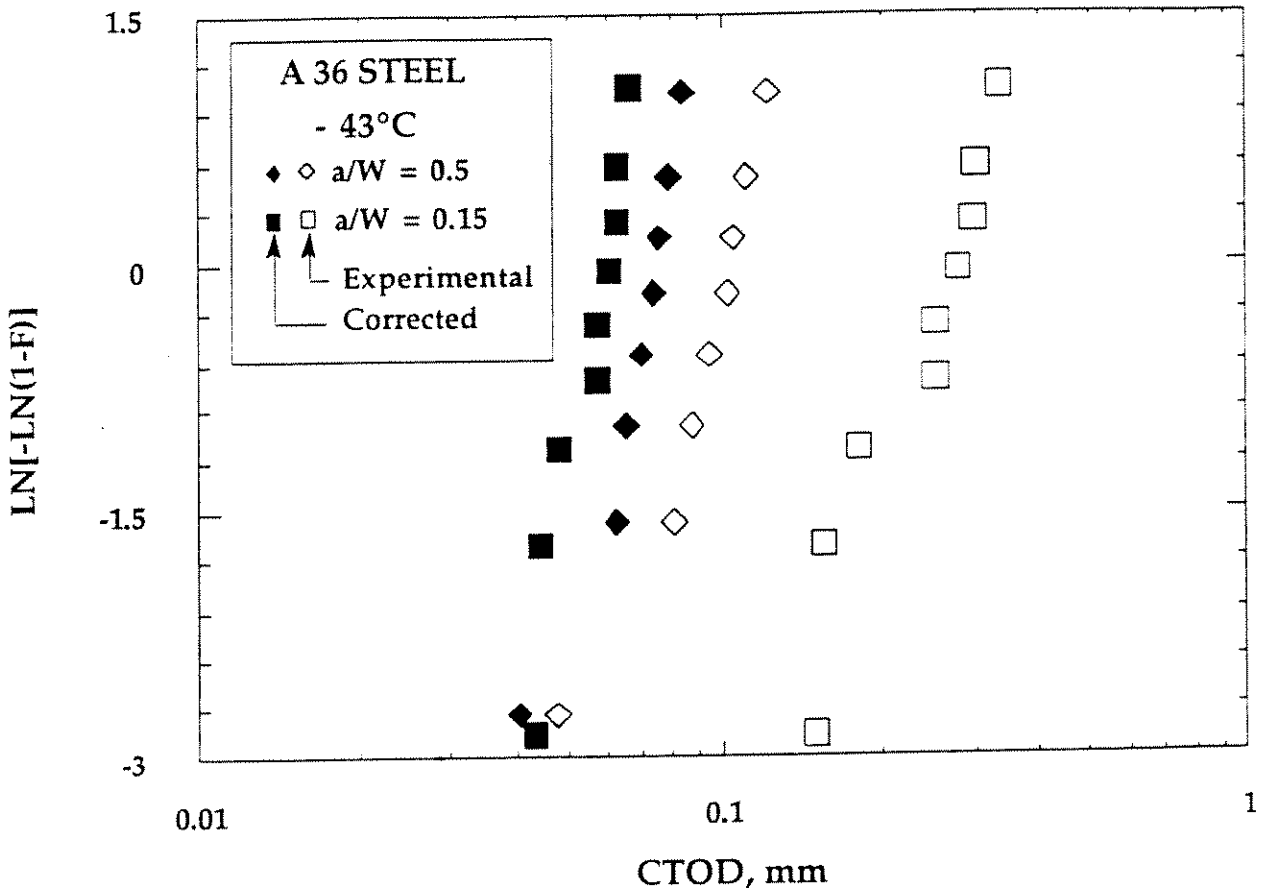

FIG. 21. Weibull plot of A 36 steel CTOD data at - 43°C.

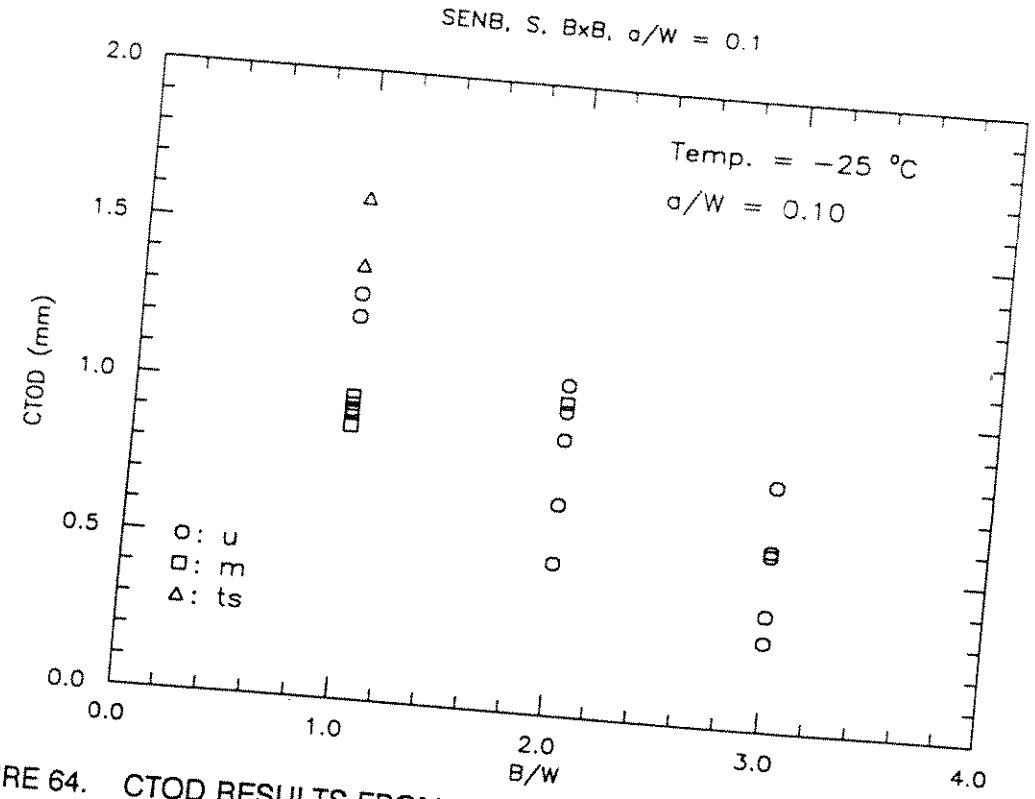

FIGURE 64. CTOD RESULTS FROM SURFACE NOTCHED SENB REPLICATE TESTS (a/W = 0.1)

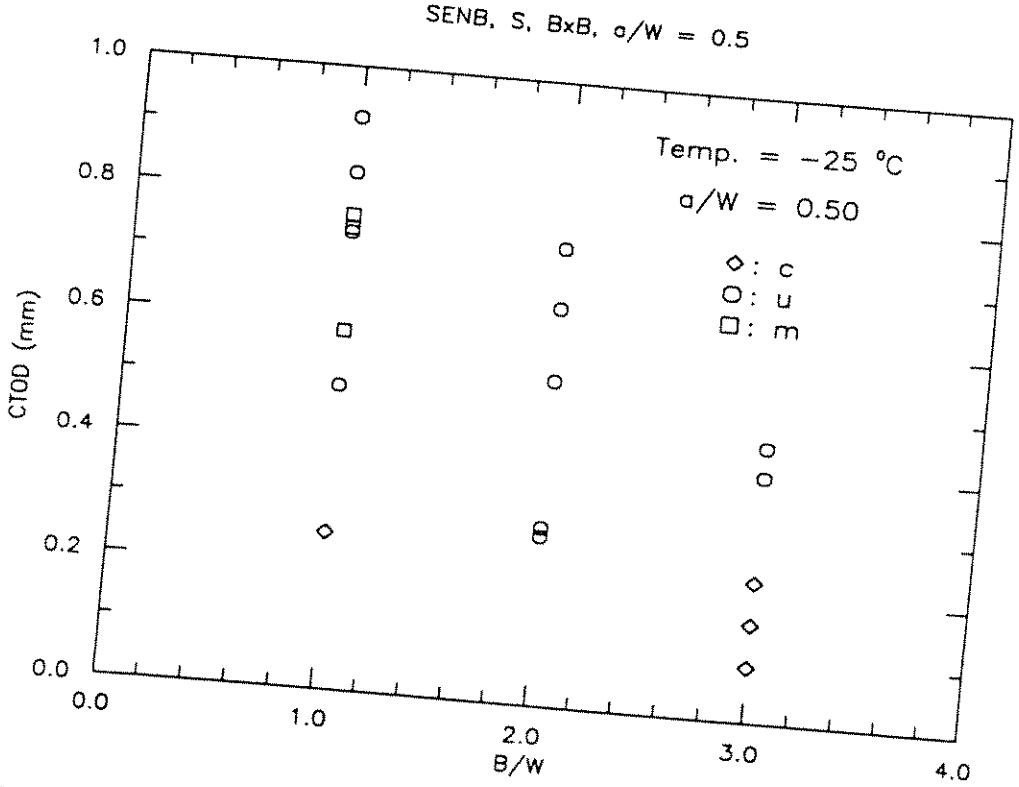

FIGURE 65. CTOD RESULTS FROM SURFACE NOTCHED SENB REPLICATE TESTS (a/W = 0.5)

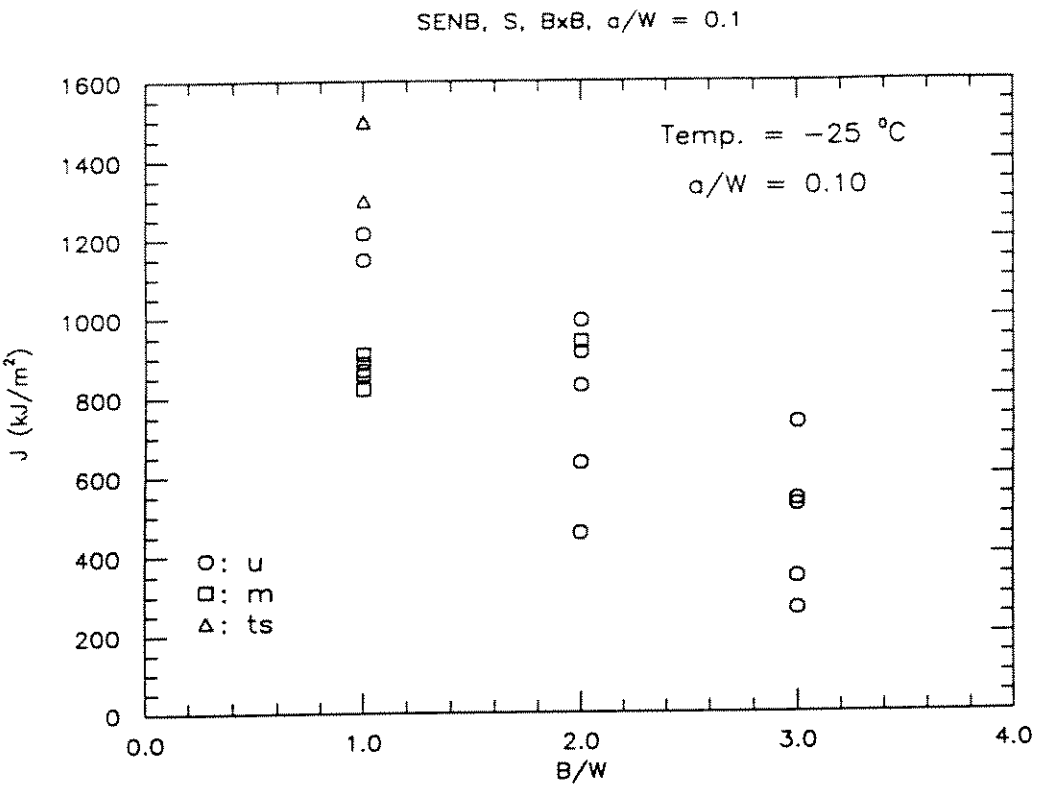

FIGURE 66. J RESULTS FROM SURFACE NOTCHED SENB REPLICATE TESTS (a/W = 0.1)

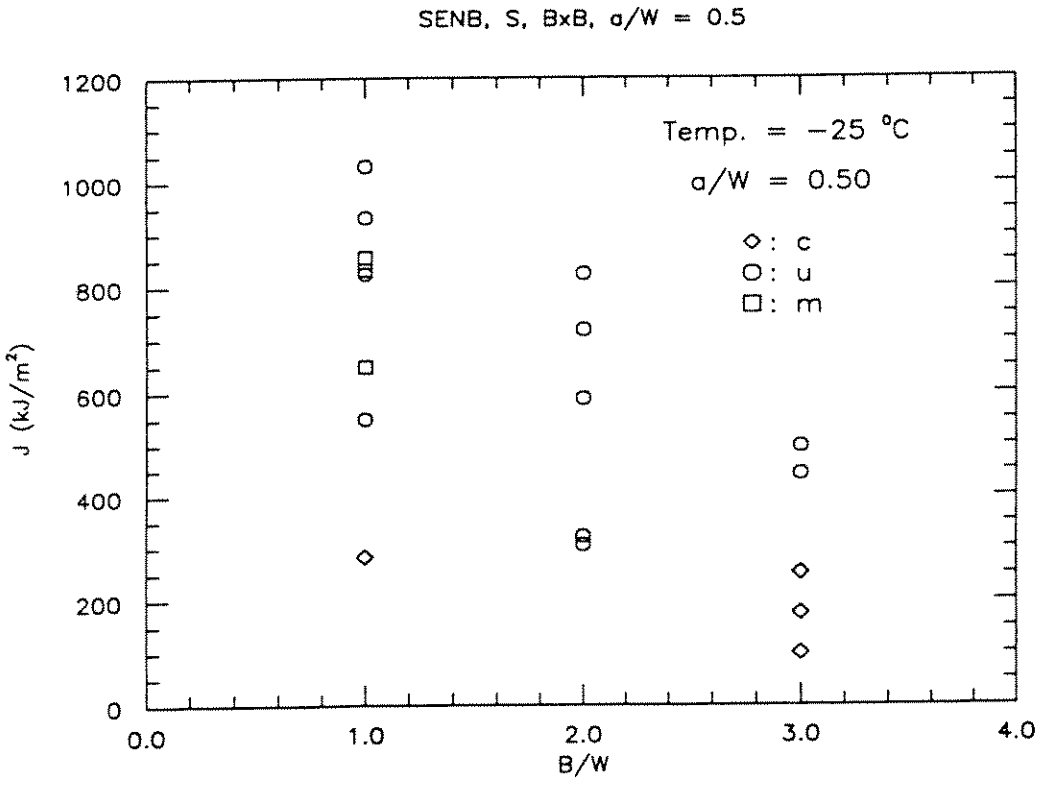

FIGURE 67. J RESULTS FROM SURFACE NOTCHED SENB REPLICATE TESTS (a/W = 0.5)

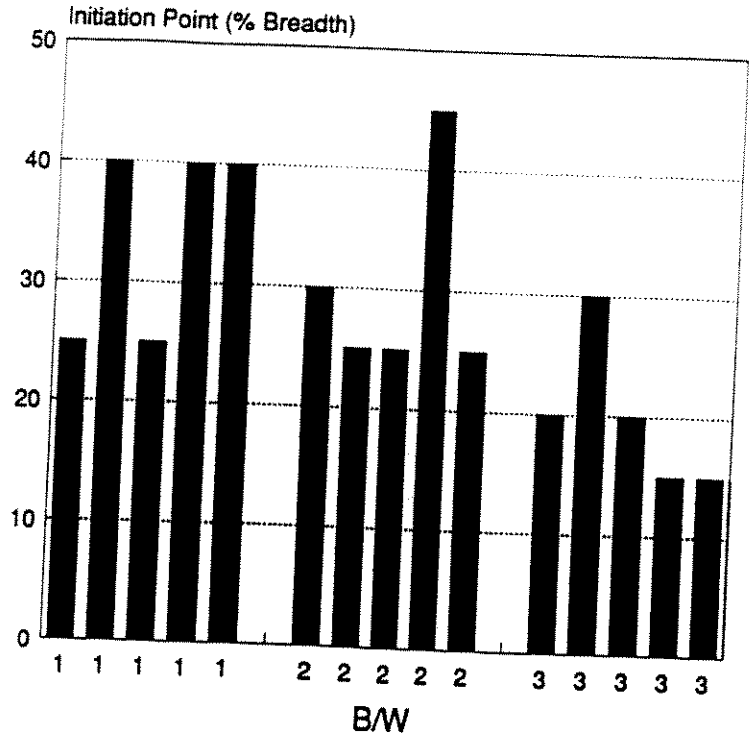

FIGURE 68. FRACTURE INITIATION POSITION IN SURFACE NOTCHED SENB REPLICATE TESTS (a/W = 0.1)

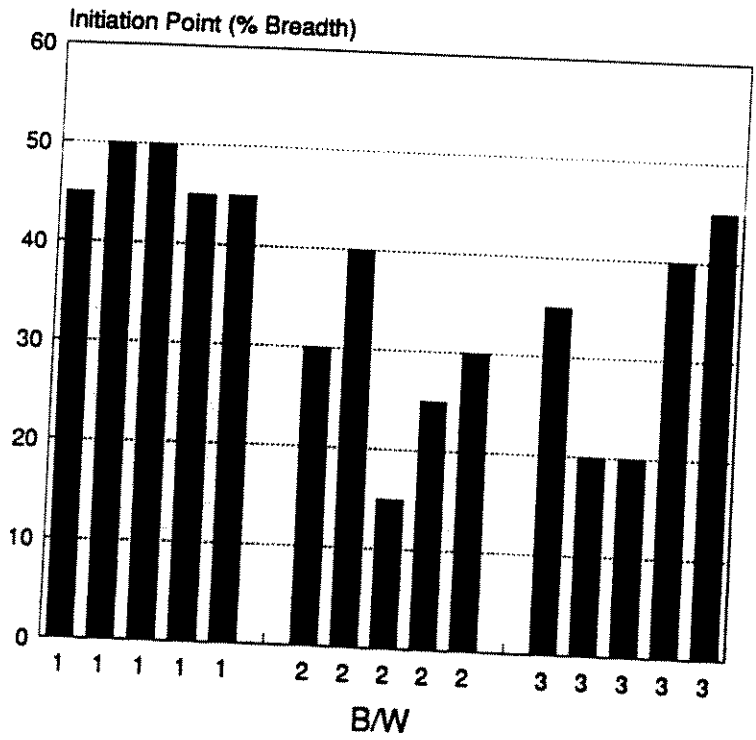

FIGURE 69. FRACTURE INITIATION POSITION IN SURFACE NOTCHED SENB REPLICATE TESTS (a/W = 0.5)

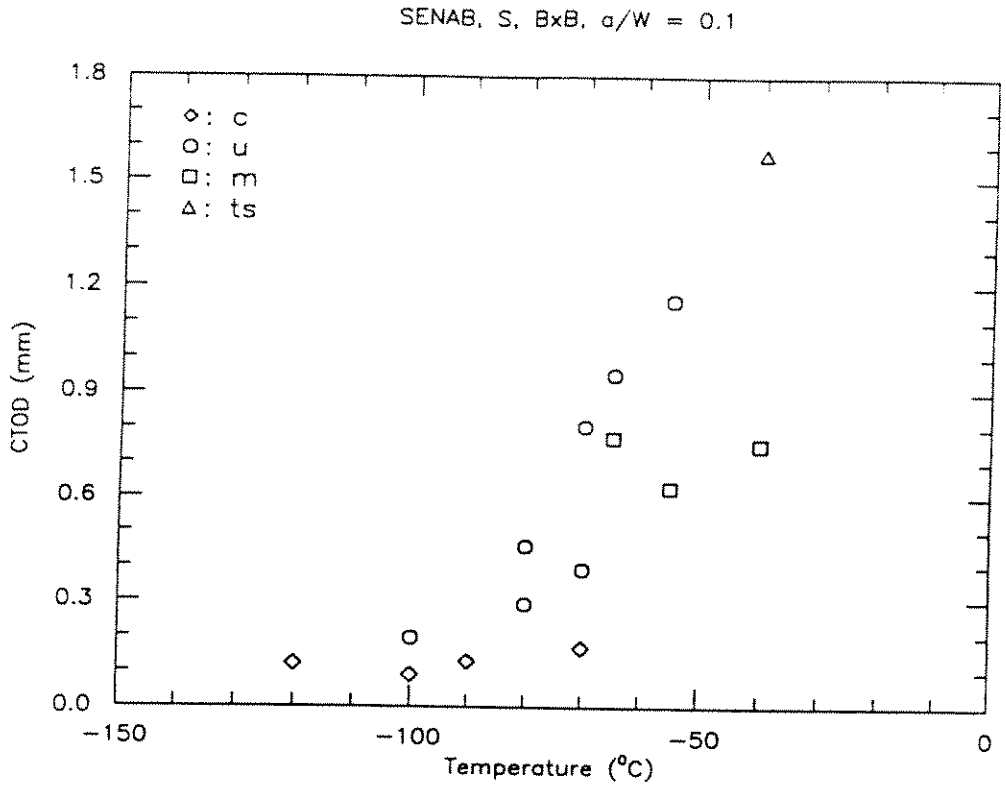

FIGURE 70. CTOD TRANSITION CURVE (SENAB, B × B, a/W = 0.1)

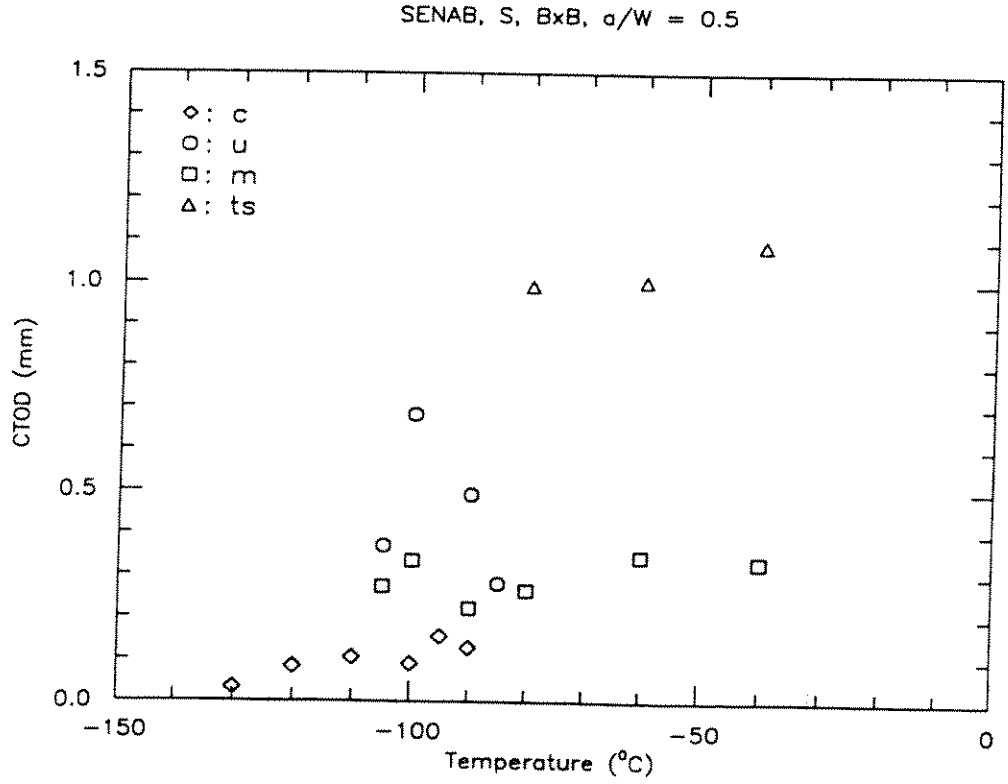

FIGURE 71. CTOD TRANSITION CURVE (SENAB, B × B, a/W = 0.5)

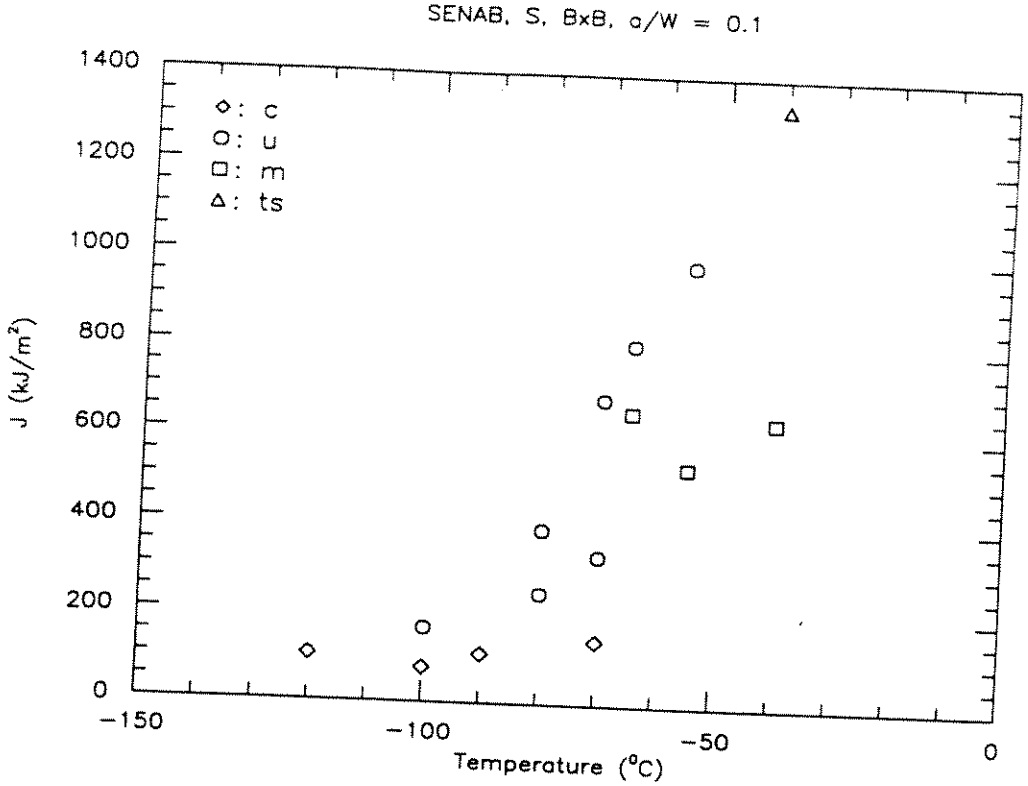

FIGURE 72. J TRANSITION CURVE (SENAB, B × B, a/W = 0.1)

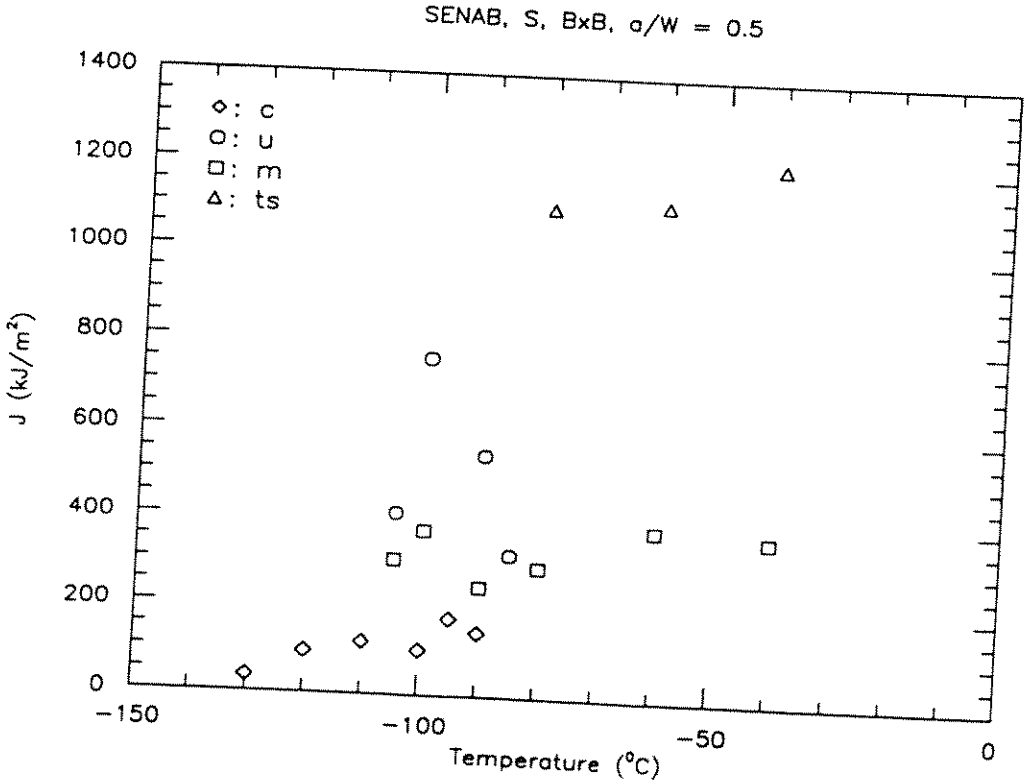

FIGURE 73. J TRANSITION CURVE (SENAB, B × B, a/W = 0.5)

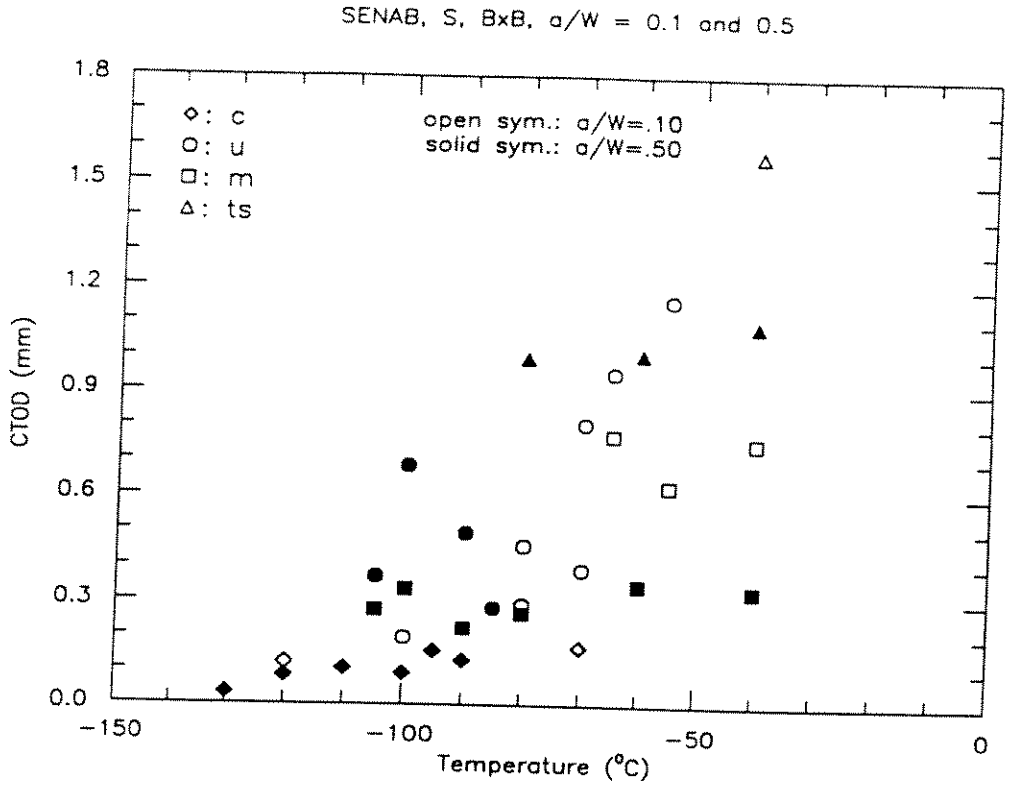

FIGURE 74. COMPARISON OF a/W = 0.1 AND a/W = 0.5 CTOD TRANSITION CURVES (SENAB, B × B)

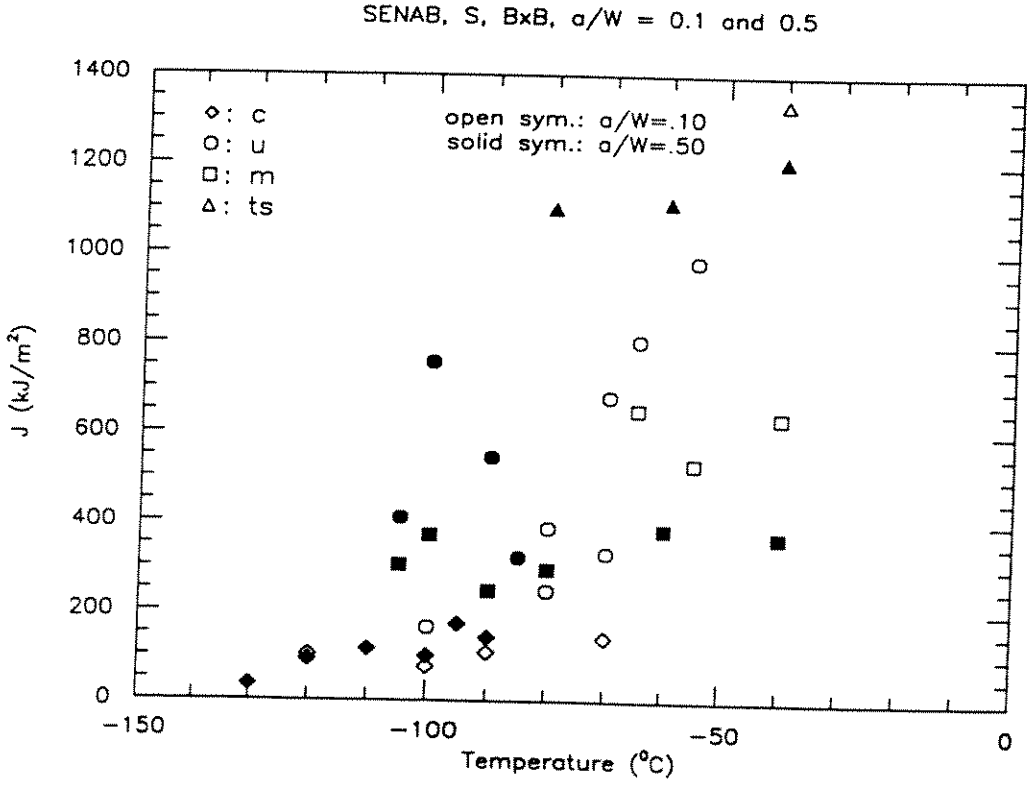

FIGURE 75. COMPARISON OF a/W = 0.1 AND a/W = 0.5 J TRANSITION CURVES (SENAB, B × B)

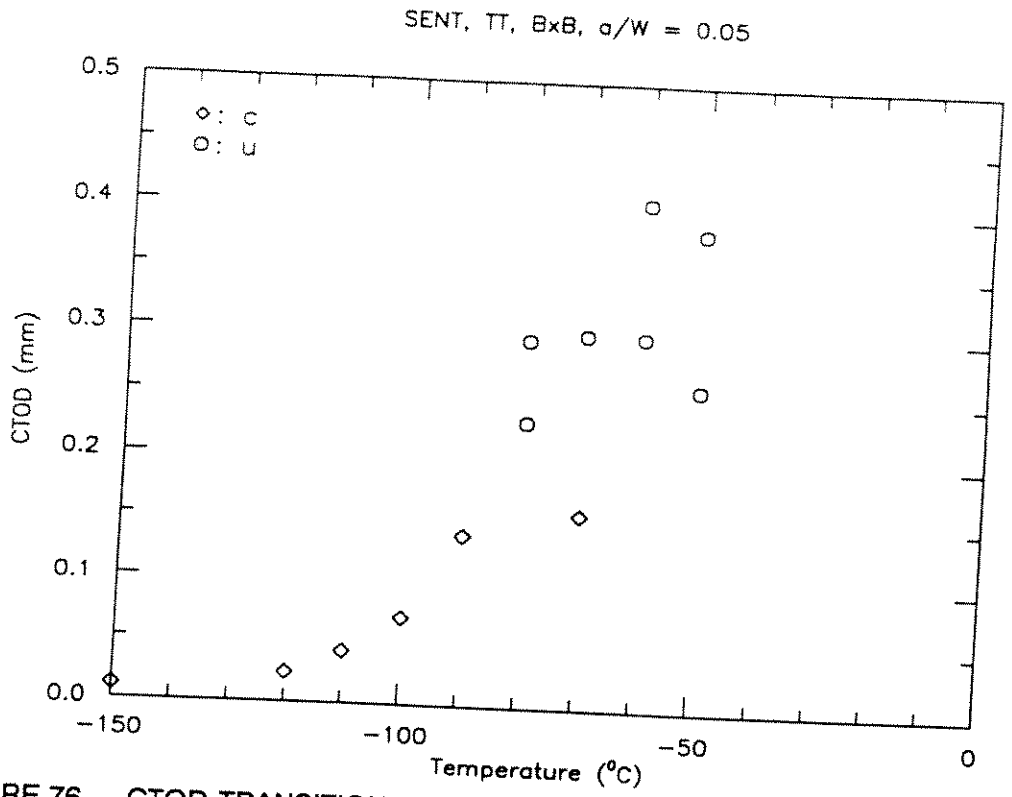

FIGURE 76. CTOD TRANSITION CURVE (SENT, B × B, a/W = 0.05, THROUGH THICKNESS NOTCHED)

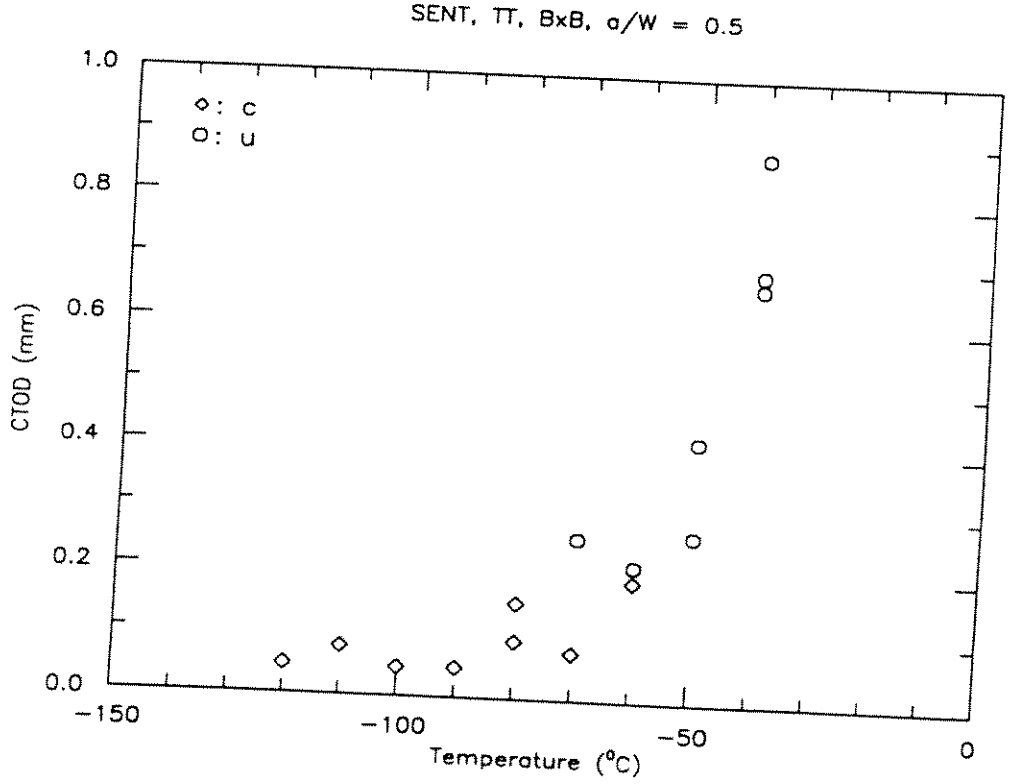

FIGURE 77. CTOD TRANSITION CURVE (SENT, B × B, a/W = 0.5, THROUGH THICKNESS NOTCHED)

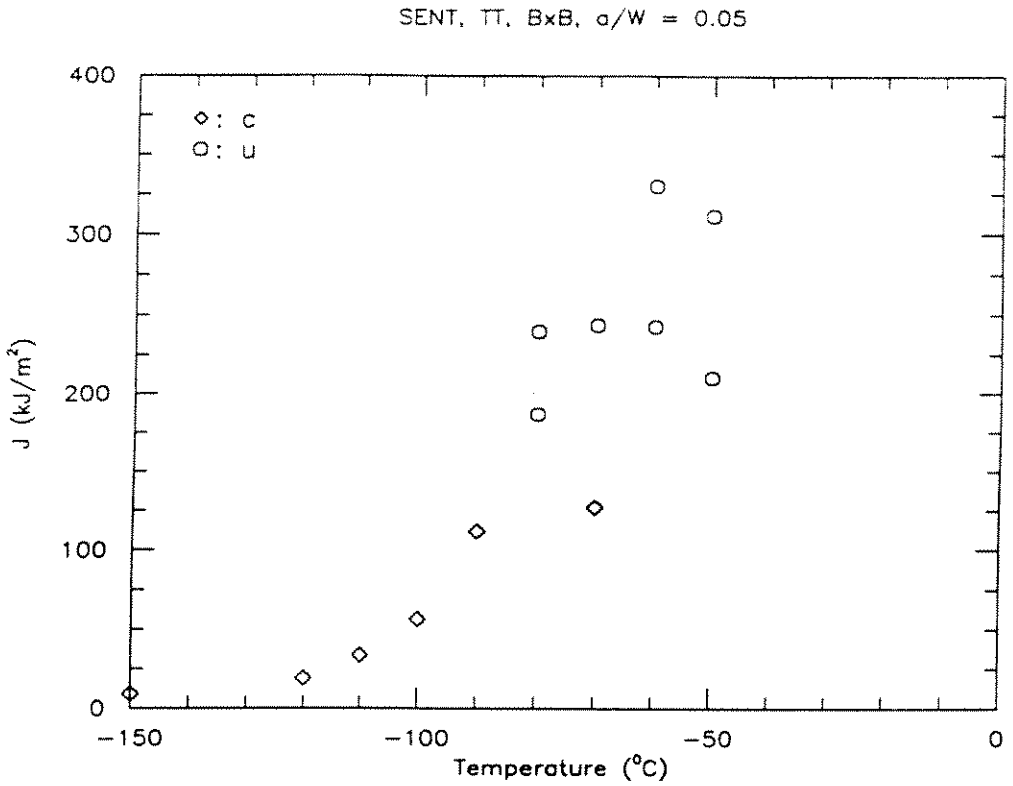

FIGURE 78. J TRANSITION CURVE (SENT, B × B, a/W = 0.05 THROUGH THICKNESS NOTCHED)

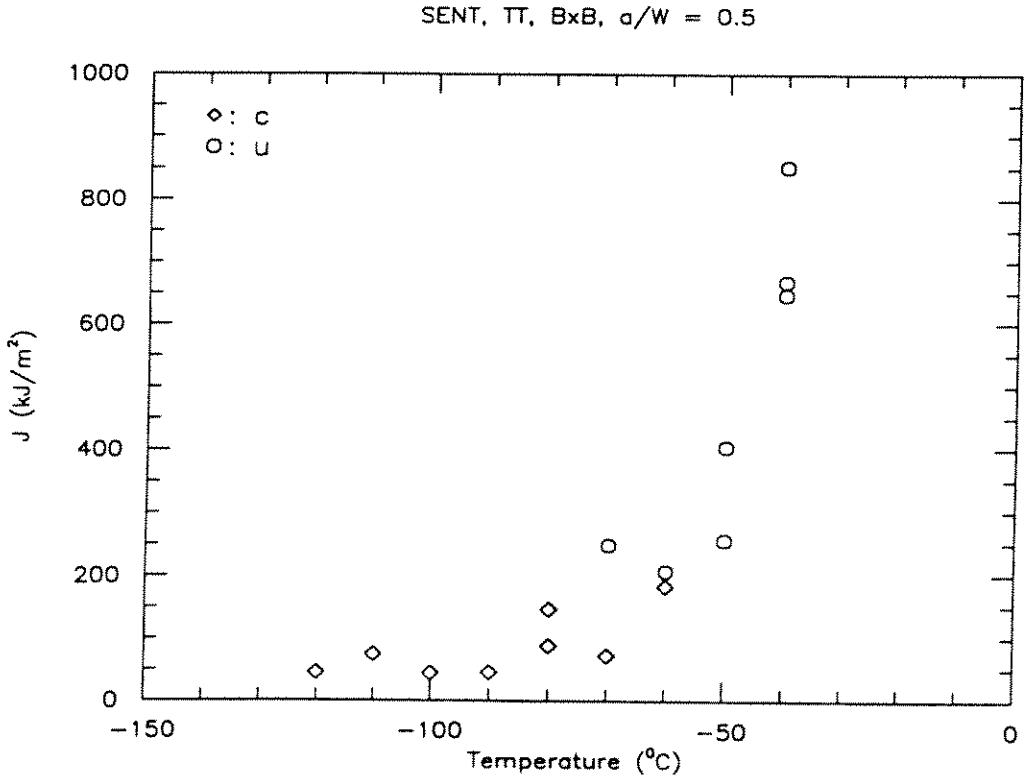

FIGURE 79. J TRANSITION CURVE (SENT, B × B, a/W = 0.5, THROUGH THICKNESS NOTCHED)

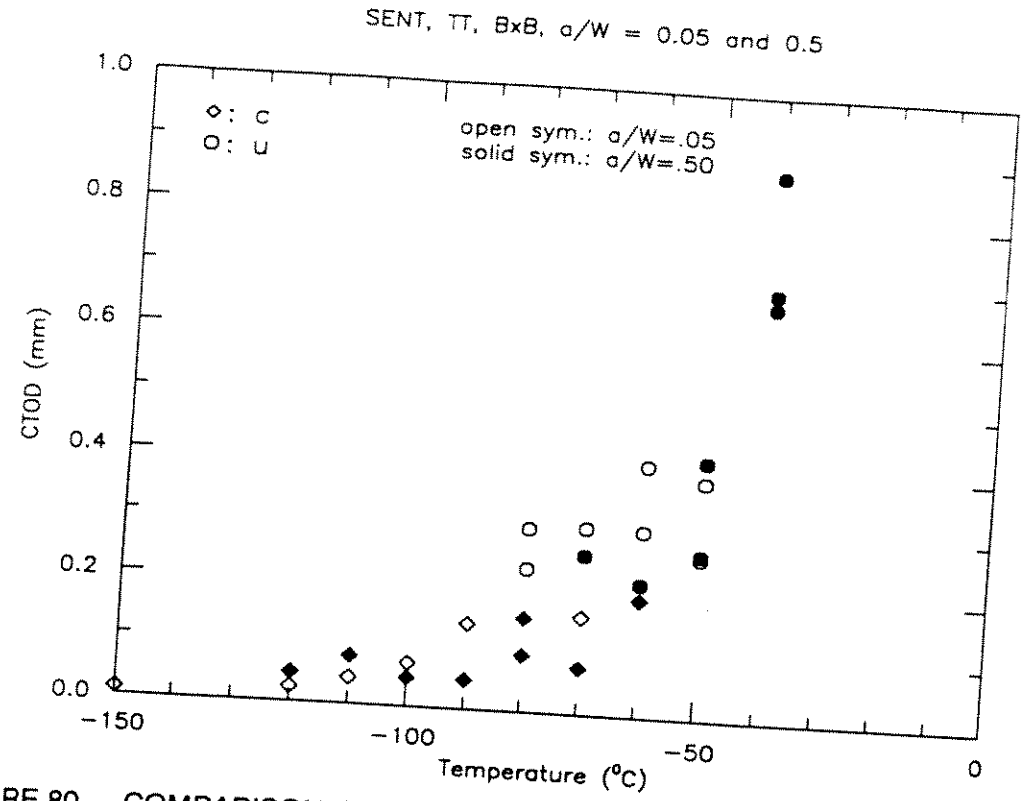

FIGURE 80. COMPARISON OF a/W = 0.05 AND a/W = 0.5 CTOD TRANSITION CURVE (SENT, B × B, THROUGH THICKNESS NOTCHED)

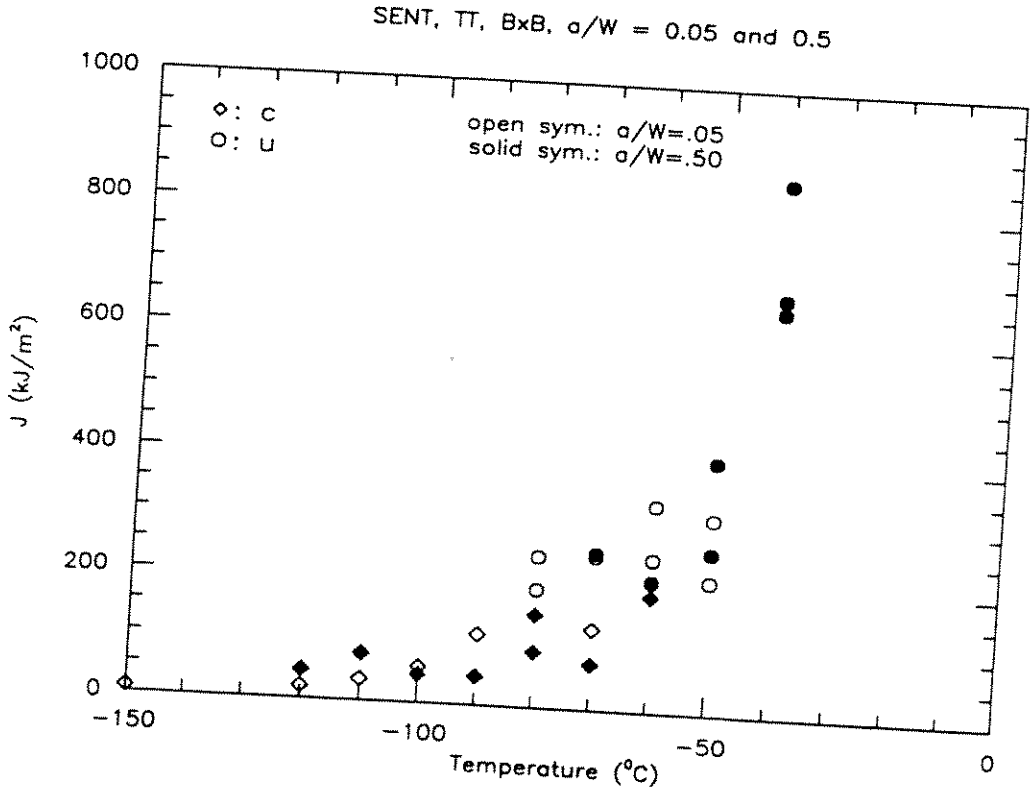

FIGURE 81. COMPARISON OF a/W = 0.05 AND a/W = 0.5 J TRANSITION CURVES (SENT, B × B, THROUGH THICKNESS NOTCHED)

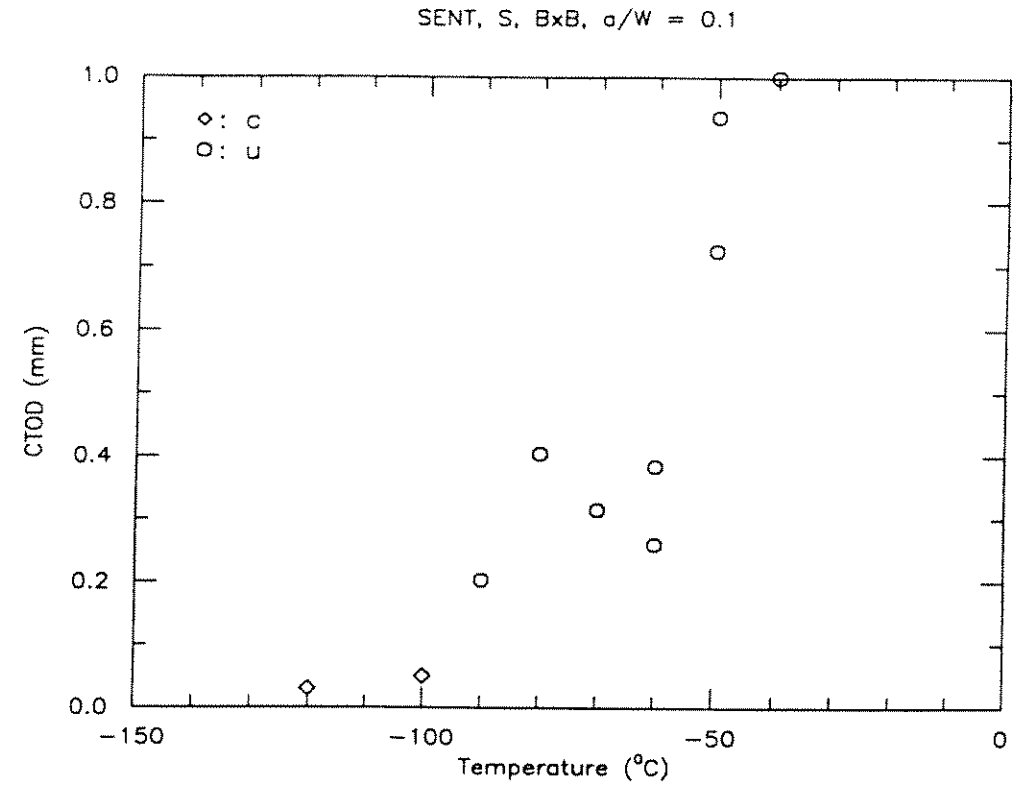

FIGURE 82. CTOD TRANSITION CURVE (SENT, BXB, a/W = 0.1, SURFACE NOTCHED)

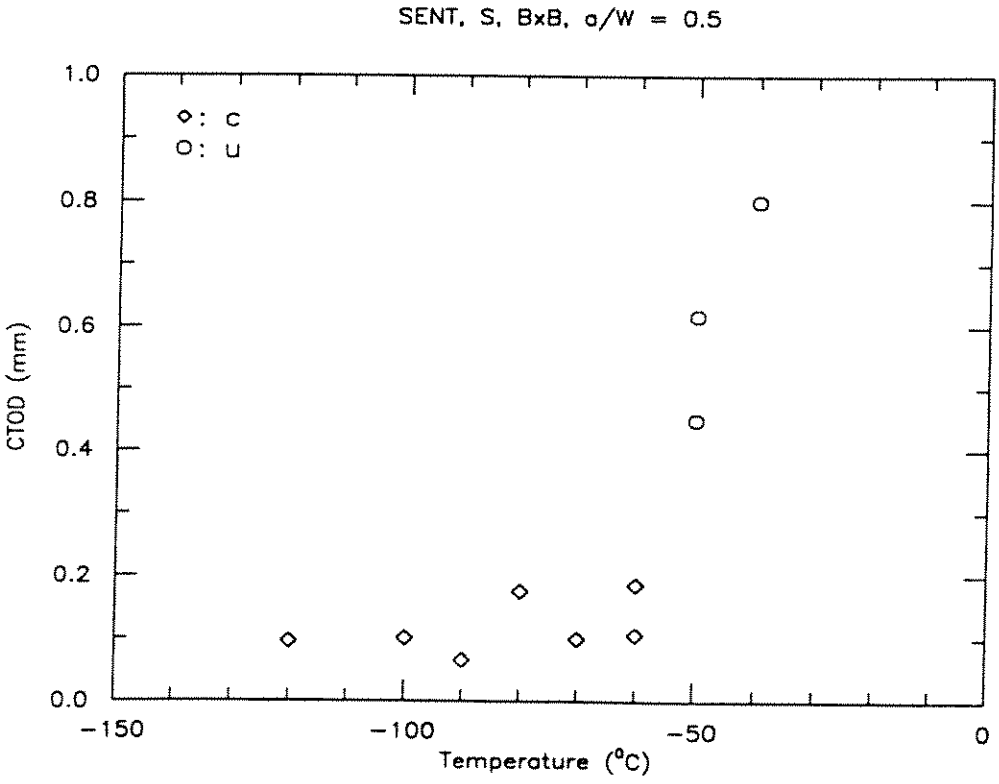

FIGURE 83. CTOD TRANSITION CURVE (SENT, BXB, a/W = 0.5, SURFACE NOTCHED)

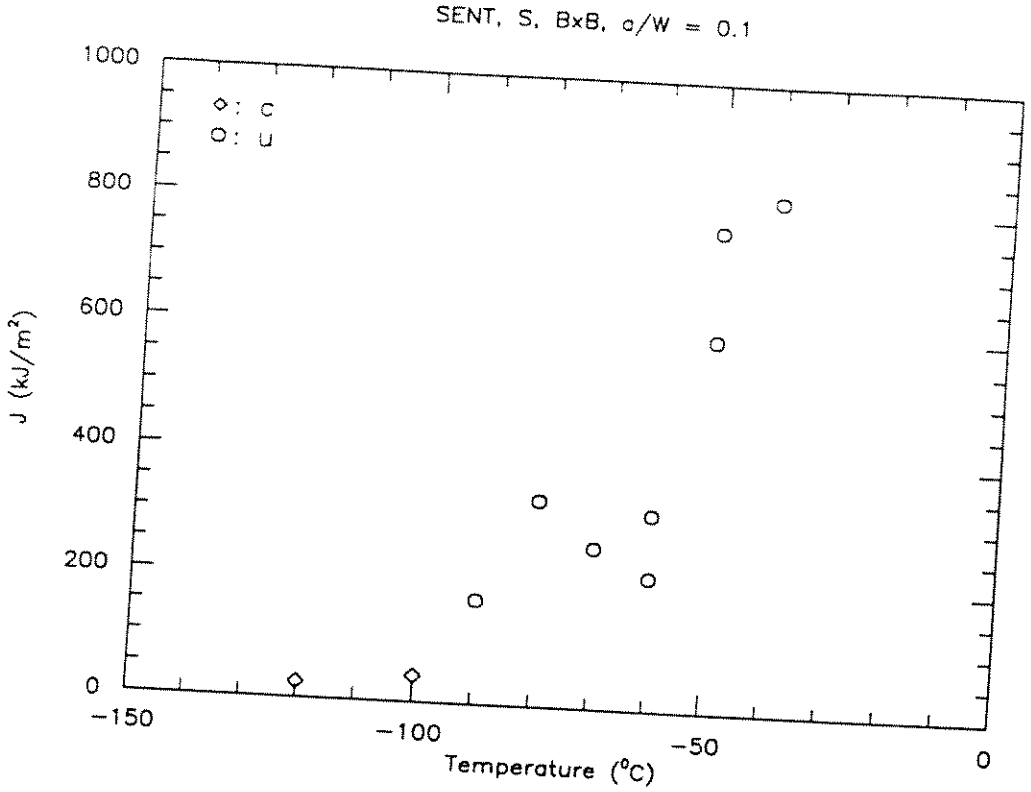

FIGURE 84. J TRANSITION CURVE (SENT, BXB, a/W = 0.1, SURFACE NOTCHED)

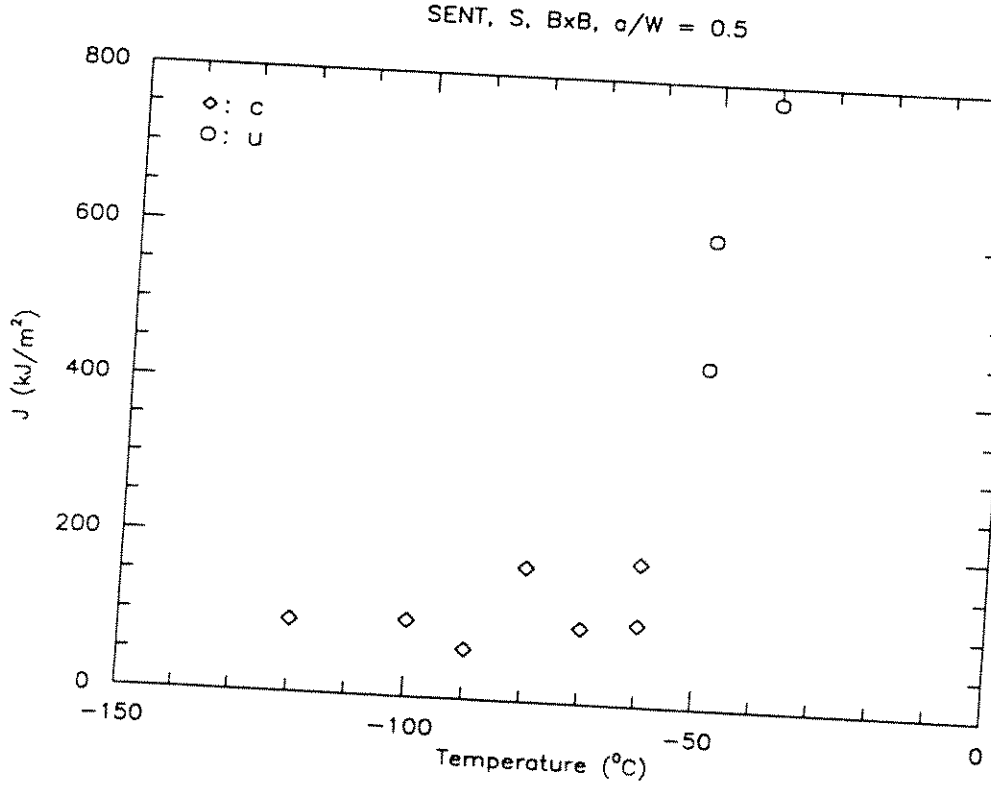

FIGURE 85. J TRANSITION CURVE (SENT, BXB, a/W = 0.5, SURFACE NOTCHED)

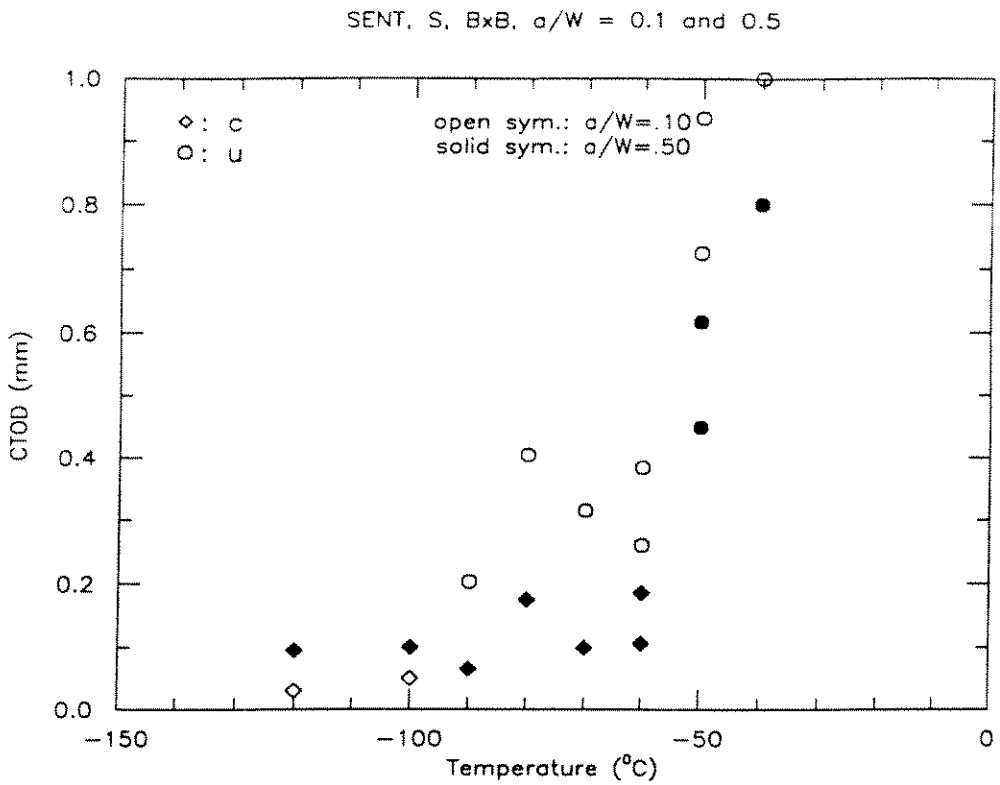

FIGURE 86. COMPARISON OF a/W = 0.1 AND a/W = 0.5 CTOD TRANSITION CURVES (SENT, BXB, SURFACE NOTCHED)

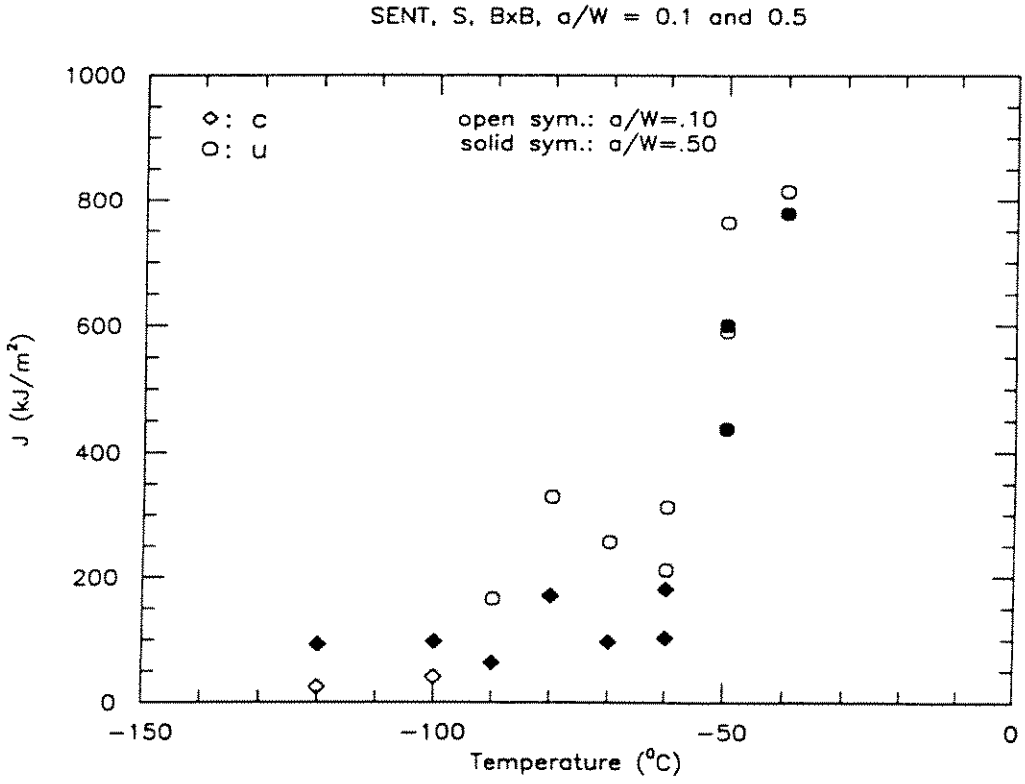

FIGURE 87. COMPARISON OF a/W = 0.1 AND a/W = 0.5 J TRANSITION CURVES (SENT, B × B, SURFACE NOTCHED)

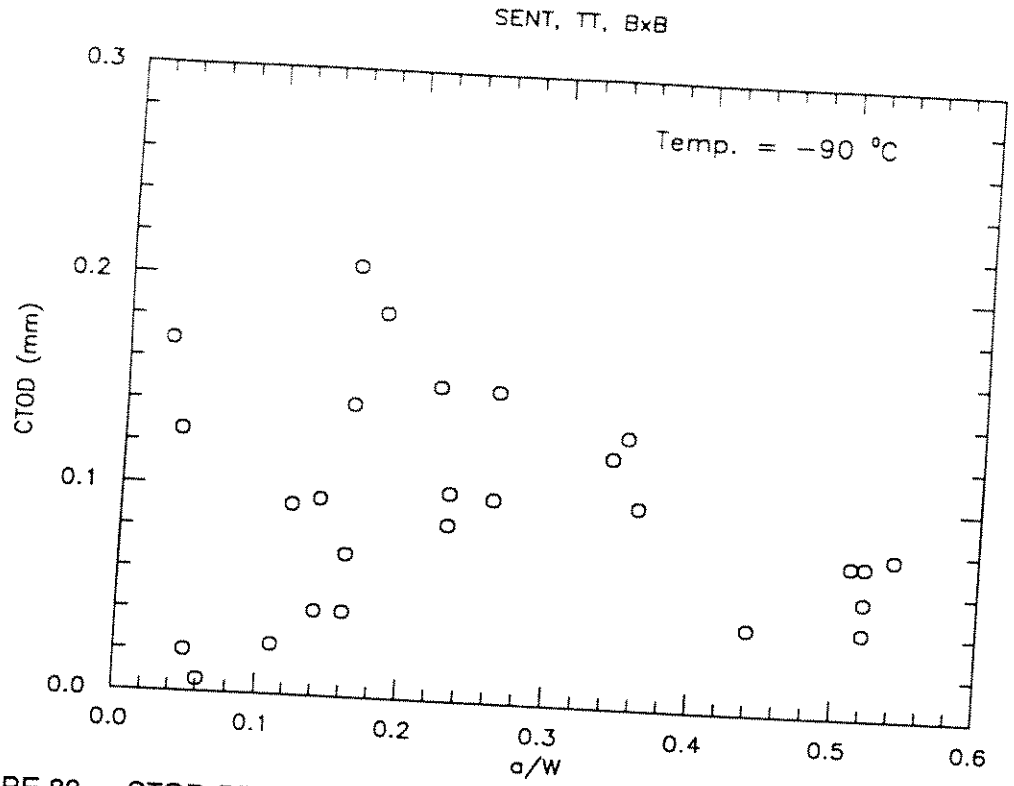

FIGURE 88. CTOD RESULTS FROM THROUGH THICKNESS NOTCHED SENT REPLICATE TESTS

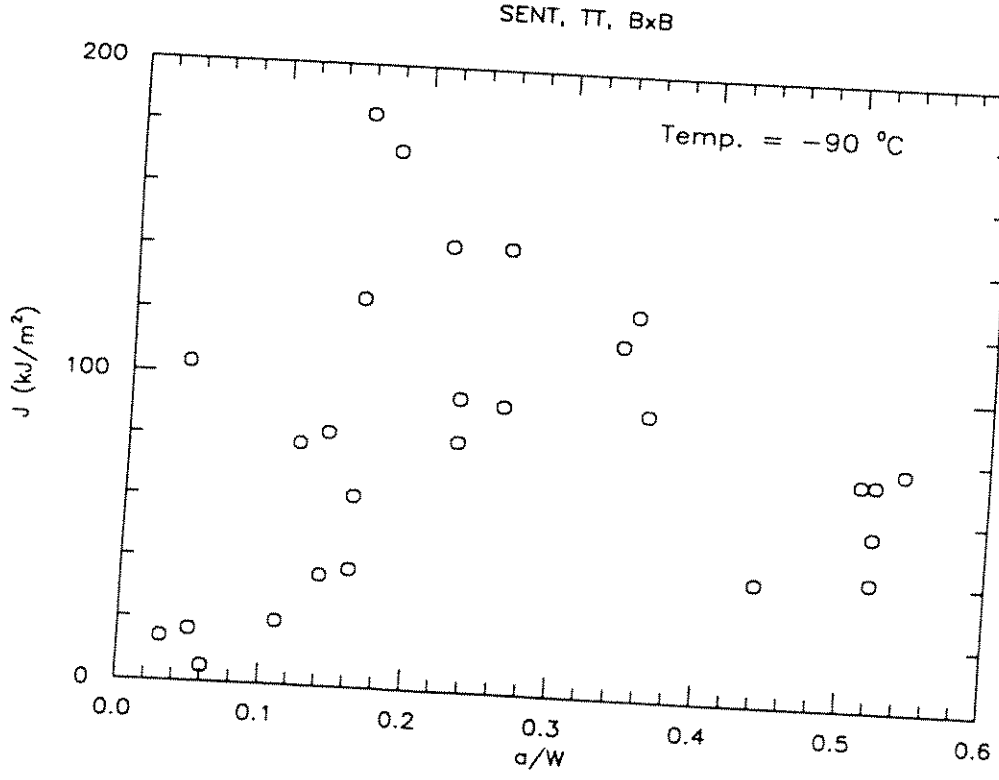

FIGURE 89. J RESULTS FROM THROUGH THICKNESS NOTCHED SENT REPLICATE TESTS

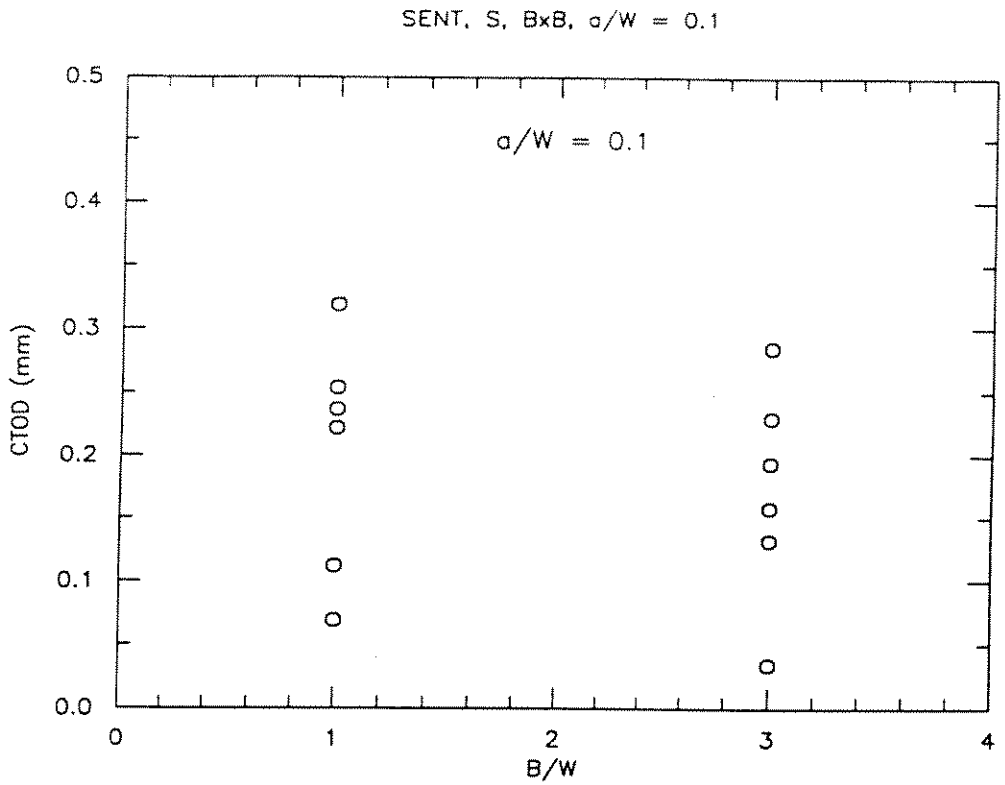

FIGURE 90. CTOD RESULTS FROM SURFACE NOTCHED SENT REPLICATE TESTS (a/W = 0.1)

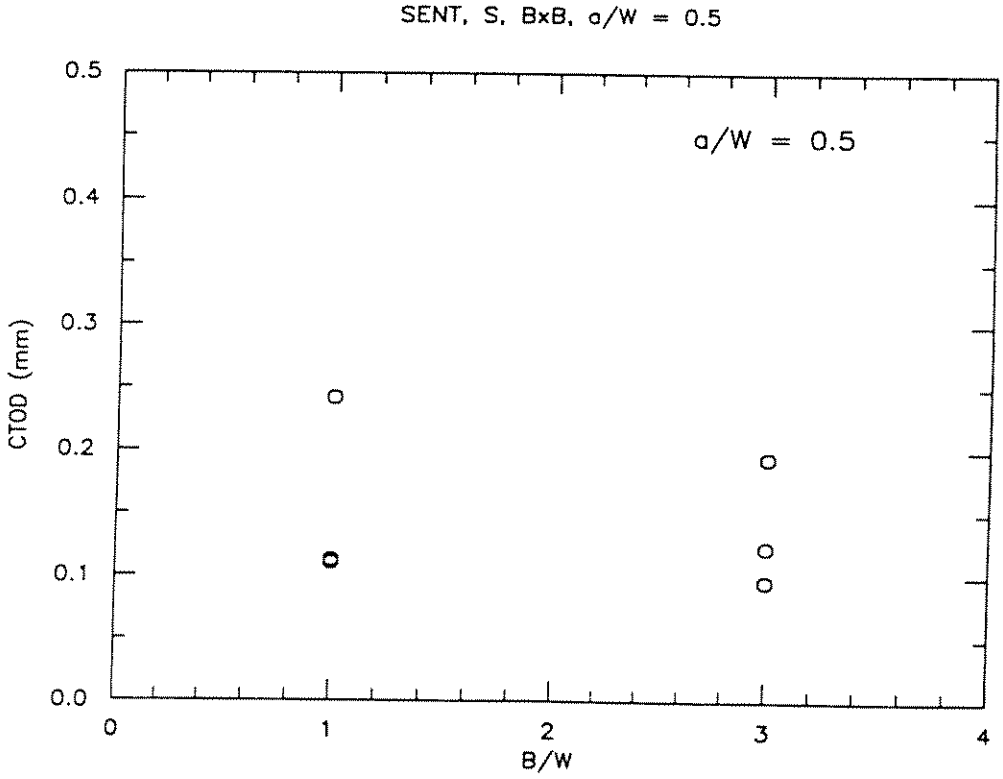

FIGURE 91. CTOD RESULTS FROM SURFACE NOTCHED SENT REPLICATE TESTS (a/W = 0.5)

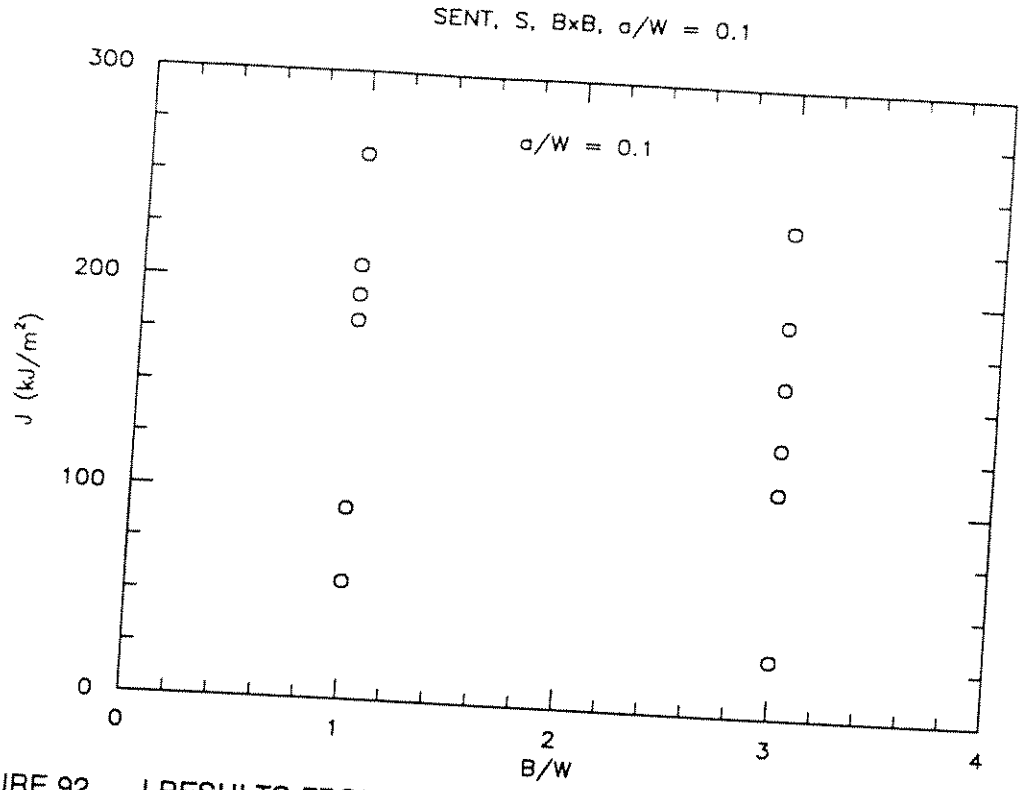

FIGURE 92. J RESULTS FROM SURFACE NOTCHED SENT REPLICATE TESTS (a/W = 0.1)

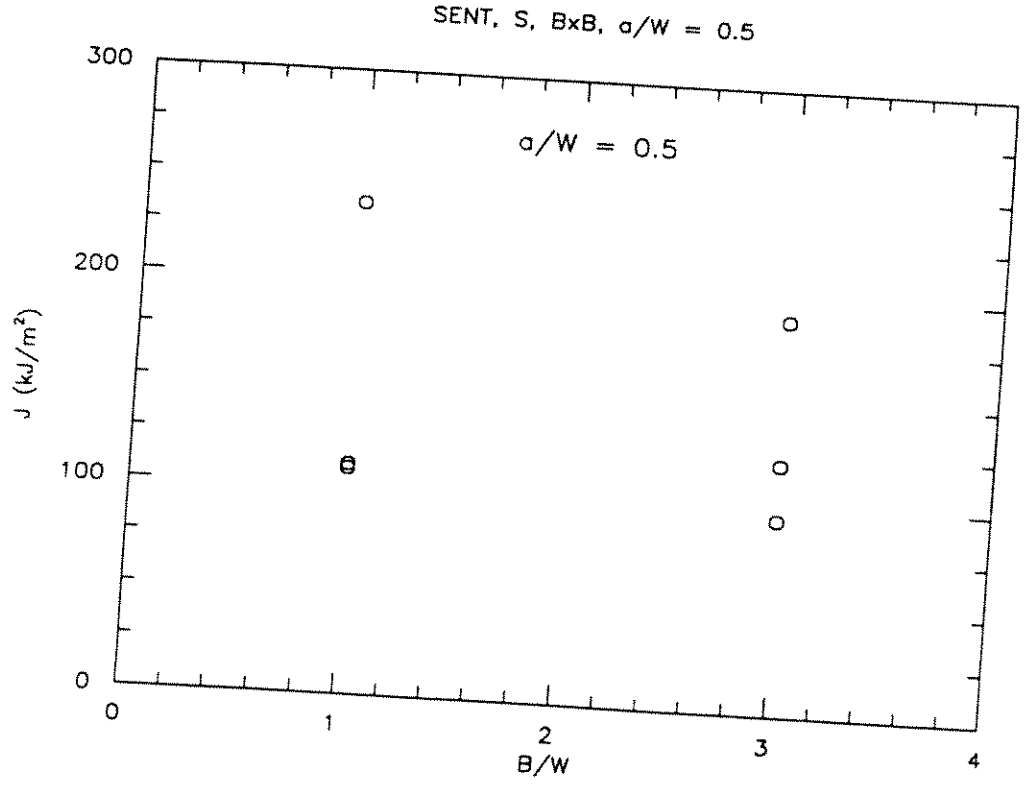

FIGURE 93. J RESULTS FROM SURFACE NOTCHED SENT REPLICATE TESTS (a/W = 0.5)

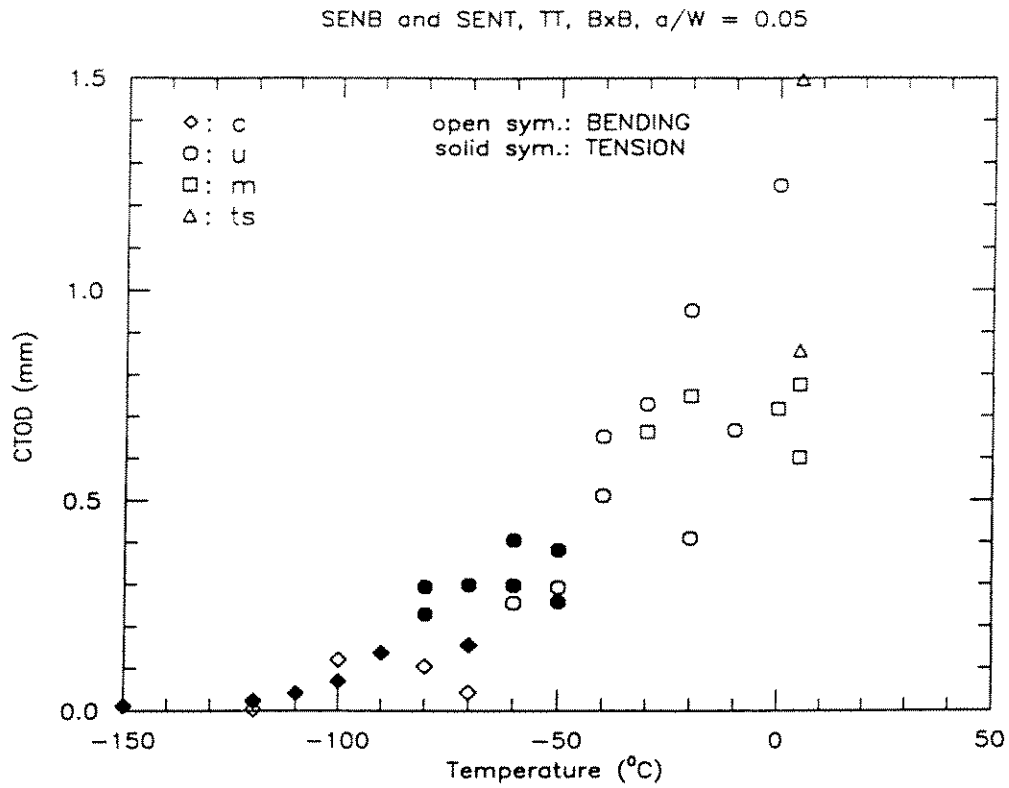

FIGURE 94. COMPARISON OF SENB AND SENT CTOD TRANSITION CURVES (a/W = 0.05, B x B, THROUGH THICKNESS NOTCHED)

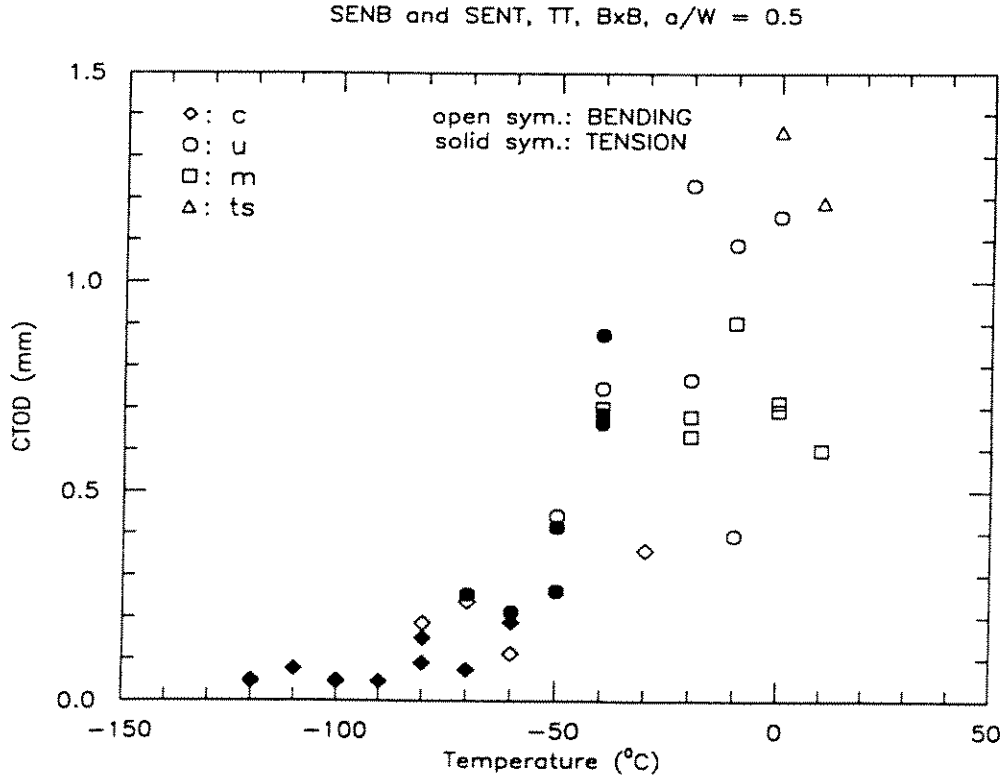

FIGURE 95. COMPARISON OF SENB AND SENT CTOD TRANSITION CURVES (a/W = 0.5, B x B, THROUGH THICKNESS NOTCHED)

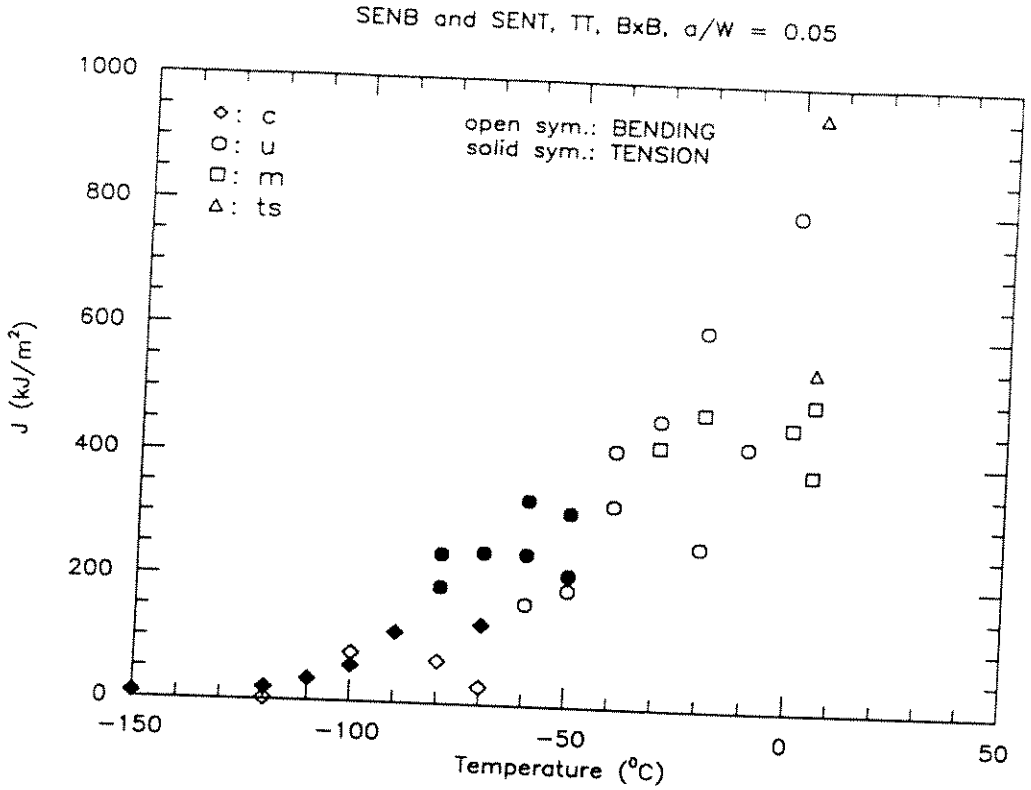

FIGURE 96. COMPARISON OF SENB AND SENT J TRANSITION CURVES (a/W = 0.05, B x B, THROUGH THICKNESS NOTCHED)

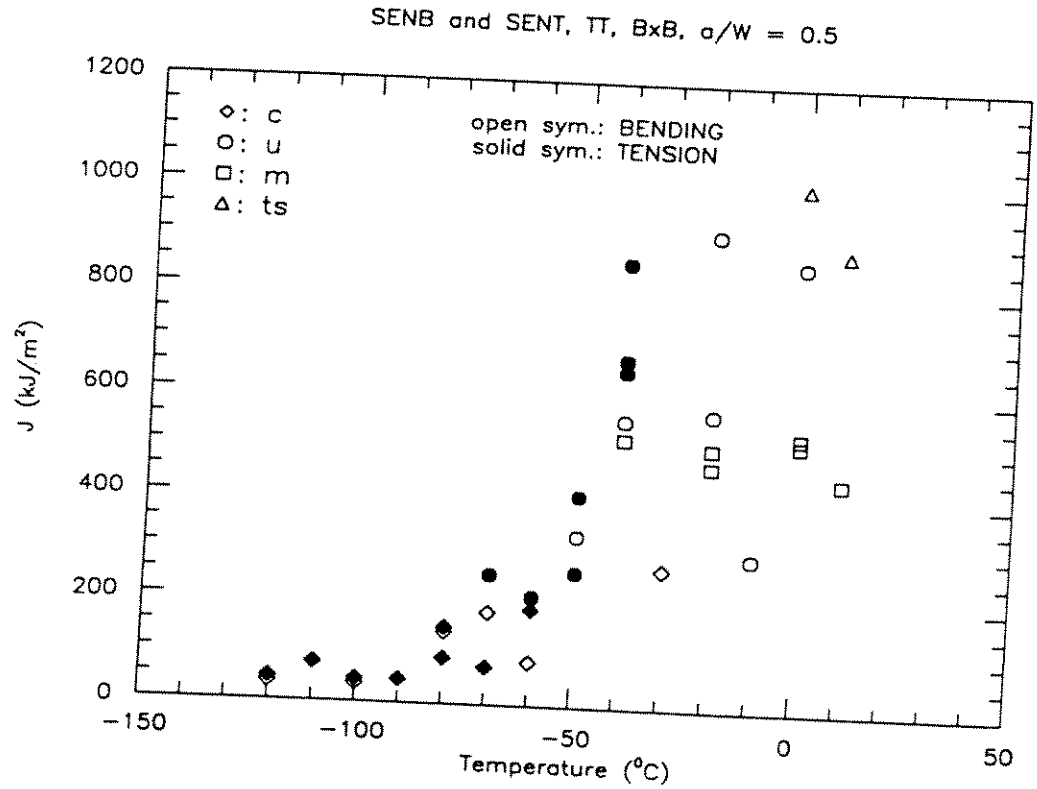

FIGURE 97. COMPARISON OF SENB AND SENT J TRANSITION CURVES (a/W = 0.5, B x B, THROUGH THICKNESS NOTCHED)

APPENDIX A

LIST OF REPORTS ISSUED DURING PROJECT

APPENDIX A

LIST OF REPORTS ISSUED DURING PROJECT

1 Dawes, M. G., Leggatt, R. H., and Slater, G., "An International Research Project to Develop Shallow Crack Fracture Mechanics Tests - European Contribution, First Progress Report," No. 5574/3/88, TWI, March 1988.

2. Pisarski, H. G., "An International Research Project to Develop Shallow Crack Fracture Mechanics Tests - North American Contribution, First Progress Report," No. J6098-1-88, EWI, April 1988.

3. Dawes, M. G., Leggatt, R. H., and Slater, G., "An International Research Project to Develop Shallow Crack Fracture Mechanics Tests - European Contribution, Second Progress Report," No. 5574/6/88, TWI, October 1988.

4. Pisarski, H. G., "International Research Project to Develop Shallow Crack Fracture Mechanics Tests - North American Contribution, Second Progress Report," No. J6098-7-88, EWI, November 1988.

5. Slater, G., Leggatt, R. H., and Dawes, M. G., "An International Research Project to Develop Shallow Crack Fracture Mechanics Tests - European Contribution, Third Progress Report," No. 5574/9/89, TWI, May 1989.

6. Gordon, J. R., "An International Research Project to Develop Shallow Crack Fracture Mechanics Tests - North American Contribution, Third Progress Report," No. J6098-10-89, EWI, May 1989.

7. Dawes, M. G., Leggatt, R. H., and Slater, G., "An International Research Project to Develop Shallow Crack Fracture Mechanics Tests - European Contribution, Fourth Progress Report," No. 5574/12/89, TWI, October 1989.

8. Gordon, J. R., "An International Research Project to Develop Shallow Crack Fracture Mechanics Tests - North American Contribution, Fourth Progress Report, No. J6098-12-89, EWI, October 1989.

9. Slater, G., Leggatt, R. H., and Dawes, M. G., "An International Research Project to Develop Shallow Crack Fracture Mechanics Tests - European Contribution, Fifth Progress Report," No. 5574/15/90, TWI, March 1990.

10. Gordon, J. R. and McGaughy, T. H., "An International Research Project to Develop Shallow Crack Fracture Mechanics Tests - North American Contribution, Fifth Progress Report, No. J6098-15-89, EWI, March 1990.

11. Leggatt, R. H., "An International Research Project to Develop Shallow Crack Fracture Mechanics Tests - European Contribution, Finite Element Modeling of 'Year 1' SENB, SENT and SENAB Tests," No. 5574/16/90, TWI, April 1990.

12. Gordon, J. R. and McGaughy, T., "An International Research Project to Develop Shallow Crack Fracture Mechanics Tests - North American Contribution, Sixth Progress Report," No. J6098-18-1990, EWI, October 1990.

13. Dawes, M. G., Leggat, R. H., and Slater, G., "An International Research Project to Develop Shallow Crack Fracture Mechanics Tests - European Contribution, Sixth Progress Report," No. 5574/20/90, TWI, December 1990.

14. Leggatt, R. H., "An International Research Project to Develop Shallow Crack Fracture Mechanics Tests - Specification of the Finite Element Analyses to be performed in Year 4 of the Project," No. 5574/22/91, TWI, February 1991.

15. Dawes, M. G., Leggatt, R. H., and Slater, G., "An International Research Project to Develop Shallow Crack Fracture Mechanics Tests - European Contribution, Seventh Progress Report," No. 5574/23/91, TWI, May 1991.

16. Gordon, J. R. and McGaughy, T. H., "An International Research Project to Develop Shallow Crack Fracture Mechanics Tests - North American Contribution, Seventh Progress Report," No. J6098-21-91, September 1991.

17. Leggatt, R. H., "An International Research Project to Develop Shallow Crack Fracture Mechanics Tests - European Contribution: Review of Finite Element Analyses Performed in Europe in Year 4 of the Project," TWI Report No. 5574/26/92, February 1992.

18. Dawes, M. G., Leggatt, R. H., and Slater, G., "An International Research Project to Develop Shallow Crack Fracture Mechanics Tests - European Contribution, Final Report," No. 5574/27/91, TWI, February 1992.

19. Gordon, J. R. and Wang Y-Y., "An International Research Project to Develop Shallow Crack Fracture Mechanics Tests - North American Contribution, Final Report on North American Finite Element Analyses," EWI Report No. J6098-23-91, May 1992.

20. Gordon, J. R. and M°Gaughy T. H., "An International Research Project to Develop Shallow Crack Fracture Mechanics Tests - North American Contribution, Final Report on North American Experimental Program, EWI Report," No. J6098-24-91, May 1992.

DOCUMENTS ISSUED TO FINITE ELEMENT CONTRIBUTORS

1. 5574/FEC/1 - Issue 2, March 1988, "Specification of Finite Element Analyses to be Performed in Year 1 of the Project" (also issued as Appendix B of First TWI Progress Report, 5574/3/88).

2. 5574/FEC/2 - April 1988, "Calculations of Projected Crack Flank Displacements," (also issued as Appendix A of Second TWI Progress Report 5574/6/88).

3. 5574/FEC/3 - April 1988, "Materials Data Sheet - Material M1," (also issued as Appendix B of Second TWI Progress Report 5574/6/88).

4. 5574/FEC/4 - Issue 2, March 1989, "Materials Data Sheet - Material M3," (also issued in Appendix 1 of Third EWI Progress Report J6098-10-89).

5. 5574/FEC/5 - December 1988, "Materials Data Sheet - Material M2," (also issued as Appendix C of Third TWI Progress Report 5574/9/89).

6. 5574/FEC/6 - March 1989, "Materials Data Sheet - Material M4," (also issued as Appendix 2 of Third EWI Progress Report J6098-10-89).

7. 5574/FEC/7 - March 1989, "Stress-Intensity Factors for Slotted, SENAB Specimens," (also issued as Appendix 3 of Third EWI Progress Report J6098-10-89).

8. 5574/FEC/8 - April 1989, "Minutes of a Meeting for Finite Element Contributors at Westin Oaks Hotel, Houston, Wednesday, March 22, 1989," (also issued, with added figures, as Appendix A of Third TWI Progress Report 5574/9/89).

9. 5574/FEC/9 - April 1989, "Simplification of Post-Processing Requirements for Year 1 Finite Element Analysis," (also issued as Appendix D of Third TWI Progress Report 5574/9/89).

APPENDIX B

STRESS INTENSITY FACTORS FOR SLOTTED SENAB SPECIMENS

Stress-intensity factors for slotted, SENAB specimens

ROBERT H. DODDS, JR.*, PEDRO M. VARGAS, and MICHAEL KEPPEL

Associate Professor and Graduate Research Assistants, respectively, Department of Civil Engineering, University of Illinois, Urbana, IL 61801*

Finite-element analyses were performed to obtain stress-intensity factors, K_I, and crack mouth opening displacements (CMOD) for single-edge notch arc bend (SENAB) specimens. A slot is machined into these specimens on the inside radius (crack side) to provide a mounting surface for displacement gages that measure the CMOD. Analyses were required to assess the influence of the slot on the specimen response and to provide geometry correction factors for shallow cracks. Results are provided for the specimens designed to test pipe materials *M2* and *M4*. The dimensions for these two specimens are provided in Figs. 1 and 2. The corresponding finite-element models are shown in Figs. 3 and 4. Stress-intensity factors and crack mouth opening displacements are determined for crack-depth to width ratios (a/W) over the range 0.05–0.60.

Plane-strain, eight-noded isoparametric elements with an elastic modulus of 30,000 ksi and a Poisson's ratio of 0.3 are employed in the finite-element models. The models are loaded with a concentrated force applied at the top center node. The crack-tip region is modeled with 6 rings of elements; the innermost ring consists of degenerate, quarter-point elements to enforce the $1/\sqrt{r}$ strain-stress singularity (see Figs. 3 and 4). This modeling scheme is adopted for each crack length. The J-integral is calculated using the the domain integral method [2]. The stress-intensity factors are then calculated from the J-integral by:

$$K_I = \sqrt{\frac{J}{E(1-\nu^2)}} \tag{1}$$

Following conventional procedures to describe geometry effects [3], stress-intensity factors and CMODs are expressed in the form:

$$K_I = \sigma \sqrt{\pi a}\ F(a/W) \tag{2}$$

$$\delta = \frac{4\sigma a}{E(1-\nu^2)}\ V(a/W) \tag{3}$$

where δ is the CMOD, E and ν the elastic constants, a and W are dimensions as indicated in Figs. 1 and 2. The functions $F(a/W)$ and $V(a/W)$ are the geometric correction factors

which equal 1 for an infinite center-cracked panel with a half crack length of a. The nominal bending stress in Eqs. (2,3), σ, is calculated by the following:

$$\sigma = \frac{3\,P\,S}{2\,W^2} \tag{4}$$

where P is the total load applied, S and W are dimensions indicated in Figs. 1 and 2. This corresponds to the bending stress on the outer fiber of a prismatic beam in the absence of a crack.

The computations were performed with the POLO-FINITE program [1] on the Civil Engineering Apollo Network at the University of Illinois. Results of the analysis are summarized in graphical form in Figs. 5 and 6. The figures also include coefficients for fourth-order polynomials fitted to the finite-element results. Table 1 compares the current results to those reported by Underwood, et al. [4] for specimens without machined slots. Underwood's results are available only for $a/W > 0.30$. The factors obtained for the two specimens are identical.

	Material "M2"		Material "M4"	
a/w	current	Ref [4]	current	Ref [4]
0.3	9.4206	9.7108	13.468	13.519
0.4	12.250	12.570	17.517	17.596
0.5	16.402	16.873	23.448	23.500
0.6	23.227	23.947	33.183	33.278

Table 1. Stress Intensity Comparisons with Ref. [4]. All units are in ksi$\sqrt{\text{in}}$

The comparison in Table 1 indicates the negligible effect of the slots on the correction functions for stress-intensity factors. Moreover, the correction factor very closely matches the solution for the usual three-point bend specimen. Similarly, the CMOD correction factors very closely match those for the three-point bend specimen.

References

1. Dodds, R., and Lopez, L., "Software Virtual Machines for Development of Finite Element Systems," *International Journal for Engineering Computations*, 3, (1986), 18-26.

2) Moran, B., and Shih, C. F., "Crack Tip and Associated Domain Integrals from Momentum and Energy Balance," *Engineering Fracture Mechanics*, 27, (1987), 615–642.

3) Tada, H., Paris, P. C., and Irwin, G. R., ed., "Stress Analysis of Cracks Handbook," Del. Research Corporation, Hellertown, Pa., (1973).

4) Underwood, J., H., Kapp, J., A., and Witherell, M., D., "Fracture Testing with Arc Bend Specimens", *Fracture Mechanics: Seventeenth Volume, ASTM STP 905*, American Society for Testing Materials, 1984, pp. 279–296.

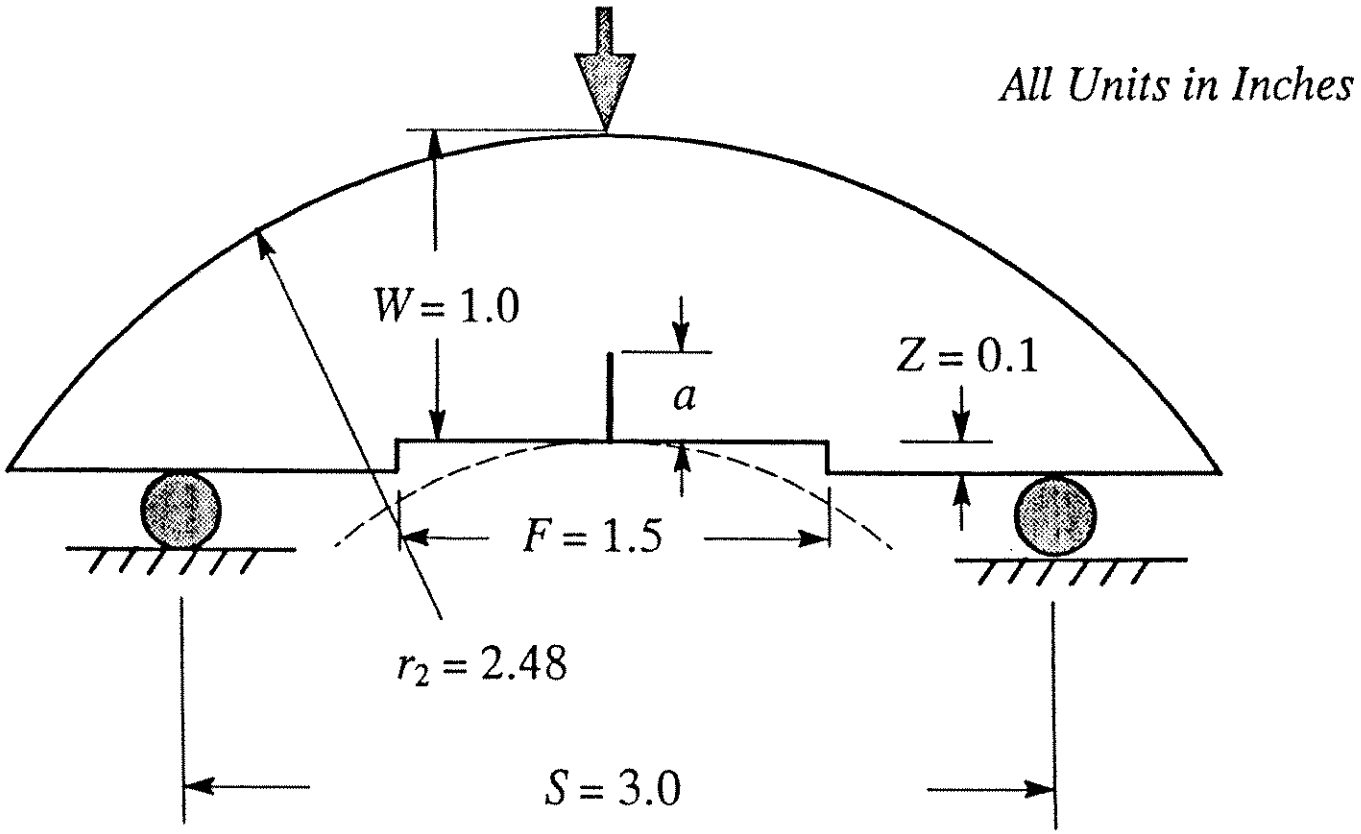

Figure 1. SENAB Specimen for Pipe Material "M2" with Machined Slot

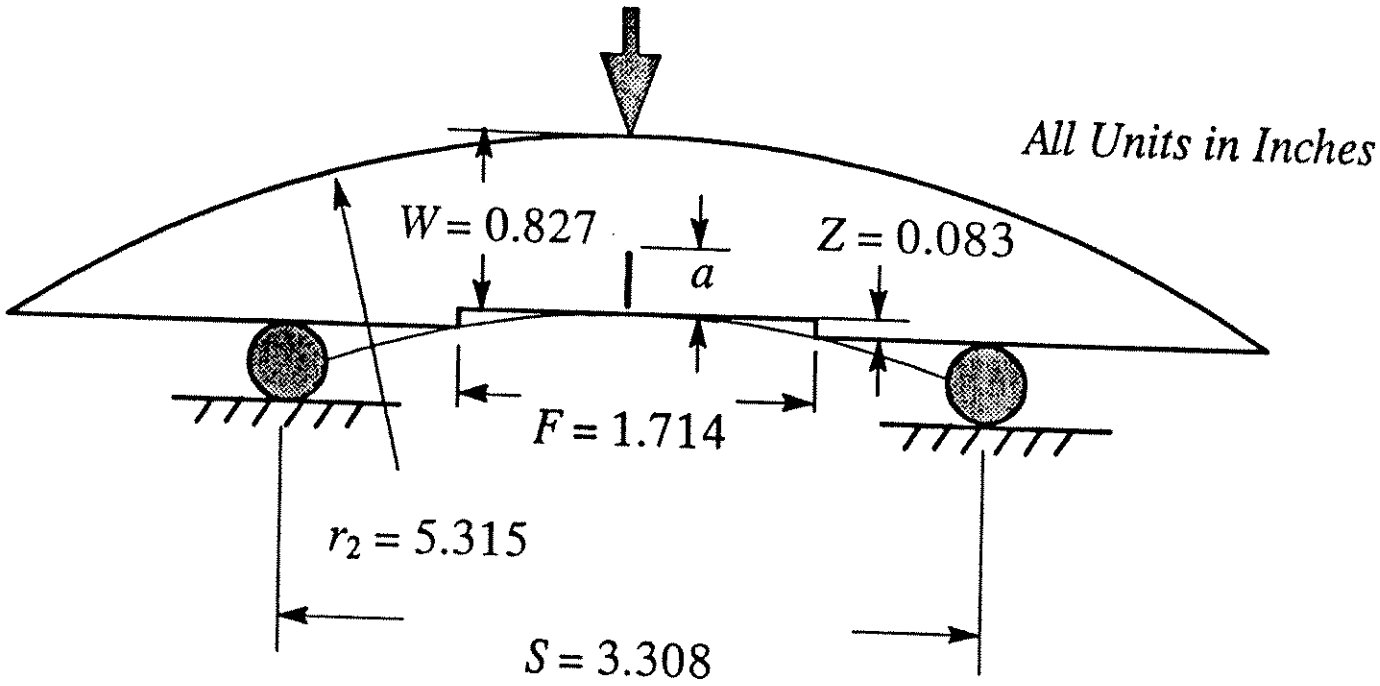

Figure 2. SENAB Specimen for Pipe Material "M4" with Machined Slot

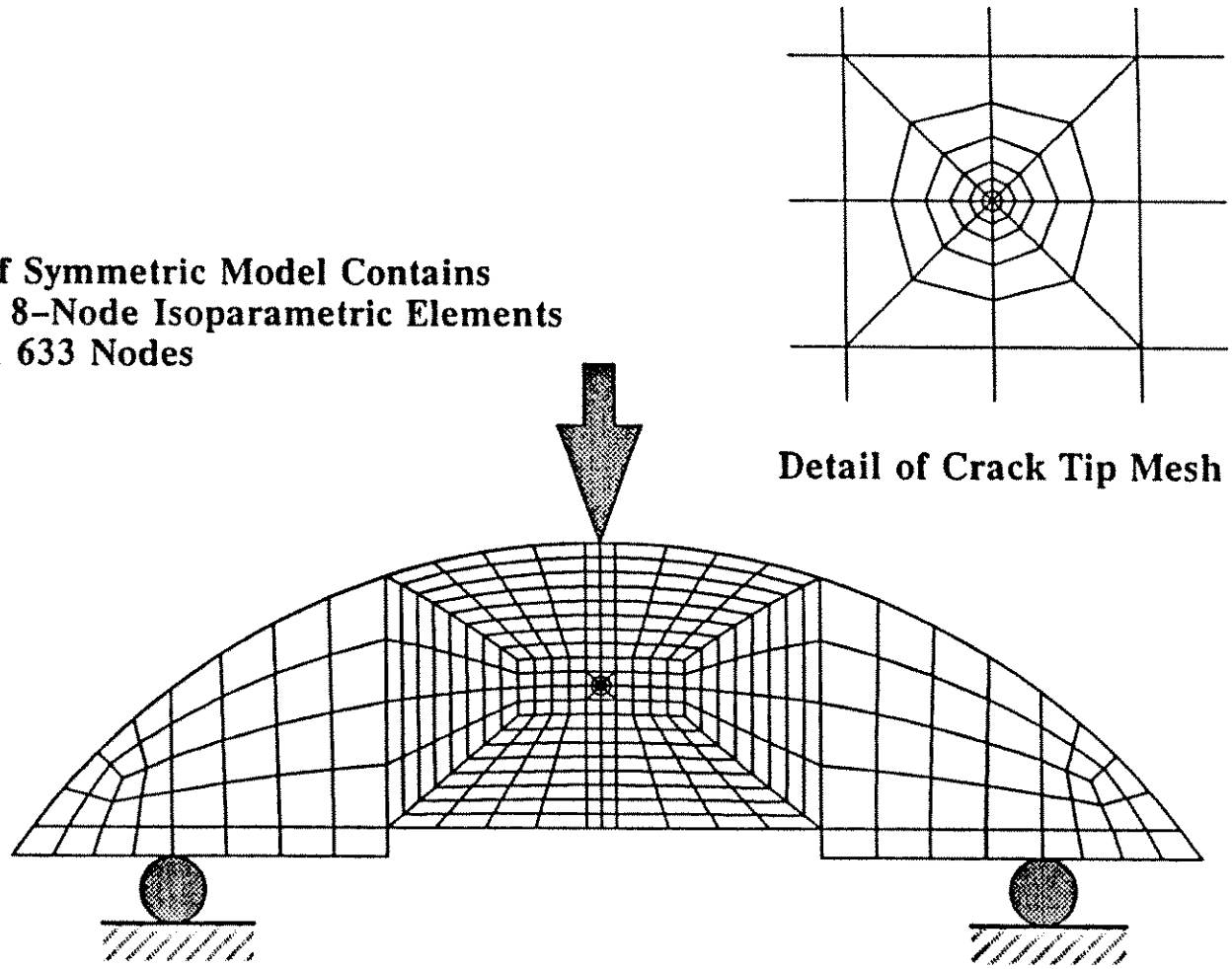

Figure 3. Finite Element Mesh for SENAB Specimen for Pipe Material "M2" with Machined Slot

Half Symmetric Model Contains
317 8–Node Isoparametric Elements
and 1024 Nodes

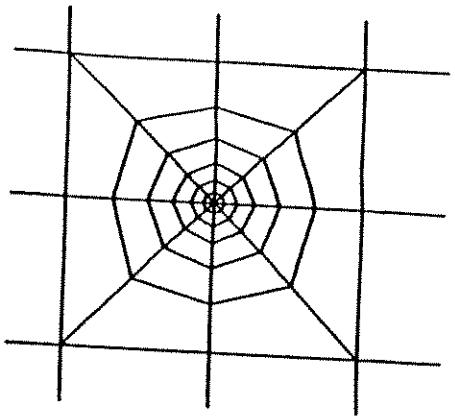

Detail of Crack Tip Mesh

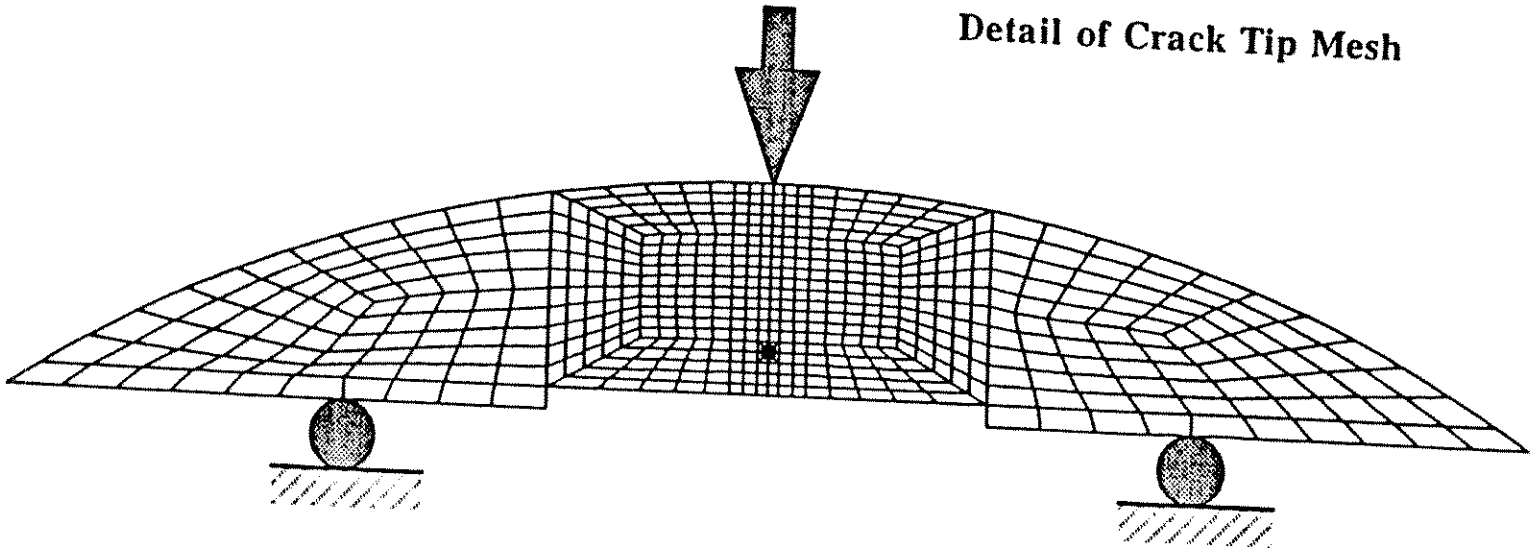

Figure 4. Finite Element Mesh for SENAB Specimen for Pipe Material "M4" with Machined Slot

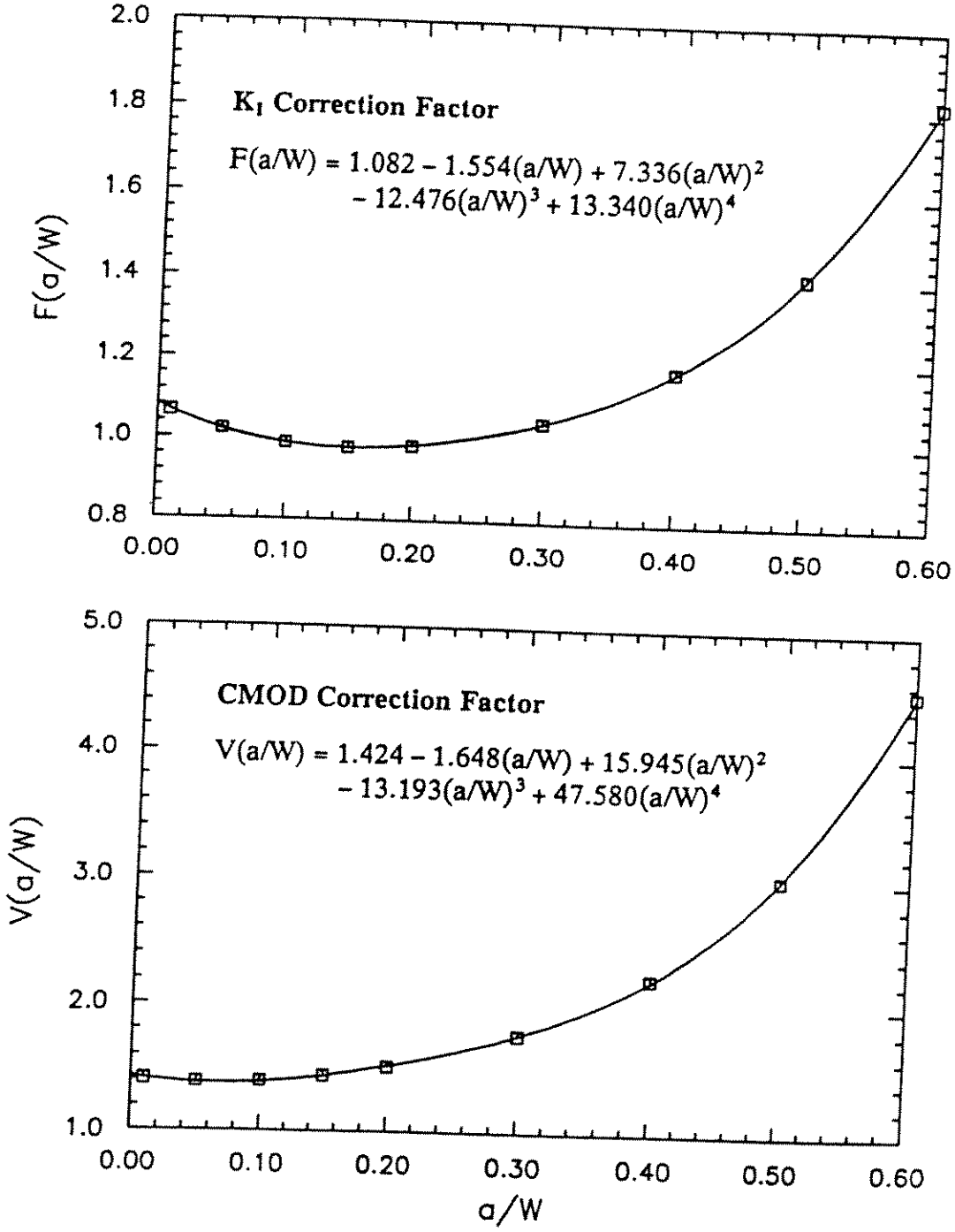

Figure 5. Correction Factors for SENAB Specimen for Pipe Material "M2" with Machined Slot